JOURNAL OF APPLIED PHYSICS

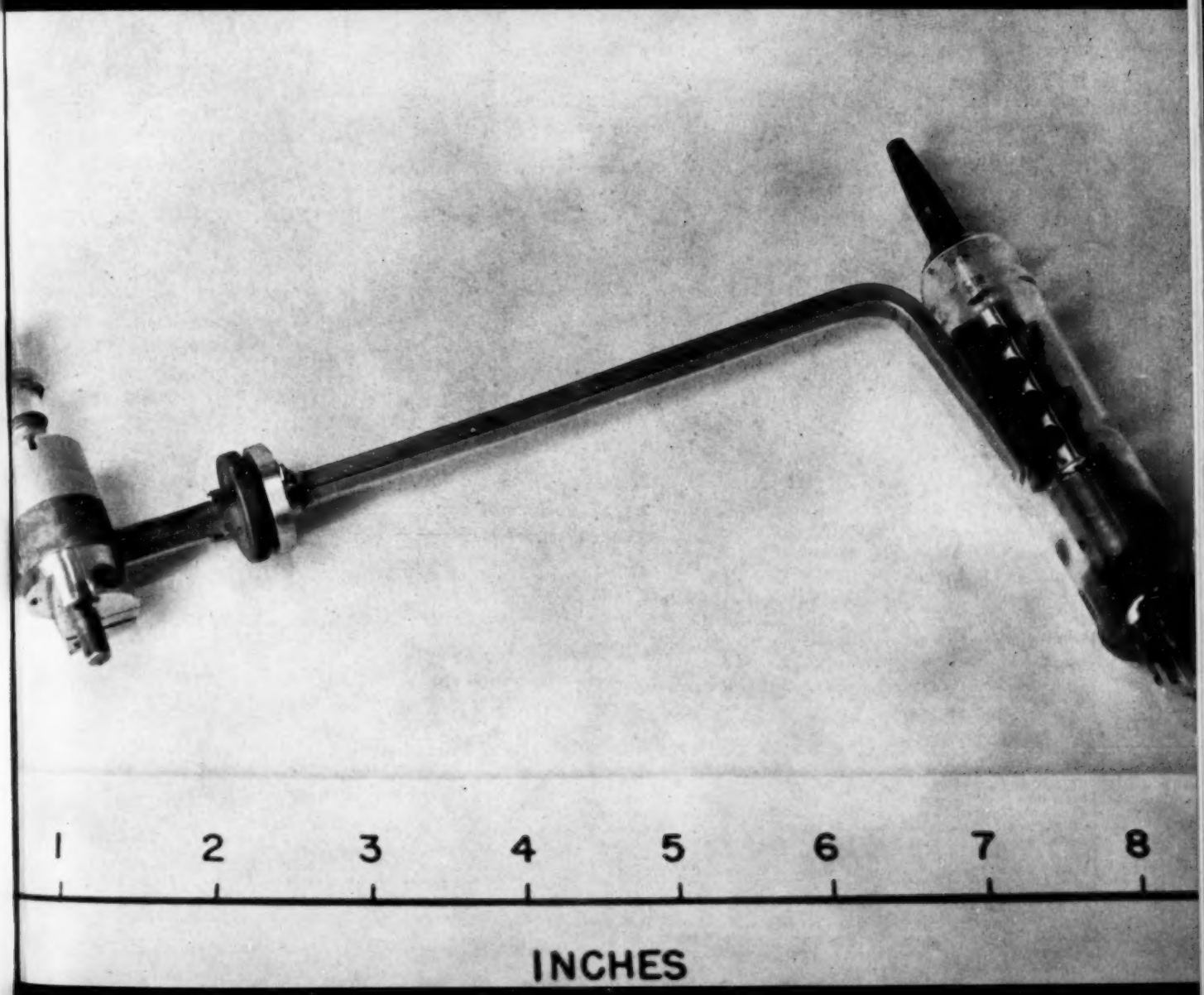

JOURNAL OF APPLIED PHYSICS

Vol. 25, No. 11 NOVEMBER, 1954

In This Issue

		Page
On the Concept of an Instantaneous Power Spectrum, and Its Relationship to the Autocorrelation Function	C. H. M. Turner	1347
Scattering from Dielectric Coated Spheres in the Region of the First Resonance	H. Scharfman	1352
Spectral Response of a Quadratic Device to Non-Gaussian Noise	T. A. Magness	1357
Electron Emission from Metals under High-Energy Hydrogen Ion Bombardment	B. Aarset, R. W. Cloud, and J. G. Trump	1365
Influence of Deuteron Bombardment and Strain Hardening on Notch Sensitivity of Mild Steel	Robert A. Meyer	1369
Effect of Velocity Distribution on Traveling-Wave Tube Gain	D. A. Watkins and N. Rynn	1375
Conditions for Porosity Formation during Diffusion	R. W. Balluffi and L. L. Seigle	1380
Calibration of a Nickel-Molybdenum Thermocouple	Richard D. Potter	1383
Theory of Stress-Strain Relations in Anisotropic Viscoelasticity and Relaxation Phenomena	M. A. Biot	1385
Electrical Noise Pulses from Polarized Dielectrics	N. P. Baumann and G. G. Wiseman	1391
Kinetics of Piles with Reflectors	V. H. Rumsey	1395
Mechanics of Two Immiscible Fluids in Porous Media	H. I. Meyer and A. O. Garder	1400
Forming Point-Contact Silicon Transistors	Harold Jacobs, Frank A. Brand, Wesley Matthei, and Alexander P. Ramsa	1406
Ferrite Phase Shifters in Rectangular Wave Guide	Benjamin Lax, Kenneth J. Button, and Laura M. Roth	1413
Radioactive and Photoelectric *p-n* Junction Power Sources	W. G. Pfann and W. van Roosbroeck	1422
Letters to the Editor:		
Failure and Survival in Fatigue	A. M. Freudenthal and E. J. Gumbel	1435
Effect of Moving Striations on Microwave Conductivity of a Coaxial Discharge	Howard L. Steele, Jr., and Peter J. Walsh	1435
Germanium-Stabilized Gray Tin	A. W. Ewald	1436
Protective Films on Magnesium Observed by Electron Diffraction and Microscopy	Shigeto Yamaguchi	1437
Entropy of Information and the Odd Ball Problem	Paul J. Kellogg and Dorothy J. Kellogg	1438
Diffusion of Boron and Phosphorus into Silicon	C. S. Fuller and J. A. Ditzenberger	1439
Stress Measurement by X-Ray Diffraction	H. R. Letner and S. R. Maloof	1440
Surface Leakage Current in Rectifiers	Melvin Cutler and Hubert M. Bath	1440
All-Glass Valves for Use in Obtaining Ultra High Vacua	Richard W. Decker	1441
Method for Elimination of Thermal Convection	Alexander Kolin	1442
Reproducibility of Diffusion Measurements: Time of Anneal and Method of Counting Radiation	C. T. Tomizuka and D. Lazarus	1443
Book Reviews		1444
Cover Photograph		1452
Proceedings of the Electron Microscope Society of America		1453
Index to Advertisers		xx

ROBERT L. SPROULL
Editor

ELMER HUTCHISSON,
EARLE C. GREGG,
Retiring Editors

Board of Editors
MAURICE A. BIOT
RAY E. BOLZ
WALLACE J. ECKERT
ROBERT D. HEIDENREICH
LOUIS A. PIPES
ROMAN SMOLUCHOWSKI
W. R. SMYTHE
ARTHUR V. TOBOLSKY
ALVIN M. WEINBERG

Publication of the
American Institute of Physics

OFFICERS
FREDERICK SEITZ,
Chairman
GEORGE B. PEGRAM,
Treasurer

GOVERNING BOARD
ROBERT F. BACHER
J. W. BUCHTA
KARL K. DARROW
S. A. GOUDSMIT
DEANE B. JUDD
HUGH S. KNOWLES
C. C. LAURITSEN
W. H. MARKWOOD, JR.
WILLIAM F. MEGGERS
PHILIP M. MORSE
BRIAN O'BRIEN
HARRY F. OLSON
GEORGE B. PEGRAM
ERIC RODGERS
RALPH A. SAWYER
FREDERICK SEITZ
WILLIAM SHOCKLEY
RICHARD M. SUTTON
J. H. VAN VLECK
MARK W. ZEMANSKY

Consultant on Printing
MELVIN LOOS

ADMINISTRATIVE STAFF
HENRY A. BARTON,
Director
WALLACE WATERFALL,
Executive Secretary
THEODORE VORBURGER,
Advertising Manager
RUTH F. BRYANS,
Publication Manager
EDITH I. NEFTEL
Circulation Manager
KATHRYN SETZE
Assistant Treasurer

The JOURNAL OF APPLIED PHYSICS, published monthly at Prince and Lemon Sts., Lancaster, Pa., is devoted to physics in its role as the science basic to other natural sciences and to the arts and industries. Previous to 1937 this publication was known as PHYSICS. The JOURNAL OF APPLIED PHYSICS publishes editorials and reviews, as well as technical papers of applied physics. Articles appearing in it are indexed regularly, according to their field, by Physics Abstracts, Chemical Abstracts, Engineering Index, Inc., Industrial Arts Index, etc.

Manuscripts should be submitted to Robert L. Sproull, Editor, Rockefeller Hall, Cornell University, Ithaca, New York. Unless otherwise stated, submission of a manuscript is a representation that it has been neither copyrighted, published, nor submitted for publication elsewhere. The authors' institutions are requested to pay a **publication charge** of **$8** per page which, if honored, entitles them to 100 reprints without further charge. Instructions will be sent with galley proofs.

Subscriptions, renewals, and orders for back numbers should be addressed to the American Institute of Physics, 57 East 55 Street, New York 22, New York.

Subscription Price	U.S. and Canada	Elsewhere
To members of the American Institute of Physics and Affiliated Societies	$10.00	$11.00
To all others	12.00	13.00

Back Number Prices

Yearly back number rate when complete year is available: **$14.00.** Single copies: **$1.25** each.

Changes of address should be sent to the American Institute of Physics; **corrected proofs** should be sent to the Publication Manager, American Institute of Physics. **Advertising rates** supplied on request. Orders, advertising copy, and cuts should be sent to the American Institute of Physics.

Entered as second class matter January 22, 1937, at the Post Office at Lancaster, Pennsylvania, under the Act of March 3, 1879. Accepted for mailing at the special rate of postage provided for in paragraph (d-2), section 34.40, P. L. & R. of 1948, authorized May 2, 1932.

New, compact

Speedomax® Instruments can modernize process control in hundreds of plants!

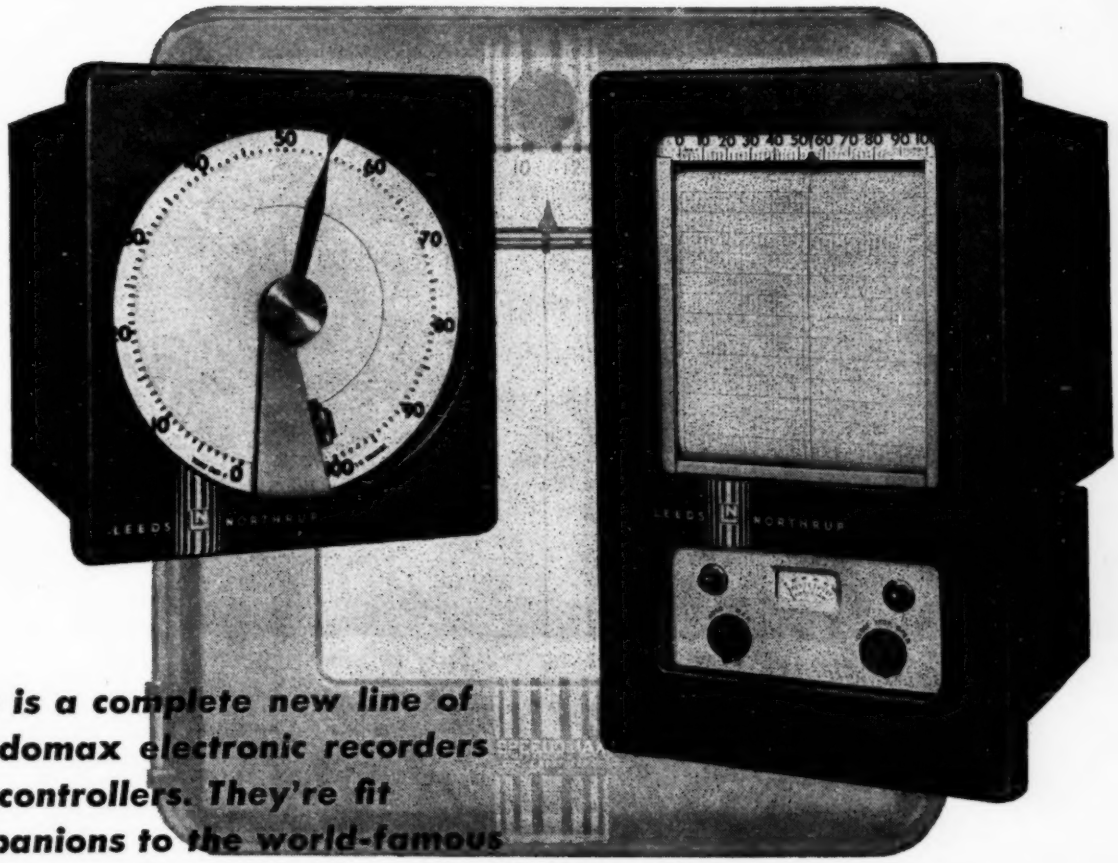

Here is a complete new line of Speedomax electronic recorders and controllers. They're fit companions to the world-famous Speedomax Type G. They are called Type H.

These new instruments can help the operation of a tremendous variety of industrial processes—including many which are perhaps now under-instrumented. And L&N's new production techniques bring Speedomax H equipments within reach of processes which couldn't formerly justify high-quality electronic potentiometers.

Especially significant to operators who now employ filled-system and deflection instruments are the benefits of electronic potentiometer performance. For instance, you can install Speedomax wherever you wish, without a thought for the distance to its sensing element. And Speedomax won't "drift" in accuracy as it ages—it stays on the job and holds the process on spec. If you damage either the sensing element or lead, you simply repair or replace on the job. Speedomax never goes back to the factory for re-calibration, so you do not need spares—thus you save both inventory and storage space.

Anyone familiar with L&N construction will see it again in Type H. The same husky components, anti-friction bearings, rigid assembly and ultra-accessability.

New features include a "fill-in-place" pen; a new, ingenious on-off control switch; more plug-in components. External leads go to a terminal board on outside back of case, for easy installation and maintenance.

One of the round-chart instrument's special features is its long scale; this is used both in setting the control point and for reading temperature. All instruments have especially easy, accurate means for moving the control point setter.

You can choose any type of control action—On-off; Proportional Action; Proportional with rate and reset actions. Any L&N office can supply details and application engineering assistance; or write us at 4978 Stenton Ave., Philadelphia 44, Pa.

LEEDS NORTHRUP
instruments *automatic controls • furnaces*

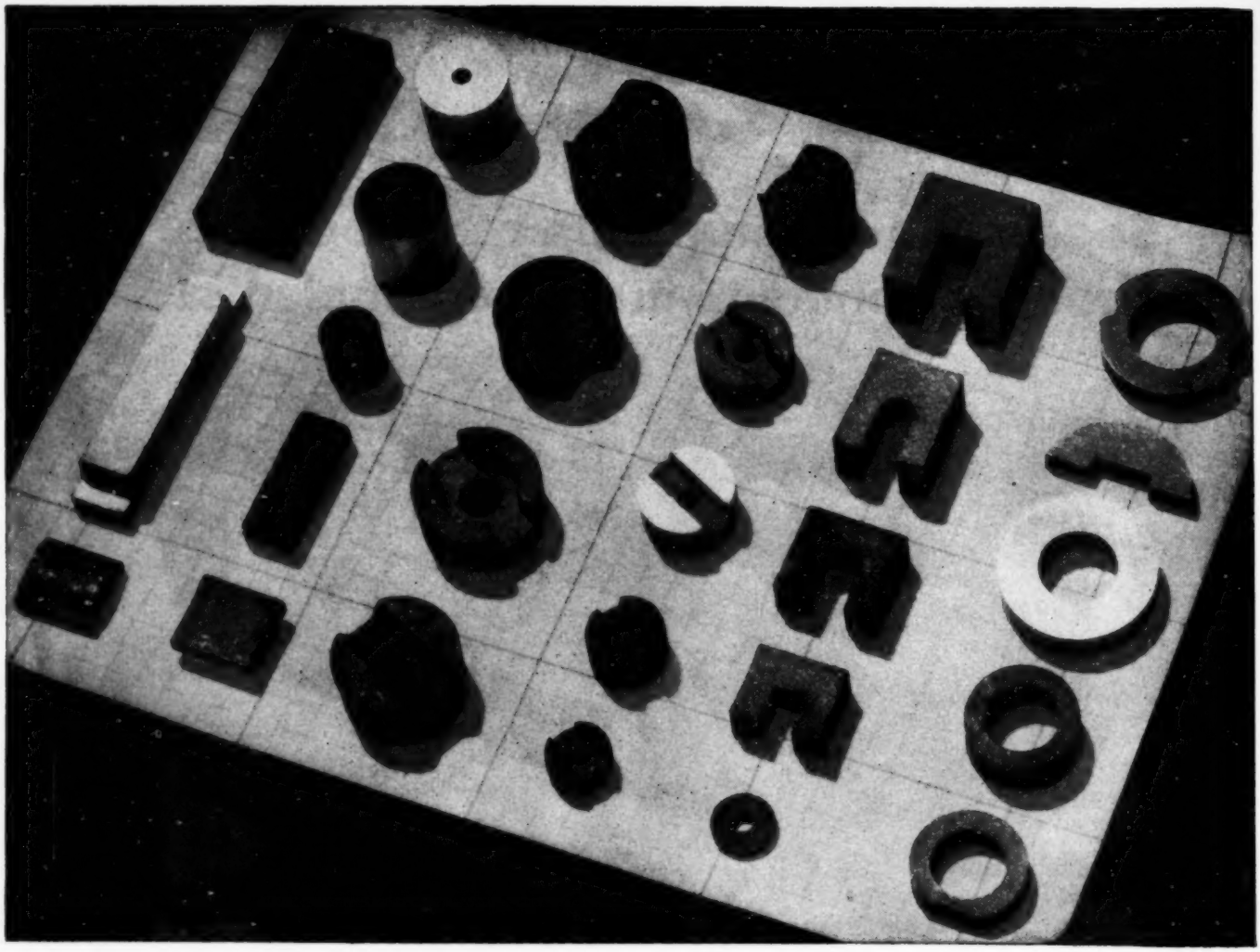

Page-full of ideas for you on *Sintered Magnets*

"MAGNETIC MATERIALS CATALOG"

Write for your copy

Contains handy data on various types of Alnico Magnets, partial lists of stock items, and information on other permanent magnet materials. Also includes valuable technical data on Arnold tape-wound cores, powder cores, and types "C" and "E" split cores in various tape gauges and core sizes.

ADDRESS DEPT. J-11

"OFF-THE-SHELF" ITEMS or SPECIAL SHAPES to suit your needs

Magnets of sintered Alnico offer endless opportunities to designers who need their useful combination of self-contained power and small bulk. A wide range of sintered Alnico shapes are carried in stock for quick shipment. Special shapes to meet an individual design need can be developed, where the quantity required is large enough to justify the tooling costs. Arnold sintered permanent magnets are fully quality-controlled and accurately held to specified tolerances. ● *We'll welcome your inquiries.*

WAD 5280

THE ARNOLD ENGINEERING COMPANY

SUBSIDIARY OF ALLEGHENY LUDLUM STEEL CORPORATION

General Office & Plant: Marengo, Illinois

DISTRICT SALES OFFICES . . . New York: 350 Fifth Ave.

Los Angeles: 3450 Wilshire Blvd. Boston: 200 Berkeley St.

Journal
of
Applied Physics

Volume 25, Number 11 November, 1954

On the Concept of an Instantaneous Power Spectrum, and Its Relationship to the Autocorrelation Function

C. H. M. TURNER
Radio Physics Laboratory, Defence Research Telecommunications Establishment, Ottawa, Canada
(Received September 30, 1953)

A definition sufficient to define a function of frequency $\rho(t,f)$ which could be regarded as the instantaneous power spectrum was given by Page. This function is not unique, since it may have added to it a complementary function of frequency $\rho_c(t,f)$ satisfying

$$\int_{-\infty}^{\infty}\rho_c(T,f)df=0$$

without changing the original signal in any way.

It is shown that when a signal is observed by different observers, starting their observations at different times, they will not derive the same "instantaneous power spectral function," and the differences between their results will be complementary functions as defined above.

It is well known that the Fourier transform of the autocorrelation function is equal to the square of the magnitude of the spectral function. Analogously, a "running autocorrelation function" is defined and it is shown that the Fourier transform of its partial differential coefficient with respect to time is an instantaneous power spectral function.

INTRODUCTION

IN a recent paper C. H. Page[1] has shown how to obtain an expression which is a function of time and frequency $\rho(t,f)$ which he regarded as a quantity representing the instantaneous power spectrum of a specified signal.

As is implied after his Eq. (5), the method is sufficient to determine $\rho(t,f)$. The expression for $\rho(t,f)$ so obtained is not unique. Since the differences between this and other possible expressions for the instantaneous power spectra were not discussed by Page, they will be examined here.

Page also assumes that the complete past history of the signal is known. It will be shown here that this assumption is not necessary, and that an instantaneous power spectrum function may be defined for a signal which has been under continuous observation for a finite time. However, as in the previous case, it is still not a unique function describing the signal, and the differences between it and other possible representations are also examined.

[1] C. H. Page, J. Appl. Phys. 23, 103 (1952).

1. STATEMENT OF PROBLEM

Let us suppose that we have a signal $G_1(t)$ as shown in Fig. 1(*i*) known theoretically for all time $t(-\infty<t<\infty)$. We shall examine the various expressions for the instantaneous power spectrum at time T which represent this signal. Further, we will suppose that there are two independent observers A and B recording the signal. They record it only after time T_α and T_β, respectively $(T_\beta>T_\alpha)$, so that earlier information about the signal is unrecorded, and may therefore be regarded as lost or unknown by the respective observers. It will be apparent from Figs. 1(ii), (iii), (iv), (v), and (vi) that*

$$G_1(t)=G_2(-\infty,T_\alpha,t)+G_3(T_\alpha,\infty,t) \quad (1)$$

$$=G_4(-\infty,T_\beta,t)+G_5(T_\beta,\infty,t) \quad (2)$$

$$=G_2(-\infty,T_\alpha,t)+G_6(T_\alpha,T_\beta,t)+G_5(T_\beta,\infty,t) \quad (3)$$

where G_3 and G_5 are the signals that are observed, and G_2 and G_4 the unrecorded or unknown signals. Were it

* The notation used is such that, for example, $G_n(T_\theta,T_\phi,t)$ has the value $G_n(t)$ when $T_\theta<t<T_\phi$, but is zero otherwise (see reference 6).

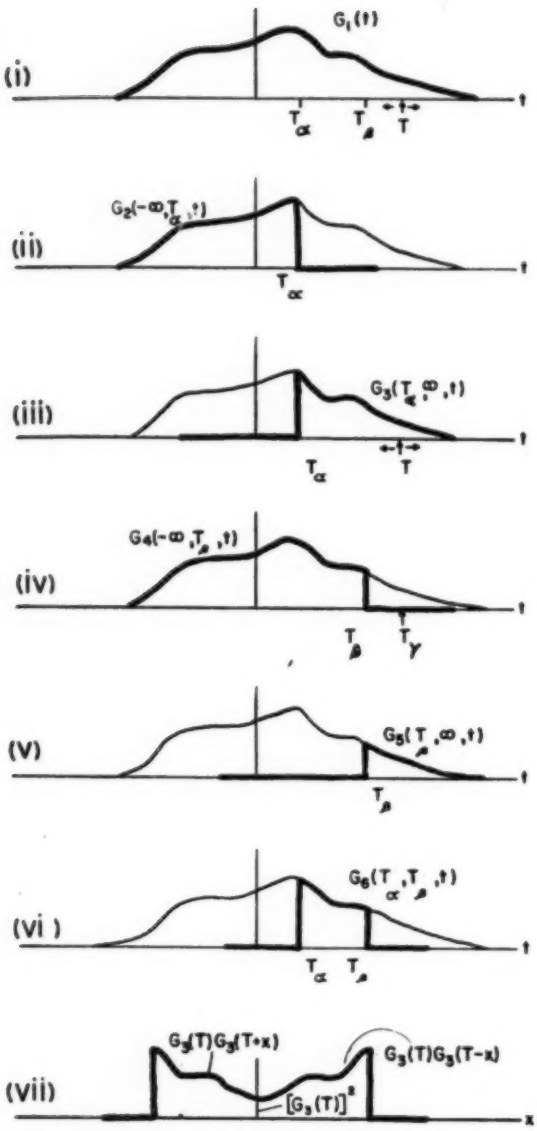

FIG. 1. (i) The time function $G_1(t)$ in the time interval $-\infty < t < \infty$. (ii) $G_2(-\infty, T_\alpha, t)$ is the value of $G_1(t)$ in the interval $-\infty < t < T_\alpha$. (iii) $G_3(T_\alpha, \infty, t)$ is that part of $G_1(t)$ recorded by observer A. (iv) $G_4(-\infty, T_\beta, t)$ is the value of $G_1(t)$ in the interval $-\infty < t < T_\beta$. (v) $G_5(T_\beta, \infty, t)$ is that part of $G_1(t)$ recorded by observer B. (vi) $G_6(T_\alpha, T_\beta, t)$ is that part of $G_1(t)$ recorded by A but not by B. (vii) Illustrating the time rate of change of the running autocorrelation coefficient $(\partial/\partial T)A_3(T,x)$. The instantaneous power spectrum is the Fourier transform of this [Eq. (28)].

not for the fact that we have presupposed $G_1(t)$ to be known for all time, each observer could, if he desired, introduce arbitrary time functions G_2 and G_4 for the signal before he started taking observations.

The problems which we now propose to examine are as follows.

1. Knowing $G_1(t)$, one may use Page's definition to obtain $\rho_1(T,f)$ for the instantaneous power spectrum. What is the difference between this expression and other possible expressions for $\rho(T,f)$ which may be used to describe the same signal?

2. Can an instantaneous power spectrum be defined by observers A and B? What differences, if any, exist between the instantaneous power spectra obtained by each observer, and are the values so obtained unique?

3. What is the relationship between the autocorrelation functions and the instantaneous power spectra of the complete signal and those recorded by the observers?

2. SOLUTION OF FIRST PROBLEM

The solution to the first problem will become clearer if we repeat here the steps which led to Page's definition of the instantaneous power spectrum $\rho(T,f)$. The subscript 1 will be omitted in this section, since the results are applicable to any aperiodic function and will be used later for the wave forms shown in Figs. 1 (i–vi). It is convenient first to define the function $g(T,f)$ as the Fourier transform of an auxiliary signal $G_T(t)$, where

$$G_T(t)=G(t) \quad \text{for } -\infty<t<T$$

and

$$=0 \quad \text{for} \quad t>T.$$

Hence

$$g(T,f)=\int_{-\infty}^{\infty} e^{-2\pi i f t}G_T(t)dt=\int_{-\infty}^{T} e^{-2\pi i f t}G(t)dt. \quad (4)$$

As Page points out, $g(T,f)$ may be regarded as the running transform or spectrum of the function $G(t)$ up to the time T.

Using Plancherel's theorem,[2] it immediately follows that

$$\int_{-\infty}^{\infty}|g(T,f)|^2df=\int_{-\infty}^{\infty}|G_T(t)|^2dt$$

$$=\int_{-\infty}^{T}|G(t)|^2dt \quad (5)$$

and hence differentiating

$$\int_{-\infty}^{\infty}\frac{\partial}{\partial T}|g(T,f)|^2df=|G(T)|^2. \quad (6)$$

Since $g(T,f)$ can be evaluated from the original signal, Page defines a new function $\rho(T,f)$ given by

$$\rho(T,f)=\frac{\partial}{\partial T}|g(T,f)|^2. \quad (7)$$

As Page points out, if $G(T)$ is the current flowing into unit resistance, Eq. (6) shows that $\rho(T,f)$ would have the dimensions of energy per unit time per unit band width, and, being a function of time and frequency, may

[2] E. C. Titchmarch, *Theory of Fourier Integrals* (Oxford University Press, London, 1948), p. 72.

be considered to be the instantaneous power spectrum of the signal.

One sees by substitution in Eq. 6, that $\rho(T,f)+\rho_c(T,f)$ is also an instantaneous power spectrum of the signal provided the complementary function $\rho_c(T,f)$ satisfies

$$\int_{-\infty}^{\infty}\rho_c(T,f)df=0. \tag{8}$$

Hence the difference between any two functions representing the instantaneous power spectra of the same wave form is a complementary function satisfying Eq. (8).

This answer to the first problem is perhaps trivial, but already throws some light on the answer to the second problem. For example, if we suppose that $\rho(T,f)$ is only specified in the interval $T_0<T<\infty$ then the corresponding time function in the same interval is given unambiguously except for sign from Eqs. (6) and (7) by

$$|G(T)|^2=\int_{-\infty}^{\infty}\rho(T,f)df. \tag{9}$$

It is now clear that although $\rho(T,f)$ has been defined' it is not unique in representing the time function $G(T)$' since the latter is unchanged by adding any complementary function satisfying Eq. (8) to the instantaneous power spectrum function. A simple example of such a complementary function is given by

$$\rho_c(T,f)=\frac{\sin 2\pi f(T-T_0)+\sin 2\pi f(T+T_0)}{2\pi T_0 f} \quad \text{for } 0<|T|<T_0. \tag{10}$$

By putting $2\pi f(T-T_0)=x$ and $2\pi f(T+T_0)=y$ it may be seen that

$$\int_{-\infty}^{\infty}\rho_c(T,f)df=0.$$

This complementary function is illustrated in Fig. 2, which shows a cross section of $\rho_c(T,f)$ at $T=\frac{1}{4}T_0$.

3. SOLUTION OF SECOND PROBLEM

Before attempting to answer the second problem, we will first define the running Fourier transform $g_n(T,f)$ for the signal $G_n(t)$, as in Eq. (4), by

$$g_n(T,f)=\int_{-\infty}^{T}e^{-2\pi ift}G_n(t)dt, \quad n=1,2,3,4,5,6 \tag{11}$$

and the corresponding instantaneous frequency spectrum (as defined by Page) by

$$\rho_n(T,f)=\frac{\partial}{\partial T}|g_n(T,f)|^2. \tag{12}$$

From the solution to the first problem it is evident that the general expression for the instantaneous frequency spectra of the signals $G_n(t)$ are given by

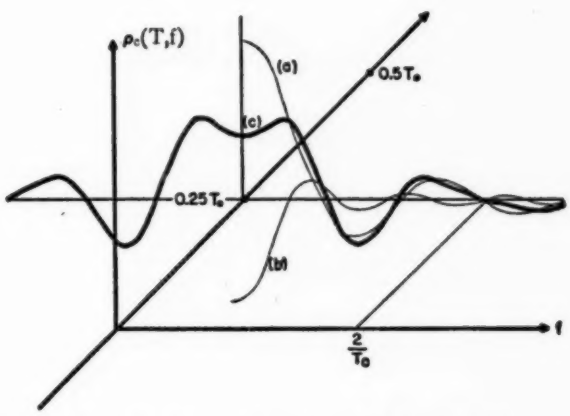

FIG. 2. Example of a complementary function $\rho_c(T,)f$.

(a) $[\sin 2\pi f(T-T_0)]/2\pi T_0 f$,

(b) $[\sin 2\pi f(T+T_0)]/2\pi T_0 f$,

(c) $\rho_c(T,f)=[\sin 2\pi f(T-T_0)+\sin 2\pi f(T+T_0)]/2\pi T_0 f$ for $0<T=T_0/4<T_0$.

$\rho_n(T,f)+\rho_{nc}(T,f)$ where $\rho_{nc}(T,f)$ is any complementary function satisfying

$$\int_{-\infty}^{\infty}\rho_{nc}(T,f)df=0. \tag{13}$$

Furthermore, from Eqs. (11), (12) it may be observed that

for $T>T_\alpha$: $g_2(T,f)$ is independent of T and $\rho_2(T,f)=0$, (14a)

$T<T_\alpha$: $g_3(T,f)=0$ and $\rho_3(T,f)=0$, (14b)

$T>T_\beta$: $g_4(T,f)$ is independent of T and $\rho_4(T,f)=0$, (14c)

$T<T_\beta$: $g_5(T,f)=0$ and $\rho_5(T,f)=0$. (14d)

Let us now return to the second problem and investigate how the instantaneous power spectrum of the record taken by observer A or by observer B differs from that of the actual signal $G_1(t)$. Using Eqs. (7) and (12), one finds that

$$\begin{aligned}\rho_1(T,f)&=\frac{\partial}{\partial T}|g_1(T,f)|^2\\&=\frac{\partial}{\partial T}|g_2(T,f)+g_3(T,f)|^2\\&=\frac{\partial}{\partial T}|g_2(T,f)|^2+\frac{\partial}{\partial T}|g_3(T,f)|^2\\&\quad+\frac{\partial}{\partial T}\{g_2\bar{g}_3+\bar{g}_2g_3\}\\&=\rho_2(T,f)+\rho_3(T,f)+\left[\frac{\partial}{\partial T}(g_2\bar{g}_3+\bar{g}_2g_3)\right].\end{aligned} \tag{15a}$$

Similarly,

$$\rho_1(T,f)=\rho_4(T,f)+\rho_5(T,f)+\left[\frac{\partial}{\partial T}(g_4\bar{g}_5+\bar{g}_4g_5)\right]. \quad (16a)$$

It will be observed that the last term in each of the Eqs. (15a) and (16a) is a particular case of complementary function satisfying Eq. (13), since

$$\int_{-\infty}^{\infty}\frac{\partial}{\partial T}(g_2\bar{g}_3)df=\frac{\partial}{\partial T}\int_{-\infty}^{\infty}(g_2\bar{g}_3)df$$

and, using Plancherel's theorem,

$$=\frac{\partial}{\partial T}\int_{-\infty}^{\infty}G_2(-\infty, T_\alpha, t)\overline{G_3(T_\alpha,\infty,t)}dt$$

and, noting that one of G_2 and G_3 is zero through the region of integration,

$$=\frac{\partial}{\partial T}(0)=0.$$

Furthermore, at time T_γ in the period which is common to both observers ($T_\alpha<T_\beta<T_\gamma<\infty$), both ρ_2 and ρ_4 are zero and therefore

$$\rho_1(T_\gamma,f)=\rho_3(T_\gamma,f)+\frac{\partial}{\partial T_\gamma}(g_2\bar{g}_3+\bar{g}_2g_3) \quad (15b)$$

$$=\rho_3(T_\gamma,f)+\frac{\partial}{\partial T_\gamma}[(g_4-g_6)(\bar{g}_5+\bar{g}_6)+(\bar{g}_4-\bar{g}_6)(g_5+g_6)]$$

$$=\rho_3(T_\gamma,f)+\frac{\partial}{\partial T_\gamma}[(g_4\bar{g}_5+\bar{g}_4g_5)-(g_6\bar{g}_5+\bar{g}_6g_5)] \quad (15c)$$

and also

$$\rho_1(T_\gamma,f)=\rho_5(T_\gamma,f)+\frac{\partial}{\partial T_\gamma}(g_4\bar{g}_5+\bar{g}_4g_5). \quad (16b)$$

We are now able to answer the questions raised in the second problem. Firstly [Eq. (15b)], the instantaneous power spectrum $\rho_1(T,f)$ for the hypothetical signal, assumed known for all past and future time, differs from that derived by an observer $\rho_3(T,f)$ by the expression

$$\frac{\partial}{\partial T_\gamma}(g_2\bar{g}_3+\bar{g}_2g_3). \quad (17)$$

This expression satisfies Eq. (8) and is therefore a complementary function. It is dependent on the Fourier transforms g_2 and g_3 of the parts of the signal before and after the commencement of observations. Naturally g_3 is unique, but g_2 corresponds to an infinite number of possible signals before the commencement of observations. Hence expression 17 represents an infinite number of complementary functions satisfying Eq. (12) and contributing nothing to the recorded signal $G_3(t)$.

Secondly, from Eqs. (15c) and (16b), the instantaneous power spectrum obtained by each observer differs by

$$\rho_3(T_\gamma,f)-\rho_5(T_\gamma,f)=\frac{\partial}{\partial T_\gamma}(g_6\bar{g}_5+\bar{g}_6g_5). \quad (18)$$

Again, this difference is a specific complementary function satisfying Eq. (8) and therefore contributing nothing to the recorded signal. It may be observed that the complementary function in expression 17, unlike that in expression 16, contains only Fourier transforms of recorded signals and to this extent is a well defined complementary function.

4. SOLUTION OF THE THIRD PROBLEM

If we define[3] the autocorrelation function of any aperiodic time series $G_1(t)$ as

$$A_1(x)=\int_{-\infty}^{\infty}G_1(t)G_1(t+x)dt \quad (19)$$

then it is well known[4] that the Fourier transform of $A_1(x)$ is equal to the square of the amplitude of the Fourier transform of $G_1(t)$; i.e.,

$$\int_{-\infty}^{\infty}A_1(x)e^{-2\pi ifx}dx=\left|\int_{-\infty}^{\infty}G_1(t)e^{-2\pi ift}dt\right|^2=|g_1(f)|^2. \quad (20)$$

Because of this connection one naturally asks whether or not there is any simple connection between the instantaneous power spectrum (which is the time differential of the square of the amplitude of a "running Fourier transform" of a signal) and the "running autocorrelation function" of the same signal.

In what follows, one first defines an expression for the "running autocorrelation function" based on Eq. (19), and then shows [Eq. (28)] how it is related to the instantaneous power spectrum.

Let $G_n(t)$ represent any one of the aperiodic signals in Fig. 1(i–vi) ($n=1, 2, \cdots 6$). Next, let us define an auxiliary signal $G_{n,T}(z)$ [as in Eq. (4)], where

$$G_{n,T}(z)=G_n(z) \quad \text{for } -\infty<z<T$$

and

$$=0 \quad \text{for} \quad z>T; \quad (21)$$

[3] Y. W. Lee, Application of Statistical Methods to Communication Problems, Massachusetts Institute of Technology Research Laboratory of Electronics, Technical Report No. 181.

[4] M. G. Kendall, *Advanced Theory of Statistics* (Charles Griffin & Company Ltd., London, 1948), Vol. 2, #30.37.

then as in Eq. (11) the running Fourier transform will be taken as

$$g_n(T,f)=\int_{-\infty}^{\infty} G_{n,T}(t)e^{-2\pi ift}dt$$

$$=\int_{-\infty}^{T} G_n(t)e^{-2\pi ift}dt. \quad (22)$$

The "running autocorrelation function" will be *defined* as

$$A_n(T,x)=\int_{-\infty}^{\infty} G_{n,T}(t)G_{n,T}(t+x)dt \quad (23)$$

$$=\int_{-\infty}^{T} G_n(t)G_n(t+x)dt \quad \text{for } -^{ve}x, \quad (24)$$

and

$$=\int_{-\infty}^{T-x} G_n(t)G_n(t+x)dt \quad \text{for } +^{ve}x, \quad (25a)$$

$$=\int_{-\infty}^{T} G_n(y-x)G_n(y)dy \quad \text{for } +^{ve}x. \quad (25b)$$

One may notice in passing that, as with all autocorrelation functions, $A_n(T,x)$ is an even function of x, and has the same value for positive and negative values of x [this is clearly confirmed by Eqs. (24) and (25b)].

Taking the partial differential coefficient of (24) and (25b) we obtain a result which will be needed later, namely:—

$$\frac{\partial}{\partial T}A_n(T,x)=G_n(T)G_n(T+x) \quad \text{for } -^{ve}x \quad (26)$$

$$=G_n(T)G_n(T-x) \quad \text{for } +^{ve}x. \quad (27)$$

We are now able to examine the relationship between the instantaneous power spectrum and the autocorrelation function. One has

$$\rho_n(T,f)=\frac{\partial}{\partial T}|g_n(T,f)|^2 \text{ and using Eq. (20)}$$

$$=\frac{\partial}{\partial T}\int_{-\infty}^{\infty} A_n(T,x)e^{-2\pi ifx}dx$$

$$=\int_{-\infty}^{\infty}\left[\frac{\partial}{\partial T}A_n(T,x)\right]e^{-2\pi ifx}dx; \quad (28)$$

i.e., the instantaneous power spectrum is equal to the Fourier transform of the time rate of change of the "running autocorrelation function."

Using Eqs. (26) and (27), (28) easily reduces to Page's Eq. (7). The representation of the integrand in (28), which is the partial differential coefficient of the running autocorrelation coefficient [(26) and (27)], is illustrated in Fig. 1(vii) for the signal $G_3(t)$. For negative values of x it is the original signal up to time T multiplied by the amplitude of the signal at time T. The mirror image of this gives its value for positive values of x. Equation (28) shows that the instantaneous power spectrum of $G_3(t)$ may therefore be regarded as the Fourier transform of the function illustrated in Fig. 1(vii).

SUMMARY

1. Page's useful definition of an instantaneous power spectrum yields a function which is not a unique representation of the instantaneous power spectrum in so far as it may have added to it any complementary function $\rho_c(T,f)$ satisfying

$$\int_{-\infty}^{\infty}\rho_c(T,f)df=0 \quad (8)$$

without changing the initial signal from which it is derived.

2. If the instantaneous power spectrum of the same signal is derived by two independent observers, then at at any time during the period of observation common to both observers the instantaneous power spectra will differ by a complementary function. Conversely, if over any interval of time two instantaneous power spectra differ only by a complementary function, then the corresponding power signals are identical during that interval of time.

3. Lastly, when a "running autocorrelation function" of the signal $G(t)$ is defined by [Eqs. (21) and (23)]

$$A(T,x)=\int_{-\infty}^{\infty} G_T(t)G_T(t+x)dt \quad (23)$$

where

$$\left.\begin{aligned} G_T(z)&=G(z) \quad \text{for } -\infty<z<T \\ &=0 \quad\quad\ \text{for } z>T \end{aligned}\right\}, \quad (21)$$

and

then Page's instantaneous power spectrum is equal to the Fourier transform of the time rate of change of the running autocorrelation function.

ACKNOWLEDGMENT

It is a pleasure to acknowledge the interest shown by Dr. C. H. Page, and his suggestion of the example shown in Fig. 2.

Scattering from Dielectric Coated Spheres in the Region of the First Resonance*

H. SCHARFMAN†
Radiation Laboratory, The Johns Hopkins University, Baltimore, Maryland‡
(Received January 4, 1954)

Formulas for the backscattering and total scattering cross sections for dielectric coating spheres of arbitrary size were developed following the methods of Hansen and of Aden and Kerker. Calculations based on the resultant formulas were made in the region of the first resonance (outside dimension of the concentric spheres is approximately 0.4 wavelength). It was found that certain choices of coating thickness and dielectric constant can lead to increases in the scattering cross sections of more than 100 percent relative to a solid metal sphere of the same outside diameter. A number of calculated and measured curves are presented, and they show the variation of the backscattering and total scattering cross sections as functions of coating thickness, coating permittivity, and outside diameter of the coating. Where both calculations and measurements were made for the same conditions, the values agree to ±2 percent.

I. INTRODUCTION

In order to study the effects of dielectric coatings on the scattering behavior of simple conducting objects, the special case of a dielectric coated conducting sphere was considered. The rigorous solution to the problem of scattering of electromagnetic plane waves by two concentric spheres has been presented by Aden and Kerker[1] following the methods of Mie,[2] Hansen,[3] and Stratton.[4] The Aden and Kerker solution is valid for any three arbitrary media and for spheres of any size. It has been applied to the problem of scattering and absorption by melting ice spheres by Langleben and Gunn.[5]

In this paper, the general solution is simplified by considering the special case of scattering from dielectric coated conducting spheres. The resulting expressions were used to calculate the variations of the backscattering and total scattering cross section as functions of coating thickness, dielectric constant, and outside diameter of the concentric spheres. The calculations were made in the region where the outside diameter was approximately 0.4 wavelength of the incident field which corresponds to the first resonance region of a single conducting sphere. For a conducting sphere coated with a lossless dielectric of suitable thickness and dielectric constant, calculations (and measurements) show that the resonant frequency is about the same as for a single conducting sphere. However, a substantial increase in both backscattering and total scattering cross sections was found. In some cases, the increase was greater than 100 percent. Two alternate interpretations of this phenomenon are presented at the end of this paper.

II. SPECIALIZATION OF THE GENERAL FORMULAS

The fields in the vicinity of two concentric spheres are shown in Fig. 1. Now let medium 1 be free space, medium 2 be a lossless dielectric, and medium 3 be a perfect conductor. Then,

$$\mu_1=\mu_2=\mu_3=\mu_0 \text{ (the permeability of free space)}, \quad (1)$$

$$g_1=g_2=0=g_0 \text{ (the conductivity of free space)}, \quad (2)$$

$$g_3=\infty, \quad (3)$$

$$\epsilon_1=\epsilon_3=\epsilon_0 \text{ (the permittivity of free space)}, \quad (4)$$

$$\epsilon_2 \geq \epsilon_1. \quad (5)$$

Under the conditions (1) through (5), the Aden and Kerker formulas for the far zone scattering coefficients

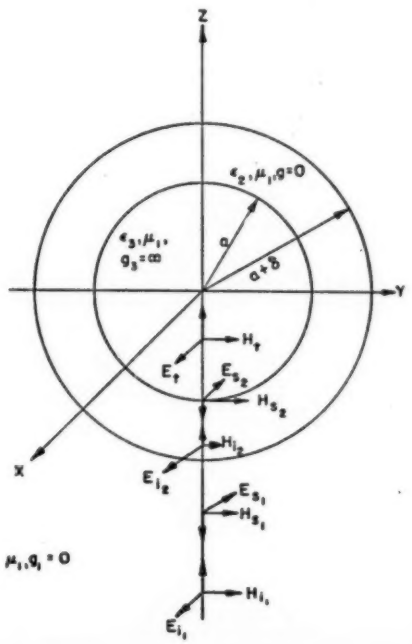

FIG. 1. Geometry of the scatterer.

* The work described in this paper was supported by Contract AF 33(616)68 between the Wright Air Development Center and the Radiation Laboratory, The Johns Hopkins University.

† This paper is a part of a thesis submitted to The Johns Hopkins University in partial fulfillment of the requirements for the D.S. in E.E.

‡ Now at Raytheon Manufacturing Company, Bedford, Massachusetts.

[1] A. L. Aden and M. Kerker, J. Appl. Phys. 1242 (1951).
[2] G. Mie, Ann. Physik 25, 377 (1908).
[3] W. W. Hansen, Phys. Rev. 47, 139 (1935).
[4] J. Stratton, *Electromagnetic Theory* (McGraw-Hill Book Company, Inc., New York, 1941).
[5] M. P. Langleben and K. L. S. Gunn, *Scattering and Absorption of Microwaves by a Melting Ice Sphere* (Scientific Report MW-5, McGill University (March, 1952).

may be greatly simplified. Using the notation of Fig. 1 and expanding the incident and scattered fields in medium 1 following Stratton[4] as

$$E_i = E_0 e^{-i\omega t} \sum_{n=1}^{\infty} i^n \frac{2n+1}{n(n+1)} [\bar{m}_{o1n}^{(1)} - i\bar{n}_{e1n}^{(1)}], \quad (6)$$

$$H_i = -\frac{k_1 E_0}{\omega\mu_1} e^{-i\omega t} \sum_{n=1}^{\infty} i^n \frac{2n+1}{n(n+1)} [\bar{m}_{e1n}^{(1)} + i\bar{n}_{o1n}^{(1)}], \quad (7)$$

$$E_s = E_0 e^{-i\omega t} \sum_{n=1}^{\infty} i^n \frac{2n+1}{n(n+1)} [a_n^s \bar{m}_{o1n}^{(3)} - ib_n^s \bar{n}_{e1n}^{(3)}], \quad (8)$$

$$H_s = -\frac{k_1 E_0}{\omega\mu_1} e^{-i\omega t} \sum_{n=1}^{\infty} i^n \frac{2n+1}{n(n+1)} \times [b_n^s \bar{m}_{e1n}^{(3)} + ia_n^s \bar{n}_{o1n}^{(3)}], \quad (9)$$

the scattering coefficients become

$$a_n^s = \frac{-j_n(A)\{h_n^{(1)}(C)[Bj_n(B)]' - j_n(C)[Bh_n^{(1)}(B)]'\} + [Aj_n(A)]'[j_n(B)h_n^{(1)}(C) - j_n(C)h_n^{(1)}(B)]}{h_n^{(1)}(A)\{\quad\uparrow\quad\} - [Ah_n^{(1)}(A)]'[\quad\uparrow\quad]}, \quad (10)$$

$$b_n^s = \frac{-j_n(A)\{[Bh_n^{(1)}(B)]'[Cj(C)]' - [Bj_n(B)]'[Ch_n^{(1)}(C)]'\} + (\epsilon_2/\epsilon_1)[Aj_n(A)]' \times [h_n^{(1)}(B)C(j_n(C)]' - j_n(B)[Ch_n^{(1)}(C)]']}{h_n^{(1)}(A)\{\quad\uparrow\quad\} - (\epsilon_2/\epsilon_1)[Ah_n^{(1)}(A)]'[\quad\uparrow\quad]}, \quad (11)$$

where

$$k_1 = \frac{2\pi}{\lambda} = \text{free space wave number}, \quad (12)$$

$$k_2 = \frac{2\pi}{\lambda}\left(\frac{\epsilon_2}{\epsilon_1}\right)^{\frac{1}{2}} = \text{wave number in the dielectric}, \quad (13)$$

$$k_1(a+\delta) = A, \quad (14)$$

$$k_2(a+\delta) = B, \quad (15)$$

$$k_2 a = C. \quad (16)$$

In terms of the scattering coefficients a_n^s and b_n^s defined above, the total scattering cross section Q_s and the backscattering cross section σ can be shown to be[1,4,6]

$$\frac{\sigma}{\lambda^2} = \frac{1}{4\pi}\left|\sum_{n=1}^{\infty} (-1)^n (2n+1)(a_n^s - b_n^s)\right|^2, \quad (17)$$

$$\frac{Q_s}{\lambda^2} = \frac{1}{2\pi} R_e \sum_{n=1}^{\infty} (2n+1)(a_n^s + b_n^s). \quad (18)$$

III. CALCULATION OF Q_s AND σ IN THE REGION OF THE FIRST RESONANCE

Using the a_n^s and b_n^s of (10) and (11), Q_s/λ^2 and σ/λ^2 from (17) and (18) were calculated for a number of different ratios of δ/a, ϵ_2/ϵ_1, and $a+\delta/\lambda$ in the region $0.1 \leq (a+\delta)/\lambda \leq 0.25$. In the latter region, σ/λ^2 for a perfectly conducting sphere ($\delta=0$) passes through its first maximum.[7] In addition, the convergence of both series in this region is sufficiently rapid to permit accuracy of better than 1 percent by considering only the first three terms of the series.

A composite plot of σ/λ^2 *versus* $(a+\delta)/\lambda$ for $\epsilon_2/\epsilon_1 = 2.56$, 4, 8, 10, 15, 25, and ∞ (solid conducting sphere) is presented in Fig. 2. The calculated a_n^s's and b_n^s's are presented in Table I. Curves of σ/λ^2 *versus* ϵ_2/ϵ_1 for a fixed δ/a and $a+\delta/\lambda$, σ/λ^2 *versus* δ/a for a fixed ϵ_2/ϵ_1 and $a+\delta/\lambda$, and Q_s/λ^2 *versus* ϵ_2/ϵ_1 for a fixed δ/a and $a+\delta/\lambda$ are presented in Figs. 3, 4, and 5. These curves show the general scattering behavior in the region of the first resonance, but the detailed behavior, particularly for large ϵ_2/ϵ_1 and δ/a, was not examined.

IV. MEASUREMENT OF THE BACKSCATTERING CROSS SECTION

Several of the calculated values of σ were checked experimentally using an indoor scattering range employing the principle of mechanically modulating the

TABLE I.

	$\delta/a = 1/6$		$a+\delta/\lambda = 0.187$	
ϵ_2/ϵ_1	a_1	a_2	a_3	
2.56	$-0.0459 - 0.2094i$	$-0.0003 - 0.0174i$	$0.0000 - 0.0006i$	
4	$-0.0454 - 0.2083i$	$-0.0003 - 0.0172i$	$0.0000 - 0.0005i$	
8	$-0.0440 - 0.2050i$	$-0.0003 - 0.0167i$	$0.0000 - 0.0005i$	
10	$-0.0431 - 0.2031i$	$-0.0003 - 0.0164i$	$0.0000 - 0.0005i$	
15	$-0.0412 - 0.1986i$	$-0.0002 - 0.0156i$	$0.0000 - 0.0005i$	
25	$-0.0363 - 0.1871i$	$-0.0002 - 0.0137i$	$0.0000 - 0.0004i$	
50	$-0.0185 - 0.1349i$	$-0.0000 - 0.0063i$	$0.0000 - 0.0001i$	
70	$-0.0001 - 0.0112i$	$-0.0000 + 0.0070i$	$0.0000 + 0.0004i$	
100	$-0.8055 - 0.3958i$	$-0.0098 - 0.0984i$	$0.0000 + 0.0006i$	
1000	$-0.1099 - 0.3147i$	$-0.0017 - 0.0411i$	$0.0000 - 0.0021i$	
10 000	$-0.0873 - 0.3822i$	$-0.0011 - 0.0387i$	$0.0000 - 0.0015i$	
Metal sphere ($a/\lambda = 0.187$)	$-0.0991 - 0.2988i$	$-0.0014 - 0.0372i$	$0.0000 - 0.0017i$	
ϵ_2/ϵ_1	b_1	b_2	b_3	
2.56	$-0.4967 + 0.5000i$	$-0.0029 + 0.0540i$	$0.0000 + 0.0016i$	
4	$-0.5547 + 0.4970i$	$-0.0038 + 0.0618i$	$0.0000 + 0.0019i$	
8	$-0.6153 + 0.4865i$	$-0.0050 + 0.0704i$	$0.0000 + 0.0021i$	
10	$-0.6310 + 0.4825i$	$-0.0053 + 0.0725i$	$0.0000 + 0.0022i$	
15	$-0.6594 + 0.4739i$	$-0.0058 + 0.0758i$	$0.0000 + 0.0023i$	
25	$-0.7085 + 0.4554i$	$-0.0064 + 0.0800i$	$0.0000 + 0.0024i$	
50	$-0.8713 + 0.3349i$	$-0.0089 + 0.0939i$	$0.0000 + 0.0027i$	
70	$-0.9831 - 0.1286i$	$-0.0179 + 0.1326i$	$0.0000 + 0.0006i$	
100	$-0.0048 + 0.0698i$	$-0.0002 + 0.0143i$	$0.0000 - 0.0007i$	
1000	$-0.3665 + 0.4819i$	$-0.0038 + 0.0615i$	$0.0000 + 0.0021i$	
10 000	$-0.4444 + 0.4969i$	$-0.0043 + 0.0657i$	$0.0000 + 0.0022i$	
Metal sphere ($a/\lambda = 0.187$)	$-0.4339 + 0.4956i$	$-0.0051 + 0.0709i$	$0.0000 + 0.0025i$	

[6] D. Kerr, *Propagation of Short Radio Waves* (McGraw-Hill Book Company, Inc., New York, 1950).

[7] L. N. Ridenour, *Radar System Engineering* (McGraw-Hill Book Company, Inc., New York, 1947).

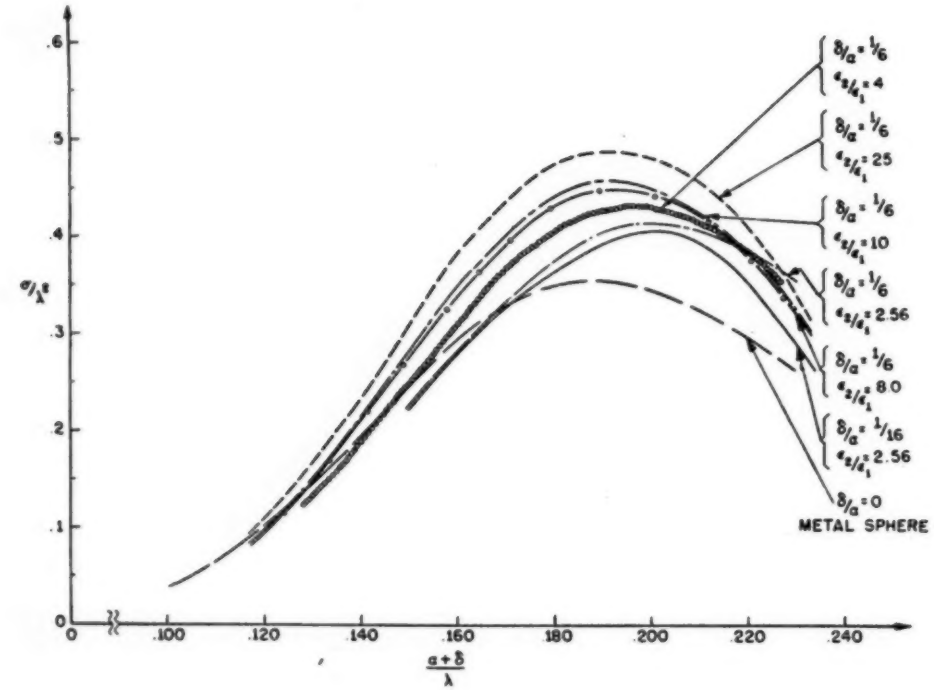

FIG. 2. Calculated backscattering cross section of coated spheres.

scatterer. A block diagram of the system is shown in Fig. 6.

A microwave oscillator feeds a hybrid T which is adjusted so that a small amount of power leaks into the detector arm and the remainder divides about equally between the horn and load arms. The horn illuminates a rotating column of styrofoam at the extremities of which are imbedded an object whose σ is known and the object whose σ is to be measured. About half of the energy scattered back to the horn reaches the detector arm where it is mixed and detected in a crystal. By virtue of the rapidly varying phase of the backscattered field with respect to the phase of oscillator field, synchronous detection[8] takes place in the crystal. The crystal output is amplified and the components of the output corresponding to the standard and unknown scatterer are separated by a commutator mounted on the drive shaft of the rotating styrofoam column and a pair of relays. The individual signals are rectified and metered from which σ can be directly calculated. Accuracy to within ± 2 percent can be obtained by this method. A more complete description of the technique can be found elsewhere.[9,10]

Several dielectric coated spheres were fabricated and their σ's measured. A comparison of calculated and

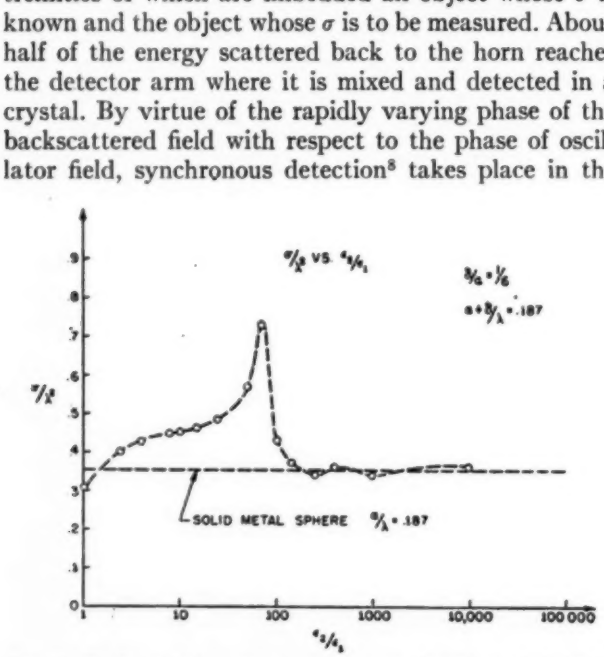

FIG. 3. Backscattering cross section as a function of dielectric constant of coating, $\delta/a=1/a$, $a+\delta/\lambda=0.187$.

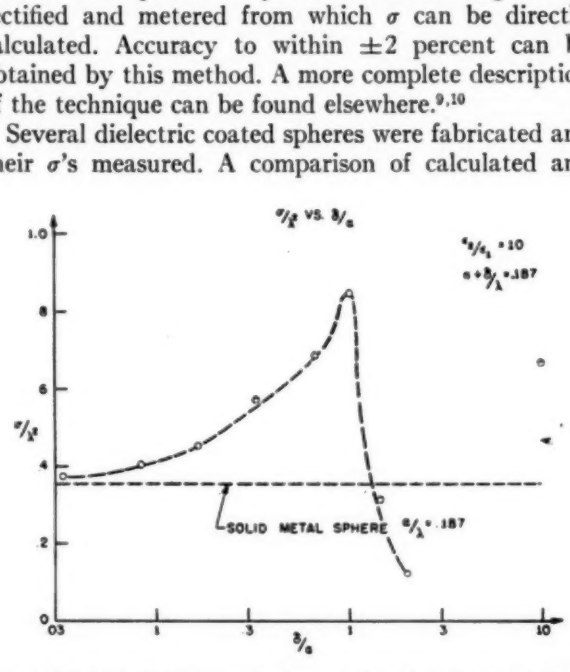

FIG. 4. Backscattering cross section as a function of coating thickness, $\epsilon_2/\epsilon_1=10$, $a+\delta/\lambda=0.187$.

[8] Brodwin, Johnson, and Waters, "Low Level Synchronous Mixing," *Convention Record of the Institute of Radio Engineers*, Part 10, Microwaves (1953).

[9] H. Scharfman, "Electromagnetic Scattering from Objects," Doctoral dissertation, Department of Electrical Engineering, The Johns Hopkins University, Baltimore, Maryland (1953).

[10] H. Scharfman and D. D. King, "Antenna Scattering Measurements by Modulation of the Scatterer," Proc. Inst. Radio Engrs. 42, No. 5, 854–858 (1954).

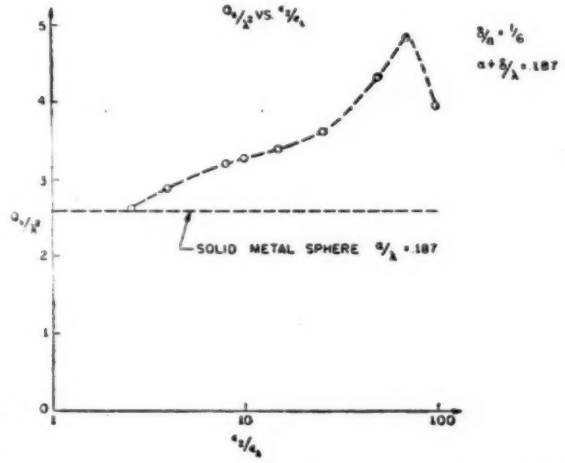

FIG. 5. Total scattering cross section as a function of dielectric constant of coating, $\delta/a=1/6$, $a+\delta/\lambda=0.187$.

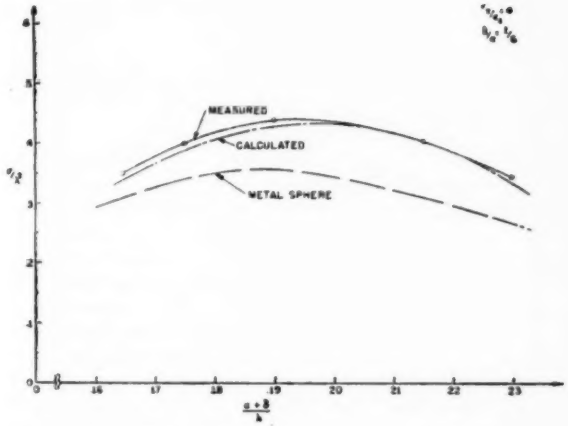

FIG. 7. Measured and calculated backscattering cross sections as a function of outside diameter of dielectric coated spheres, $\epsilon_2/\epsilon_1=4$, $\delta/a=1/6$.

measured values is presented in Figs. 7, 8, and 9. The measured and calculated values agree within the ascribed accuracy.

V. INTERPRETATION OF THE RESULTS

The curves of Figs. 2–9 have one salient feature in common. They indicate that it is possible to increase the scattering cross section of perfectly conducting spheres by replacing the outer shell of conducting material with a lossless dielectric. By a suitable choice of ϵ_2/ϵ_1 and δ/a at a particular frequency, increases of approximately 100 percent can be attained in both the total scattering cross section and the backscattering cross section.

Although the solution of the electromagnetic boundary value problem completely explains this phenomena, it does so in complex mathematical terms which are only applicable to the chosen geometry and which require considerable time to evaluate. An approximate physical description of the phenomena is therefore presented so that one may consider the qualitative effect of variation of the parameters. In addition the approximate description may be useful in obtaining qualitative results for the scattering behavior of dielectric coated nonspherical conducting objects.

To find an approximate physical description, one may consider a perfectly conducting sphere as a fat dipole. Indeed, the largest scattering coefficient for a perfectly conducting sphere is seen to be (from Table I) the b_1 term which corresponds to the dipole mode. The effect of replacing some of the conductor by a lossless dielectric can then be thought of as a method of increasing the capacitance at the poles of the inner conducting sphere. There then results an increased charge density at the poles, a corresponding increase in current density on the surface of the inner conducting sphere, and a resultant increase in the scattered field.

To check this theory two of the fabricated dielectric coated conducting spheres were modified as in Fig. 10a and 10b. With the objects orientated such that the incident electric field was perpendicular to the plane of the cut out rings of dielectric, the σ's were the same as for

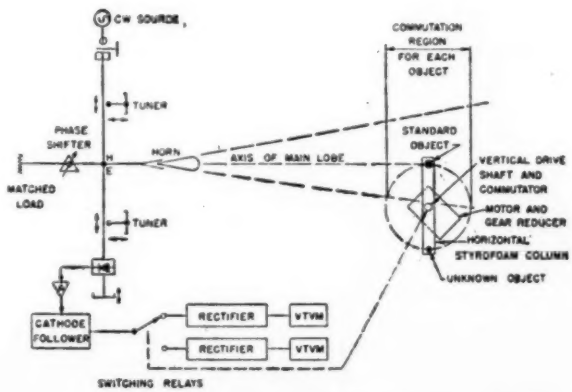

FIG. 6. Schematic diagram of system for measurement of backscattering cross section.

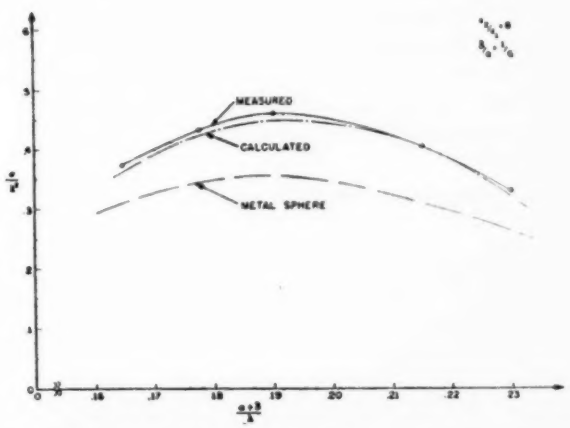

FIG. 8. Measured and calculated backscattering cross sections as a function of outside diameter of dielectric coated spheres, $\epsilon_2/\epsilon_1=8$, $\delta/a=1/6$.

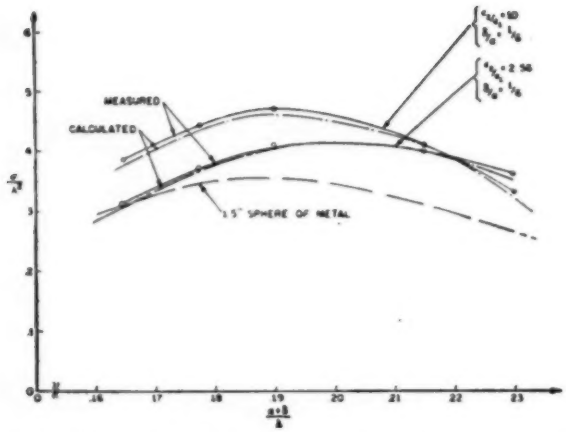

FIG. 9. Measured and calculated backscattering cross sections as a function of outside diameter of dielectric coated spheres, $\epsilon_2/\epsilon_1=2.56$ and 10, $\delta/a=1/6$.

the completely coated spheres. However, when the objects were oriented such that the incident electric field was parallel to the plane of the cut out rings, σ decreased 5 percent and 20 percent for the objects of Figs. 10a and 10b, respectively. This appears to justify the assumption that the portion of the dielectric coating at the poles of the conducting sphere causes the major portion of the increase of σ.

It would also appear reasonable, on the basis of the dipole end loading theory, to expect that thin coatings of high dielectric constant material would have effects similar to thicker coatings of lower dielectric constant material. A few calculations were carried out holding $\epsilon_2/\epsilon_1=1000$, $a+\delta/\lambda=0.187$, and varying δ/a. For $\delta/a=1/30$, σ/λ^2 was found to increase to 0.401, and it is to be expected that for a somewhat different value of $a+\delta/\lambda$ a greater value could be found.

VI. CONCLUSION

It has been shown both theoretically and experimentally that a dielectric coated conducting sphere can be made to have a greater backscattering and total scattering cross section than a single conducting sphere of the same outside diameter. The nature of the scattering as functions of the various parameters has been examined, and an approximate physical description of the phenomenon has been presented.

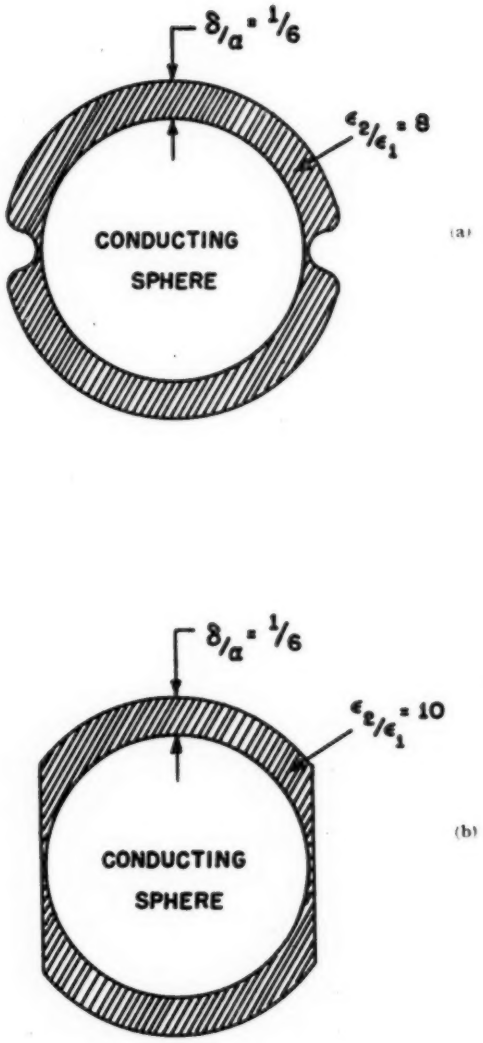

FIG. 10. Cross section of modified dielectric coated conducting spheres.

VII. ACKNOWLEDGMENT

The author wishes to thank Dr. D. D. King and Dr. C. F. Miller for their help and encouragement throughout the course of this work. The author is also indebted to Dr. M. I. Aissen for his many suggestions concerning the mathematical treatment and computation, and Mrs. J. H. Lewis for doing the computations.

JOURNAL OF APPLIED PHYSICS VOLUME 25, NUMBER 11 NOVEMBER, 1954

Spectral Response of a Quadratic Device to Non-Gaussian Noise*

T. A. MAGNESS†
University of California, Marine Physical Laboratory of the Scripps Institution of Oceanography, La Jolla, California
(Received February 17, 1954)

In order to compute the spectral response of a quadratic device to noise, a fourth-order moment P of the input noise is sufficient, P being a function of three independent time delays. The function P_1 by which this fourth moment for a non-Gaussian noise differs from the corresponding moment for a Gaussian noise having the same spectrum is examined. The Fourier transform of this function is Q_1, a function of three frequencies. Q_1 is capable of an interpretation in terms of nonlinear correlations between noise components at different frequencies. A specialization of Q_1 leads to E, a function of two frequencies which is a measure of the correlation between the squares of the envelopes associated with those frequencies.

Several networks involving quadratic nonlinear elements are examined to illustrate the theory. It is shown that while the function P makes it possible to compute the complete spectral response of the network, the function E (together with the spectrum of the input) is sufficient in order to find the spectral density at zero frequency. Finally, for three examples of non-Gaussian processes, the corresponding P_1, Q_1 and E functions are computed.

I. INTRODUCTION

THE now-famous theorem of Wiener[1] and Khintchine[2] which relates the autocorrelation and spectrum of a time series enables one to describe analytically the spectral response of a linear device to a noise input. Use of this technique has led to the solution of a large number of problems in communication and information theory.[3,4] However, there are many situations in communications engineering—and in particular in the detection of weak signals in noise[5]—which involve rectification of noise, and when this is the case, the autocorrelation function of the input *may* not contain sufficient information to permit one to predict the spectrum of the output. When the rectification involved consists simply of squaring or of cross-multiplying, it will be seen presently that a fourth-order moment of the input noise serves this purpose. But first it is desirable to present definitions and background material on noise problems.

By "noise" will be meant a real, stationary, random,[6,7] or stochastic[2] process; i.e., an ensemble of time series $x(t)$ governed by the set of probability densities

$$W_1[x_1],$$
$$W_2[x_1,x_2;\, t_2-t_1],$$
$$\cdots$$
$$W_n[x_1,\cdots,x_n;\, t_2-t_1,\cdots,t_n-t_{n-1}],$$
$$\cdots$$

where $W_1[x_1]dx_1$ is the probability of finding $x(t_1)$ between x_1 and x_1+dx_1; $W_2[x_1,x_2;t_2-t_1]dx_1dx_2$ is the probability of finding $x(t_1)$ between x_1 and x_1+dx_1, and $x(t_2)$ between x_2 and x_2+dx_2; $\cdots$; $W_n[x_1,\cdots,x_n;\, t_2-t_1,\cdots,t_n-t_{n-1}]dx_1\cdots dx_n$ is the probability of finding: $x(t_1)$ between x_1 and x_1+dx_1; $\cdots$; and $x(t_n)$ between x_n and x_n+dx_n. Note that the probability density associated with a set of points $t_1,\cdots,t_n$ is a function of the differences $t_2-t_1,\cdots,t_n-t_{n-1}$ and not of the absolute positions of the points on the t axis; this is a consequence of the stationary character of x. The process will be assumed to satisfy the ergodic hypothesis which says, in effect, that the probability densities associated with the ensemble are identical with the probability densities associated with a single typical function.[8] For example, the mean m may be defined either as the mathematical expectation of $x(t)$ for fixed t and over different functions x,

$$m=\mathcal{E}\{x(t)\}\equiv\int_{-\infty}^{\infty}x_1W_1[x_1]dx_1, \tag{1}$$

or as $x(t)$ for a particular function x averaged over t,

$$m=\langle x(t)\rangle\equiv\lim_{T\to\infty}(1/2T)\int_{-T}^{T}x(t)dt. \tag{1.1}$$

The autocorrelation function $R(\tau)$ is defined by

$$R(\tau)=\mathcal{E}\{[x(t)-m][x(t-\tau)-m]\}$$
$$=\langle[x(t)-m][x(t-\tau)-m]\rangle. \tag{2}$$

* This work represents one of the results of research carried out under contract with the Bureau of Ships, Navy Department.

† On leave of absence from the Marine Physical Laboratory of the Scripps Institution of Oceanography of the University of California.

Contribution from Scripps Institution of Oceanography, University of California, New Series No. 713.

[1] N. Wiener, Acta Math. 55, 117 (1930).

[2] A. Khintchine, Math. Ann. 109, 604 (1934).

[3] C. E. Shannon, Bell System Tech. J. 27, 379, 623 (1948).

[4] N. Wiener, *Extrapolation, Interpolation, and Smoothing of Stationary Time Series* (John Wiley & Sons, Inc., New York, 1949).

[5] Carl Eckart, *The Measurement and Detection of Steady A.C. and D.C. Signals in Noise*, University of California, Marine Physical Laboratory of the Scripps Institution of Oceanography, SIO Ref. 51-39 (October 4, 1951).

[6] H. Cramer, Ann. Math. Ser. 2, 41, 215 (1940).

[7] James, Nichols, and Phillips, *Theory of Servomechanisms*, Radiation Laboratory Series, Book No. 25 (McGraw-Hill Book Company, Inc., New York, 1947).

[8] See reference 7, p. 271.

We shall assume $R(\tau)$ to be integrable;‡ it has as its Fourier transform the (uniformly) continuous function $S(\omega)$,

$$S(\omega)=\int_{-\infty}^{\infty} R(\tau)e^{-i\omega\tau}d\tau,$$
$$R(\tau)=(1/2\pi)\int_{-\infty}^{\infty} S(\omega)e^{i\omega\tau}d\omega, \tag{3}$$

where $S(\omega)$, according to the Wiener-Khintchine theorem, is the power spectrum of $x(t)$.

If $u(t)$ is the result of an "operation" on $x(t)$, e.g.,

(i) $$u(t)=\int_{-\infty}^{\infty} a(\sigma)x(t-\sigma)d\sigma, \tag{4}$$

where $a(t)$ is an integrable function of time,§

(ii) $u(t)=[x(t)]^2$,

(iii) $u(t)=(d/dt)x(t)$, etc.,

$u(t)$ will be another stochastic process and very often it is in theory possible to compute the probability densities associated with u from a knowledge of those associated with x.[9] However, this approach is far too general to be feasible in very many cases, and in practice one is usually content to predict to only a limited extent the behavior of the output, e.g., to predict its first-order probability density and/or power spectrum.

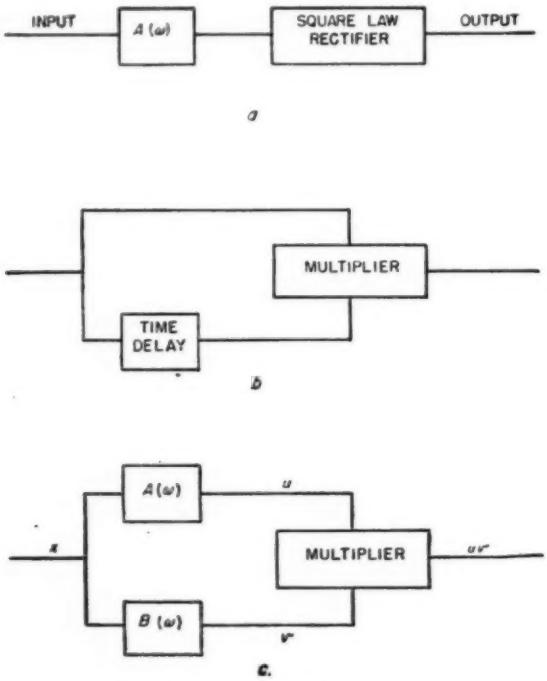

FIG. 1. Elementary quadratic devices.

There are two important classes of problems which fall into the latter category and which have been successfully attacked; *viz*, problems in which (a) the operation is linear, or (b) the noise is Gaussian. If the operation is linear [as in Eq. (4)], then regardless of the other statistics of $x(t)$, $S_u(\omega)$, the spectrum of u, is related to the spectrum of x by

$$S_u(\omega)=S(\omega)|A(\omega)|^2, \tag{5}$$

where

$$A(\omega)=\int_{-\infty}^{\infty} a(t)e^{-i\omega t}dt,$$
$$a(t)=(1/2\pi)\int_{-\infty}^{\infty} A(\omega)e^{i\omega t}d\omega. \tag{6}$$

On the other hand, if the noise $x(t)$ is Gaussian, i.e., if W_n is the nth-order normal distribution,[10] then the statistics of x (and very often the statistics of u) are completely determined by the autocorrelation function of x.[11–13]

The problem which we have set out to investigate is the determination of the spectrum of the output of a quadratic device when the input is a (possibly) non-Gaussian noise. We use the term "quadratic device" to mean an electronic network in which there is a quadratic operation, either square law rectification or cross-multiplication, which may be preceded and/or followed by linear operations. Block diagrams of some quadratic networks are shown in Fig. 1. Consider in particular the network shown in Fig. 1c (the networks in Figs. 1a, 1b, being but special cases of that shown in 1c), where $A(\omega)$ and $B(\omega)$ represent real linear filters and $u(t)$ and $v(t)$ their respective outputs when the input is $x(t)$. Then $w(t)=u(t)v(t)-\langle uv\rangle$ has autocorrelation

$$\langle w(t)w(t-\tau)\rangle=\int_{-\infty}^{\infty}\int\int\int d\sigma_1\cdots d\sigma_4 a(\sigma_1)b(\sigma_2)a(\sigma_3)b(\sigma_4)$$
$$\times[\langle x(t-\sigma_1)x(t-\sigma_2)x(t-\tau-\sigma_3)x(t-\tau-\sigma_4)\rangle$$
$$-\langle x(t-\sigma_1)x(t-\sigma_2)\rangle\langle x(t-\sigma_3)x(t-\sigma_4)\rangle], \tag{7}$$

$a(t)$ and $b(t)$ being the time responses of filters $A(\omega)$ and $B(\omega)$. Thus, in order to compute this *second*-order moment of w, one needs a *fourth*-order moment of x. This is characteristic of problems involving quadratic devices and provides the motivation for this paper.

‡ Throughout this paper, "integrable" will mean the function belongs to both L_1 and L_2; see N. Wiener, *The Fourier Integral* (Dover Publications, New York).

§ This operation will be referred to hence as "linear filtering." The filter will be called real or complex according as $a(t)$, the time response of the filter to a δ-function input (see reference 7, p. 30), is real or complex. The filter is realizable only if $a(t)$ vanishes for negative argument (see reference 4, p. 12).

[9] H. E. Singleton, *Theory of Nonlinear Transducers*, Mass. Inst. Technol. Research Lab. Electronics, Tech. Rept. No. 160 (August 12, 1950).

[10] H. Cramer, *Mathematical Methods of Statistics* (Princeton University Press, Princeton, 1946), Chapter 24.

[11] S. O. Rice, Bell System Tech. J. **23**, 282 (1944); **24**, 109 (1945).

[12] M. Kac and A. J. F. Siegert, J. Appl. Phys. **18**, 383 (1947).

[13] D. Middleton, "*Noise and Nonlinear Communication Problems*," Symposium on Applications of Autocorrelation Analysis to Physical Problems, Woods Hole, Massachusetts (June 13–14, 1949).

II. A FOURTH-ORDER MOMENT

The noise function will be represented by the real stochastic process $x(t)$ for which the moments

$$\langle x(t)\rangle = 0,$$
$$\langle x(t)x(t-\tau)\rangle = R(\tau), \tag{8}$$
$$\langle x(t)x(t-\tau_1)x(t+\tau_2)x(t+\tau_3)\rangle = P(\tau_1,\tau_2,\tau_3)$$

exist. It is with the function $P(\tau_1,\tau_2,\tau_3)$ that we shall be most concerned in this section. By (a) rearranging the factors of the fourth moment occurring in Eq. (8) and (b) translating along the time axis, one can show that P satisfies certain relations of the form

$$\text{(a)}\quad P(\tau_1,\tau_2,\tau_3) = P(\tau_1,\tau_3,\tau_2) = P(-\tau_2,-\tau_1,\tau_3), \tag{9}$$
$$\text{(b)}\quad P(\tau_1,\tau_2,\tau_3) = P(-\tau_1,\tau_1+\tau_2,\tau_1+\tau_3).$$

If, in addition, we have (c) that the mechanism generating $x(t)$ is isotropic in time, then

$$\text{(c)}\quad P(\tau_1,\tau_2,\tau_3) = P(-\tau_1,-\tau_2,-\tau_3); \tag{10}$$

this last condition will not generally be fulfilled, however.

Consider next the function $P_1(\tau_1,\tau_2,\tau_3)$ defined by the equation

$$P(\tau_1,\tau_2,\tau_3) = R(\tau_1)R(\tau_2-\tau_3)+R(\tau_2)R(\tau_3+\tau_1) + R(\tau_3)R(\tau_1+\tau_2)+P_1(\tau_1,\tau_2,\tau_3). \tag{11}$$

The reader will recognize $P-P_1$ as the corresponding fourth moment when x is a Gaussian time series. Thus, if we restrict our attention to moments of order no higher than four, P_1 is a measure of the "non-Gaussianness" of the time series. If x has the property that $x(t)$ and $x(t-\tau)$ become statistically independent as $|\tau|$ becomes large, it will follow that

$$\lim_{s\to\infty} P_1(a_1s+b_1, a_2s+b_2, a_3s+b_3) = 0, \tag{12}$$

for all a_i, b_i such that $a_1^2+a_2^2+a_3^2>0$ (i.e., $P_1\to 0$ along any linear path). We shall make the further assumption that P_1 goes to zero sufficiently rapidly to make it an integrable function. Then it will possess a Fourier transform Q_1:

$$Q_1(\omega_1,\omega_2,\omega_3) = \int_{-\infty}^{\infty}\int\int P_1(\tau_1,\tau_2,\tau_3) \times e^{-(\omega_1\tau_1+\omega_2\tau_2+\omega_3\tau_3)}d\tau_1 d\tau_2 d\tau_3, \tag{13}$$

$$P_1(\tau_1,\tau_2,\tau_3) = (1/2\pi)^3\int_{-\infty}^{\infty}\int\int Q_1(\omega_1,\omega_2,\omega_3) \times e^{i(\omega_1\tau_1+\omega_2\tau_2+\omega_3\tau_3)}d\omega_1 d\omega_2 d\omega_3.$$

The function Q_1 is real when $x(t)$ is isotropic in time; for, denoting the complex conjugate with a bar, we have

$$\begin{aligned}\bar{Q}_1(\omega_1,\omega_2,\omega_3) &= \int_{-\infty}^{\infty}\int\int P_1(\tau_1,\tau_2,\tau_3) \times e^{i(\omega_1\tau_1+\omega_2\tau_2+\omega_3\tau_3)}d\tau_1 d\tau_2 d\tau_3 \\ &= \int_{-\infty}^{\infty}\int\int P_1(-\tau_1,-\tau_2,-\tau_3) \times e^{-i(\omega_1\tau_1+\omega_2\tau_2+\omega_3\tau_3)}d\tau_1 d\tau_2 d\tau_3 \\ &= \int_{-\infty}^{\infty}\int\int P_1(\tau_1,\tau_2,\tau_3) \times e^{-i(\omega_1\tau_1+\omega_2\tau_2+\omega_3\tau_3)}d\tau_1 d\tau_2 d\tau_3 \\ &= Q_1(\omega_1,\omega_2,\omega_3).\end{aligned} \tag{14}$$

It is clear now that both second- and fourth-order statistics of x are specified when P is given; for,

$$R(\tau) = \lim_{s\to\infty} P(0,s,s-\tau)/R(0)$$

and

$$R^2(0) = \lim_{s\to\infty} P(0,s,s). \tag{15}$$

The effect produced on $P(\tau_1,\tau_2,\tau_3)$ by passing $x(t)$ through a real filter may be deduced as follows: if $u(t)$ is related to $x(t)$ according to Eq. (4) with $a(t)$ real, then the new fourth moment is

$$\begin{aligned}P_u(\tau_1,\tau_2,\tau_3) &= \langle u(t)u(t-\tau_1)u(t+\tau_2)u(t+\tau_3)\rangle \\ &= \int_{-\infty}^{\infty}\int\int\int d\sigma_1\cdots d\sigma_4 a(\sigma_1)\cdots a(\sigma_4) \\ &\quad\times\langle x(t-\sigma_1)x(t-\sigma_2-\tau_1)x(t-\sigma_3+\tau_2) \\ &\quad\times x(t-\sigma_4+\tau_3)\rangle \\ &= R_u(\tau_1)R_u(\tau_2-\tau_3)+R_u(\tau_2)R_u(\tau_3+\tau_1) \\ &\quad+R_u(\tau_3)R_u(\tau_1+\tau_2)+P_{u1}(\tau_1,\tau_2,\tau_3),\end{aligned} \tag{16}$$

where

$$R_u(\tau) = \int_{-\infty}^{\infty}\int a(\sigma_1)a(\sigma_2)R(\sigma_1-\sigma_2-\tau)d\sigma_1 d\sigma_2, \tag{17}$$

and

$$P_{u1}(\tau_1,\tau_2,\tau_3) = \int_{-\infty}^{\infty}\int\int\int d\sigma_1\cdots d\sigma_4 a(\sigma_1)\cdots a(\sigma_4) \times P_1(\sigma_2-\sigma_1+\tau_1, \sigma_1-\sigma_3+\tau_2, \sigma_1-\sigma_4+\tau_3). \tag{18}$$

In the frequency domain, the formulas corresponding to Eqs. (17) and (18) are Eq. (5) and

$$Q_{u1}(\omega_1,\omega_2,\omega_3) = Q_1(\omega_1,\omega_2,\omega_3)\bar{A}(\omega_1)A(\omega_2)A(\omega_3)\bar{A}(\omega_3+\omega_2-\omega_1). \tag{19}$$

The most important property of Q_1 has yet to be stated; meanwhile it is instructive both for the sake of completeness and also in order to provide a model for later calculations to include a proof of the statement which will be referred to in this paper as the Wiener-Khintchine theorem.

Wiener-Khintchine Theorem. The autocorrelation function and power spectrum of a stochastic process form a Fourier pair.

Proof: Consider a family of complex, ideal band-pass filters $G_\alpha(\omega)$,

$$G_\alpha(\omega)=1, \quad |\omega-\omega_2|\leqq\Delta/2 \qquad =0 \quad \text{otherwise}, \tag{20}$$

where ω_α ranges over the entire frequency axis and $\omega_{-\alpha}=-\omega_\alpha$. Let $\xi_\alpha(t)$ denote the (complex) output of $G_\alpha(\omega)$ when the input is $x(t)$:

$$\xi_\alpha(t)=\int_{-\infty}^{\infty} g_\alpha(\sigma)x(t-\sigma)d\sigma, \tag{21}$$

where

$$g_\alpha(t)=(1/2\pi)\int_{-\infty}^{\infty} G_\alpha(\omega)e^{i\omega t}d\omega. \tag{22}$$

Note that since $g_{-\alpha}(t)=\bar{g}_\alpha(t)$, $\xi_{-\alpha}(t)=\bar{\xi}_\alpha(t)$. Now let $\xi_1(t)$ and $\xi_2(t)$ be a pair of $\xi_\alpha(t)$ and consider the product

$$\xi_1(t)\bar{\xi}_2(t)=\int_{-\infty}^{\infty}\int g_1(\sigma_1)\bar{g}_2(\sigma_2)x(t-\sigma_1)x(t-\sigma_2)d\sigma_1 d\sigma_2. \tag{23}$$

The time average of this expression is

$$\langle\xi_1\bar{\xi}_2\rangle=\int_{-\infty}^{\infty}\int g_1(\sigma_1)\bar{g}_2(\sigma_2)R(\sigma_1-\sigma_2)d\sigma_1 d\sigma_2; \tag{24}$$

letting $S(\omega)$ be *defined* by Eq. (3), the above expression may be transformed to

$$\langle\xi_1\bar{\xi}_2\rangle=(1/2\pi)\int_{-\infty}^{\infty} S(\omega)G_1(\omega)\bar{G}_2(\omega)d\omega. \tag{24.1}$$

Hence, from the nature of the $G_\alpha(\omega)$ and from the uniform continuity of $S(\omega)$, we have

(i) for sufficiently small Δ, $\langle\xi_1\bar{\xi}_2\rangle=0$ when $\omega_1\neq\omega_2$,

(ii) $\langle|\xi_1|^2\rangle=S(\omega_1')(\Delta/2\pi)$, where $\omega_1-\Delta/2\leqq\omega_1'\leqq\omega_1+\Delta/2$,

or

$$\text{(i')} \quad \lim_{\Delta\to 0}(2\pi/\Delta)\langle\xi_1\bar{\xi}_2\rangle=0, \quad \omega_1\neq\omega_2.$$

$$\text{(ii')} \quad \lim_{\Delta\to 0}(2\pi/\Delta)\langle|\xi_1|^2\rangle=S(\omega_1), \tag{25}$$

the limit being approached uniformly in ω_1. Since $\langle|\xi_1|^2\rangle$ is a measure of the power of $x(t)$ contained between the frequencies $\omega_1-\Delta/2$ and $\omega_1+\Delta/2$, $\lim_{\Delta\to 0}(2\pi/\Delta)\langle|\xi_1|^2\rangle$ yields the power density at the frequency ω_1, q.e.d.

The remainder of this section is devoted to a theorem involving fourth moments which is analogous to the W-K theorem for second moments. Let $\xi_1(t), \cdots, \xi_4(t)$ be the (complex) outputs of four filters $G_1(\omega), \cdots, G_4(\omega)$ [as in Eq. (20)] with center frequencies $\omega_1, \cdots, \omega_4$, when the common input is $x(t)$. Take the product

$$\xi_1(t)\xi_2(t)\xi_3(t)\bar{\xi}_4(t)=\int_{-\infty}^{\infty}\int\int\int d\sigma_1\cdots d\sigma_4 \times\bar{g}_1(\sigma_1)g_2(\sigma_2)g_3(\sigma_3)\bar{g}_4(\sigma_4) \times x(t-\sigma_1)x(t-\sigma_2)x(t-\sigma_3)x(t-\sigma_4), \tag{26}$$

and average

$$\langle\bar{\xi}_1\xi_1\xi_3\bar{\xi}_4\rangle=\int_{-\infty}^{\infty}\int\int\int d\sigma_1 d\sigma_2 d\sigma_3 d\sigma_4 \times\bar{g}_1(\sigma_1)g_2(\sigma_2)g_3(\sigma_3)\bar{g}_4(\sigma_4) \times P(\sigma_1-\sigma_4, \sigma_4-\sigma_2, \sigma_4-\sigma_3). \tag{27}$$

If one now substitutes

$$P(\sigma_1-\sigma_4, \sigma_4-\sigma_2, \sigma_4-\sigma_3)=R(\sigma_1-\sigma_2)R(\sigma_3-\sigma_4) +R(\sigma_1-\sigma_3)R(\sigma_2-\sigma_4)+R(\sigma_1-\sigma_4)R(\sigma_2-\sigma_3) +P_1(\sigma_1-\sigma_4, \sigma_4-\sigma_2, \sigma_4-\sigma_3), \tag{28}$$

the integral may be separated into two parts: the first, I_1 involving the R's and the second, I_2, involving P_1.

The first integral is simply

$$I_1=\langle\bar{\xi}_1(t)\xi_2(t)\rangle\langle\xi_3(t)\bar{\xi}_4(t)\rangle+\langle\bar{\xi}_1(t)\xi_3(t)\rangle\langle\xi_2(t)\bar{\xi}_4(t)\rangle +\langle\bar{\xi}_1(t)\bar{\xi}_4(t)\rangle\langle\xi_2(t)\xi_3(t)\rangle. \tag{29}$$

The second integral may be transformed to

$$I_2=(1/2\pi)^3\int_{-\infty}^{\infty}\int\int Q_1(\lambda_1,\lambda_2,\lambda_3)\bar{G}_1(\lambda_1)G_2(\lambda_2)G_3(\lambda_3) \times\bar{G}_4(\lambda_3+\lambda_2-\lambda_1)d\lambda_1 d\lambda_2 d\lambda_3$$

$$=(1/2\pi)^3\int_{\omega_i-\Delta/2}^{\omega_i+\Delta/2}\int\int Q_1(\lambda_1,\lambda_2,\lambda_3) \times G_4(\lambda_3+\lambda_2-\lambda_1)d\lambda_1 d\lambda_2 d\lambda_3. \tag{30}$$

As the Fourier transform of an integrable function Q_1 is uniformly continuous; this permits the representation

$$I_2=(1/2\pi)^3 Q_1(\omega_1',\omega_2',\omega_3') \times\int_{\omega_i-\Delta/2}^{\omega_i+\Delta/2}\int\int G_4(\lambda_3+\lambda_2-\lambda_1)d\lambda_1 d\lambda_2 d\lambda_3, \tag{30.1}$$

where $\omega_i-\Delta/2\leqq\omega_i'\leqq\omega_i+\Delta/2$, $i=1, 2, 3$. Thus we see that

(i) for sufficiently small Δ, I_2 vanishes unless

$$\omega_4=\omega_3+\omega_2-\omega_1; \tag{31}$$

(ii) when Eq. (31) is satisfied, the triple integral occurring in Eq. (30.1) may be evaluated as $2\Delta^3/3$, leading to

$$I_2=2/3(\Delta/2\pi)^3Q_1(\omega_1',\omega_2',\omega_3'). \tag{30.2}$$

These results may be incorporated into

Theorem

$$\text{(i)}\quad \lim_{\Delta\to 0}(2\pi/\Delta)^3\langle\bar{\xi}_1\xi_2\xi_3\bar{\xi}_4\rangle=0 \text{ when } \omega_4\neq\omega_3+\omega_2-\omega_1.$$

$$\begin{aligned}\text{(ii)}\quad \lim_{\Delta\to 0}(2\pi/\Delta)^3\{&\langle\bar{\xi}_1\xi_2\xi_3\bar{\xi}_4\rangle-\langle\bar{\xi}_1\xi_2\rangle\langle\xi_3\bar{\xi}_4\rangle\\&-\langle\bar{\xi}_1\xi_3\rangle\langle\xi_2\bar{\xi}_4\rangle-\langle\bar{\xi}_1\bar{\xi}_4\rangle\langle\xi_2\xi_3\rangle\}\\&=2/3Q_1(\omega_1,\omega_2,\omega_3),\end{aligned} \tag{32}$$

when Eq. (31) is satisfied, the limit being approached uniformly in ω_1, ω_2, ω_3.

III. THE ENVELOPE CORRELATION FUNCTION

The concept of the envelope and phase of a stationary time series has been given precise meaning in a recent paper of Bunimovitch.[14] His approach may be outlined as follows: given $x(t)$, a real stationary time series, one can form a new time series $y(t)$ which will be in "quadrature" with $x(t)$ by performing on the latter the "Hilbert" transformation,

$$y(t)=\lim_{T\to\infty}(1/\pi)\int_{-T}^{T}[x(t-\sigma)/\sigma]d\sigma. \tag{33}$$

Then $X(t)=x(t)+iy(t)$ is a complex time series for which the spectrum is, for positive argument, proportional to the spectrum of x, while for negative argument it is zero. If $X(t)$ is put into polar form $X(t)=\rho(t)\exp i\theta(t)$, $\rho(t)$ is by definition the "envelope" and $\theta(t)$ the "phase" of the original time series and

$$\begin{aligned}x(t)&=\rho(t)\cos\theta(t),\\y(t)&=\rho(t)\sin\theta(t).\end{aligned} \tag{34}$$

Let us now define

$$x_a(t)=\xi_a(t)+\bar{\xi}_a(t), \tag{35}$$

where $\xi_a(t)$ is as defined in Sec. II; $x_a(t)$ may also be identified with the output of a *real* ideal band-pass filter $H_a(\omega)$,

$$\begin{aligned}H_a(\omega)&=1, \quad |\omega\pm\omega_a|\leqq\Delta/2,\\&=0 \quad \text{otherwise},\end{aligned} \tag{36}$$

when the input is $x(t)$. Then $2\xi_a(t)$ and $x_a(t)$ bear the same relation to one another as $X(t)$ and $x(t)$, above. Accordingly, $2|\xi_a(t)|$ is the envelope of the time series $x_a(t)$.

[14] V. I. Bunimovitch, J. Tech. Phys. (U.S.S.R.) **19**, 1231 (1949).

By combining Eqs. (25) and (32) one can write

$$\langle|\xi_1\xi_2|^2\rangle-\langle|\xi_1|^2\rangle\langle|\xi_2|^2\rangle\doteq 2/3Q_1(\omega_1,\omega_2,\omega_1)(\Delta/2\pi)^3$$

when $\omega_1\neq\omega_2$,

$$\begin{aligned}\langle|\xi_1|^4\rangle-\langle|\xi_1|^2\rangle^2\doteq S^2(\omega_1)(\Delta/2\pi)^2\\+2/3Q_1(\omega_1,\omega_1,\omega_1)(\Delta/2\pi)^3.\end{aligned} \tag{37}$$

Thus one sees that the function $Q_1(\omega_1,\omega_2,\omega_1)$ may be interpreted as a measure of the correlation between the squares of the envelopes of $x_1(t)$ and $x_2(t)$. It is for this reason that the (real, continuous) function

$$E(\omega_1,\omega_2)\equiv Q_1(\omega_1,\omega_2,\omega_1)=Q_1(\omega_1,\omega_1,\omega_2), \tag{38}$$

will be referred to hence as the "envelope correlation function" of the time series $x(t)$. Clearly, $E(\omega_1,\omega_2)=E(\omega_2,\omega_1)=E(-\omega_1,\omega_2)$. Note that both E and Q_1 are "densities" in that each must be multiplied by the third power of band width in order to have physical significance.

If $x(t)$ is passed through a (real) linear filter of admittance $A(\omega)$, the output $u(t)$ will have envelope correlation function [see Eq. (19)]

$$E_u(\omega_1,\omega_2)=E(\omega_1,\omega_2)\,|A(\omega_1)A(\omega_2)|^2. \tag{39}$$

It is possible to express $D(\tau_1,\tau_2)$, the Fourier transform of $E(\omega_1,\omega_2)$, in terms of the function $P_1(\tau_1,\tau_2,\tau_3)$ in the following manner:

$$\begin{aligned}D(\tau_1,\tau_2)&=(1/2\pi)^2\int_{-\infty}^{\infty}\int E(\omega_1,\omega_2)e^{i(\omega_1\tau_1+\omega_2\tau_2)}d\omega_1d\omega_2\\&=(1/2\pi)^2\int_{-\infty}^{\infty}\int\int ds_1ds_2ds_3\\&\quad\times\int_{-\infty}^{\infty}\int d\omega_1d\omega_2P_1(s_1,s_2,s_3)\\&\quad\times\exp i(\omega_1\tau_1+\omega_2\tau_2-\omega_1s_1-\omega_2s_2-\omega_1s_3)\\&=\int_{-\infty}^{\infty}P_1(s,\tau_2,\tau_1-s)ds.\end{aligned} \tag{40}$$

It is important to point out here that $E(\omega_1,\omega_2)$ is *not* a correlation density in the strict sense of the word; indeed, if one divides Eq. (37) by $(\Delta/2\pi)^3$ and takes the limit as $\Delta\to 0$, one sees that

$$\begin{aligned}\lim_{\Delta\to 0}(2\pi/\Delta)^3[\langle|\xi_1\xi_2|^2\rangle-\langle|\xi_1|^2\rangle\langle|\xi_2|^2\rangle]\\=2\pi\delta(\omega_1-\omega_2)S(\omega_1)S(\omega_2)+2/3E(\omega_1,\omega_2).\end{aligned} \tag{37.1}$$

Thus, one must append to $2/3E(\omega_1,\omega_2)$ the function $2\pi\delta(\omega_1-\omega_2)S(\omega_1)S(\omega_2)$ in order to make it a correlation density. Consequently, E should not be expected to possess all of the properties of such a function. For

example, E need not be positive definite: we have in Example 2 of Sec. V an instance in which $E(\omega_1,\omega_1)$ is negative for some ω_1.

Unlike the function $Q_1(\omega_1,\omega_2,\omega_3)$, the envelope correlation function is capable of a description in terms of limits of mean products of outputs of *real* ideal bandpass filters. For, if $H_1(\omega)$ and $H_2(\omega)$ are two such filters [as in Eq. (36)] with center frequencies ω_1 and ω_2 and if $x_1(t)$ and $x_2(t)$ are their respective outputs when the inputs are $x(t)$, then

Corollary

$$\text{(i)}\quad \lim_{\Delta\to 0}(2\pi/\Delta)^3[\langle x_1^2x_2^2\rangle-\langle x_1^2\rangle\langle x_2^2\rangle] = 8/3E(\omega_1,\omega_2),\quad \omega_1\neq\omega_2. \tag{41}$$

$$\text{(ii)}\quad \lim_{\Delta\to 0}(2\pi/\Delta)^3[\langle x_1^4\rangle-3\langle x_1^2\rangle^2]=4E(\omega_1,\omega_1).$$

Proof of this corollary is effected by a straightforward application of the Theorem, Sec. II, to Eq. (41) when $x(t)$ is as defined in Eq. (35).

IV. APPLICATION TO QUADRATIC DEVICES

As it was demonstrated in Sec. I, in order to determine the spectral response of a quadratic device to a noise input it is necessary to have knowledge not only of the spectrum of the input but also of the P_1 function of the input. It is our intention in this section to show how, given this additional information, one proceeds to calculate the spectrum of the output.

Let us return to the example which was left incomplete in Sec. I. The autocorrelation of $w(t)=u(t)v(t)-\langle uv\rangle$ as given by Eq. (7) may now be rewritten as

$$\begin{aligned}R_w(\tau)=\int\int\int\int_{-\infty}^{\infty} d\sigma_1\cdots d\sigma_4 a(\sigma_1)b(\sigma_2)a(\sigma_3)b(\sigma_4)\\ \times[R(\sigma_1-\sigma_3-\tau)R(\sigma_2-\sigma_4-\tau)\\ +R(\sigma_1-\sigma_4-\tau)R(\sigma_2-\sigma_3-\tau)\\ +P_1(\sigma_1-\sigma_4-\tau,\sigma_4-\sigma_2+\tau,\sigma_4-\sigma_3)].\end{aligned} \tag{7.1}$$

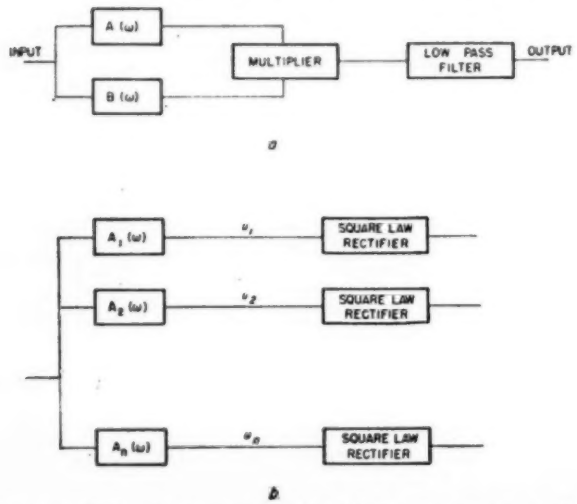

FIG. 2. Additional networks to which the theory may be applied.

The spectrum of w is obtained by taking the Fourier transform,

$$\begin{aligned}S_w(\omega)&=\int_{-\infty}^{\infty}R_w(\tau)e^{-i\omega\tau}d\tau\\ &=(1/2\pi)\int_{-\infty}^{\infty}S(\omega_1)S(\omega_1+\omega)[|A(\omega_1)B(\omega_1+\omega)|^2\\ &\quad+\bar{A}(\omega_1)B(\omega_1)B(\omega_1+\omega)\bar{A}(\omega_1+\omega)]d\omega_1\\ &\quad+(1/2\pi)^2\int\int_{-\infty}^{\infty}Q_1(\omega_1,\omega_1+\omega,\omega_2)\\ &\quad\times\bar{A}(\omega_1)A(\omega_2)B(\omega_1+\omega)\bar{B}(\omega_2+\omega)d\omega_1d\omega_2.\end{aligned} \tag{42}$$

It is of interest to set $\omega=0$ in Eq. (42) and obtain

$$\begin{aligned}S_w(0)&=(1/2\pi)\int_{-\infty}^{\infty}S^2(\omega_1)[|A(\omega_1)B(\omega_1)|^2\\ &\quad+\bar{A}(\omega_1)^2B^2(\omega_1)]d\omega_1+(1/2\pi)^2\int\int_{-\infty}^{\infty}E(\omega_1,\omega_2)\\ &\quad\times\bar{A}(\omega_1)A(\omega_2)B(\omega_1)\bar{B}(\omega_2)d\omega_1d\omega_2.\end{aligned} \tag{42.1}$$

This result is of use when the quadratic operation is followed by low pass filtering (or averaging) as shown in Fig. 2a; when this is the case, the spectral density at zero frequency of the output of the quadratic element often contains sufficient information regarding the noise, since the higher frequency fluctuations are suppressed.[5,15] The fact that Q_1 may be replaced by E not only simplifies considerably the formula, but also exhibits another important property of the envelope correlation function.

In the problem of the detection of signals in noise, networks such as shown in Fig. 2b are sometimes employed.[15] Without going into the details of the detection problem, we can still investigate how our theory applies to such circuitry. The device consists of N real operations performed in parallel on the common input $x(t)$:

$$u_n(t)=\int_{-\infty}^{\infty}a_n(\sigma)x(t-\sigma)d\sigma, \tag{43}$$

where

$$a_n(t)=(1/2\pi)\int_{-\infty}^{\infty}A_n(\omega)e^{-i\omega t}d\omega; \tag{44}$$

and

$$w_n(t)=u_n^2(t)-\langle u_n^2\rangle,\quad n=1,2,\cdots,N. \tag{45}$$

First of all, one can obtain the spectrum of the output w_n of a single "channel" as a special case of Eq. (42):

[15] Philip Rudnick, J. Appl. Phys. 24, 128 (1953).

$$S_n(\omega)=(1/\pi)\int_{-\infty}^{\infty} S(\omega_1)S(\omega_1+\omega)\times|A_n(\omega_1)A_n(\omega_1+\omega)|^2d\omega_1+(1/2\pi)^2\int\int_{-\infty}^{\infty} Q_1(\omega_1,\omega_1+\omega,\omega_2)\bar{A}_n(\omega_1)\times A_n(\omega_1+\omega)A_n(\omega_2)A_n(\omega_2+\omega)d\omega_1d\omega_2. \quad (46)$$

The spectral density at zero frequency is then

$$S_n(0)=(1/\pi)\int_{-\infty}^{\infty} S^2(\omega_1)|A_n(\omega_1)|^4d\omega_1+(1/2\pi)^2\int\int_{-\infty}^{\infty} E(\omega_1,\omega_2)\times|A_n(\omega_1)A_n(\omega_2)|^2d\omega_1d\omega_2. \quad (46.1)$$

It is interesting to observe that if $A_n(\omega)$ is a (real) narrow band filter with center frequency ω_n and effective band width Δ (rad/sec), then Eq. (46.1) can be approximated by

$$S_n(0)\doteq 4S^2(\omega_n)|A_n(\omega_n)|^4(\Delta/2\pi)+4E(\omega_n,\omega_n)|A_n(\omega_n)|^4(\Delta/2\pi)^2. \quad (46.2)$$

Thus, $S_n(0)$ differs from the value it would have for Gaussian noise $[E(\omega_n,\omega_n)=0]$ by a term which is second order in $\Delta/2\pi$. This is in agreement with the principle which has been stated by Rice,[11] Middleton[13] and others that the statistics of a narrow band of any noise approach Gaussian as the band width approaches zero.

The cross correlation between two outputs w_m and w_n can also be determined:

$$R_{mn}(\tau)=\langle w_m(\tau)w_n(t-\tau)\rangle=\int\int\int\int\int_{-\infty}^{\infty} d\sigma_1\cdots d\sigma_4 a_m(\sigma_1)a_m(\sigma_2)a_n(\sigma_3)a_n(\sigma_4)\times[2R(\sigma_1-\sigma_4-\tau)R(\sigma_1-\sigma_3-\tau)+P_1(\sigma_1-\sigma_4-\tau,\sigma_4-\sigma_2+\tau,\sigma_4-\sigma_3)]. \quad (47)$$

The cross spectrum is then

$$S_{mn}(\omega)=\int_{-\infty}^{\infty} R_{mn}(\tau)e^{-i\omega\tau}d\tau=(1/\pi)\int_{-\infty}^{\infty} S(\omega_1)S(\omega_1+\omega)\bar{A}_m(\omega_1)\times A_m(\omega_1+\omega)A_n(\omega_1)\bar{A}_n(\omega_1+\omega)d\omega_1+(1/2\pi)^2\int\int_{-\infty}^{\infty} Q_1(\omega_1,\omega_1+\omega,\omega_2)\bar{A}_m(\omega_1)\times A_m(\omega_1+\omega)A_n(\omega_2)\bar{A}_n(\omega_2+\omega)d\omega_1d\omega_2. \quad (48)$$

The value of the cross spectrum at zero frequency provides a measure of the correlation between the low frequency parts of w_m and w_n and is given by

$$S_{mn}(0)=(1/\pi)\int_{-\infty}^{\infty} S^2(\omega_1)|A_m(\omega_1)A_n(\omega_1)|^2d\omega_1+(1/2\pi)^2\int\int_{-\infty}^{\infty} E(\omega_1,\omega_2)\times|A_m(\omega_1)A_n(\omega_2)|^2d\omega_1d\omega_2. \quad (48.1)$$

Note that if A_m and A_n are non-overlapping filters $(A_m(\omega)A_n(\omega)\equiv 0)$, then the correlation between the low frequency parts of w_m and w_n is due entirely to the envelope correlation function.

V. EXAMPLES

Included below are three examples of non-Gaussian processes for which the P_1, Q_1 and E functions have been computed. In each case, statistics of second order —the autocorrelation and spectrum—have been studied already in some detail, but little attention has previously been directed toward fourth-order statistics.

1. Square of a Gaussian Time Series

Let $u(t)$ be a Gaussian time series with first and second moments

$$\langle u(t)\rangle=0,\qquad \langle u(t)u(t-\tau)\rangle=r(\tau), \quad (49)$$

where for simplicity we demand that $r(\tau)$ be integrable and $r(0)=1$. Then $x(t)=u^2(t)-1$ will be the non-Gaussian noise which we shall examine. This noise could be realized physically by applying, say, "white" thermal noise to a linear filter $A(\omega)$, where $A(\omega)$ is chosen to impart to its output the desired spectral character [see Eq. (5)], and then rectifying quadratically the filter output.

It is well known that

$$R(\tau)=\langle x(t)x(t-\tau)\rangle=2r^2(\tau), \quad (50)$$

but the fourth moment involving x is more difficult to obtain. The method used by the author was to express $\langle x(t)x(t-\tau)x(t+\tau_2)x(t+\tau_3)\rangle$ in terms of 8th-, 6th-, 4th-, and 2nd-order moments of the Gaussian variables $u(t)$, $u(t-\tau_1)$, $u(t+\tau_2)$, $u(t+\tau_3)$, and then to evaluate these moments by differentiating the appropriate characteristic function.[10] One is thus led to the result

$$P_1(\tau_1,\tau_2,\tau_3)=16[r(\tau_1)r(\tau_1+\tau_2)r(\tau_2-\tau_3)r(\tau_3)+r(\tau_2)r(\tau_2-\tau_3)r(\tau_3+\tau_1)r(\tau_1)+r(\tau_3)r(\tau_3+\tau_1)r(\tau_1+\tau_2)r(\tau_2)]. \quad (51)$$

P_1 is clearly integrable and has as its Fourier transform

the (real, non-negative) function

$$Q_1(\omega_1,\omega_2,\omega_3)=16(1/2\pi)\times\int_{-\infty}^{\infty}[s(\lambda)s(\lambda+\omega_1)s(\lambda+\omega_2)s(\lambda+\omega_2+\omega_3)+s(\lambda)s(\lambda+\omega_2)s(\lambda+\omega_3)s(\lambda+\omega_3+\omega_1)+s(\lambda)s(\lambda+\omega_3)s(\lambda+\omega_1)s(\lambda+\omega_1+\omega_2)]d\lambda, \quad (52)$$

where

$$s(\omega)=\int_{-\infty}^{\infty}r(\tau)e^{-i\omega\tau}d\tau. \quad (53)$$

The envelope correlation function is then

$$E(\omega_1,\omega_2)=16(1/2\pi)\int_{-\infty}^{\infty}[2s(\lambda)s^2(\lambda+\omega_1)s(\lambda+\omega_1+\omega_2)+s(\lambda)s(\lambda+\omega_1)s(\lambda+\omega_2)s(\lambda+\omega_1+\omega_2)]d\lambda, \quad (54)$$

and

$$(1/2\pi)^2\int_{-\infty}^{\infty}\int E(\omega_1,\omega_2)d\omega_1 d\omega_2 ,$$

$$=16\int_{-\infty}^{\infty}[2r^2(\tau)+r^4(\tau)]d\tau>0. \quad (55)$$

2. Random Telegraph Signal[11,16]

Let $x(t)$ be either $+1$ or -1 so that it is of the form of a flat top wave. Let the zero crossings be distributed along the t axis in such a manner that the probability of a crossing between t and $t+dt$ is (in the limit) equal to μdt and is independent of what happens outside the interval $(t, t+dt)$. It is known then that

$$R(\tau)=e^{-2\mu|\tau|}, \quad (56)$$

and an extension of the type of argument which leads to Eq. (56) will show

$$P_1(\tau_1,\tau_2,\tau_3)=-[g_1(\tau_1,\tau_2,\tau_3)+g_2(\tau_1,\tau_2,\tau_3)+g_3(\tau_1,\tau_2,\tau_3)], \quad (57)$$

where

except when

$$g_1=e^{-2\mu[|\tau_1|+|\tau_2-\tau_3|]}\begin{cases}\tau_2,\tau_3>0,\ \tau_1>-\min(\tau_2,\tau_3)\\ \tau_2,\tau_3<0,\ \tau_1<\min(-\tau_2,-\tau_3),\end{cases}$$

$$g_2=e^{-2\mu[|\tau_2|+|\tau_3+\tau_1|]}\begin{cases}\tau_1>0,\ \tau_3<0,\ \tau_2>-\min(\tau_1,-\tau_3)\\ \tau_1<0,\ \tau_3>0,\ \tau_2<\min(-\tau_1,\tau_3),\end{cases}$$

$$g_3=e^{-2\mu[|\tau_3|+|\tau_1+\tau_2|]}\begin{cases}\tau_1>0,\ \tau_2<0,\ \tau_3>-\min(\tau_1,-\tau_2)\\ \tau_1<0,\ \tau_2>0,\ \tau_3<\min(-\tau_1,\tau_2).\end{cases} \quad (58)$$

[16] G. W. Kenrick, Phil. Mag. (January, 1929).

The functions g_i are all integrable and possess Fourier transforms which, combined, yield

$$Q_1(\omega_1,\omega_2,\omega_3)=-(1/2\mu)^3\times[24+4(\lambda_1^2+\lambda_2^2+\lambda_3^2+\lambda_4^2)-8\lambda_1\lambda_2\lambda_3\lambda_4]/(1+\lambda_1^2)(1+\lambda_2^2)(1+\lambda_3^2)(1+\lambda_4^2), \quad (59)$$

where (1) $\omega_4=\omega_3+\omega_2-\omega_1$ and (2) $\lambda_i=\omega_i/2\mu$. The envelope correlation function is then

$$E(\omega_1,\omega_2)=-(1/2\mu)^3\times[24+8(\lambda_1^2+\lambda_2^2-\lambda_1^2\lambda_2^2)]/(1+\lambda_1^2)^2(1+\lambda_2^2)^2; \quad (60)$$

note that $E(\omega_1,\omega_1)$ is negative when $\lambda_1^2<3$.

3. The Shot Effect[11]

Let

$$u(t)=\sum_{\tau=-\infty}^{\infty}f(t-\tau_\tau), \quad (61)$$

where $f(t)$ is a real valued, integrable function and where the epochs τ_τ are randomly and independently distributed in time with density μ; then $x(t)=u(t)-\mathcal{E}\{u\}$ will be the non-Gaussian process to be examined.

Using Middleton's[17] generalization of the Campbell theorem, it can be shown that the characteristic function of any finite set of $u_\lambda\equiv u(t_\lambda)$, $\lambda=1, 2, \cdots N$, is

$$\phi_N(\eta_1,\cdots,\eta_N)=\mathcal{E}\{\exp[i\sum_{\lambda=1}^{N}u_\lambda\eta_\lambda]\}=\exp\left\{\mu\int_{-\infty}^{\infty}\{\exp[i\sum_{\lambda=1}^{N}\eta_\lambda f(t+t_\lambda)]-1\}dt\right\},\quad N=1, 2, \cdots. \quad (62)$$

This system of equations completely defines u (and subsequently x) as a stochastic process, and moments involving the u_λ may be computed by differentiating ϕ_N as in Example 1.

For example,

$$R(\tau)=\mu\int_{-\infty}^{\infty}f(t)f(t-\tau)dt, \quad (63)$$

and

$$S(\omega)=\mu|F(\omega)|^2, \quad (64)$$

where

$$F(\omega)=\int_{-\infty}^{\infty}f(t)e^{-i\omega t}dt. \quad (65)$$

The P_1 function is

$$P_1(\tau_1,\tau_2,\tau_3)=\mu\int_{-\infty}^{\infty}f(t)f(t-\tau_1)f(t+\tau_2)f(t+\tau_3)dt, \quad (66)$$

and its transform is

$$Q_1(\omega_1,\omega_2,\omega_3)=\mu\bar{F}(\omega_1)F(\omega_2)F(\omega_3)\bar{F}(\omega_3+\omega_2-\omega_1). \quad (67)$$

[17] D. Middleton, J. Appl. Phys. 22, 1143 (1951).

The envelope correlation function is[11]

$$E(\omega_1,\omega_2)=\mu|F(\omega_1)F(\omega_2)|^2 =S(\omega_1)S(\omega_2)/\mu. \quad (68)$$

It is of interest to allow the density of pulses μ to increase while keeping the total power in x constant: let

$$x_\mu(t)=\sum_\nu f_\mu(t-\tau_\nu)-\mathcal{E}\{\sum_\nu f_\mu\}, \quad (69)$$

where $f_\mu(t)=f(t)/\sqrt{\mu}$. The spectrum of x_μ is

$$S_\mu(\omega)=|F(\omega)|^2, \quad (70)$$

while

$$Q_{\mu 1}(\omega_1,\omega_2,\omega_3)=\bar{F}(\omega_1)F(\omega_2)F(\omega_3)\bar{F}(\omega_3+\omega_2-\omega_1)/\mu. \quad (71)$$

Thus we see that as $\mu\to\infty$, S_μ remains fixed while $Q_{\mu 1}\to 0$; or, insofar as fourth-order statistics are concerned, x_μ becomes Gaussian.

[11] Note the non-negative character of E. This is a fundamental property of processes which can be represented by Eq. (61).

ACKNOWLEDGMENT

The significance of fourth-order moments in the analysis of non-Gaussian noises was first brought to the author's attention by Professor Carl Eckart, and it was at the latter's suggestion that this investigation was originally begun. The author is also indebted to other members of the laboratory staff, and in particular to Dr. Philip Rudnick, for providing indispensable help and encouragement.

JOURNAL OF APPLIED PHYSICS VOLUME 25, NUMBER 11 NOVEMBER, 1954

Electron Emission from Metals under High-Energy Hydrogen Ion Bombardment

B. Aarset,* R. W. Cloud, and J. G. Trump
Department of Electrical Engineering, Massachusetts Institute of Technology, Cambridge, Massachusetts

(Received April 9, 1954)

Measurements of the electron emission from Mg, Al, Fe, Ni, Au, and Pb surfaces bombarded by atomic (H_1^+) and molecular (H_2^+) hydrogen ions with energies from 0.7 to 2.0 Mev showed a diminishing emission with ion energy and little dependence on either atomic number or on the field intensity at the metal surface. Measurements of this type are of interest in connection with the mechanism of high voltage discharges in vacuum. The expected variation of secondary emission with angle of incidence and with conditioning was found. The emission ratios are compared with measurements by others at lower ion energies.

INTRODUCTION

ALTHOUGH secondary electron emission by the impact of positive ions on metal surfaces has been measured by several workers, there has been considerable diversity in the type and energy of the bombarding ion, and in the nature and condition of the metal surfaces. This work has shown that emission does not vary greatly for different metals and ions but does exhibit considerable energy dependence. For ion energies up to one kilovolt the electron emission per positive ion is less than unity. At higher energies the emission ratio for normally incident ions may increase to 10 or 15. Linford[1] using mercury ions with energies from 0.7 to 2.35 Mev obtained from the common metals an electron emission per ion which increased from 7 to 9 in this energy range. Exceptionally high ratios of 25 and 20 were observed from evaporated sodium and potassium targets. Until the present study, 400 kev was the highest energy used with the light ions, hydrogen, and helium. In this study by Hill *et al.*[2] a tendency was noted for the secondary electron emission to reach a maximum and then decrease at higher energies; this maximum was reached at about 100 kev for H_2^+ and 300 kev for He^+.

The influence of the nature of the ion has been investigated with various results. Hill used H_1^+, H_2^+, and He^+ and found increasing secondary emission with increasing ion mass. Healea and Houtermans[3] used He, Ne, and A ions and found decreasing emission with increasing ion mass. Bourne[4] obtained the maximum emission from ions of intermediate mass and observed increasing yield with ion energy up to the limit of his range, 140 kev.

An important factor in these experiments is the condition of the target surface. Contamination and adsorbed gases increase the emission and must be minimized to obtain consistent results. Hill found that a half-hour bombardment of a new target with 400-kev ions reduced the secondary emission as much as 50 percent. Linford heated the target by electron bombardment and lowered the secondary emission by amounts

* On leave to Massachusetts Institute of Technology from the Department of Physics, University of Oslo, Norway, September 1951–1953.

[1] L. H. Linford, Phys. Rev. **47**, 279–282 (1935).

[2] Hill, Buechner, Clark, and Fisk, Phys. Rev. **55**, 463–470 (1939).

[3] M. Healea and C. Houtermans, Phys. Rev. **58**, 608–610 (1940).

[4] H. C. Bourne, "Study of Theory of Voltage Breakdown in High Vacuum," Doctorate thesis in electrical engineering, Massachusetts Institute of Technology (1952).

up to 50 percent of its initial value. Allen[5] found that the emission decreased to a stable value when a fresh target was bombarded for about 10 minutes. For 200-kev ions on Ni the decrease was about 25 percent; outgassing the target at red heat further reduced the secondary emission to about half of the latter value.

In the present work, the vacuum was produced by mercury diffusion pumps trapped with liquid air. Before readings were taken, the target was bombarded for two hours or more to produce stable emission values. Although this technique is representative of good electrode conditioning in high-voltage acceleration tubes it is presumed that the secondary electron emission is still influenced by the layers of residual contamination over the true metal surface.

THEORIES

Kapitza,[6] considering high-energy alpha-particle bombardment of metals, described secondary emission as thermionic emission resulting from the kinetic energy released by the ion at the point of impact. He took into account the trapping of electrons energized at considerable depths below the surface and analyzed the effect of glancing incidence. He found agreement between the observed energy distribution of secondary electrons and the expected energy distribution from such thermionic emission. This process, permissible at higher ion energies, permits multiple electron emission.

Oliphant,[7] concerned with low ion energies below 1000 ev, noted a two-step process in the electron emission. As it approaches the metal surface, the ion may be neutralized by high field emission and drop to the ground state by electron emission, or it may continue into the metal and transfer its excitation energy to an electron in the metal which may then be emitted. This theory agrees with the characteristic shape of the energy distribution curve of the secondary electrons. Hagstrum[8] believes it is more probable that the excited atom is de-excited by a metal electron jumping directly to the ground state of the atom, while the excited electron receives the excess energy and is emitted. There is general acceptance that at higher ion energies the process gradually shifts to thermionic emission and depends primarily on the kinetic energy of the ion.

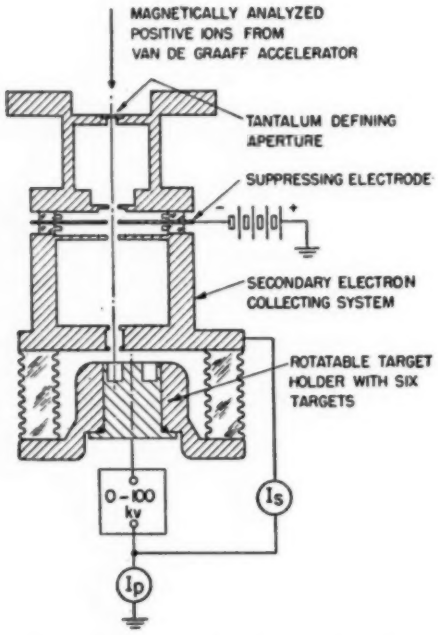

FIG. 1. Arrangement for measuring the secondary electron emission under high-energy hydrogen ion bombardment.

SOURCE OF HIGH-ENERGY IONS

The high-energy ions were produced in a 2-Mev pressurized Van de Graaff accelerator. The ion source was a capillary dc arc in hydrogen mounted in the terminal. A 90-degree magnetic analyzer was used after acceleration to obtain the H_1^+ or H_2^+ ions as required. The generator voltage was stabilized by utilizing the mass 2-ion beam which delivered signals to slits placed in its path beyond the analyzer. The generator voltage was varied from 0.7 to 2 Mev and produced a very steady proton beam of about 0.5 microampere over most of this energy range.

EMISSION MEASUREMENTS

Figure 1 shows the target assembly, the collector, and the defining apertures toward which the analyzed beam of high-energy ions was directed. Line-up of the beam with the axis of the chamber and the system of defining diaphragms was facilitated by substituting a polished quartz disk for the target; the assembly could be easily aligned by adjusting its position while watching the fluorescent spot produced by the ion beam on the quartz.

A negative bias of 600 volts on the suppressing electrode was found sufficient to repel secondary electrons from both sides, thus preventing unwanted electrons from reaching the collector and the escape of secondary electrons from the collecting system.

Six targets were mounted in a holder which could be rotated without breaking the vacuum. The surfaces of the targets, their holder, and also the surface of the collector facing the target were polished and chemically cleaned. High voltages could be applied between target and collector to investigate the effect of extracting gradients up to 40 kv/cm on the target surface. The aperture facing the target was estimated to cause less than 5 percent distortion of the gradient across the face of the target. The source for the collector-to-target voltage was a pressure-insulated transformer-rectifier unit for voltages up to 40 kilovolts and dry cells for low bias voltages.

[5] J. S. Allen, Phys. Rev. **55**, 336–339 (1939).
[6] P. L. Kapitza, Phil. Mag. **45**, 989–998 (1923).
[7] M. L. E. Oliphant, Proc. Roy. Soc. (London) **A127**, 373–406 (1930).
[8] H. D. Hagstrun, Phys. Rev. **89**, 244–255 (1953).

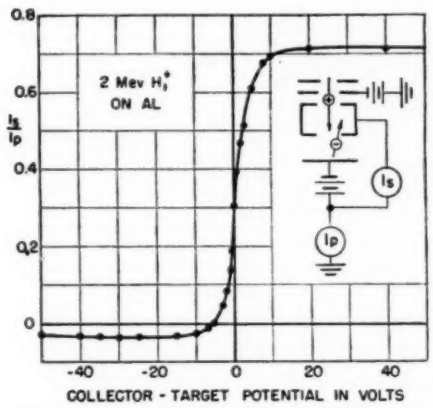

FIG. 2. Dependence of emission ratio on the collector-target voltage.

When a fresh target was bombarded with protons the yield of secondary electrons would drop rapidly at first and then level off to a constant value. Two to three hours of bombardment seemed to be necessary to reach steady reproducible measurements.

Figure 2 shows the influence of collector voltage on the measured ratio of collector current I_s to total ion beam current I_p. With positive collector voltage the electron current I_s increased rapidly and reached an equilibrium value at 20 volts. This suggests that most of the secondary electrons are emitted with energies under this value. With negative collector voltage the current I_s passed through zero at about -5 volts and then increased with opposite sign reaching a broad maximum at about -25 volts. Further increase of the negative collector voltage to several kilovolts causes this reversed-polarity current to decrease to 5 percent of its maximum value. This decrease, shown in Fig. 3, is evidence that this current is primarily electron emission caused by reflected ions impinging on the collector rather than photoelectric emission as has occasionally been suggested.[1] At low voltages, many of the reflected ions will hit the collector at various angles with consequently enhanced electron emission. At higher negative collector voltages, the reflected ions will be focussed toward the aperture and tend to enter the Faraday cage; photoelectric emission would be unaffected by this field.

SECONDARY ELECTRONS PRODUCED BY H_1^+ AND H_2^+ ION BOMBARDMENT

Table I gives the results of bombarding thick targets of different metals with protons and molecular hydrogen

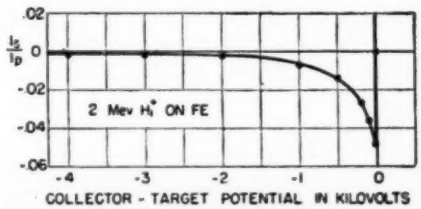

FIG. 3. Reversed emission ratios at high repressing potentials.

TABLE I. Secondary electron emission by hydrogen ions on metals.

Metal	Type of ion	Ion energy in Mev 0.7	0.85	1.0	1.3	1.6	2.0
Mg	H_1^+	1.22	1.09	1.01	0.88	0.78	0.67
Al		1.31	1.15	1.08	0.86	0.77	0.68
Fe		1.23	1.16	1.09	0.94	0.80	0.69
Ni		1.28	1.23	1.17	0.92	0.79	0.69
Au		1.3	1.16	1.05	0.91	0.81	0.68
Pb		1.22	1.11	1.00	0.86	0.77	0.66
Al	H_2^+	3.71	3.4	3.24	2.85	2.58	2.24
Ni		3.76	3.44	3.22	2.86	2.53	2.26
Au		3.760	3.44	3.17	2.81	2.50	2.21

ions. As suggested by Hill *et al.*,[2] one might expect the secondary electron yield produced by one H_2^+ ion to be roughly equal to that produced by two protons, each with one-half the energy of the H_2^+ ion, plus one electron with energy $V/3680$. A plot of one-half the secondary emission yield against one-half the H_2^+ energy should therefore be expected to run higher than H_1^+ emission curve by an amount given by the secondary emission yield of the electron. The difference shown in Fig. 6 between the reduced H_2^+ curve and the proton curve is too small to fully verify this theory.

INFLUENCE OF FIELD INTENSITY AT THE EMISSION SURFACE

Figure 4 shows the secondary electron emission plotted against the gradient at the surface of the target. Within the accuracy of the experiment the gradient had no influence on the secondary electron emission in the region 0 to +36 kv/cm. These measurements thus confirmed other studies in this laboratory showing gradient independence[9] and emphasize again the importance of particle energy rather than gradient in high-voltage breakdown in vacuum gaps.[10]

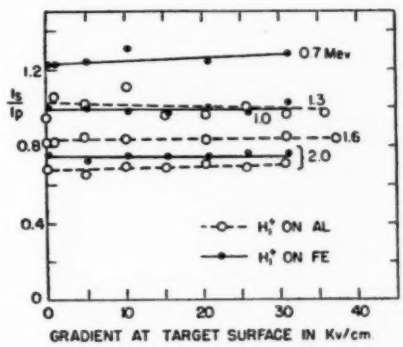

FIG. 4. Dependence of emission ratio on gradient at the target surface.

[9] Webster, Van de Graaff, and Trump, J. Appl. Phys. **23**, 264-266 (1952).

[10] J. G. Trump and R. J. Van de Graaff, J. Appl. Phys. **18**, 327–332 (1947).

EFFECT OF ANGLE OF INCIDENCE

Six cone-shaped targets of aluminum, each with a different angle ranging from 30 to 90 degrees between the cone axis and the surface, were mounted in the target holder and successively bombarded by a 1.6-Mev proton beam approaching axially. Figure 5 shows the secondary yield as a function of the angle θ between the incident proton beam and the tilted target surface. Although each target was not completely conditioned, the yield was adjusted to approximate the same state of conditioning by assuming that conditioning is related to total amount of collected charge. The result shows good agreement with Allen,[5] who found that the secondary emission yield was proportional to the cosecant of θ. The equation $I_s/I_p = 0.825 \csc\theta$ is seen to approximate the emission *versus* beam angle curve. Assuming the continued validity of this relationship it is evident that in actual acceleration tubes in which almost tangential incidence of the positive ions is frequent, the secondary electron emission from such bombardment may be extremely high.

CONCLUSIONS

The comparison in Fig. 6 of these electron emission measurements with results of others over a wide range of lower energies sustains the previous impression that the emission reaches a peak and diminishes at the higher ion energies. The emission is not assisted by high field intensities at the bombarded surface and shows little variation from one metal to another. The cosecant θ dependence of emission with angle θ between beam and surface reflects the importance of the limited depth from which energized electrons can escape. The adequate conditioning of the target material by extended ion bombardment was found essential.

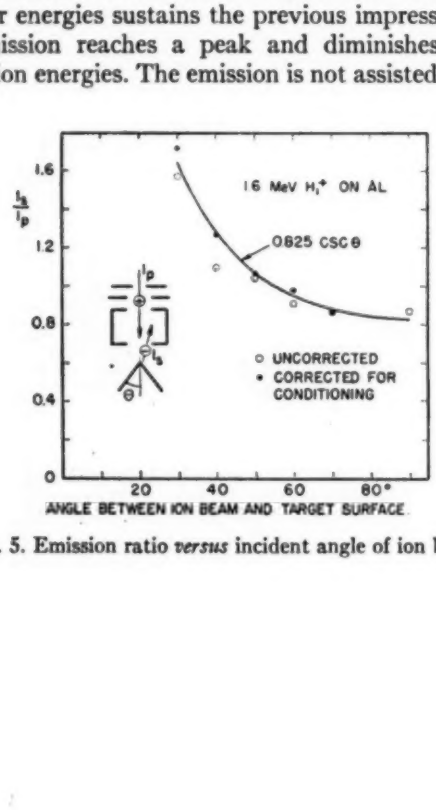

FIG. 5. Emission ratio *versus* incident angle of ion beam.

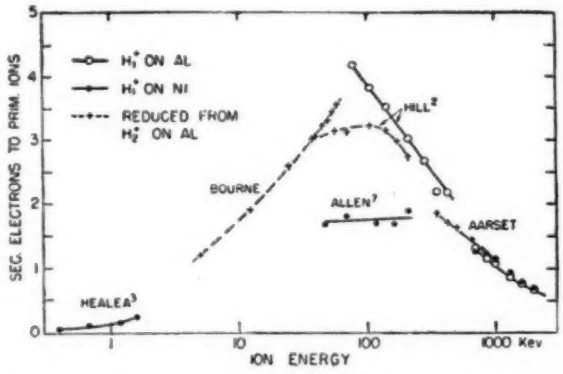

FIG. 6. Comparison over a wide energy range of the electron emission ratios measured by different workers using hydrogen ions on aluminum or nickel.

This work suggests that the electron emission under positive ion bombardment is not quantitatively adequate to produce instability by the particle interchange mechanism[10] in high vacuum breakdown. For such instability the product of the emission ratios at the anode and cathode surfaces should exceed unity, yet the ratio of positive ions emitted under electron bombardment is known to be less than 0.001, and the present study shows that the electron emission ratio is generally less than 10 and is uninfluenced by gradient.

The reported measurements do not, however, distinguish the nature of the secondary emission, whether electrons or negative ions. The existence of negative ions in this secondary emission deserves investigation as they could be the influential factors in the particle interchange mechanism.

ACKNOWLEDGMENTS

The assistance of a grant from the National Science Foundation in support of this work is gratefully acknowledged.

Influence of Deuteron Bombardment and Strain Hardening on Notch Sensitivity of Mild Steel*†

ROBERT A. MEYER
U. S. Naval Radiological Defense Laboratory, San Francisco, California
(Received February 22, 1954)

Schnadt-type impact specimens of SAE 1019 steel were irradiated with 18.6-Mev deuterons for the purpose of studying the influence of radiation on the brittle property as measured by the change in transition temperature. The effect was compared with that of two, five, and ten percent strain hardening. Microhardness studies were made to determine the extent and location of the radiation effect. An integrated flux of 29.6 microampere-hr per cm² shifted the transition temperature from −1°C to 18°C. The embrittling action was not a linear function of dose. Hardness was increased from 180 to 380 Knoop numbers. It was found to depend on the depth of penetration as well as the integrated flux. While radiation caused an effect similar to strain hardening, the nature of this effect was different. Annealing studies showed recovery of the irradiated material occurred between 260°C and 480°C. An interstitial vacancy diffusion process was indicated. Activation energies increased as recovery progressed. Recovery of the five percent strain hardened material occurred between 315°C and 371°C and would appear to be relaxation of internal stresses by the movement of dislocations.

INTRODUCTION

WITHIN recent years considerable research has been done on the effect of nuclear radiation to the physical properties of metals. Slater[1] and Dienes[2] have written excellent summaries of the theoretical and experimental work done to date. A number of mechanisms have been proposed to explain the observed changes. In view of this, it was thought desirable to attempt to determine which model seemed most correct. Bruckner[3] has shown that the introduction of carbon to steel affects the ease of propagation of microfractures across the grain. This in turn raises the transition temperature, the temperature at which the mode of fracture changes from shear to cleavage.[4–7] Cold working steel will also cause the transition temperature to shift upwards[8] as the stress for plastic deformation is increased. Some experiments have shown that radiation affects the plastic property of metal in a manner similar to adding carbon to steel.[9,10] In other experiments it would appear that the effect is similar to that of cold working. Seitz[11] has proposed that cold work produces dislocations and vacancies but probably does not generate interstitials in significant numbers. If radiation produces equal numbers of interstitials and vacancies, then there should be an observable difference between cold work and radiation effects.

In this investigation a comparison between these effects is made by studying the brittle property of steel as indicated by changes in the transition temperature under impact loads. The effects measured are relative changes as the exact mechanism of the transition between shear and cleavage fracture in steel is not understood. The extent and location of the radiation effect is determined by making microhardness studies.

EXPERIMENTAL PROCEDURE

The steel chosen for study was SAE 1019 as it has a very sharp transition temperature occurring in a convenient range. The principle chemical constituents are summarized in Table I. To relieve rolled-in stresses, the stock was preheated for 20 minutes and then stress relieved under atmospheric conditions for one hour at 620°C. Material for strain hardening studies was prepared from 36.6 cm lengths of bar stock elongated in tension. A Baldwin-Southwork Tensile machine with a maximum capacity of 120 000 pounds was used. The rate of straining was approximately 1000 psi per 30 seconds.

The type of impact specimen selected was a Schnadt, reduced in all its dimensions (Fig. 1). This configuration permitted irradiating a maximum percentage of the

TABLE I. Principle chemical constituents of steel tested other than iron.

Constituent	Percent by weight
Carbon	0.1900
Manganese	0.7210
Silicon	0.0060
Sulfur	0.0340
Phosphorus	0.0100
Chromium	0.0610
Nickel	0.0450
Molybdenum	0.0470
Aluminum	0.0042
Copper	0.0530
Cobalt	0.0042

* This work was supported by the Bureau of Ships, U. S. Navy.
† Part of a dissertation submitted to Yale University in partial fulfillment of the requirements for the Ph.D. degree.

[1] J. C. Slater, J. Appl. Phys. **22**, 237 (1951).
[2] G. J. Dienes, U. S. Atomic Energy Commission report AECU-2196, (April, 1952).
[3] W. H. Bruckner, Welding J. **30**, 459S (1951); **29**, 467S (1950).
[4] C. Zener and J. H. Hollomon, Am. Soc. Metals **33**, 163 (1944).
[5] N. Davidenkov and P. Sakhavov, Tech. Phys. U.S.S.R. **5**, 758 (1938).
[6] E. Orowan, Repts. Progr. Phys. **XII**, 186 (1949).
[7] C. H. Lorig, Trans. Am. Soc. Metals **44**, 30 (1952).
[8] E. Folkhand, Welding J. (August, 1951).
[9] E. Orowan, Am. Soc. Metals Symposium (June, 1950).
[10] W. Shockley, Seminar of Am. Soc. Metals 131 (1948).
[11] F. Seitz, Advances in Physics **1**, 43 (1952).

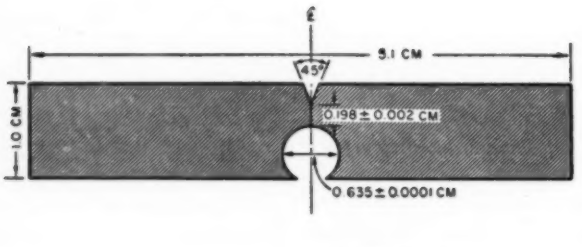

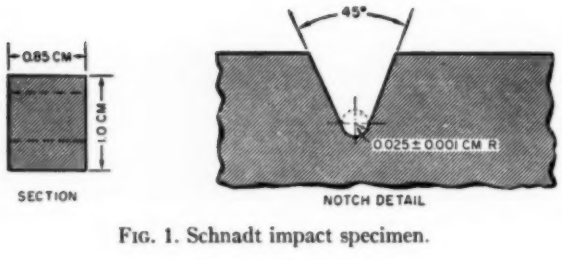

FIG. 1. Schnadt impact specimen.

portion of the metal that would fracture under impact and utilized the entire cross section of the collimated cyclotron beam so that a number of samples could be bombarded at one time. It was also desirable as the material tested is under a triaxial tensile load. At the time of fracture, the hole is filled with a hardened steel pin through which is passed the impact force of the hammer. The amount of energy expended in deforming the pin is negligible. A web cross section of 0.198×0.85 cm was used since the ratio of energy absorbed in shear fracture to that of cleavage is ten to one. This value corresponds well with the shear-cleavage ratio obtained in the standard Charpy bar test. Furthermore, the chance of data scatter was reduced because the transverse plastic contraction for shear fracture was not as excessive as that for smaller cross sections. The impact specimens were prepared under controlled machining procedures and rates in order to minimize the effect of machining strains and temperature. The longitudinal axis of all specimens was taken parallel to the direction of rolling in an attempt to exclude the effect of rolled-in inclusions. The notch radius was checked frequently to insure that it was maintained even though some investigators do not seem to feel it is very critical.[12] During the machining of strain hardened material, a high-velocity air jet was used for cooling to prevent annealing. It had been noted that oil cooling was not satisfactory.

Impact testing of the samples was done on a Baldwin-Southwork plastic impact machine having a maximum energy of 16 ft-lb. The desired temperatures for fracturing were obtained by immersing the samples in a bath until thermal equilibrium had been reached. A mixture of acetone and dry ice was used for values below 0°C, water for values between 0°C and 88°C, and transformer oil for values above this. The specimens were transferred to the jig with tongs that had also been immersed in the bath. The time required for this operation was five seconds. Since the temperature of the specimen increased at a maximum rate of only 0.14°C per second at 0°C, it was felt that the transfer technique was adequate, especially in view of the fact that the interior temperatures would change at a slower rate.

The conditions of irradiation and annealing temperatures were simulated in order to determine the effect on the base metal. For irradiation, specimens were placed in a Dewar flask filled with liquid nitrogen for a period of time equal to that required for irradiation. These were stored at room temperature and then fractured. In the case of annealing, specimens were annealed in a dried helium atmosphere to prevent oxidation at temperatures ranging from 430°C to 650°C (±1°C). After fracturing, samples were polished, etched for 20 seconds with two percent Nital at room temperature, and then checked under a microscope at a magnification of 125X.

The impact specimens were irradiated on the 60-in. cyclotron at the University of California using special low-temperature equipment developed and built by North American Aviation Company. A six-sided turret was used for mounting. Three samples were placed on each side with their notches along the same horizontal center line. A 0.025 mm copper foil was placed over them to check the integrator and also get distribution of the flux. The turret was placed inside a cooling chamber through which helium was blown that was cooled to liquid nitrogen temperature. Two Dural foils were used as windows for the external beam. Deuterons of 19.6-Mev energy were used for the bombarding particles because of their greater range in steel than other available particles from the 60-in. cyclotron. However, the energy of the particles on striking the specimens was 18.6 Mev because of passing through the above-mentioned copper and Dural foils. Since previous experiments have shown an integrated flux of 10^{16} to 10^{18} particles per cm^2 will produce observable effects,[13–15] the samples were irradiated in excess of 10^{17} deuterons per cm^2. The average value for the total radiation on each sample was 6.66×10^{17} or 29.6 microampere-hr per cm^2. Six samples received approximately one-half this amount, 16.2 microampere-hr per cm^2 each, to see if the shift in transition temperature was a linear function of dose. Two rectangular blocks designed for the purpose of hardness tests received 29.2 and 60.0 microampere-hr per cm^2. In the former case, the block had a thermocouple placed 1.0 mm below the surface at the point of maximum beam intensity to give an estimate of the internal temperatures of the steel during irradiation.

The horizontal profile of the integrated flux was

[12] R. V. Southwell *et al.*, Trans. Am. Soc. Mech. Engrs. **56**, 97 (1934).

[13] R. E. Jamison and T. H. Blewitt, Phys. Rev. **86**, 641 (1952).

[14] T. H. Blewitt and R. R. Coltman, U. S. Atomic Energy Commission report AECD 3095.

[15] Harmon, Eidam, and Greib, Quart. Progr. Rept., Purdue Univ. (July 1 to September 30, 1952).

determined by cutting the 0.025 mm copper foil into 2.0 mm strips and counting the gamma activity of 250-day half-life Zn^{65}. The vertical profile was obtained by cutting each of these 2.0 mm strips into 1.0×2.0 mm rectangles and counting them in the same manner.

Since the estimated penetrating power of 19.6-Mev deuterons is 0.5 mm,[16] it was necessary to turn the samples to the opposite side and reirradiate. Room temperature was used for storage. It was felt this was adequate as cold work effects on mild steel do not anneal out within the period of time considered

Hardness measurements were made with a Tukon microhardness tester, the value being expressed in Knoop hardness numbers (KHN). Initial measurements on the irradiated steel were made on the block which received an integrated flux equal to that of the impact specimens (Block A). After irradiation, a taper was ground on the block. Hardness *versus* integrated flux measurements were taken in the direction of the maximum flux gradient which was parallel to the vertical direction of the beam. Hardness *versus* depth of penetration measurements were taken perpendicular to this in a direction along the taper.

Isothermal annealing studies were made on the block which received 60.0 microampere-hr per cm² (Block B). The block was composed of four strips joined together by two pins. A wedge-shaped piece of steel 2.54×10.1 cm and varying from 0.610 to 0.229 mm covered the block on the beam side. This reduced the energy of the beam, thus producing maximum hardness on the surface of the strips without further machining. The taper allowed for error in the hardness *versus* depth of penetration measurements previously made on the other block. A 0.025 mm copper foil was placed on the beam side of the collimating slit. In addition a foil was placed next to the wedge. This procedure was introduced since hardness measurements on Block A suggested checking the flux distribution on either side of the collimating slit to determine the degree of dispersion.

EXPERIMENTAL RESULTS

The energy absorption for fracture of the untreated steel as a function of temperature is given in Fig. 2. The transition temperature was found to be −1.1°C. The mean deviation was ±2°C. Tests showed that the thermal conditions of irradiation, approximately liquid nitrogen temperature, had no effect on the transition temperature. However, annealing temperatures over 540°C caused a downward shift. Polished sections of these samples showed recrystallization had taken place. For this reason all annealing temperatures had to be kept to 540°C or lower. The transition temperature for two, five, and ten percent strain hardened steel is 8.5°C, 9.5°C, and 14.5°C, respectively. No change was noted in the energy absorption for cleavage fracture.

[16] Aron, Hoffmen, and Williams, U. S. Atomic Energy Commission report AECU-663.

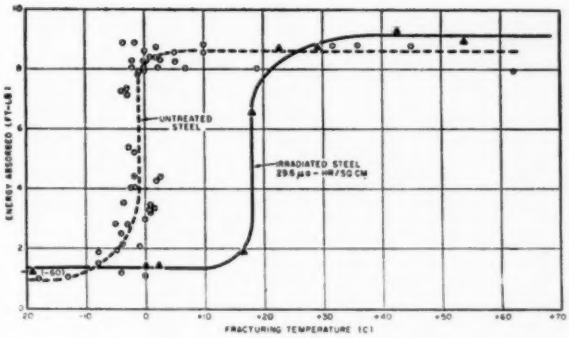

FIG. 2. Transition curve for untreated and irradiated impact specimens.

The energy required for shear fracture was less than that of the untreated steel. This decrease was more pronounced for greater amounts of cold work. At ten percent, the stock was beginning to neck down. Consequently, five percent strained material was used for annealing studies. Specimens annealed at temperatures ranging from 204°C to 315°C showed no recovery. Those annealed at temperatures above 371°C showed complete recovery.

No shift in transition temperature, from that of the untreated steel, was observed when impact specimens received a flux of 16.2 microampere-hr per cm². However, a flux of 29.6 microampere-hr per cm² shifted the transition temperature upwards to 18°C (Fig. 2). This is even greater than the shift for severe cold working conditions of ten percent strain. The energy absorption value for cleavage fracture remained 50 percent higher than that of the basic steel. The value for shear fracture remained seven percent higher. It will be noted that the transition curve for the irradiated steel has a slope similar to that of the untreated steel. This similarity between them was assumed to exist in determining other transition curves in order to reduce the number of irradiated specimens required for various annealing temperatures. Furthermore, it was also assumed that the curves would have a mean divergence of ±2°C. Transition curves were determined for specimens irradiated and then annealed at temperatures ranging from 260°C to 590°C. At 260°C, there was very little recovery. At 315°C, the transition temperature was lowered from 18°C to 8.8°C, thereby showing partial recovery of the radiation effect had commenced. At 480°C, the transition temperature had shifted down to 0°C and could be considered to be at the original state.

The percent recovery is expressed as

$$\phi=(S-A/S-C)\times 100, \qquad (1)$$

where S is the shift of transition temperature for the strained or irradiated sample, A is the transition temperature for the annealed sample, and C is the transition temperature for the untreated steel. Letting ϕ equal zero at 260°C and considering the errors, the

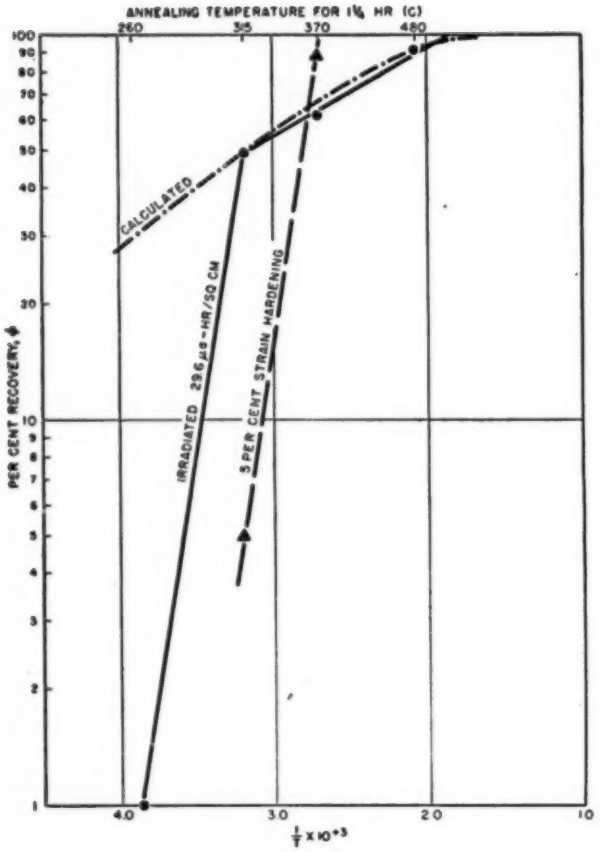

FIG. 3. Transition temperature recovery for irradiated and strain hardened steel.

temperature at which recovery is complete is estimated to be 530°C. Figure 3 shows the percent recovery as a function of the inverse temperature for irradiated and strain hardened specimens. It would appear that a diffusion process may be occurring of the form $\phi = f(e^{-H/RT})$.

Temperature measurements were made to determine the relation between the flux of the deuteron beam and the temperature of the metal during irradiation. The estimated maximum temperature of the specimen was −40°C on the surface and 50°C within. However, peak fluxes lasted only five to twenty seconds. Since the highest average beam flux was 13.5 microamperes per hr per cm², the average temperature was −55°C and 20°C, respectively.

Hardness measurements made on the untreated steel showed an average value of 180 KHN (±2 percent). For stock strained five percent, the hardness was 178 KHN (±8 percent). Hardness as a function of distance from the steel surface first encountered by the deuterons is given in Fig. 4 for an integrated flux of 29.6 microampere-hr per cm². Maximum hardness occurred at 0.42 mm, which is approximately 85 percent of the deuteron's range in steel, and then rapidly decreased to zero at 0.49 mm. For the first 70 percent of the range, the increase was only 20 percent of the total observed. Hardness values at constant depths of penetration reached a maximum and were symmetrical about the point of highest integrated flux. There was no change after successive annealing at temperatures ranging from 150°C to 260°C. A measurement of the 0.43 mm penetration area indicated that no annealing effect occurred after a period of six weeks had elapsed between measurements. Hardness as a function of integrated flux is given in Fig. 5. It will be noted that no saturation effect had occurred up to 60 microampere-hr per cm². Isothermal annealing curves for the strips receiving a total integrated flux of 60 microampere-hr per cm² are given in Fig. 6.

The integrated flux curves obtained from the foils placed on either side of Block B showed some beam dispersion had occurred. The beam was approximately 1.3 and 1.8 mm wider than the 6.33 mm collimating slit.

DISCUSSION

Observations show that there is an embrittling action in mild steel due to irradiation. This effect is not a linear function of the integrated flux. The increase in transition temperature may be considered to be due to deuteron produced interstitial-vacancy pairs affecting the normal movement of dislocation and slip within the grain, when the specimen is under external stresses. This leads one to believe that there is a fine dispersion of these interstitial-vacancy pairs, which is consistent with the observation of Maloof[17] who found that steel was embrittled by a fine dispersion of particles within the grain. It would also seem that some minimum number must be present per unit volume to influence the plastic property of the steel. Evidence of this is given by the absence of a shift in the transition temperature for a 16.2 microampere-hr per cm² integrated flux. In addition, the hardness was found to be a nonlinear function of the integrated flux.

The experiment suggested two other possibilities to explain the embrittlement. First, the steel could have been embrittled by hydrogen formed by the deuteron-proton reaction of Fe^{54} and Fe^{58}. However, Seabrook[18] has shown that this will not exist if the sample is

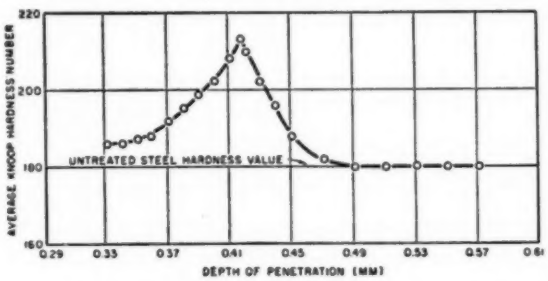

FIG. 4. Hardness *vs* depth of beam penetration total current of 29.6 μa-hr per sq cm.

[17] S. R. Maloof, Trans. Am. Soc. Metals 44, 264 (1952).
[18] J. B. Seabrook *et al.*, Trans. Am. Inst. Mining Met. Engrs. 188, 1317 (1950).

allowed to remain at room temperature for 72 hours. Since the impact specimens were not fractured earlier than five days after irradiation, any such effect must be considered negligible. Second, the embrittlement might be due to precipitation hardening caused by ionization. The deuteron gives up a great deal of energy by ionization at the beginning of its range in steel.[19] This energy would locally heat the metal and a precipitate could be formed. However, the fact that the maximum hardness occurs at the latter portion of the deuteron's range also makes this possibility negligible.

Theoretically, the number of interstitials produced should be greatest at the latter portion of the deuteron's range, this being the region where elastic collision occurs and the atoms are displaced from their lattice sights by the deuterons. Therefore, the hardness of the steel should be changed most near the end of the range. As mentioned above, the effect was present. This further confirms the view that interstitial-vacancy pairs are responsible for the radiation effects observed.

It has been previously noted that the critical shear stress of some metals is increased by irradiation.[14] The observed embrittlement of the steel indicates this is taking place, for an increased shear stress results in a higher cleavage stress which enhances the probability of brittle fracture. Moreover, the energy required to fracture the specimens in shear is seven percent higher after irradiation. This effect is contrary to that of strain hardening, as the energy for shear fracture varies inversely with the degree of cold work.

Annealing studies, made on irradiated impact specimens, indicate that recovery may be the result of recombination of the Frenkel defects by an interstitial-vacancy diffusion process. The activation energy

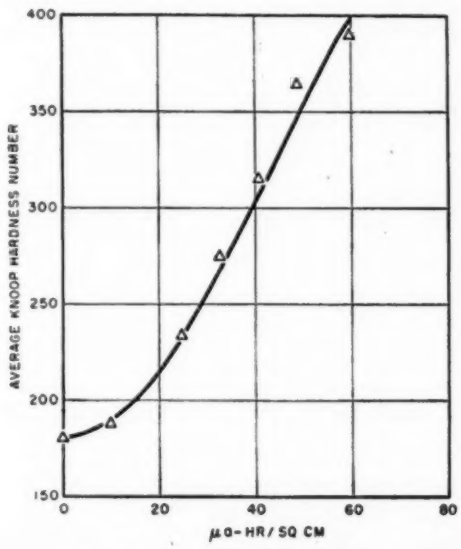

FIG. 5. Increase in hardness *vs* total deuteron beam current.

[19] F. Seitz, Trans. Faraday Soc. No. 5, 271 (1949).

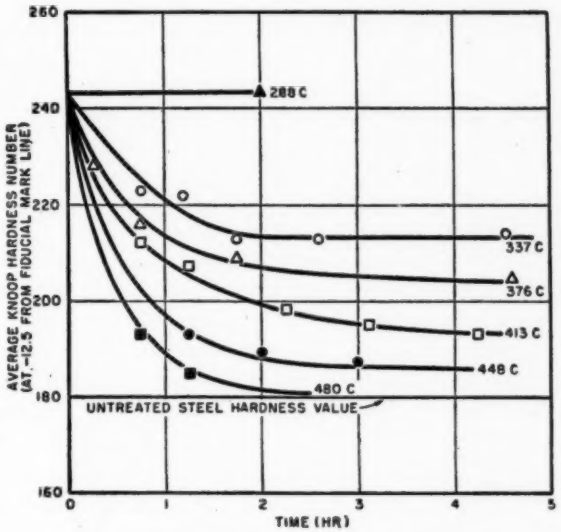

FIG. 6. Isothermal recovery curve of hardness increases due to 60 μa-hr per sq cm beam.

for this recovery[20–22] was found to be approximately 6900 cal/mole between 315°C and 480°C. However, the rate of recovery is greater between 260°C and 315°C. Therefore, the activation energy is lower. These values are abnormally low, especially in view of the fact that the radiation effect does not anneal out at room temperature during the time the impact specimens are stored. This suggests that the computed activation energies are not necessarily the actual values for recombination of the defects. It would seem recovery is not solely a function of the interstitial diffusion process but strongly dependent on the number of defects present per unit volume above a minimum number. That is, no shift in the transition temperature will be evident when the defects are less than some number N_0. However, when

$$N = N_0 + N', \tag{2}$$

where $N' \ll N_0$, there will be a marked shift in the transition temperature. Thus, a small reduction of the number of defects will bring about a large reduction in transition temperature which manifests itself as if a large number of defects are annealing out and thereby gives a low activation energy.

Similar to the transition temperature recovery of irradiated specimens, hardness recovery may also be considered an interstitial diffusion process, where the rate of change of interstitial-vacancy pairs is

$$dn/dt = D_0(n - n_0)\exp(-H/RT), \tag{3}$$

$n_0 - n$ being the number of interstitial vacancy pairs at any time t. From this equation the activation

[20] A. S. Nowick, J. Appl. Phys. 22, 1182 (1951).
[21] C. Wert, J. Appl. Phys. 21, 1196 (1950); Phys. Rev. 79, 601 (1950).
[22] A. D. LeClaire, Progr. Metal Phys. 1, 306 (1949).

energy may be expressed as

$$H=R\ln(t_1/t_2)(T_1T_2/T_2-T_1). \quad (4)$$

Numerical values of H can be determined at various degrees of hardness using Fig. 6. The values obtained are not constant over the entire range. They vary from less than 12 000 calories per mole as recovery commences to 25 000 calories per mole when no further recovery occurs for extended annealing times. Variable activation energies as recovery progresses have been mentioned in the literature.[23–25] When recovery commences, there are present large numbers of Frenkel defects which elastically distort the lattice and lower the energy barrier between the interstitial and vacancy. However, annealing of the defects will allow the distorted lattice to relax to a more normal configuration and a higher activation energy is then required for further interstitial diffusion.

A comparison of the recovery temperatures for irradiated and strain hardened steel indicates that the annealing processes are different. In the latter case complete recovery occurs within a temperature interval of 55°C. Consideration of this temperature interval indicates that the annealing effect may be due to the relief of interval stresses by the movement of dislocations.

In the case of strain hardened material, the increased scatter of hardness points and reduction of the impact energy necessary for shear fracture are probably caused by narrow regions of residual strains[26] that hinder the movement of slip planes. However, when sufficient stress is applied to initiate fracture, this residual energy will assist in its propagation. Less external energy is then required to fracture the impact specimen.

CONCLUSION

Deuteron bombardment affects the impact property of mild steel in a manner similar to strain hardening, although the nature of this effect appears to be different. That is, both radiation and strain hardening raise the transition temperature; but annealing studies indicate that radiation recovery occurs by interstitial-vacancy diffusion while strain hardening anneals out in a different manner, possibly by the movement of dislocations.

Measurements show the extent of the radiation effect is determined by the number of deuterons per cm² striking the metal. An integrated flux exceeding 16.2 microampere-hr per cm² is necessary to produce an observable change in the transition temperature. However, hardness begins to increase for a value of approximately ten microampere-hr per cm². Furthermore, the hardness increases by a factor of five at 85 percent of the deuteron's range. This localizes the major portion of the radiation effect at approximately 0.42 mm below the surface of the notch and hole on the impact specimens.

The increase of hardness with depth of penetration leads to the conclusion that the deuteron radiation effect is a production of interstitial-vacancy pairs. It could not be determined from the measurements made whether the defects were acting singularly or in some combination. However, hardness annealing studies lead to the belief that the first effect is the recombination of single defects at low activation energies. As recovery progresses, the remaining defects will be of the cluster type. These have greater stability and explain the residual hardness effect at the lower annealing temperatures. The combined effect of these processes can account for the observed variable activation energy.

The author would like to express his appreciation to Professor E. R. Parker of the University of California who provided valuable guidance in the execution of this problem. He is also indebted to Professor M. L. Wiedmann of Yale University for his suggestions and continued interest and to Dr. Alan Andrews and other members of the North American Aviation group at Berkeley, California, for many helpful discussions. The cooperation of this group, in operating the special low-temperature and counting equipment, and the University of California Metallurgy Department, in permitting use of their test equipment, is greatly appreciated.

[23] A. W. Overhauser, U. S. Atomic Energy Commission report AECU-2358 (November, 1952).
[24] G. J. Dienes, Phys. Rev. **91**, 1283 (1953).
[25] A. W. Overhauser, Phys. Rev. **92**, 530(A) (1953).
[26] G. B. Greenough, Proc. 7th Intern. Congr. Appl. Mech. **1**, 431 (1948).

Effect of Velocity Distribution on Traveling-Wave Tube Gain

D. A. WATKINS AND N. RYNN
Stanford University, Stanford, California
(Received February 22, 1954)

The density-function method is applied to the one-dimensional model of the traveling-wave tube to determine the effect of velocity distribution on traveling-wave tube performance. For narrow velocity spreads, a term is introduced into the root equation for the incremental propagation constants which is like the space charge term $4QC$ and directly added thereto. This term is proportional to the ratio of the variance of the distribution to the square of the gain parameter C. For a typical tube, thermal velocities are found to reduce the gain by less than one part in 10^4. In a tube employing confined magnetic focusing, and employing a high perveance beam, the velocity spread resulting from space charge lowers the gain by about 1 percent.

INTRODUCTION

In a previous paper[1] one of the authors described a method of solving one-dimensional small-signal electron beam problems so as to include a velocity distribution. The purpose of the present paper is to apply this method to Pierce's[2] one-dimensional model of the traveling-wave tube and thereby show the effect of velocity distribution on traveling-wave tube gain. In a previous issue of this journal Parzen and Goldstein[3,4] treated this problem by considering that the electron beam in a traveling-wave tube could be regarded as a gas in which the process of acceleration of the beam from the cathode to its final drift potential and the ac process of interaction with an electromagnetic wave thereafter are both "isothermal." This approximation, which is not valid, leads to the prediction of very large effects as illustrated by their example in which the gain of a typical tube is reduced to 65 percent compared with the same tube with no velocity spread. That well designed and well constructed tubes show no such discrepancy between measured gain and theoretical gain neglecting velocity spread is in itself substantial evidence that the effect of velocity spread is small. This is further illustrated by electron beam measurements of helix impedance[5] in which good agreement between theory and experiment was obtained. In a specific case with Parzen and Goldstein's factor ignored, the measured impedance and the calculated impedance were in the ratio 0.86. Employing their theory would make this same ratio 4.2. In other words the helix would be required to have an impedance which is four times the theoretical value.

Estimates of collision frequency and mean free path in an electron cloud have been worked out by Vlasov.[6] Application of his results indicates that the average number of collisions per electron during its flight through a typical traveling-wave tube is less than one percent. Since thermal equilibrium is achieved through the mechanism of collisions, this would suggest that there are not enough collisions for equilibrium to be established. Rather, their almost total absence is justification for ignoring them as will be done in the remainder of this paper.

FORMULATION

In the usual small-signal analyses of electron beam devices without velocity spread, the state of the electron stream is described by the well-known dependent variables charge density, convection current, and velocity which are single-valued functions of time and distance along the stream. When a velocity spread is to be taken into account, the state of the electron stream may be described by a density function, $F_t(z,u,t)$,* such that $[F_t(z,u,t)/e]dzdu$ is the number of electrons between z and $z+dz$ with velocity (in the z direction) between u and $u+du$ at the time t. The magnitude of the electronic charge is e. The convection current, $i_t(z,t)$, and the linear charge density, $\rho_t(z,t)$, are related to the density function as follows:

$$i_t(z,t) = -\int_{-\infty}^{\infty} uF_t(z,u,t)du; \tag{1}$$

$$\rho_t(z,t) = -\int_{-\infty}^{\infty} F_t(z,u,t)du. \tag{2}$$

The dependent velocity variable used in analyses without velocity spread has no direct counterpart when the density function is used. Rather, the velocity is treated as an independent variable like time and distance so that the electron stream moves in time through a two-dimensional phase space whose coordinates are z and u. As a consequence of conservation of energy and conservation of electrons, the Liouville theorem of statistical mechanics states that the density function, $F_t(z,u,t)$, has the property that its total derivative with

[1] D. A. Watkins, J. Appl. Phys. **23**, 568 (1952).
[2] J. R. Pierce, *Traveling-Wave Tubes* (D. Van Nostrand Company, Inc., New York, 1950).
[3] P. Parzen and L. Goldstein, J. Appl. Phys. **22**, 398 (1951).
[4] M. E. Hines, J. Appl. Phys. **22**, 1385 (1951) (Letter to the Editor commenting on Reference 3).
[5] D. A. Watkins and A. E. Siegman, J. Appl. Phys. **24**, 917 (1953).
[6] A. Vlasov, J. Phys. **9**, 25 (1945).

* In reference 1 this was called the *distribution function*. *Density function* is the commonly accepted name.

respect to time is zero. Thus,

$$\frac{dF_t(z,u,t)}{dt}=0. \tag{3}$$

In terms of partial derivatives, this may be written

$$\frac{\partial F_t(z,u,t)}{\partial t}+u\frac{\partial F_t(z,u,t)}{\partial z}+\frac{du}{dt}\frac{\partial F_t(z,u,t)}{\partial u}=0. \tag{4}$$

This is the Boltzmann transport equation neglecting collisions. If the electron stream is acted upon by an electric field in the z direction the acceleration du/dt is related to the electric field $[-\partial V_t(z,t)/\partial z]$ through the force equation

$$\frac{du}{dt}=\eta\frac{\partial V_t(z,t)}{\partial z}, \tag{5}$$

where η is the magnitude of the electronic charge-to-mass ratio, and all the units are mks.

Separating all quantities into dc and ac parts, as is commonly done in small-signal analyses, we have

$$\begin{aligned} F_t(z,u,t)&=F_0(z,u)+F(z,u)e^{j\omega t};\\ V_t(z,t)&=V_0(z)+V(z)e^{j\omega t};\\ i_t(z,t)&=-I_0+i(z)e^{j\omega t}. \end{aligned} \tag{6}$$

Substitution of Eqs. (5) and (6) into Eq. (4) leads to an equation for the ac parts which is

$$j\omega F(z,u)+u\frac{\partial F(z,u)}{\partial z}+\eta\frac{\partial V}{\partial z}\frac{\partial F_0(z,u)}{\partial u}+\eta\frac{\partial V_0}{\partial z}\frac{\partial F(z,u)}{\partial u}=0, \tag{7}$$

where products of ac quantities have been neglected. For a traveling-wave tube the dc potential, V_0, is constant in the circuit portion of the tube so that $\partial V_0/\partial z=0$, and Eq. (7) simplifies to

$$j\omega F(z,u)+u\frac{\partial F(z,u)}{\partial z}+\eta\frac{\partial V}{\partial z}\frac{\partial F_0(u)}{\partial u}=0. \tag{8}$$

We will call this the *electronic equation* for it corresponds to the single-valued-velocity electronic equation of Pierce[7] put in differential form and allowing a velocity distribution. It relates the ac density function $F(z,u)$ to the ac potential $V(z)$. This equation is to be combined with Pierce's *circuit equation*[8] which relates the potential $V(z)$ to the ac convection current $i(z)$ which in turn is related to $F(z,u)$ through Eq. (1). Dropping the functional notation, the circuit equation is

$$V=\left[\frac{\Gamma\Gamma_1(E^2/\beta^2P)}{2(\Gamma_1^2-\Gamma^2)}-j\frac{\Gamma}{\omega C_1}\right]i, \tag{9}$$

where the notation is that used by Pierce. In deriving Eq. (9), Pierce has replaced the operator $\partial/\partial z$ with $-\Gamma$. If we reverse that process and employ the following new variables together with Eq. (1)

$$\begin{aligned} \frac{E^2}{2\beta^2P}&=K;\\ C_1&=\frac{\beta_e}{2K\omega Q};\\ \phi&=\beta_eCz=2\pi CN;\\ V(z)&=V'(\phi)e^{-j(\phi/C)};\\ \Gamma_1&=j(1+bC)\beta_e;\\ F(z,u)&=F'(\phi,u)e^{-j(\phi/C)}. \end{aligned} \tag{10}$$

Equation (9) becomes

$$\begin{aligned} C^2\frac{\partial V'}{\partial\phi}-j2CV'+bC(2+bc)\int_\phi V'd\phi&\\ =-jK\Big\{(1+bC)[C+2QC(1+bC)]&\\ \times\int_{-\infty}^{\infty}u\left[F'-j\frac{1}{C}\int_\phi F'd\phi\right]du&\\ +2QC\int_{-\infty}^{\infty}u\left[C^2\frac{\partial^2F'}{\partial\phi'}-j3C\frac{\partial F'}{\partial\phi}\right.&\\ \left.+j\frac{1}{C}\int_\phi F'd\phi\right]du\Big\},& \end{aligned} \tag{11}$$

and Eq. (8) becomes

$$j\omega F'+\beta_eu\left[C\frac{\partial F'}{\partial\phi}-jF'\right]=\beta_e\eta\left[\frac{\partial V'}{\partial\phi}-jV'\right]\frac{\partial F_0}{\partial u}. \tag{12}$$

Thus Eqs. (11) and (12) are two equations in V' and F' which are to be solved simultaneously subject to the appropriate boundary conditions at $\phi=0$, the input to the traveling-wave tube. The notation is that used by Pierce except for the new symbols required by the use of the density function which have been defined here. At the entrance to a traveling-wave tube there is an applied voltage V_i. Since the electron stream must enter unmodulated, the ac part of the density function F' must be zero at the input. If the traveling-wave tube is matched to the signal source at the input we have the

[7] See reference 2, p. 13.
[8] See reference 2, Eq. (7.8), p. 112.

additional requirement that

$$\frac{\partial V}{\partial z}=-\Gamma_1 V_i \quad \text{at} \quad z=0.$$

Thus we have three boundary conditions which are

$$\left.\begin{aligned} F'(\phi,u)&=0\\ V'(\phi)&=V_i\\ \frac{\partial V'}{\partial \phi}&=-jbCV_i \end{aligned}\right\} \quad \text{at} \quad \phi=0. \tag{13}$$

The solution to Eqs. (11) and (12) subject to these conditions is carried out by means of the Laplace transform such that the distance variable ϕ corresponds to the Laplace transform variable δ and $V'(\phi)$ and $F'(\phi,u)$ go into $\mathfrak{V}(\delta)$ and $\mathfrak{F}(\delta,u)$, respectively. With the use of Eq. (13), Eqs. (11) and (12) become when transformed

$$C^2\delta\mathfrak{V}-C^2V_i-2C\mathfrak{V}+\frac{bC(2+bC)}{\delta}\mathfrak{V}+j\frac{C(2+bC)V_i}{\delta}=jKA\int_{-\infty}^{\infty}u\mathfrak{F}du, \tag{14}$$

$$\mathfrak{F}=\frac{-\beta_e[(\delta C-j)\mathfrak{V}-CV_i]\dfrac{\partial F_0}{\partial u}}{j\omega+\beta_e u(\delta C-j)}, \tag{15}$$

where

$$A=-C\left(1+bC+4QCb+2b^2QC^2-j\frac{b}{\delta}-2j\frac{b^2QC}{\delta}+2\delta^2QC^2-j6\delta QC\right)+\left(\frac{j}{\delta}+\frac{4QCb}{\delta}+4QC\right). \tag{16}$$

Noting that $C^3=KI_0/4V_0$, where I_0 is the dc current and V_0 is the dc beam voltage which we will take to correspond to the average velocity of the stream, and using $\beta_e=\omega/u_0$ where u_0 is the average velocity, an integration of Eq. (15) by parts leads to

$$\int_{-\infty}^{\infty}u\mathfrak{F}du=-\frac{2jC}{K\delta^2}[(\delta C-j)\mathfrak{V}-CV_i]\xi; \tag{17}$$

$$\xi=\frac{u_0}{I_0}\int_{-\infty}^{\infty}\frac{\delta^2C^2F_0du}{[j+(u/u_0)(\delta C-j)]^2}, \tag{18}$$

since $F_0(\phi,\pm\infty)=0$. An examination of ξ reveals that it is of the order of magnitude unity although this is not obvious at first glance. We also take b and QC to be of magnitude unity or less and assume that C is small compared with unity. Hindsight tells us that we will be interested in δ when its magnitude is about unity. With these restrictions Eqs. (14) and (17) can be greatly simplified to yield, when combined, the following expression for $\mathfrak{V}$ in terms of V_i and the parameters of the system.

$$\mathfrak{V}=\frac{\delta^2V_i}{\delta^3+jb\delta^2+(4QC\delta+jb4QC+j)\xi}. \tag{19}$$

At this point the outstanding problem is the evaluation of ξ which will be discussed in the following sections.

NO VELOCITY SPREAD

For no velocity spread, the dc density function F_0, is a Dirac delta function with an appropriate coefficient such that

$$\int_{-\infty}^{\infty}uF_0du=I_0.$$

Its form is as follows

$$F_0=(I_0/u_0)\delta(u-u_0), \tag{20}$$

where $\delta(u-u_0)$ is the delta function. When this is inserted into Eq. (18), the integration is readily carried out with the result that

$$\xi=1. \tag{21}$$

For this case Eq. (19) becomes

$$\mathfrak{V}=\frac{\delta^2V_i}{\delta^3+jb\delta^2+4QC\delta+jb4QC+j}. \tag{22}$$

This expression for the transformed ac voltage corresponds exactly to that given by Pierce for no circuit loss ($d=0$). The root equation which is formed by setting the denominator of Eq. (22) equal to zero is[9]

$$\delta^3+jb\delta^2+4QC\delta+jb4QC+j=0. \tag{23}$$

This is a third-degree equation specifying the incremental propagation constants δ_1, δ_2, and δ_3 of the three forward waves of the system.

RECTANGULAR DENSITY FUNCTION

One of the more tractable density functions which may be considered is that of the rectangular density function shown in Fig. 1. This is expressed mathematically by

$$\left.\begin{aligned} &F_0=(I_0/2\Delta u_0) \quad u_0-\Delta<u<u_0+\Delta;\\ &F_0=0 \quad \text{otherwise.} \end{aligned}\right\} \tag{24}$$

If this is inserted into Eq. (18), ξ becomes

$$\xi=\frac{1}{2\Delta}\int_{u_0-\Delta}^{u_0+\Delta}\frac{\delta^2C^2du}{[j+(u/u_0)(\delta C-j)]^2}. \tag{25}$$

[9] See reference 2, Eq. (7.14), p. 113.

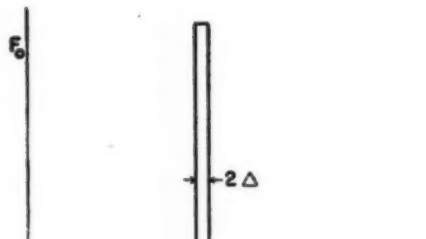

FIG. 1. The rectangular density function.

This is readily evaluated and simplified to

$$\xi=\frac{-j\delta^2}{\left[\delta^2+\left(\frac{\Delta}{u_0C}\right)^2\right][C\delta-j]}. \tag{26}$$

Since in obtaining Eq. (19) we took C to be small compared with unity, consistency requires us to drop the term $C\delta$ in the denominator of Eq. (26) so that

$$\xi=\frac{\delta^2}{\left[\delta^2+\left(\frac{\Delta}{u_0C}\right)^2\right]}. \tag{27}$$

The term (Δ/u_0C) may be retained because Δ/u_0 may be of magnitude comparable to C. It will be useful in the next section to have ξ expressed in terms of the normalized variance of the distribution where the variance is defined by

$$\sigma^2=\frac{\langle(u-u_0)^2\rangle_{Av}}{u_0^2}. \tag{28}$$

This is readily worked out for the rectangular case and is found to be

$$\sigma^2=\tfrac{1}{3}(\Delta/u_0)^2. \tag{29}$$

Inserting this into Eq. (27), ξ becomes

$$\xi=\frac{\delta^2}{\left[\delta^2+3\frac{\sigma^2}{C^2}\right]}. \tag{30}$$

When this is used with Eq. (19), the expression for the transformed voltage becomes

$$v=\frac{[\delta^2+S]V_i}{\delta^3+jb\delta^2+(4QC+S)\delta+jb(4QC+S)+j}, \tag{31}$$

and the root equation is

$$\delta^3+jb\delta^2+(4QC+S)\delta+jb(4QC+S)+j=0, \tag{32}$$

where

$$S=3(\sigma^2/C^2). \tag{33}$$

If Eq. (32) is compared with Eq. (23), the corresponding equation for no velocity spread, it is seen that wherever $4QC$ appeared we have now added S. Thus the effect of velocity spread is like the effect of space charge for this case. We need calculate no new curves to show this effect since the curves given by Pierce[10] may be applied by noting that S is like $4QC$ and may be added directly thereto. In Eq. (31), however, note that S appears in the numerator in a way that is not like $4QC$. Its effect there is to alter the initial value of each of the three waves. Since in practical cases S is commonly small compared with unity, this is of minor importance.

HALF-MAXWELLIAN DISTRIBUTION

When the velocity spread of interest is associated with the thermal spread in the emission velocities at the cathode, F_0 has the half-Maxwellian form (see Fig. 2) given by

$$F_0=2\alpha I_0 s(u-u_s)\exp[-\alpha(u^2-u_s^2)], \tag{34}$$

where

$$\alpha=m/2kT_c, \tag{35}$$

and $s(u-u_s)$ is the unit step function defined by

$$\begin{aligned} s(u-u_s)&=0 \quad u<u_s;\\ s(u-u_s)&=1 \quad u>u_s. \end{aligned} \tag{36}$$

The velocity of the slowest electrons in the stream is u_s given by

$$u_s=[2\eta U_0]^{\frac{1}{2}}, \tag{37}$$

where U_0 is the dc potential of the traveling-wave tube circuit with respect to that of the potential minimum in front of the cathode if the emission is space-charge limited or, of the cathode itself, if the emission is temperature limited. m is electronic mass, k is Boltzmann's constant, and T_c is the cathode temperature in degrees Kelvin. Note that U_0 will be slightly less than V_0 which we have taken to correspond to the average velocity rather than the slowest velocity. Inserting Eq. (34) into

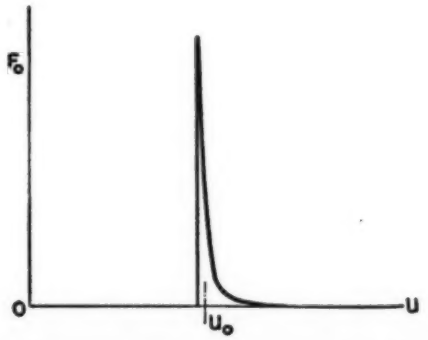

FIG. 2. The half-Maxwellian density function.

[10] See reference 2, Fig. 8.10, p. 126.

Eq. (18) we have

$$\xi=2\alpha u_0\int_{u_s}^{\infty}\frac{\delta^2C^2\exp[-\alpha(u^2-u_s^2)]du}{[j+(u/u_0)(\delta C-j)]^2}. \quad (38)$$

This integral cannot be evaluated explicitly. Some of the attempted approximations lead to the introduction of new roots into the root equation [the denominator of Eq. (19) set equal to zero]. Since no roots were added in the case of the rectangular function which was integrable without approximation, these are undesirable results. Further, we would not expect the number of roots to be different for the two cases to the same order of approximation. We are interested in finding the perturbation of the three waves found for the no-velocity-spread case.

An evaluation of Eq. (38) by expansion in terms of moments about the mean leads to

$$\xi\simeq 1-\frac{3}{4}\left(\frac{kT_e}{eV_0}\right)^2\frac{1}{\delta^2C^2}-j\left(\frac{kT_e}{eV_0}\right)^3\frac{1}{\delta^3C^3}+\frac{45}{16}\left(\frac{kT_e}{eV_0}\right)^4\frac{1}{\delta^4C^4}+\cdots. \quad (39)$$

Since δ is of the order of magnitude unity, this is approximately

$$\xi\simeq\frac{\delta^2}{\delta^2+\frac{3}{4}(kT_e/eV_0)^2\frac{1}{C^2}}, \quad (40)$$

for $(kT_e/eV_0)1/C<1$. Alternatively, the approximation may be made that the half-Maxwellian distribution is equivalent to the rectangular distribution as long as they are both narrow and if their zeroth and second moments about the mean are equal. We may then use Eq. (30) directly by inserting the appropriate value for the variance. This is found to be (for narrow distributions)

$$\sigma^2\simeq\frac{1}{4}\left(\frac{kT_e}{eV_0}\right)^2, \quad (41)$$

and S is approximately given by

$$S\simeq\frac{3}{4}\left(\frac{kT_e}{eV_0}\right)^2\frac{1}{C^2}\quad S<1, \quad (42)$$

so that Eqs. (30) and (40) are equivalent. Applying this to the example chosen by Parzen and Goldstein[3] in which $kT_e/e=0.1$ volt, $C=0.015$, and $V_0=500$ volts, we find $S=1.33(10)^{-4}$. The effect of this on the gain of the increasing wave in a tube with QC and d equal to zero may be found through the use of Fig. 8.14 of reference 2 which shows that

$$\frac{\partial x_1}{\partial(4QC)}\simeq-0.28, \quad (43)$$

where x_1 is the real part of the incremental propagation constant, δ_1, of the increasing wave. Thus, the gain for $S=1.33(10)^{-4}$ compared with the gain for $S=0$ is approximately

$$\frac{x_1|[S=1.33(10)^{-4}]}{x_1|[S=0]}=1-4.3(10)^{-5},$$

the change being less than 1 part in 10^4.

VELOCITY SPREAD DUE TO SPACE-CHARGE POTENTIAL DEPRESSION

In traveling-wave tubes using confined flow[11] the potential at the center of a solid cylindrical beam is lower than at the outside edge due to space charge. For this case the variance of the velocity distribution is given approximately by

$$\sigma^2=4.78(10)^6\frac{I_0^2}{V_0^3}.$$

A tube built at Stanford has $I_0/V_0^{\frac{3}{2}}=8(10)^{-6}$ and $C=0.15$. For this tube

$$\sigma^2=3.06(10)^{-4},$$
$$S=0.0407,$$

so that the reduction in gain is 1.3 percent.

CONCLUSION

The fact that the foregoing analysis shows that the velocity spreads encountered in ordinary traveling-wave tubes have a very small effect on the performance is a useful result because it further increases our confidence in Pierce's one-dimensional model. If an occasion arises in which the velocity spread parameter S is not small the foregoing results can be applied to determine the order of magnitude of the effect. In addition, there is some indication† that nonlinear effects in traveling-wave tube attenuators produce velocity distributions which result in reduced linear gain in later sections of the tube. The foregoing analysis may prove useful in explaining some of these phenomena.

This work was supported jointly by the U. S. Airforce, the U. S. Army, and the U. S. Navy.

[11] J. R. Pierce, *Theory and Design of Electron Beams* (D. Van Nostrand Company, Inc., New York, 1950), p. 151.

† J. J. Caldwell, Hughes Research and Development Laboratories (private communication).

Conditions for Porosity Formation during Diffusion*

R. W. BALLUFFI† AND L. L. SEIGLE‡
Atomic Energy Division, Sylvania Electric Products, Inc., Bayside, New York
(Received February 27, 1954)

Formal relationships defining the regions of the diffusion zone where porosity tends to form during the Kirkendall effect are developed. The surfaces at which the intrinsic diffusional flux of each component reaches a maximum are also considered. The results are applicable to diffusion systems subject to the usual boundary conditions where the solution $N_1 = N(x/\sqrt{t})$ holds. The results are discussed in relation to presently available experimental findings.

INTRODUCTION

A NUMBER of investigators[1–6] have recently found porosity formation and other structural changes in the diffusion zones of specimens undergoing the Kirkendall effect. The occurrence and distribution of porosity varies from system to system and depends upon the type of diffusion couple used. Several detailed discussions of the mechanism of this porosity formation have appeared elsewhere.[7,8] In the sandwich couples studied to date the porosity has been found in the side of the couple initially containing the higher concentration of the faster diffusing component. In the case of copper/alpha brass[1,4] and copper/nickel[2,4] couples the maximum amount of porosity forms and remains near the Kirkendall markers in the side of the couple containing the higher concentration of zinc and copper, respectively. However, in silver/gold couples the region of maximum porosity does not remain near the Kirkendall markers but instead moves continuously away towards the silver side of the couple.[3,5,6] In vapor-solid couples where the faster diffusing component is diffused into the specimen from the vapor phase, no porosity appears in the copper/alpha brass and copper/nickel[4,6] systems but a region of porosity is produced in silver/gold couples.[4,6]

The purpose of the present work is to develop the formal relationships defining the regions in the diffusion zone where porosity tends to form. The surfaces at which the intrinsic diffusional flux of each component reaches a maximum are also considered. The results are applicable to diffusion systems subject to the usual suitable boundary conditions where the solution $N_1 = N(x/\sqrt{t})$ holds. This general problem has been considered by Seith and Kottmann[3] and also by Heumann and Kottmann,[5] who have obtained somewhat different results. It turns out that all of the desired relationships may be obtained by making the usual change of variable $\lambda \equiv x/\sqrt{t}$ and employing the solution $N_1 = N(\lambda)$ in the appropriate diffusion equations. Since the relationships are obtained in general functional form an application to a specific system is also presented. The results are then discussed in relation to the experimental findings which are now available.

I. THE PLANE IN THE DIFFUSION ZONE WHERE POROSITY JUST TENDS TO FORM

In all cases the coordinate system to which diffusion is referred must be clearly distinguished. We assume unidirectional diffusion in the x direction. As Darken[9] has indicated, two general reference systems may be most readily employed to describe diffusion during the Kirkendall effect: (1) a system fixed with respect to the nondiffused ends of the couple (e.g., a system with the origin at the position in space of the original join); (2) a system fixed with respect to a plane embedded in the specimen. By assigning an independent intrinsic diffusivity to each component, Darken has described the flux of component 1 across a unit plane fixed with respect to the origin at the position of the original join by

$$j_1 = -\left[D_1 \frac{\partial c_1}{\partial x} - c_1 v\right]. \tag{1}$$

In this expression the term $-D_1(\partial C_1/\partial x)$ represents the flux of 1 diffusing past a plane embedded in the specimen which is in turn moving with a velocity v with respect to the above origin as a result of the unequal diffusion rates of 1 and 2. Consideration of the fluxes diffusing past any moving plane shows that

$$v = (D_1 - D_2)\frac{\partial N_1}{\partial x}. \tag{2}$$

The rotal rate of transport across a plane fixed with respect to the origin may be alternatively described in

* This work was sponsored by the U. S. Atomic Energy Commission and was done under Contract AT-30-1 GEN 367.
† University of Illinois, Urbana, Illinois.
‡ Atomic Energy Division, Sylvania Electric Products, Inc., Bayside, New York.
[1] H. Bückle and J. Blin, J. Inst. Metals **80**, 385 (1952).
[2] R. S. Barnes, Proc. Phys. Soc. (London) **B65**, 512 (1952).
[3] W. Seith and A. Kottmann, Angew. Chem. **64**, 379 (1952).
[4] R. W. Balluffi and B. H. Alexander, J. Appl. Phys. **23**, 953 (1952); **23**, 1237 (1952).
[5] T. Heumann and A. Kottmann, Z. Metallkunde **44**, 139 (1953).
[6] R. W. Balluffi and L. L. Seigle, J. Appl. Phys. **25**, 607 (1954).
[7] F. Seitz, Acta Met. **1**, 355 (1953).
[8] R. W. Balluffi, Acta Met. **2**, 194 (1954).
[9] L. S. Darken, Trans. Am. Inst. Mining Met. Engrs. **175**, 184 (1948).

terms of the "chemical diffusivity" (D) by

$$j_1=-D\frac{\partial c_1}{\partial x}. \tag{3}$$

The chemical diffusivity, therefore, includes both the effect of mass flow in the specimen and diffusion with respect to the flowing specimen. The relationship between diffusivities is, therefore,

$$D=N_1D_2+N_2D_1. \tag{4}$$

At the plane embedded in the specimen where porosity just tends to form the divergence of the mass flow must disappear. At this point the mass flow must go through either a maximum or minimum. On one side of this point where the divergence is positive porosity will tend to form since each small unit volume is losing mass and on the other side the specimen will gain mass and expand. At such a point, therefore,

$$\frac{\partial v}{\partial x}=\frac{\partial}{\partial x}\left[(D_1-D_2)\frac{\partial N_1}{\partial x}\right]=0. \tag{5}$$

By defining $(D_1-D_2)\equiv g(\lambda)$ and employing the solution $N_1=N(\lambda)$, where $\lambda\equiv x/\sqrt{t}$, and using (4) and the relationship

$$\frac{\partial^2 N_1}{\partial\lambda^2}=-\frac{1}{D}\frac{\partial N_1}{\partial\lambda}\left(\frac{\lambda}{2}+\frac{\partial D}{\partial\lambda}\right), \tag{6}$$

obtained from Ficks' second law, Eq. (5) may be expressed as

$$\left(\lambda-2g(\lambda)\frac{\partial N_1}{\partial\lambda}\right)+\frac{\partial N_1}{\partial\lambda}\cdot\frac{2}{g(\lambda)}\left(D_1\frac{\partial D_2}{\partial N_1}-D_2\frac{\partial D_1}{\partial N_1}\right)=0. \tag{7}$$

The relation (7) is an equation in λ which may possess a number of roots $\lambda_i=A_i$. The plane (or planes) bounding the regions of porosity formation must therefore remain at constant composition.

As we have shown elsewhere[6] the embedded Kirkendall markers which are initially placed at the origin remain at constant composition and at a constant value of λ which is defined by the equation

$$\lambda-2g(\lambda)\cdot\frac{\partial N_1}{\partial\lambda}=0. \tag{8}$$

Since the second term in Eq. (7) does not necessarily vanish for all values of λ the plane (or planes) where porosity tends to form is not necessarily embedded in the specimen. It may move relative to the flowing specimen since the compositions defined by (7) are generally not the same as the composition at the plane of the Kirkendall markers defined by Eq. (8). This point may be proved as follows. Let us suppose a specific case where $\lambda=B$ satisfies (8). We also fix D as a function of λ, thereby fixing $(\partial N_1/\partial\lambda)_{\lambda=B}$. Under these conditions according to (4) we may vary $(\partial D_2/\partial N_1)_{\lambda=B}$ and $(\partial D_1/\partial N_1)_{\lambda=B}$, while holding $g(\lambda)\equiv(D_1-D_2)_{\lambda=B}$ constant. By using this method the value of the second term in (7) may be varied at will while holding the first term equal to 0. Under these circumstances (7) is not satisfied by $\lambda=B$. It seems, therefore, that the plane (or planes) defining the regions of porosity formation may appear anywhere in the diffusion zone depending upon the behavior of the intrinsic diffusivities. However, under the special conditions that the diffusivities do not vary with concentration $(\partial D_1/\partial N_1=\partial D_2/\partial N_1=0)$, or that the ratio of diffusivities remains constant $(D_1/D_2=K)$ this plane will obviously coincide with the plane of the Kirkendall markers.

II. THE PLANE WHERE THE FLUX OF ONE COMPONENT RELATIVE TO THE FLOWING SPECIMEN IS A MAXIMUM

We now consider the point in the flowing specimen past which the flux of component 1 is a maximum. A necessary condition for this point is

$$\frac{\partial}{\partial x}\left(D_1\frac{\partial N_1}{\partial x}\right)=\frac{\partial}{\partial x}(N_1v)+\frac{\partial N_1}{\partial t}=0. \tag{9}$$

By using the same procedure as in the previous section (9) may be expressed as

$$D_1\left(\lambda-2g(\lambda)\frac{\partial N_1}{\partial\lambda}\right)+2N_1\frac{\partial N_1}{\partial\lambda}\left(D_1\frac{\partial D_2}{\partial N_1}-D_2\frac{\partial D_1}{\partial N_1}\right)=0. \tag{10}$$

The relation (10) is an equation in λ which may possess a number of constant roots $\lambda_i=C_i$. The plane (or planes) where the flux of component 1 is a maximum, therefore, remain at constant composition. Using a similar derivation the corresponding equation for species 2 appears as

$$D_2\left(\lambda-2g(\lambda)\frac{\partial N_1}{\partial\lambda}\right)-2(1-N_1)\frac{\partial N_1}{\partial\lambda}\left(D_1\frac{\partial D_2}{\partial N_1}-D_2\frac{\partial D_1}{\partial N_1}\right)=0. \tag{11}$$

Since (10) and (11) have the same general form as (7), we again conclude that the planes where the individual fluxes have maximum values may appear anywhere in the diffusion zone depending upon the behavior of the intrinsic diffusivities. Since (10) and (11) differ, the planes for components 1 and 2 will not necessarily coincide. However, these planes will both appear at the Kirkendall marker plane under the diffusivity conditions given in Sec. I. This conclusion does not agree with the results of Seith and Kottmann[3] who have stated that the fluxes should have maximum values at the Kirkendall marker plane.

III. APPLICATION TO A SPECIFIC SYSTEM

In order to apply the above general equations to a specific case let us consider the problem of a sandwich type couple made up of two pure metals when the chemical diffusivity remains constant and the intrinsic diffusivities vary linearly with composition. In this case,

$$\begin{cases} D_2 = DN_1 \\ D_1 = D(1+N_1) \\ D_1 - D_2 = g(\lambda) = D \\ \dfrac{dN_1}{d\lambda} = -\dfrac{1}{2(\pi D)^{\frac{1}{2}}} \cdot \exp(-\lambda^2/4D). \end{cases} \tag{12}$$

Substituting (12) into (8) we obtain

$$\lambda + \left(\frac{D}{\pi}\right)^{\frac{1}{2}} \cdot \exp(-\lambda^2/4D) = 0 \tag{13}$$

for the equation defining the value of λ at the Kirkendall interface. Equation (13) has a single negative root which indicates that the markers are moving into the side of the couple initially containing the higher concentration of the higher diffusivity component as would be expected. By substituting (12) into (7) we find that the plane of incipient porosity formation occurs at the origin ($\lambda = 0$). Substitution into (10) and (11) gives the expressions

$$\begin{aligned} \lambda + \frac{1}{(1+N_1)}\left(\frac{D}{\pi}\right)^{\frac{1}{2}} \exp(-\lambda^2/4D) = 0 \\ \lambda + \frac{1}{N_1}\left(\frac{D}{\pi}\right)^{\frac{1}{2}} \exp(-\lambda^2/4D) = 0, \end{aligned} \tag{14}$$

for the values of λ at the planes where fluxes of 1 and 2 respectively reach maximum values. It is clear that these equations possess different single negative roots and that the planes are located in different places in the negative side of the couple.

IV. DISCUSSION

All of the experimental observations of porosity made to date seem to be consistent with the results of the previous sections. However, it must be remembered that it is unlikely that the boundary of the region of porosity formation can ever actually be observed exactly. The fact that there is a tendency for porosity to form is no guarantee that porosity actually will form since a certain supersaturation of vacancies must be reached before precipitation of holes can occur.[7,8]

Our results predict that as a result of the variation of the intrinsic diffusivities with composition the plane of incipient porosity formation will not necessarily be located in the specimen at the Kirkendall marker interface but will move relative to the flowing specimen. This may be the case in silver/gold sandwich type couples where the porous zone is found to move in approximately the expected parabolic manner with time.[3,5,6] In this system, the holes which remain behind as the plane where porosity tends to form sweeps through the specimen, evidently sinter together, and therefore it is easily possible to follow the region of strong porosity formation. In other couples such as copper/alpha brass and copper/nickel,[1,2,4] the porous zone remains most highly concentrated near the Kirkendall markers and, therefore, either the plane where porosity just tends to form remains close to the Kirkendall markers or else the majority of holes formed during the diffusion cycle do not sinter but remain in the specimen.

The fact that porosity is generated in vapor-solid silver/gold couples where silver vapor is diffused into gold,[4,6] may be expected on the basis of the previous results. It is interesting to notice that the maximum porosity in both sandwich type and vapor-solid type silver/gold couples appears in about the same composition range, namely 70–85 atomic percent silver. Since the diffusion penetration curves are approximately linear in this region in both couples, we may postulate along with Seith and Kottmann[3] that the value of $(D_{Ag} - D_{Au})$ goes through a maximum near this composition. Obviously, direct measurements of this quantity must be made to verify this possibility. In other vapor-solid couples (such as copper/alpha brass and copper/nickel) where no porosity has been found to occur,[4,6] it is probable that regions were present where porosity tended to form but that sufficiently high supersaturations were not achieved for holes to form.

JOURNAL OF APPLIED PHYSICS VOLUME 25, NUMBER 11 NOVEMBER, 1954

Calibration of a Nickel-Molybdenum Thermocouple

RICHARD D. POTTER*
Metallurgy Research Branch, Michelson Laboratory, U. S. Naval Ordnance Test Station, Inyokern, China Lake, California
(Received March 29, 1954)

A report is made of a calibration of a nickel (*A*) *versus* molybdenum thermocouple up to 2242°F (50 mv).

INTRODUCTION

In extending work on thermoelectric functions to cover metals like alpha brass and aluminum, some difficulty was experienced in spot welding the usual types of thermocouples, such as chromel-alumel, iron-constantan, and copper-constantan, to the sample material. Experimenting with various commercial wires, it was found that "*A*" nickel and molybdenum both spot welded satisfactorily to brass and aluminum.

A brief review of the literature did not show any useful calibration data on nickel-molybdenum thermocouples.[1,2] Finch had made thermoelectric data comparisons of several metals referred to platinum, including nickel and molybdenum.[3] In his work, nickel was shown to have approximately the same thermoelectric response as alumel and molybdenum about the same as chromel.

In order to use nickel and molybdenum as thermocouple elements, it was necessary to make calibration checks of nickel-molybdenum couples against standard thermocouples. The results of the calibration are reported here in both curve and table form with temperature-degrees Fahrenheit *versus* millivolts (abs).

DISCUSSION AND RESULTS

Materials used were "*A*" nickel and molybdenum wires, both 0.020 inch in diameter. The nickel wires used in the calibration were from coil stock whereas the molybdenum was supplied in straight lengths about three feet long.

In previous work of the author,[4] a stock of chromel-alumel thermocouple wires was calibrated against a standard platinum couple. The calibration of the nickel-molybdenum couples was made against the calibrated chromel-alumel stock using the open circuit thermocouple (OTC) technique.[4] Each of the four wires, nickel, molybdenum, chromel, and alumel, was individually spot-welded to a short length of 0.040-inch diameter platinum wire with about a quarter of an inch between each spot weld in the series. The OTC assembly was then heated and cooled in a purified helium atmosphere contained within an electrically heated furnace where the hot junctions of the thermocouples were in the center of a four-inch constant-temperature zone. Cold junction reference was 32°F.

Data were recorded on a Speedomax X-X millivolt recorder with the thermoelectric outputs of chromel-alumel and nickel-molybdenum couples plotted simultaneously. From these plots, temperature values were obtained at 0.5-millivolt intervals of the nickel-molybdenum output in reference to the chromel-alumel plot. The original values of temperature-degrees Fahrenheit *versus* millivolts (abs) are plotted in Fig. 1. In consideration of the accuracy and sensitivity of the equipment and the standardization of the chromel-alumel stock, these values are felt to be accurate to ±2°F for the nickel and molybdenum wire stocks used. Since, for the use intent of this work, it has not been necessary to compare other stocks of nickel and molybdenum wires to this calibration, other investigators should make spot checks of wire stocks, particularly in the anomaly range of 400°F to 900°F caused by the specific heat effect of the Curie transformation of nickel.

From the 0.50-millivolt interval data of the original calibration, calculations were made to extend the data to 0.10-millivolt values with ratio interpolation. Table I is the result of these calculations. Ratio interpolation assumes a straight line between the calibration points and therefore is usually less accurate than the original data or true curve; however, it facilitates interpolating between the tabled values over a one-millivolt range.

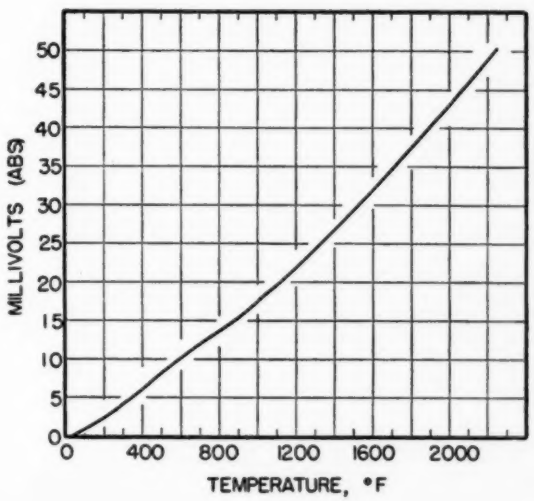

FIG. 1.

* Head of the Metallurgy Research Branch.
[1] American Society for Metals Review of Metal Literature, Vol. 1 through 9, 1944–1952.
[2] Reference Tables for Thermocouples, National Bureau of Standards Circular No. 508, United States Department of Commerce, May 7, 1951.
[3] D. I. Finch (American Society for Metals, *Metals Handbook*, Cleveland, 1948), p. 32.
[4] R. D. Potter, Metal Progr. 64, 80–81 (November, 1953).

TABLE I. Nickel-molybdenum thermocouple.

	To convert millivolts to degrees Fahrenheit							Cold junction 32°F					
mv	0	0.1	0.2	0.3	0.4	0.5	0.6	0.7	0.8	0.9	1.0	mv	°F per 0.01 mv
	Degrees Fahrenheit												
0	32	40	47	55	62	70	77	85	92	99	107	0	0.75
1	107	114	120	127	133	140	146	153	159	166	173	1	0.66
2	173	179	185	191	197	203	209	215	221	227	233	2	0.60
3	233	239	244	250	255	261	266	272	277	283	289	3	0.56
4	289	295	300	306	311	316	321	327	332	338	343	4	0.54
5	343	348	353	359	364	369	374	380	385	390	395	5	0.52
6	395	400	405	410	415	420	425	430	435	440	445	6	0.50
7	445	449	454	459	464	469	474	479	484	489	494	7	0.49
8	494	498	503	508	513	518	523	528	533	538	543	8	0.49
9	543	548	553	558	563	568	573	578	583	588	594	9	0.51
10	594	599	605	610	616	621	627	632	638	643	648	10	0.54
11	648	654	659	665	670	676	681	687	692	698	703	11	0.55
12	703	709	715	721	727	732	738	743	749	755	761	12	0.58
13	761	767	772	778	784	789	795	801	807	813	818	13	0.57
14	818	823	828	834	839	844	849	855	860	865	871	14	0.53
15	871	876	881	886	891	896	901	906	911	916	922	15	0.51
16	922	927	932	937	942	947	952	957	962	967	972	16	0.50
17	972	977	982	987	992	996	1001	1006	1011	1016	1020	17	0.48
18	1020	1025	1029	1034	1039	1043	1048	1053	1058	1063	1067	18	0.47
19	1067	1072	1076	1081	1085	1090	1094	1099	1103	1108	1113	19	0.46
20	1113	1117	1122	1126	1131	1135	1140	1144	1149	1153	1157	20	0.44
21	1157	1161	1166	1170	1175	1179	1184	1188	1193	1197	1201	21	0.44
22	1201	1205	1209,	1214	1218	1222	1226	1231	1235	1239	1244	22	0.43
23	1244	1248	1252	1257	1261	1265	1269	1274	1278	1282	1286	23	0.42
24	1286	1290	1294	1299	1303	1307	1311	1316	1320	1324	1328	24	0.42
25	1328	1332	1336	1340	1344	1348	1352	1356	1360	1364	1368	25	0.40
26	1368	1372	1376	1380	1384	1388	1392	1396	1400	1404	1408	26	0.40
27	1408	1412	1416	1420	1424	1428	1432	1436	1440	1444	1448	27	0.40
28	1448	1452	1456	1460	1464	1468	1472	1476	1480	1484	1488	28	0.40
29	1488	1492	1496	1500	1504	1507	1511	1515	1519	1523	1526	29	0.38
30	1526	1530	1534	1538	1542	1545	1549	1553	1557	1561	1564	30	0.38
31	1564	1568	1572	1576	1580	1583	1587	1591	1595	1599	1602	31	0.38
32	1602	1606	1610	1614	1618	1621	1625	1629	1633	1637	1640	32	0.38
33	1640	1644	1647	1651	1655	1658	1662	1666	1670	1674	1677	33	0.37
34	1677	1681	1684	1688	1692	1695	1699	1703	1707	1711	1714	34	0.37
35	1714	1718	1721	1725	1729	1732	1736	1740	1744	1748	1751	35	0.37
36	1751	1755	1758	1762	1765	1769	1772	1776	1779	1783	1787	36	0.36
37	1787	1791	1794	1798	1801	1805	1808	1812	1815	1819	1823	37	0.36
38	1823	1827	1830	1834	1837	1841	1844	1848	1851	1855	1859	38	0.36
39	1859	1863	1866	1870	1873	1877	1880	1884	1887	1891	1895	39	0.36
40	1895	1899	1902	1906	1909	1913	1916	1920	1923	1927	1931	40	0.36
41	1931	1935	1938	1942	1945	1949	1952	1956	1959	1963	1966	41	0.35
42	1966	1970	1973	1977	1980	1984	1987	1991	1994	1998	2001	42	0.35
43	2001	2005	2008	2012	2015	2019	2022	2026	2029	2033	2036	43	0.35
44	2036	2040	2043	2047	2050	2054	2057	2061	2064	2068	2071	44	0.35
45	2071	2075	2078	2082	2085	2089	2092	2096	2099	2103	2106	45	0.35
46	2106	2109	2113	2116	2120	2123	2127	2130	2134	2137	2140	46	0.34
47	2140	2143	2147	2150	2154	2157	2161	2164	2168	2171	2174	47	0.34
48	2174	2177	2181	2184	2188	2191	2195	2198	2202	2205	2208	48	0.34
49	2208	2211	2215	2218	2222	2225	2229	2232	2236	2239	2242	49	0.34

The values listed in Table I and interpolation to whole numbers of degrees Fabrenheit are considered accurate to plus or minus five times the listed degrees Fahrenheit per 0.01-millivolt interpolation value but not better than ± 2°F. At the calibration points, the table values check the original calibration within 2°F.

JOURNAL OF APPLIED PHYSICS VOLUME 25, NUMBER 11 NOVEMBER, 1954

Theory of Stress-Strain Relations in Anisotropic Viscoelasticity and Relaxation Phenomena

M. A. Biot*
Shell Development Company, New York, New York
(Received March 19, 1954)

A thermodynamic derivation is given for the representation of a system having viscoelastic or relaxation properties by means of a potential and dissipation function familiar in Lagrangian mechanics. This leads to modes of relaxation which are used as normal coordinates to derive general expressions for operational tensors relating stress and strain. A large variety of phenomena involving interaction of diffusion, chemical reaction, heat transfer, mechanical deformation, etc., is included in this theory.

I. INTRODUCTION

THE behavior of systems having both elasticity and viscosity under applied forces or exhibiting relaxation is usually analyzed by considering a simple mechanical model constituted by interconnected springs and dashpots. An arbitrary system of this type made up of a lattice of points connected by such springs and dashpots may be considered as an n degree of freedom system which is defined by two quadratic forms, the potential energy and the dissipation function. It is first shown in Sec. II by applying Onsager's theorem and the thermodynamics of irreversible phenomena that this model may represent the behavior of a very wide variety of phenomena in the process of their response to external action in the vicinity of equilibrium. Such phenomena may involve the application of external stresses, chemical reactions due to departure from chemical equilibrium, heat transfer, etc., and the coupling between these phenomena. The present treatment therefore includes Zener's theory of thermoelastic damping as a particular case. Also included are the effects of a liquid solvent which have been found experimentally in rock creep tests. We show that we may extend the concepts of potential energy and dissipation function to cover all these cases leading to their treatment by the methods of Lagrangian mechanics.

Section III derives the existence of modes of relaxation, i.e., solutions for which all variables are proportional to a decreasing real exponential of time. Properties of decay constants and other properties of these modes such as orthogonality are examined. Use of these modes is made in Sec. IV in order to solve for the forces or external actions in terms of a limited number of external or observed coordinates, and it is found that the most general behavior of external coordinates may be represented by a model made of a number of Maxwell type materials plus a spring and a dashpot all in parallel.

Section V deals with the stress-strain relations of a continuum and introduces the concept of operational tensor as a generalization for the elastic moduli of the theory of elasticity.

Section VI deals with the particular form of these tensors for special cases of symmetry of the material. The possibility of multiple symmetry in the same material depending on the strain rate is pointed out.

The results are also applicable to electric network theory and give expression for the direct and cross-impedances of a $2k$ terminal RC network. Extension to an LC network is also quite straightforward as it amounts to replacing p by p^2.

II. THERMODYNAMIC DERIVATION OF THE FUNDAMENTAL EQUATION OF RELAXATION PHENOMENA

We consider a general thermodynamic system with n degrees of freedom defined by n state variables q_i. These degrees of freedom are of a quite general nature. They may include coordinates, local temperatures, piezoelectric charges, concentrations such as induced by chemical or solubility processes, etc. Correlatively we assume that the system is under the action of external forces in the generalized sense denoted by Q_i such that $Q_i dq_i$ represents the energy furnished to the system. These forces may be externally applied stresses, electromotive forces, or may result from deviations of Gibbs and chemical potential from the equilibrium state. No external forces are associated with the temperature variables.

We also assume the system to be linear, i.e., that the coordinates q_i and their derivatives are linear functions of the forces Q_i. The system includes a large reservoir at a constant temperature T and the total system is closed, i.e., exchanges no heat with the outside. Under those circumstances the entropy and the internal energy are quadratic functions of the state variables.

We define the zero level of the entropy for the state where all variables are zero and T is the uniform temperature of this equilibrium state. Part of the state variables will be local temperature increments concentration increments, etc. Where no forces are applied, the entropy of the system in the vicinity of the zero level is a maximum and we may write

$$TS = -\tfrac{1}{2} \sum^{ij} a_{ij} q_i q_j = -V, \qquad (2.1)$$

where V is a positive definite quadratic form. The

* Consultant.

constant temperature T is introduced here as a factor simply for convenience. When forces are applied this is replaced by

$$TS=-\tfrac{1}{2}\sum^{ij} a_{ij}q_iq_j+\sum^{i}\beta_iq_i. \tag{2.2}$$

If the system is displaced from the zero level by applying the forces very slowly so that the system is displaced reversibly by a succession of equilibrium states, expression (2.2) would constantly satisfy the conditions that the entropy is a maximum, namely,

$$\partial S/\partial q_i=0. \tag{2.3}$$

We now investigate the significance of the linear terms in expression (2.2) for the entropy. We separate the system into two parts, a system I to which the forces Q_i are applied and a system II constituted by the large reservoir at the constant temperature T. Conservation of energy requires that the total heat absorbed by system I is

$$dh=dU_{\mathrm{I}}-\sum^{i} Q_idq_i, \tag{2.4}$$

where U_{I} is the internal energy of I. Hence the reservoir acquires an increment of entropy

$$dS_{\mathrm{II}}=-\frac{dU_{\mathrm{I}}}{T}+\sum^{i}\frac{Q_idq_i}{T}. \tag{2.5}$$

Denoting by S_{I} the entropy of system I we have for the total entropy

$$dS=dS_{\mathrm{I}}-\frac{dU_{\mathrm{I}}}{T}+\sum^{i}\frac{Q_idq_i}{T}. \tag{2.6}$$

Now in the vicinity of the origin $q_i=0$, for a reversible process in which the forces Q_i are constantly in equilibrium with the system, we have

$$dS_{\mathrm{I}}=\frac{dU_{\mathrm{I}}}{T}-\sum^{i} Q_idq_i. \tag{2.7}$$

But at the origin equilibrium requires $Q_i=0$ by definition, hence at the origin

$$dS_{\mathrm{I}}=\frac{dU_{\mathrm{I}}}{T}. \tag{2.8}$$

We conclude for $q_i=0$,

$$T\frac{\partial S}{\partial q_i}=Q_i=\beta_i. \tag{2.9}$$

Expression (2.2) for the total entropy becomes

$$TS=-\tfrac{1}{2}\sum^{ij} a_{ij}q_iq_j+\sum^{i} Q_iq_i. \tag{2.10}$$

By putting equal to zero the derivatives $\partial S/\partial q_i$ we obtain n linear relations between the forces and the coordinates which correspond to equilibrium conditions of the system under those forces.

We now apply Onsager's theorem[1] to expression (2.10). This theorem is concerned with the case where the derivatives $\partial S/\partial q_i$ are not zero, i.e., where we have a departure from equilibrium. These derivatives are considered as forces associated with time rates of change of the state variables q_i. The theorem states that these rates are linear functions of these derivatives and that the coefficients constitute a symmetric matrix. We write

$$T\frac{\partial S}{\partial q_i}=\tfrac{1}{2}\sum^{j} b_{ij}\dot{q}_i \tag{2.11}$$

with $b_{ij}=b_{ji}$. Since

$$T\sum^{i}\frac{\partial S}{\partial q_i}\dot{q}_i=\tfrac{1}{2}\sum^{ij} b_{ij}\dot{q}_i\dot{q}_j=D \tag{2.12}$$

is proportional to the rate of change of entropy which is always positive, we conclude that the quadratic form D is positive definite.

The fundamental relation between forces and state variables may therefore be written in the general form,

$$\sum^{j} a_{ij}q_j+\sum^{j} b_{ij}\dot{q}_j=Q_i. \tag{2.13}$$

These equations may also be written in the familiar Lagrangian form

$$\frac{\partial V}{\partial q_i}+\frac{\partial D}{\partial \dot{q}_i}=Q_i \tag{2.14}$$

We see that V plays the role of a potential energy and D that of a dissipation function. The system therefore is represented by a mechanical model of springs and dashpots connecting two by two a lattice of $n/3$ spacially distributed points with n independent coordinates and corresponding forces Q_i applied at these points. For simplicity we shall refer hereafter to the state variables q_i as coordinates.

III. RELAXATION MODES AND RELAXATION SPECTRUM

The general equations (2.13) are written for convenience

$$\sum^{j} A_{ij}q_j=Q_i \tag{3.1}$$

with

$$A_{ij}=a_{ij}+pb_{ij} \tag{3.2}$$

and the time operator

$$p=d/dt. \tag{3.3}$$

For studying the properties of these equations it is

[1] S. R. De Groot, *Thermodynamics of Irreversible Processes* (Interscience Publishers Inc., New York, 1952).

important to treat first the homogeneous equations

$$\sum^{j} A_{ij}q_j=0. \tag{3.4}$$

If p is considered as a parameter we see that the homogeneous equations lead to an eigenvalue problem. An algebraic equating for the characteristic values of p is obtained by equating to zero the determinant of the coefficients A_{ij},

$$\Delta=\det(A_{ij})=0. \tag{3.5}$$

For the sake of generality we shall say that this equation is of the nth degree and that there are n roots but will consider that in addition to possible multiple and zero roots some of the roots may be infinite. We denote the roots of equation (3.5) by $-\lambda_s$. Let us assume first that the roots are all distinct, finite, and different from zero. The general solution of the homogeneous Eqs. (3.4) is then

$$q_j=\sum^{s} \phi_j^{(s)}e^{-\lambda_s t}. \tag{3.6}$$

To each root $-\lambda_s$ corresponds a solution

$$q_j^{(s)}=\phi_j^{(s)}e^{-\lambda_s t} \tag{3.7}$$

which is called a relaxation mode. That the roots $-\lambda_s$ are real and negative is easily seen as follows. We consider two modes

$$\begin{aligned} q_j^{(s)}&=\phi_j^{(s)}e^{-\lambda_s t},\\ q_j^{(r)}&=\phi_j^{(r)}e^{-\lambda_r t} \end{aligned} \tag{3.8}$$

corresponding to the two roots $-\lambda_s$, $-\lambda_r$. That these solutions are orthogonal is established by the usual procedure of substituting each solution in the equation then multiplying each equation for the solutions $\phi_j^{(s)}$ by $\phi_i^{(r)}$ and those for $\phi_j^{(r)}$ by $\phi_i^{(s)}$. Adding each set of equations gives the two relations

$$\begin{aligned} \sum^{ij} a_{ij}\phi_j^{(s)}\phi_i^{(r)}-\lambda_s\sum^{ij} b_{ij}\phi_j^{(s)}\phi_i^{(r)}=0,\\ \sum^{ij} a_{ij}\phi_j^{(r)}\phi_i^{(s)}-\lambda_r\sum^{ij} b_{ij}\phi_j^{(r)}\phi_i^{(s)}=0. \end{aligned} \tag{3.9}$$

Because of the symmetry $a_{ij}=a_{ji}$ and $b_{ij}=b_{ji}$ the quadratic forms are the same in both equations, and by subtraction of Eq. (3.9) we find that if λ_s and λ_r are distinct, this implies

$$\sum^{ij} a_{ij}\phi_j^{(s)}\phi_i^{(r)}=\sum^{ij} b_{ij}\phi_j^{(s)}\phi_i^{(r)}=0. \tag{3.10}$$

These equations express the orthogonality of the modes. It is easily verified that they cannot be satisfied if the modes are complex conjugates because of the property that the quadratic forms are positive. So the modes are real. Moreover if we put $s=r$ in (3.9) we find

$$\lambda_s=\frac{\sum^{ij} a_{ij}\phi_i^{(s)}\phi_j^{(s)}}{\sum^{ij} b_{ij}\phi_i^{(s)}\phi_j^{(s)}}=\frac{V}{D}, \tag{3.11}$$

where V and D are positive definite forms corresponding to the potential energy V and the dissipation function D (in which we replace q_i by $\phi_i^{(s)}t$). Therefore, all roots $-\lambda_s$ are real and negative.

Now these properties are not restricted to the case where all roots are distinct, finite, and different from zero. In case of a multiple root $-\lambda_s$ of multiplicity α, we may determine α orthogonal modes corresponding to this root. Also, in the case of an infinite root we have a mode which is simply a column of constants independent of time. The case of a zero root corresponds to a solution of the type

$$q_j^{(s)}=\phi_j^{(s)}t. \tag{3.12}$$

This will be further clarified by considering the system from the standpoint of normal coordinates in the next section.

In most physical systems a great many variables are "hidden," i.e., we do not observe them. External forces are only applied to k coordinates $q_1\cdots q_k$ while the $n-k$ others constitute what we shall call the internal system. This is expressed by writing Eqs. (3.1) in the form

$$\left[\begin{array}{c|c} N & S \\ \hline T & M \end{array}\right]\begin{bmatrix} q_1 \\ q_k \\ q_{k+1} \\ \vdots \\ q_n \end{bmatrix}=\begin{bmatrix} Q_1 \\ Q_k \\ 0 \\ \vdots \\ 0 \end{bmatrix}. \tag{3.13}$$

The matrix M represents an internal subsystem of $n-k$ degrees of freedom which is of the same general nature as the total system with its own $n-k$ relaxation constants σ_s and modes corresponding to roots $-\sigma_s$ of the determinant of the submatrix $[M]$,

$$M=\det[M]=0. \tag{3.13}$$

The relaxation constants λ_s correspond to a set of relaxation times which if a great many degrees of freedom are considered may be said to constitute a spectrum. The spectrum σ_s of a subsystem will depend of course on the particular subsystem which is considered as internal. It is also a consequence of the properties of the type of matrices involved that the roots σ_s are located between the roots λ_s because the system defined by the matrix M may be considered as the original system of determinant Δ in which k restraints, $q_1=q_2=\cdots q_k=0$, have been introduced.

IV. NORMAL COORDINATES AND GENERALIZED FORCES

We perform a change of coordinates from q_i to ξ_s by the n linear relations

$$q_i=\sum^{s} \phi_i^{(s)}\xi_s, \tag{4.1}$$

where $\phi_i^{(s)}$ is the modal column of the sth relaxation mode. The ξ's are called the normal coordinates. The

Lagrangian Eq. (2.14) then becomes

$$\frac{\partial V}{\partial \xi_s}+\frac{\partial D}{\partial \dot{\xi}_s}=\Xi_s \tag{4.2}$$

where the generalized normal force Ξ_s corresponding to the coordinate ξ_s is given by

$$\Xi_s=\sum^{j} \phi_j^{(s)} Q_j. \tag{4.3}$$

We normalize the $\phi_j^{(s)}$ columns in such a way that for each s

$$\sum^{ij} b_{ij}\phi_i^{(s)}\phi_j^{(s)}=1 \tag{4.4}$$

except for the case where $\lambda_s=\infty$ where we normalize by

$$\sum^{ij} a_{ij}\phi_i^{(s)}\phi_j^{(s)}=1. \tag{4.5}$$

Then we may write for $\lambda_s\neq\infty$,

$$\begin{aligned} V&=\tfrac{1}{2}\sum^{s}\lambda_s\xi_s^2,\\ D&=\tfrac{1}{2}\sum^{s}\dot{\xi}_s^2 \end{aligned} \tag{4.6}$$

and for $\lambda_s=\infty$,

$$\begin{aligned} V&=\tfrac{1}{2}\sum^{i}\xi_s^2,\\ D&=0. \end{aligned} \tag{4.7}$$

The Lagrangian equations for the normal coordinates are thus the n equations

$$\begin{aligned} (p+\lambda_s)\xi_s&=\Xi_s,\\ \xi_s&=\Xi_s, \end{aligned} \tag{4.8}$$

where the last equation corresponds to modes of infinite root λ_s. These are n equations which are quite general and may correspond to any case of multiplicity of λ_s or to zero and infinite roots. In the case of α multiplicity of a root λ_s the corresponding Eq. (4.8) is simply repeated α times.

Equations (4.8) are immediately solved in terms of the coordinates

$$\begin{aligned} \xi_s&=\frac{\Xi_s}{p+\lambda_s},\\ \xi_s&=\Xi_s. \end{aligned} \tag{4.9}$$

With these results we may solve the fundamental Eq. (3.1) for the variables q_j in terms of the forces Q_j. Substituting ξ_s in (4.1) and using (4.3) for Ξ_s, we find

$$q_i=\sum_{j=1}^{k} Q_j\left[\sum^{s}\frac{C_{ij}^{(s)}}{p+\lambda_s}+C_{ij}\right]. \tag{4.10}$$

The summation $\sum^{s}$ is extended to all the *distinct* roots λ_s.

$$C_{ij}^{(s)}=\phi_i^{(s)}\phi_j^{(s)} \tag{4.11}$$

if λ_s is a single root and

$$C_{ij}^{(s)}=\sum^{s}\phi_i^{(s)}\phi_j^{(s)} \tag{4.12}$$

is the summation extended to all the modes of the multiplicity α if λ_s is a multiple root. The value of C_{ij} is the same expression as (4.11) and (4.12) corresponding to the infinite roots, single or multiple. From these expressions it is seen that the diagonal terms $C_{ii}^{(s)}$ and C_{ii} are always positive and that the coefficients are symmetric, i.e.,

$$C_{ij}^{(s)}=C_{ji}^{(s)},\quad C_{ij}=C_{ji}. \tag{4.13}$$

In expression (4.10) the summation is extended from $j=1$ to $j=k$ over all forces Q_j which are taken different from zero. The k first equations therefore give the observed variables q_1 and q_k in terms of the forces Q_1 to Q_k applied to those coordinates.

Now we would like to solve these equations back and express the k applied forces in terms of the observed coordinates. This is best done by going back to the original Eqs. (3.13).

We consider the subsystem represented by the equation

$$\left[M\right]\begin{bmatrix} q_{k+1}\\ q_n \end{bmatrix}=0. \tag{4.14}$$

This system may be represented by its $n-k$ normal coordinates $\xi_{k+1}\cdots\xi_n$. The complete n degree of freedom system may be represented by these normal coordinates and by the k coordinates $q_1\cdots q_k$. The potential energy and the dissipation function for this system may then be written

$$\begin{aligned} V&=\tfrac{1}{2}\sum^{ij} a_{ij}q_iq_j+\sum^{is} a_{is}'q_i\xi_s+\tfrac{1}{2}\sum^{s}\sigma_r\xi_s^2,\\ D&=\tfrac{1}{2}\sum^{ij} b_{ij}\dot{q}_i\dot{q}_j+\sum^{is} b_{is}'\dot{q}_i\dot{\xi}_s+\tfrac{1}{2}\sum^{s}\dot{\xi}_s^2, \end{aligned} \tag{4.15}$$

where i and j vary from 1 to k and s from $k+1$ to n. As before we note that if one of the roots σ_s of M is infinite, the normalization of the mode can be done in such a way that the corresponding ξ_s^2 term in the dissipation function does not appear while there is a term ξ_s^2 in the potential energy. In that case, however, the condition that D is positive definite also requires that all coefficient b_{is}' corresponding to that mode vanish. Similarly since V is also positive definite if there are zero values of σ_s all corresponding coefficients a_{is}' must be zero.

With normal coordinates for the subsystem, the

equations for the complete system become

$$\left[\begin{array}{cc|cc} A_{11} & A_{1k} & A_{1,k+1}' & A_{1n}' \\ A_{k1} & A_{kk} & A_{k,k+1}' & A_{kn}' \\ \hline A_{k+1,1}' & A_{k+1,k}' & \beta_{k+1} & \\ & & & \ddots \\ A_{n1}' & A_{nk}' & 0 & \beta_{nn} \end{array}\right]\left[\begin{array}{c} q_1 \\ q_k \\ \hline \xi_{k+1} \\ \\ \xi_n \end{array}\right]=\left[\begin{array}{c} Q_1 \\ Q_k \\ \hline \\ 0 \\ \\ \end{array}\right], \tag{4.16}$$

where $A_{ij}=a_{ij}+pb_{ij}$, $A_{is}'=a_{is}'+pb_{is}'$ and $\beta_s=p+\sigma_s$ or 1, depending on whether σ_s is finite or infinite. We now solve the last $n-k$ equations for ξ_s. If $\sigma_s\neq\infty$, we may write

$$\xi_s=-\sum_{j=1}^{k}\frac{A_{sj}'q_j}{p+\sigma_s} \tag{4.17}$$

and, if $\sigma_s=\infty$,

$$\xi_s=-\sum_{j=1}^{k}A_{sj}'q_j=-\sum_{j=1}^{k}a_{sj}'q_j. \tag{4.18}$$

We also note that, if $\sigma_s=0$,

$$\xi_s=-\sum_{j=1}^{k}b_{sj}'q_j. \tag{4.19}$$

Substituting these values of ξ in the first k equations, we find

$$Q_i=\sum^{j}T_{ij}q_j \tag{4.20}$$

with

$$T_{ij}=A_{ij}-\sum^{s}\frac{A_{is}'A_{sj}'}{p+\sigma_s}. \tag{4.21}$$

If σ_s is zero or infinite for any particular mode the last term is replaced, respectively, by

$$A_{is}'A_{sj}'=A_{is}'b_{sj}', \tag{4.22}$$

$$A_{is}'A_{sj}'/p+\sigma_s=A_{is}'a_{sj}'. \tag{4.23}$$

All coefficients in (4.20) are symmetric

$$T_{ij}=T_{ji}. \tag{4.24}$$

The coefficients may be written

$$T_{ij}=\sum^{s}\frac{p}{p+\sigma_s}D_{ij}^{(s)}+D_{ij}+D_{ij}'p, \tag{4.25}$$

where

$$\begin{aligned} D_{ij}^{(s)}&=\psi_i^{(s)}\psi_j^{(s)}, \\ D_{ij}&=a_{ij}-\sum^{s}\frac{a_{is}'a_{sj}'}{\sigma_s}, \\ D_{ij}'&=b_{ij}-\sum^{s}b_{is}'b_{sj}', \\ \psi_i^{(s)}&=a_{is}'/\sigma_s^{\frac{1}{2}}-\sigma_s^{\frac{1}{2}}b_{is}'. \end{aligned} \tag{4.26}$$

All diagonal terms of the matrix T_{ij} are positive. This may be seen directly from the expression (4.26) for $D_{ii}^{(s)}$. As regards D_{ii} and D_{ii}' they must be positive because the ratio Q_i/q_i and $Q_i/\dot{q}_i$ must be positive for $p=0$ and $p=\infty$, respectively. Expression (4.25) of T_{ij} shows that any relaxation phenomena may be represented by a spring, a dashpot, and a sum of a great many elements made up of a Maxwell type material corresponding to the operator

$$(p/p+\sigma_s)D_{ij}^{(s)}. \tag{4.27}$$

Such a Maxwell material is represented by a spring and dashpot in series. We thus have shown that a mechanical model of springs and dashpots in series and in parallel may represent a very wide variety of relaxation effect involving not only mechanical, but chemical, thermodynamic phenomena, etc., and coupled effects between them.

V. APPLICATION TO THE GENERAL STRESS-STRAIN RELATIONS IN AN ANISOTROPIC CONTINUUM

We shall apply the previous theory to the formulation of the stress-strain relations in a viscoelastic material or more generally to any material exhibiting relaxation effects. We assume the deformation of this material under stress to be made of the variation of many degrees of freedom both internal and external. The internal degrees of freedom may be of mechanical, chemical, or other physical nature. In this case the nine stress components

$$\sigma_{\mu\nu}=\begin{Bmatrix} \sigma_{xx} & \sigma_{xy} & \sigma_{xz} \\ \sigma_{yx} & \sigma_{yy} & \sigma_{yz} \\ \sigma_{zx} & \sigma_{zy} & \sigma_{zz} \end{Bmatrix} \tag{5.1}$$

applied to the faces of an elementary cube of material play the role of applied generalized forces $Q_1\cdots Q_k$ $(k=9)$ considered in the previous section. The nine corresponding observed coordinates $q_1\cdots q_k$ are the nine components of the strain tensor,

$$e_{\mu\nu}=\begin{Bmatrix} e_{xx} & e_{xy} & e_{xz} \\ e_{yx} & e_{yy} & e_{yz} \\ e_{zx} & e_{zy} & e_{zz} \end{Bmatrix}. \tag{5.2}$$

Because of the symmetry

$$\sigma_{\mu\nu}=\sigma_{\nu\mu}, \quad e_{\mu\nu}=e_{\nu\mu} \tag{5.3}$$

we have only six independent components of these tensors. We now apply relations (4.20) and (4.25) to this material and write

$$\sigma_{\mu\nu}=\sum^{ij}P_{\mu\nu}^{ij}e_{ij} \tag{5.4}$$

with

$$P_{\mu\nu}^{ij}=\sum^{s}\frac{pD_{\mu\nu}^{ij(s)}}{p+\sigma_s}+D_{\mu\nu}^{ij}+pD_{\mu\nu}'^{ij}. \tag{5.5}$$

This is an operational tensor having the following sym-

metry properties:

$$P_{\mu\nu}{}^{ij}=P_{\nu\mu}{}^{ij}=P_{\mu\nu}{}^{ji}, \quad P_{\mu\nu}{}^{ij}=P_{ij}{}^{\mu\nu}. \tag{5.6}$$

These properties are the same as those of the elastic moduli of the theory of elasticity and we may therefore treat these operators in a similar way. By solving these equations with respect to the strain, we shall obtain a similar expression with an operator having the same form as in Eq. (4.10).

In expression (5.5) the summation is extended to all internal relaxation constants σ_s. Since the solid has a great many internal degrees of freedom there may be in some cases an almost continuous distribution of relaxation modes. This will correspond to a spectrum or spectral density distribution of the relaxation constant. With a density distribution function $\gamma(\sigma)$ we may write

$$P_{\mu\nu}{}^{ij}=p\int_0^\infty \frac{D_{\mu\nu}{}^{ij}(\sigma)\gamma(\sigma)}{p+\sigma}d\sigma+D_{\mu\nu}{}^{ij}+pD_{\mu\nu}{}'^{ij}. \tag{5.7}$$

This operational tensor is an analytic function of the time operator p. The more general representation of the operational tensors $P_{\mu\nu}{}^{ij}$ is therefore a set of 21 analytic functions of p constituting a symmetric six by six matrix. Under the integral, due account must be taken of the possibility of degeneracy of the modes in evaluating the product $D_{\mu\nu}{}^{ij}(\sigma)\gamma(\sigma)$. From expressions (4.26) we see that we may write

$$D_{\mu\nu}{}^{ij}(\sigma)=\psi_{\mu\nu}(\sigma)\psi^{ij}(\sigma). \tag{5.8}$$

VI. SPECIAL CASES OF SYMMETRY

The operational equations (5.4) may be simplified if we introduce the assumption that the material has a certain degree of symmetry. We shall discuss two examples, the case of cubic symmetry and the case of isotropy.

We proceed as in the classical theory of elasticity, where in the present case the operational tensor plays the same role as the elastic moduli. The relation between stress and strain must remain invariant under certain symmetry operations. In elasticity a cubic crystal has three elastic constants. Similarly in our case cubic symmetry leads to three operational tensor components. If we take the coordinate axes along the cubic axes the stress strain relations become

$$\begin{aligned}
\sigma_{xx}&=2Qe_{xx}+Re,\\
\sigma_{yy}&=2Qe_{yy}+Re,\\
\sigma_{zz}&=2Qe_{zz}+Re,\\
\sigma_{xy}&=2Se_{xy},\\
\sigma_{yz}&=2Se_{yz},\\
\sigma_{zx}&=2Se_{zx},
\end{aligned} \tag{6.1}$$

with $e=e_{xx}+e_{yy}+e_{zz}$. The three operators are

$$\begin{aligned}
Q&=\sum^{s}\frac{pQ^s}{p+\sigma_s}+Q+Q'p,\\
R&=\sum^{s}\frac{pR^s}{p+\sigma_s}+R+R'p,\\
S&=\sum^{s}\frac{pS^s}{p+\sigma_s}+S+S'p.
\end{aligned} \tag{6.2}$$

The quantities Q^s, Q, Q', R^s, $\cdots$ etc. are characteristic constants of the material, and σ_s are the internal relaxation constants. The summation may be replaced by an integration with a spectral distribution.

In the case of isotropy the number of operators is further restricted. The condition of invariance under any rotation implies

$$Q=S \tag{6.3}$$

and the stress-strain relations for the isotropic case become

$$\begin{aligned}
\sigma_{xx}&=2Qe_{xx}+Re,\\
\sigma_{yy}&=2Qe_{yy}+Re,\\
\sigma_{zz}&=2Qe_{zz}+Re,\\
\sigma_{xy}&=2Qe_{xy},\\
\sigma_{yz}&=2Qe_{yz},\\
\sigma_{zx}&=2Qe_{zx}.
\end{aligned} \tag{6.4}$$

The two operators Q and R are invariants of the form (6.2) and are the formal analogs of the Lame constants in the theory of elasticity. The case of hydrostatic stress is obtained by putting

$$\begin{aligned}
\sigma_{xx}&=\sigma_{yy}=\sigma_{zz},\\
\sigma_{xy}&=\sigma_{yz}=\sigma_{zx}=0,
\end{aligned} \tag{6.5}$$

with

$$3\sigma=\sigma_{xx}+\sigma_{yy}+\sigma_{zz}, \tag{6.6}$$

we find

$$\sigma=(\tfrac{2}{3}Q+R)e. \tag{6.7}$$

The operator $\frac{2}{3}Q+R$ is equivalent to a bulk modulus. The existence of this operator in the general form correspond to the assumption of bulk relaxation or volume creep. This may of course occur at high pressure or for porous materials. If $\frac{2}{3}Q+R$ is a constant, then the material obeys Hooke's law under hydrostatic pressure. Denoting by K the elastic bulk modulus this requires a relation between the operators Q and R,

$$\tfrac{2}{3}Q+R=K. \tag{6.8}$$

Equations (6.4) are then expressed by means of a single operator Q,

$$\begin{aligned}
\sigma_{xx}&=2Qe_{xx}+(K-\tfrac{2}{3}Q)e,\\
\sigma_{xy}&=2Qe_{xy}.
\end{aligned} \tag{6.9}$$

Very often the assumption is made that the material is

incompressible. In this case the operator R is infinite and $e=0$, but the product Re is finite and the limiting relation (6.7) is

$$\sigma = Re. \tag{6.10}$$

It is convenient to introduce this negative hydrostatic pressure σ in the relations (6.4) and write

$$\begin{aligned} \sigma_{xx}-\sigma &= 2Qe_{xx}, \\ \sigma_{yy}-\sigma &= 2Qe_{yy}, \\ \sigma_{zz}-\sigma &= 2Qe_{zz}, \\ \sigma_{xy} &= 2Qe_{xy}, \\ \sigma_{yz} &= 2Qe_{yz}, \\ \sigma_{zy} &= 2Qe_{zz}. \end{aligned} \tag{6.11}$$

In this case also a single operator Q is necessary to characterize the material.

There is need to call attention to a difference between the operational stress-strain relations and the theory of elasticity with respect to symmetry properties. This is the possibility of occurrence of multiple or mixed symmetry. If we note that $P_{\mu\nu}{}^{ij}$ is written in terms of the tensor

$$D_{\mu\nu}{}^{ij(s)} \quad D_{\mu\nu}{}^{ij} \quad D'_{\mu\nu}{}^{ij}, \tag{6.12}$$

it is not contradictory to assume that each of these tensors has its own symmetry. The material would then exhibit different symmetries, each of which would predominate at various strain rates.

ACKNOWLEDGMENTS

The author is indebted to the Shell Development Company for permission to publish the present work which has been sponsored during the past years as part of a research program on the mechanical properties of rock at the Exploration and Production Research Division in Houston, Texas.

JOURNAL OF APPLIED PHYSICS VOLUME 25, NUMBER 11 NOVEMBER, 1954

Electrical Noise Pulses from Polarized Dielectrics*

N. P. BAUMANN AND G. G. WISEMAN
University of Kansas, Lawrence, Kansas
(Received April 5, 1954)

Electrical noise pulses have been observed at elevated temperatures in polarized dielectrics (electrets) made of carnauba wax and of a vinyl acetate polymer. Pulse rate *versus* time was observed for electrets heated at a uniform rate and the results differ from those previously reported by others. Experiments devised to determine the origin of the pulses indicate that they are associated with the decay of volume polarization rather than with real surface charge. The total charge associated with the pulses from carnauba wax electrets is at least 5 percent of the maximum electret charge.

INTRODUCTION

ELECTRICAL noise pulses from electrets were first reported by Gutmann[1] but his mode of detection and the nature of his results were not given. Boyer[2] measured random electrical noise pulses in a number of plastics which were subjected to fields of 4 kv/cm to 118 kv/cm. More recently, Kojima and Kato[3] investigated noise pulses from electrets which were being heated at a uniform rate from room temperature to a temperature high enough to destroy the electret's charge. Kojima and Kato used two electrets which had been prepared by subjecting identical specimens of a carnauba wax and rosin mixture to the same electrical and thermal treatment. One electret was used for observing the noise pulses, the other for measuring the surface charge.

The present work was undertaken to verify and extend the work of Kojima and Kato. In this study, however, both the noise pulses and the charge measurements were made on the same electret primarily because incidental experiments revealed that electrets which have been given apparently identical thermal and electrical treatment are often unlike. Moreover, surface charge measurements were made by the conventional dissectible capacitor method,[4,5] rather than by the induction voltmeter method used by Kojima and Kato because the dissectible capacitor method allows a much smaller air gap between the measuring electrode and the electret. The average electric field E causing depolarization within a "short-circuited" electret with one air gap is (in mks units)

$$E=\sigma/\epsilon_0(d_2/d_1)+K, \tag{1}$$

where σ is the net surface charge of the electret, d_1 is

* Supported by the U. S. Signal Corps.

[1] F. Gutmann, Revs. Modern Phys. **20**, 457 (1948). This article reviews experimental and theoretical work on electrets. It contains an extensive bibliography.

[2] R. F. Boyer, J. Appl. Phys. **21**, 469 (1950).

[3] S. Kojima and K. Kato, J. Phys. Soc. (Japan) **6**, 207 (1951).

[4] M. Eguchi, Phil. Mag. **49**, 178 (1925).

[5] B. Gross, J. Chem. Phys. **17**, 866 (1949). This paper presents a two-charge theory of electrets.

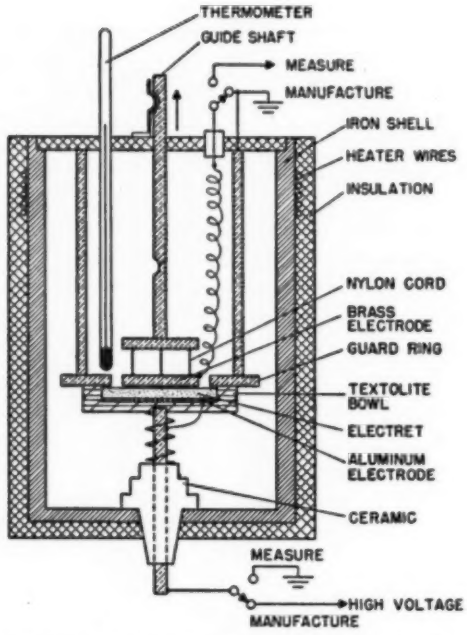

FIG. 1. Dissectible capacitor for polarization of samples and observation of electrical noise pulses.

the thickness of the air gap, d_2 is the thickness of the electret, and K is the low-frequency dielectric constant of the electret substance. Equation (1) implies that the growth and decay rates of an electret's charge are strongly dependent upon the air gap, especially at elevated temperatures where the electret is easily depolarized, an observation which was verified by an independent experiment. It is true that measurement by the dissectible capacitor method subjects the electret to a strong depolarizing field during each charge measurement, but the depolarizing time can easily be reduced to about five seconds. Consequently, the aggregate depolarization of typical electrets is less for the dissectible capacitor method than for the induction voltmeter method.

An attempt was made to determine the nature and origin of the noise pulses. A rough quantitative value for the charge associated with the various size pulses was obtained.

EQUIPMENT

A special dissectible capacitor was constructed inside a cylindrical oven (Fig. 1). It was designed so that the dielectric material could be melted, cooled with the electric field applied, and then measured, all without taking the electret from the oven.

The guard ring was incorporated primarily to improve the accuracy of the surface charge measurements. It served the additional purpose of leveling the Textolite bowl containing the electret material. The upper electrode served as a ground plate during electret manufacture, as a pickup electrode during pulse measurements, and as an induction plate during surface charge measurements. The lower electrode served as the high-voltage electrode during manufacture and as the ground plate during measurements of both noise pulses and surface charge. Nylon cord was found to be a satisfactory material for suspending the upper electrode from the guide shaft; some solid insulating materials generate spurious noise pulses of their own.

The circuits for controlling temperature and measuring surface charge are shown in Fig. 2. The electrometer was calibrated after each measurement by duplicating the observed deflection with the calibrating circuit shown. The noise pulses were amplified by a Sands Model 100 linear amplifier and a battery-powered preamplifier. An oscilloscope was used to observe the shape of the noise pulses. The pulses were counted either on a scale of 100 counter or on a ten-channel discriminator.

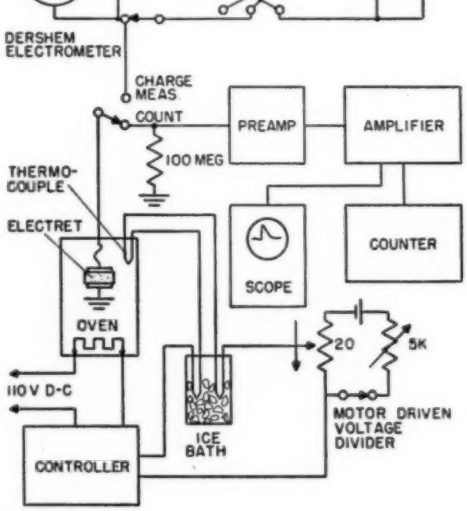

FIG. 2. Oven and associated equipment used for measurement of surface charge and noise pulses. Resistances are in ohms, capacitances are in microfarads.

RESULTS

In the first group of experiments, electrets were polarized by allowing melted carnauba wax to solidify and cool to room temperature with an electric field applied. The resulting electrets were maintained at room temperature for a short period after which they were warmed at a nearly uniform rate until the softening temperature was reached. The electrical noise pulses generated by the electret during the warming process are represented in Fig. 3. A number of general features are presented here: no pulses appear until the surface charge has reversed to the homocharge polarity, the maximum pulse rate occurs at a temperature slightly above 65°C (approximately coincidental with maximum surface charge), and the pulses disappear before the charge disappears completely.

Carnauba wax-rosin electrets were made to duplicate those reported by Kojima and Kato. They behaved in essentially the same fashion as the electret of Fig. 3, whereas Kojima and Kato obtained no pulses until after the charge had attained its maximum, and their maximum pulse rate occurred where the charge decayed most rapidly.

Electrets of polyvinyl acetate† prepared and measured in a similar manner gave the results shown in Fig. 4. The details vary, but the general behavior is similar to that of the carnauba wax electrets. The chief difference is the sudden onset of a myriad of very small pulses at 43°C and their sudden cessation 40 minutes later. No significance should be attached to the shape of the curve for the small pulses since it varied markedly among different electrets.

The amplifier circuit of Fig. 2 was calibrated by a known-voltage pulser. Using a ten-channel discriminator in place of the counter, curves similar to those of

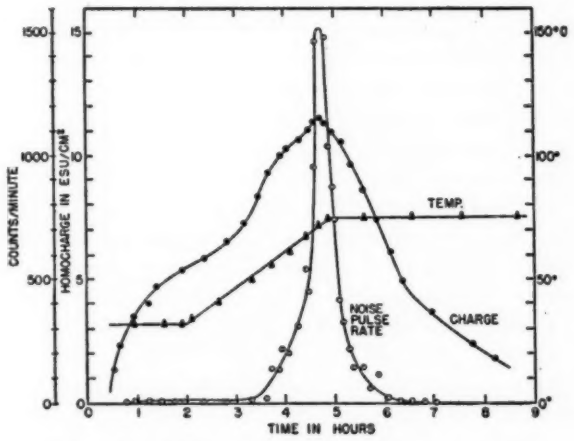

FIG. 3. Surface charge and pulse behavior of a carnauba wax electret polarized in a field of 12 kv/cm and heated from room temperature to 75°C.

Fig. 3 were obtained for each of the 10 channels for a single electret. The channels were set to respond to pulse sizes from 0.5 to 12 millivolts. By graphically integrating these curves and using the previous calibration, the total charge associated with the sum of all pulses was found to be 5 percent of the maximum charge attained by the electret.

Attempts were made to determine whether the noise pulses originate from the electret's heterocharge (volume polarization) or from its homocharge (real surface charge).‡

An unpolarized carnauba wax disk 0.7 cm thick was given a "sprayed-on" surface charge by momentarily applying a potential of 20 kilovolts across it at room temperature. The ensuing decay of surface charge and the noise pulses for this specimen are indicated in

† Gelva V-7 obtained from Shawinigan Products Company, 350 Fifth Avenue, New York.

‡ See reference 5 for an interpretation of electret charges.

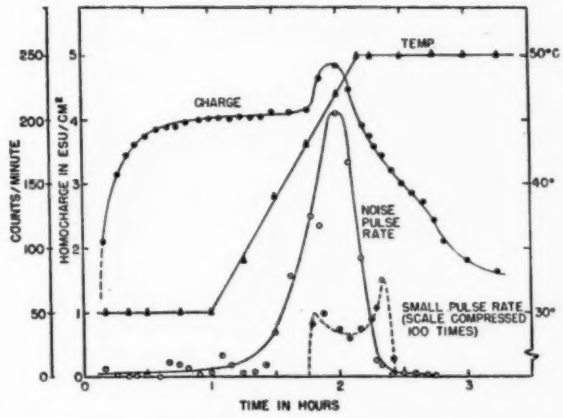

FIG. 4. Surface charge and pulse behavior of a polyvinyl acetate electret polarized in a field of 18 kv/cm and heated from room temperature to 50°C.

Fig. 5. The number of pulses was much less than for true electrets, and the greatest count rate was observed immediately after the field was removed although a slight increase occurred at 65°C. Nearly identical results were obtained for a carnauba wax disk which had been given only a molding charge of the same initial value.

An electret which had both its faces turned off in a lathe gave the same type of pulse and charge behavior as a "normal" electret (Fig. 3).

Electrodes were cemented to an electret by thin layers of petroleum jelly, thus largely eliminating the usual air gap. No charge measurements can be made on such a specimen but its pulse behavior with increasing temperature was similar to that of a normal electret. Another electret which had a thin coating of aluminum evaporated on both faces gave a pulse behavior differing little from that of a normal electret.

Electrets were also made from initially unpolarized carnauba wax disks. The disks were heated to a temperature slightly below the softening point (approximately 75°C) at which time the electric field was applied and the electret cooled. The charge behavior was the same as for normal electrets, but the pulse behavior was markedly different; only a few scattered pulses were observed. Similar pulse behavior was also

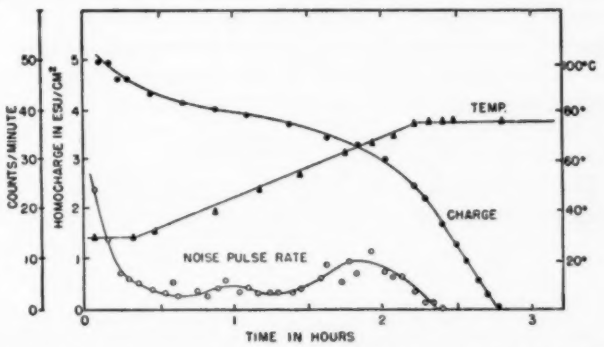

FIG. 5. Surface charge and pulse behavior of 0.7-cm thick disk of carnauba wax to which a field of 30 kv/cm was momentarily applied to give a "sprayed-on" charge.

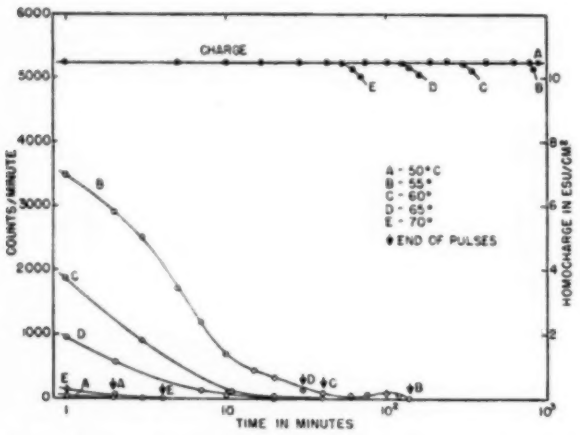

FIG. 6. Surface charge and pulse behavior of a group of carnauba wax electrets which were allowed to decay at a fixed high temperature. These specimens were 0.6 cm thick and were polarized in a field of 10 kv/cm.

observed for a disk which was given the same treatment after aluminum surfaces were evaporated on both faces.

A separate group of electrets was made from molten wax cooled in a field of 12 kv/cm at a constant rate of 2°C/hr to a final fixed temperature ranging from 50°C to 70°C. The charge and pulse behavior for each electret was observed as its charge decayed. The results are shown in Fig. 6. At these temperatures the charge of each electret reverses and attains the maximum allowed by air breakdown before the first charge reading can be taken following removal of the field. The rate of charge decay increased with the increase of final temperature. The greatest total number of decay pulses as well as the greatest pulse rate occurred for the electret of this group whose final temperature was 55°C. In every case the pulse rate was greatest immediately after removal of the field and the pulses quit well before the surface charge dropped below that of air breakdown.

Pulse shapes were observed on an oscilloscope. Most of the pulses had a rise time of less than 5 microseconds followed by an exponential decay estimated to be that determined primarily by the capacity of the electret and the input resistance of the preamplifier. A typical pulse is shown on the oscilloscope of Fig. 2. Many of the pulses, however, had an irregular decay probably caused by a pileup of succeeding pulses. With few exceptions, the pulses observed were unidirectional, having the same polarity as that of the adjacent electrode during manufacture.

DISCUSSION OF RESULTS

The present results agree with the theory of electrets proposed by Gross[5] in which two oppositely directed polarizations decay simultaneously, the surface homocharge decaying more slowly than the volume heterocharge.

Kojima and Kato report that their investigations suggest that the pulses are caused by the decay of the homocharge. The present results are, however, better explained by assuming that the pulses are caused by a decay of the heterocharge. To give pulses of proper polarity, a decaying homocharge would have to transfer its charge to the adjacent electrode. The results of the various surface treatments seem to preclude this. Sporadic ohmic decay of the homocharge inside the electret would give pulses of the wrong polarity.

Solidification in the forming field is essential for the formation of pulse-giving electrets of carnauba wax. It is believed that this process gives rise to cooperatively polarized aggregates of wax molecules superficially analogous to the domains of ferromagnetism.

It is not known how much of the total volume polarization of an electret may decay by pulses since, unfortunately, the value of 5 percent previously cited can serve only as a lower limit since imperfectly shaped pulses tend to lower the value by an unpredictable amount. Measurements of the total decay charge represented by the pulses may show it to exceed the greatest value of the surface charge and thus provide a further verification of the Gross theory.

The results shown in Fig. 6 of electrets decaying at constant temperatures indicate that the pulse rate is affected much more by the temperature than by the measured surface charge. Moreover, Fig. 6 indicates a threshold temperature of approximately 55°C which agrees with the temperature at which the heated electrets (Fig. 3) show a marked increase in pulse rate. This behavior agrees with what one expects from the Gross theory of two competing mechanisms. The inference can be made that low temperatures inhibit the depolarizing processes which give rise to pulses whereas high temperatures promote competing processes such as ohmic conductivity.

The mechanism giving rise to these pulses is believed to differ from that given by Boyer[2] who attributes the electrical noise observed by him to humidity-dependent localized breakdowns in the polymer chains which permit trapped ions to move through. No dependence on humidity was noted in the present experiments and the large number of charge carriers involved in each pulse (a typical pulse corresponds to a transfer of 10^7 electron charges) indicates the unlikelihood of this mechanism here. The assumption of cooperative dipole groups is consistent with all of the present observations.

Kinetics of Piles with Reflectors

V. H. RUMSEY*
Ohio State University, Columbus, Ohio
(Received January 25, 1954)

An integral equation for the time-dependent reaction is derived on the basis of the two-group model of neutron multiplication. When the effective multiplication constant is given, the solution reduces to a determination of the mean time T between consecutive generations, which is largely controlled by the circulation of neutrons in the reflector. If the steady distribution is known, T can be calculated from a simple formula.

To illustrate the orders of magnitude which are involved, T was calculated for a small pile surrounded by an infinite reflector. A value of $T=450$ microseconds was obtained assuming a mean lifetime in the core of 50 microseconds and a mean lifetime in the reflector of 14 000 microseconds.

STATEMENT OF THE PROBLEM

THE problem is to determine how the reaction (the number of fissions per second) changes with time in a pile consisting of a small core of fissile material, having a multiplication constant much greater than unity, surrounded by a reflector. It is assumed that we are given k_e, the effective multiplication constant, i.e., the average number of fissions of the second generation arising from one fission of the first generation.

The simple analysis based on a "one-group" model[1] of neutron diffusion may be very inaccurate in this case because it does not take into account the fact that many of the fast neutrons produced by fission in the core enter the reflector, are slowed down, and then returned to the core as thermal neutrons.

THE TIME-DEPENDENT EQUATION (IN DELAYED NEUTRONS)

The "two-group" model is adopted, in which all neutrons are classified either as thermal or "fast." The two-group time-dependent equations for the fast and thermal densities are difficult to solve, owing to the considerable algebraic manipulation involved in taking into account the boundary conditions. In place of this, the following method is adopted, in which the boundary conditions are taken into account at the outset. Let

$p_f(R,r)dv$ = probability that a fast neutron which is born at the point R (coordinates X, Y, Z) dies at the point $r(x,y,z)$ in the volume $dv=dxdydz$, (1)

and

$t_f(R,r)$ = the average time between birth at R and death at r. (2)

Fast neutrons die by being converted to thermal neutrons or by being captured (resonance capture). The quantities $p_t(R,r)$ and $t_t(R,r)$ are similarly defined for thermal neutrons. Let

$F(r,t)dvdt$ = the number of fast neutrons produced during time dt in the volume dv at the point $r(x,y,z)$. (3)

Similarly let $T(r,t)$ be the rate of production of thermal neutrons per unit volume.

Then

$pF(r,t)=k$ times the rate of dying of thermal neutrons at the point r in the core, and

$pF(r,t)=0$ for points r outside of the core,

where

p = probability of escaping resonance capture,

and

k = multiplication constant of the fissile medium.

Thus

$$pF(r,t)=k\int_A dv_1 T[r_1,\, t-t_t(r_1,r)]p_t(r_1,r)$$

for points r in the core, (4)

where $\int_A$ denotes integration over the entire system (core plus reflector).

Similarly

$$T(r_1,t)=p_1\int_C dv_2 F[r_2,\, t-t_f(r_2,r_1)]p_f(r_2,r_1), \quad (5)$$

where $\int_C$ denotes integration over the core and p_1 denotes the value of p at the point r_1: if r_1 is in the core $p_1=p$, otherwise $p_1=1$.

Substituting for T from (5) in (4) gives the following equation:

$$pF(r,t)=k\int_A p_1 dv_1\int_C dv_2 F[r_2,\, t-t_f(r_2,r_1) - t_t(r_1,r)]p_f(r_2,r_1)p_t(r_1,r). \quad (6)$$

* Formerly with Chalk River Laboratories N.R.C.; now with Atomic Energy of Canada, Ltd.

[1] *The Science and Engineering of Nuclear Power*, edited by Clark Goodman (Addison-Wesley Press, Inc., Cambridge, 1947), Vol. 11.

We seek a solution of the form

$$F(r,t)=F_i(r)\exp\omega_i t, \tag{7}$$

summed over all possible values of i.

Substituting from (7) in (6) and equating coefficients of $\exp\omega_i t$ we find that $F_i(r)$ is a solution of

$$pF(r)=k\int_A p_1 dv_1\int_C dv_2 F(r_2)\exp[-\omega t_f(r_2,r_1) -\omega t_i(r_1,r)]p_f(r_2,r_1)p_i(r_1,r), \tag{8}$$

and ω_i is the value of ω belonging to that solution.

After a relatively short time, the most positive ω_i predominates. If we denote this dominant value by w, the distribution $F(r,t)$ then has the form

$$F(r,t)=F(r)\exp wt. \tag{9}$$

Under these conditions the concept of k_e may be employed as follows. Suppose that we put into the otherwise empty system a distribution of fast neutrons $F(r)$. Then $pk_e=k$ times the fraction of the total number of fast neutrons put into the system which are captured as thermal neutrons in the core.

If $T(r_1)$ is the distribution of thermal neutron sources arising from the fast neutron sources $F(r_2)$, then

$$T(r_1)=p_1\int_C dv_2 F(r_2)p_f(r_2,r_1).$$

The number of thermal neutrons captured in the core is then

$$\int_C dv\int_A dv_1 T(r_1)p_i(r_1,r) =\int_C dv\int_A p_1 dv_1\int_C dv_2 F(r_2)p_f(r_2,r_1)p_i(r_1,r) \tag{10}$$

$$\therefore\quad k_e=\frac{k\int_C dv\int_A p_1 dv_1\int_C dv_2 F(r_2)p_f(r_2,r_1)p_i(r_1,r)}{p\int_C dv F(r)}.$$

If, now, we integrate (8) over the core, we obtain the equation

$$1=\frac{k\int_C dv\int_A p_1 dv_1\int_C dv_2 F(r_2)\exp[-wt_f(r_2,r_1)-wt_i(r_1,r)]p_f(r_2,r_1)p_i(r_1,r)}{p\int_C dv F(r)}, \tag{11}$$

which is identical to Eq. (10) except that $\exp[-wt_f(r_2,r)-wt_i(r_1,r)]$ in Eq. (11) takes the place of $1/k_e$ in Eq. (10). Since we are given that k_e differs from unity by a few percent, it is permissible to use the approximation

$$\exp[-wt_f-wt_i]\doteq 1-w(t_f+t_i). \tag{12}$$

Substituting from Eq. (12) in (11) gives

$$1=k_e-Tw, \tag{13}$$

where

$$T=\frac{\int_C dv_3\int_A p_2 dv_2\int_C dv_1 F(r_1)p_f(r_1,r_2)p_i(r_2,r_3)[t_f(r_1,r_2)+t_i(r_2,r_3)]}{\frac{p}{k}\int_C dv F(r)}. \tag{14}$$

Equation (13) is identical to the equation for w obtained from one group theory (when applied to systems for which one group theory gives a good approximation) provided that we replace the one group mean lifetime by our quantity T. Examination of Eq. (14) shows that T is precisely the average time between consecutive generations in the steady state, because

$$F(r_1)p_f(r_1,r_2)p_2p_i(r_2,r_3)dv_1dv_2dv_3$$

is, by definition of the p's and t's, the fraction of fast neutrons born by fission in dv_1 which are captured as thermal neutrons in dv_3 after the time

$$t_f(r_1,r_2)+t_i(r_2,r_3).$$

The numerator of Eq. (14) is therefore the sum of all possible times between one fission and the next. Again, in the steady state a fraction p/k of the neutrons produced by fission are eventually captured in the core and therefore the denominator of Eq. (14) represents the number of all such times between fissions. It follows that T is the average time between consecutive fissions.

Since k_e is almost unity, the mean lifetime T can be

found from Eq. (14), within a few percent, by using the steady-state distribution in place of $F(\mathbf{r})$. The integrals can then be evaluated with comparative ease as described below.

THE EFFECT OF DELAYED NEUTRONS

Let c be the fraction of thermal neutrons captured by fissionable nuclei which produce delayed neutrons, and η the number of fast neutrons emitted, either promptly or after a delay, per thermal neutron captured in this way.

If there are many types of delayed sources let

R_i = number of delayed sources of type i,
λ_i = decay constant of sources of type i,
μ_i = probability that when a delayed source is produced it will be of type i.

As before $F(\mathbf{r},t)$ represents the density of fast neutron sources.

In place of Eq. (6) we now have

$$p\int_C F(\mathbf{r},t)dv = k(1-c)\int_C dv_3\int_A p_2 dv_2 \times\int_C dv_1 F[\mathbf{r}_1, t-t_f(\mathbf{r}_1,\mathbf{r}_2)-t_i(\mathbf{r}_2,\mathbf{r}_3)] \times p_f(\mathbf{r}_1\mathbf{r}_2)p_i(\mathbf{r}_2\mathbf{r}_3)+\eta\textstyle\sum_i \lambda_i R_i, \quad (15)$$

where

$$\frac{dR_i}{dt} = \frac{k\mu_i}{\eta p}c\int_C dv_3\int_A p_2 dv_2 \times\int_C dv_1 F[\mathbf{r}_1, t-t_f(\mathbf{r}_1\mathbf{r}_2)-t_i(\mathbf{r}_2\mathbf{r}_3)] \times p_f(\mathbf{r}_1\mathbf{r}_2)p_i(\mathbf{r}_2\mathbf{r}_3)-\lambda_i R_i. \quad (16)$$

In order to proceed as before we assume that the distribution of delayed sources, as well as the distribution of prompt sources, differs slightly from the steady-state source distribution. Then the spatial distribution of the total source (i.e., the spatial part of $F(\mathbf{r},t)$) is approximately the same as the steady-state distribution. Note that in a liquid pile the distribution of delayed sources depends on the liquid flow. However, since c is usually less than 1 percent the assumption concerning $F(\mathbf{r},t)$ is usually valid.

Proceeding as before, we see that $F(\mathbf{r},t)=F(\mathbf{r})f(t)$ plus terms which die out in a very short time.

Owing to the various delayed neutron periods λ_i, we assume here that $f(t)$ has the form

$$f(t)=\sum_j A_j \exp W_j t \quad (17)$$

(the various values of W_j being due to the different decay periods λ_i), and that R_i can be represented by

$$R_i=\sum_j B_{ji}\exp W_j t. \quad (18)$$

Proceeding as before we finally obtain the equation

$$W_j T=(k_e-1-c)+c\sum_i \frac{\lambda_i\mu_i}{W_j+\lambda_i}, \quad (19)$$

assuming $|k_e-1|\ll 1$ and $c\ll 1$, where k_e and T are given in Eqs. (10) and (14).

Thus Eqs. (17) and (18) represent the solution of Eqs. (15) and (16). Equation (19) is identical to the conventional one-group equation provided that we replace the one-group mean lifetime by our quantity T.

If k_e varies with time the solution cannot be expressed in the above form. Equations (15) and (16) can, however, be put into a simpler form if the percentage change of k_e in time T is very small. Assuming that

$$F(\mathbf{r},t)=F(\mathbf{r})f(t)$$

(as before) we can then put

$$F(\mathbf{r}, t-t_f-t_i)=F(\mathbf{r})\left[f(t)-(t_f+t_i)\frac{df}{dt}\right].$$

Making this substitution in (15) and (16) we obtain the usual equations:

$$\frac{dN}{dt}=\frac{N}{T}(k_e-1-c)+\sum_i \lambda_i R_i, \quad (20)$$

$$\frac{dR_i}{dt}=\mu_i c\frac{N}{T}-\lambda_i R_i, \quad (21)$$

where

$$N=\frac{Tf(t)\int_C F(\mathbf{r})dv}{\eta}. \quad (22)$$

Since $F(\mathbf{r})f(t)$ represents the density of fast sources, N is approximately proportional to the number of thermal neutrons in the core (since c is small).

EVALUATION OF THE MEAN LIFETIME

Assuming that the steady-state neutron distribution is known, we need to know $p_f(\mathbf{r}_1,\mathbf{r}_2)$, $p_i(\mathbf{r}_1,\mathbf{r}_2)$, $t_f(\mathbf{r}_1,\mathbf{r}_2)$ and $t_i(\mathbf{r}_1,\mathbf{r}_2)$ in order to evaluate T from Eq. (14). For the present, let us omit the subscripts i and f and consider simply the properties of neutron sources and the neutron densities which they generate. Suppose that a unit source is placed at the point $\mathbf{r}=R$. Then, by definition, $p(R,\mathbf{r})$ is the rate of dying at the point $\mathbf{r}$. Thus $p(R,\mathbf{r})$ is given by

$$\tau D\nabla^2 p = p \quad \text{for} \quad \mathbf{r}\neq R, \quad (23)$$

where

τ = mean lifetime in the medium, (24)

and

D = diffusion coefficient in the medium. (25)

The condition for a unit source at $r=R$ is represented by

$$\int\int_{S\to R} D\tau\nabla p\cdot\mathbf{n}dS\to 1 \tag{26}$$

as the surface S shrinks around the point $r=R$, where $\mathbf{n}$ represents a unit inward normal to S. The quantity $y(R,r)=\tau(r)p(R,r)$ is the density at r due to a unit source at R, and therefore satisfies the usual boundary conditions; i.e., y and $D\nabla y\cdot\mathbf{n}$ are continuous at the boundary between the core and reflector.

The average time between birth at R and death at r, $t(R,t)$, can be obtained from the relation:

$$p(R,r)=\text{rate of dying at } r=N/t(R,r), \tag{27}$$

where $N=$ number of neutrons present in the system at any instant, which are destined to die at r. (28)

Thus

$$N=\int_A y(R,r_1)p(r_1,r)dv_1. \tag{29}$$

and

$$\frac{y(R,r)t(R,r)}{\tau(r)}=p(R,r)t(R,r)=\int_A dv_1 y(R,r_1)p(r_1,r)$$

$$=\frac{\int dv_1 y(R,r_1)y(r_1,r)}{\tau(r)}. \tag{30}$$

The reciprocity theorem states that

$$\tau(r)p(R,r)=y(R,r)=y(r,R)=\tau(R)p(r,R). \tag{31}$$

It follows from Eq. (30) that

$$t(R,r)=t(r,R). \tag{32}$$

If $S(r)$ represents any source distribution

$$\int_A dv_1 S(r_1)p(r_1,r_2)t(r_1,r_2)$$

$$=\int_A\int_A dv_1dv_3 S(r_1)y(r_1,r_3)y(r_3,r_2)/\tau(r_2)$$

(see Eq. (30))

$$=\int_A dv_3\rho(r_3)y(r_3,r_2)/\tau(r_2), \tag{33}$$

where

$$\tau D\nabla^2\rho=\rho-\tau S. \tag{34}$$

Thus we have the following interesting relations:

$y(R,r)t(R,r)$ is the density at r due to the source distribution $y(R,r_1)$[R fixed] where $y(R,r_1)$ is the density at r_1 due to a unit source at R, and

$\int_A dv_1 S(r_1)p(r_1,r)t(r_1,r)$ is the density at r due to the source distribution $\rho(r_2)$ where $\rho(r_2)$ is the density at r_2 due to the source distribution S.

Using these relations the formula for T [Eq. (14)] can be expressed entirely in terms of the p functions by means of Eq. (30) or, alternatively, can be reduced, by means of Eq. (33), to the form

$$T=\int_C q_t dv \Big/ \int_C \rho_t dv, \tag{35}$$

where

$$q_t=\tau_t D_t\nabla^2 q_t+\tau_t(\rho_t+pq_f/\tau_f), \tag{36}$$

$p=$ resonance escape probability,
$=1$ in the reflector,
$\rho_t=$ steady-state density of thermal neutrons,

$$q_f=\tau_f D_f\nabla^2 q_f+\tau_f\rho_f, \text{ and} \tag{37}$$

$\rho_f=$ steady-state density of fast neutrons.

Thus if the steady-state solution is known, T can be calculated quite easily by solving Eq. (37) for q_f and substituting in Eq. (36) to obtain q_t.

To illustrate the orders of magnitude which are involved, T was calculated for a small pile surrounded by an infinite reflector. A value of $T=450$ microseconds was obtained assuming a mean lifetime in the core of 50 microseconds and a mean lifetime in the reflector of 14 000 microseconds. This theory has been applied to the analysis of experiments involving piles with reflectors.[2]

ACKNOWLEDGMENT

This work was described in a secret report CRP 316 (Chalk River Laboratories Atomic Energy Project, January, 1947) which has recently been declassified. It is a pleasure to acknowledge the help given by A. G. Ward (who suggested the problem) and by Boris Davison.

APPENDIX

It has been suggested by the referees that it would be worth while to include an alternative derivation of Eq. (14) based on the material in S. Glasstone and M. C. Edlund, *The Elements of Nuclear Reactor Theory* (D. Van Nostrand Company, Inc., New York, 1952). The derivation given by the referees follows.

The general reactor equation with variable absorptions and an arbitrary slowing down kernel, $P(r,r^1)$—notation

[2] V. H. Rumsey, Can. J. Phys. (July, 1954).

as in Glasstone and Edlund, Chapter XII—is

$$\frac{1}{v}\frac{d\Phi}{dt}=D\Delta\Phi-\sum_a\Phi+\int\frac{k}{p}\sum_a P(\mathbf{r},\mathbf{r}^1)\Phi(\mathbf{r}^1)d\mathbf{r}^1. \tag{A1}$$

Let N be total slow neutron population. Then, by *definition* of k_{eff},

$$\frac{dN}{dt}=\frac{k_{\text{eff}}-1}{l}N=\frac{N}{T}. \tag{A2}$$

Integration of Eq. (1) over all space gives

$$\frac{dN}{dt}=\left[\int D\Delta\phi d\mathbf{r}-\int\sum_a\Phi d\mathbf{r}+\int\int\frac{k}{p}\sum_a P(\mathbf{r},\mathbf{r}^1)\Phi(\mathbf{r}^1)d\mathbf{r}d\mathbf{r}^1\right]$$

$$=\frac{\left[\int D\Delta\phi d\mathbf{r}-\int\sum_a\Phi d\mathbf{r}+\int\int\frac{k}{p}\sum_a P\Phi d\mathbf{r}^1d\mathbf{r}\right]vN}{\int\Phi d\mathbf{r}}. \tag{A3}$$

So that, by comparison with (2),

$$T=\frac{\int\Phi d\mathbf{r}}{v\left[\int D\Delta\phi d\mathbf{r}-\int\sum_a\Phi d\mathbf{r}+\int\int\frac{k}{p}\sum_a P(\mathbf{r},\mathbf{r}^1)\Phi(\mathbf{r}^1)d\mathbf{r}^1d\mathbf{r}\right]},$$

or, upon dividing numerator and denominator by $\int\sum_a\Phi d\mathbf{r}$,

$$T=\frac{\tau}{1-\frac{D}{\sum_a}\frac{\int\Delta\phi d\mathbf{r}}{\int\sum_a\Phi d\mathbf{r}}-\frac{\int\int\frac{k}{p}\sum_a P(\mathbf{r},\mathbf{r}^1)\Phi(\mathbf{r}^1)d\mathbf{r}^1d\mathbf{r}}{\int\Phi d\mathbf{r}}},$$

which is essentially Rumsey's result when $P(\mathbf{r},\mathbf{r}^1)$ is the one-group kernel.

JOURNAL OF APPLIED PHYSICS VOLUME 25, NUMBER 11 NOVEMBER, 1954

Mechanics of Two Immiscible Fluids in Porous Media

H. I. MEYER AND A. O. GARDER
Research Department, United Gas Corporation, Shreveport, Louisiana
(Received January 4, 1954)

Flow of two and three immiscible fluids in porous media is considered in which the various fluids are separated into different saturation zones by gravity. An equation of flow for any one fluid is derived with the condition that the other fluids must be stationary. This equation is then applied to solve the question of the maximum rate of flow of one fluid into a well from a radially symmetrical porous medium without producing the other fluid or fluids present in the formation. Different well geometries and fluid systems are considered. These problems are sometimes called "coning" problems.

INTRODUCTION

THERE are many problems in the fields of hydrology and reservoir mechanics in which systems involving two immiscible fluids of different densities flowing in porous media must be considered. Typical fluid systems are: air-water, water-salt water, oil-water, gas-oil, and gas-oil-water systems. The treatment in this paper concerns hydrocarbon-water systems under radial flow conditions but the methods used are of a general nature and may be immediately extended to other types of problems and to linear systems. All problems of this type are characterized by the existence of a free surface between the fluids whose shape is a function of the dynamics of the flowing fluids.

We shall consider three separate but similar problems. I. The production of oil or gas from a reservoir which has an underlying water table. II. The production of oil from a reservoir which has an overlying gas sand. III. Oil production from a reservoir with both an underlying water stratum and an overlying gas cap.

In all cases the problem will be to determine the maximum allowable flow of oil into the well with different completion practices without the gas or the water zone invading (coning into) the producing section of the well. In order to simplify the analytic treatment of this problem, the reservoir is assumed to be homogeneous, to extend radially from the well a distance which is large with respect to the well diameter; and the fluids are assumed initially to lie in this reservoir in horizontal layers.

The first question treated is that of determining the maximum oil flow into a well in the presence of a water cone. This theoretical maximum is obtained as a function of the depth of penetration of the well below the top of the oil layer (or zone) and the thickness of the oil zone at the drainage radius. The identical problem is solved for a gas well and a formula for maximum flow rate is obtained as a function of the depth of penetration, the reservoir thickness, and the bottom-hole pressure. For comparison purposes, the formulas are evaluated in engineering units. In a later paragraph the same problem is considered, including the influence of an impermeable barrier extending radially into the formation at the base of the well.

The second problem considered is the analogous one of determining the maximum rate of oil production under the condition that the gas cone shall not invade the producing section of the well.

In the third problem, formulas are obtained for the optimum depth at which the casing should be perforated and for the oil flow rate in a three-phase reservoir.

The mathematical treatment in this paper is based on the theory of fluid flow in porous media as presented by Hubbert.[1] Use may be made of the more general potential function defined by Hubbert which takes into account the capillary pressure at fluid interfaces by a shift of the origin of the z coordinates involved. The *form* of the final equations is identical and it does not seem justified to complicate this paper by these considerations.

There has been some prior work on this type of problem. Leverett, Lewis, and True[2] made use of dimensional models to study the form of the interface. Muskat treated the problem by making simplifying assumptions concerning the fluid behavior but his procedure is somewhat tedious; it is outlined in his book,[3] chapter 5. His results may be compared to those presented here.

THE BASIC EQUATION

We wish to use a formula previously derived for the simple case of radial flow of a single fluid into a well. In order to show that we may apply the formula to the two and three-fluid cases considered in the present paper, we first give a simple derivation.

Let h be the reservoir thickness, and let r_1 and r_2 be the drainage radius and the well radius, respectively. Let the flow be radial into a well which penetrates the reservoir. We choose the axis of the well as $r=0$, and the base of the formation as $z=0$; we suppose the reser-

[1] M. K. Hubbert, J. Geol. (November–December, 1948). Hubbert seems to have been the only one to propose a theory of flow in porous media with a rigorous respect for the mathematical and physical principles involved. This work appears to have been largely ignored.

[2] Leverett, Lewis, and True, "Dimensional Model Studies of Oil Field Behavior," Am. Inst. Mining Met. Engrs., Petroleum Div., reprint pp. 217–236 (1942–1943).

[3] Morris Muskat, *Physical Principles of Oil Production* (McGraw-Hill, Book Company, Inc., New York, 1949).

voir bounded above and below by impermeable surfaces $z=0$ and $z=h$.

If we assume the fluid to be incompressible, the potential function, as defined by Hubbert, becomes

$$\phi(r,z)=gz+\frac{p-p'}{\rho}$$

in which p is the pressure at the point (r,z), p' is a constant reference pressure, ρ is the density of the fluid and g is the gravitational constant.

Since the integral of the normal velocity over any closed surface within the flow region is zero (continuity criterion), we may use the boundary conditions of our problem to obtain

$$2\pi\int_0^h v_r(r,z)r\,dz=-Q, \quad r_2\leq r\leq r_1, \tag{1}$$

where Q is the volume of flow into the well per unit of time and $v_r(r,z)$ is the radial velocity of the fluid at the point (r,z).

Also, we may write Darcy's approximation

$$v_r(r,z)=-\sigma\frac{\partial\phi}{\partial r} \tag{2}$$

in the form

$$\phi(r,z)=\frac{1}{\sigma}\int_r^{r_1} v_r(\rho,z)\,d\rho+\phi_1, \quad r_2\leq r\leq r_1, \tag{3}$$

where ϕ_1 is the value of the potential function at the drainage radius r_1, $\sigma=(k\rho/\mu)$, where k is the permeability of the formation, ρ is the density, and μ, the viscosity of the fluid.

We may then use (1) and (3) to obtain

$$Q=\frac{2\pi\sigma}{\ln\frac{r}{r_1}}\left\{\int_0^h \phi(r,z)\,dz-h\phi_1\right\}, \quad r_2\leq r\leq r_1. \tag{4}$$

This is the formula which we wish to generalize for use in cases other than a single-fluid system.

We will consider only one case, *viz.*, we suppose that a fluid (oil) is flowing into a well which penetrates the reservoir to a depth D and that a second heavier fluid (water) lies below the oil.* We suppose that the pressure gradient in the well has caused the water to cone up, so that the interface between the fluids is no longer a horizontal plane, but forms a more general surface with equation $z=f(r)$.

If $\phi_0(r,z)$ is the potential function of the oil, if we set $\phi_0(r_1,z)=\phi_1$ and if we choose our coordinate system as shown in Fig. 1, then it is shown by Hubbert that

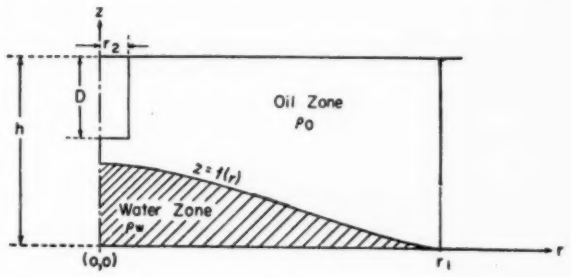

FIG. 1.

for any point (r,z) such that $z\leq f(r)$, the potential function of the oil in the region occupied by the water becomes

$$\phi_0(r,z)=\alpha z+\phi_1, \quad \alpha=\frac{\rho_0-\rho_w}{\rho_0}g. \tag{5}$$

It is important to observe that (5) is valid only if the water is at rest.

From the above derivation of formula (4), it is clear that it will be valid in the present case provided (1) and (3) are valid. But we certainly have, as before, that

$$2\pi\int_{f(r)}^h v_r(r,z)r\,dz=-Q, \quad r_2\leq r\leq r_1.$$

Since $v_r(r,z)=0$ if $z\leq f(r)$, the relation (1) holds.

Also, it is clear that (3) holds at any point (r,z) above the interface $z=f(r)$. If (r,z) is a point below the interface, i.e., $z\leq f(r)$, let r^* satisfy the equation $z=f(r^*)$, so that (r^*,z) is a point on the interface which lies in the same horizontal plane as (r,z). We then have, from (5),

$$\begin{aligned}\frac{1}{\sigma}\int_r^{r_1} v_r(\rho,z)\,d\rho&=\frac{1}{\sigma}\int_{r^*}^{r_1} v_r(\rho,z)\,d\rho=-\int_{r^*}^{r_1}\frac{\partial\phi_0}{\partial r}\,dr\\&=\phi_0(r^*,z)-\phi_1=\alpha z\\&=\phi_0(r,z)-\phi_1.\end{aligned}$$

Hence, (3) holds above and below the interface.

The important point to be observed here is that the possibility of extending (3), and therefore (4), to a system involving more than one fluid depends upon the fact that (5) gives the potential of the flowing fluid outside the region which it occupies. But (5) will hold only if the other fluids in the system are at rest. From this observation, it will be clear that Eq. (4) may be used to determine the flow of a single fluid into a well in the presence of a water or a gas cone provided only that the fluids in the cones are not moving. This will be true in the cases considered in the present paper.

WATER CONING IN AN OIL WELL

This section is concerned with the amount of rise of an underlying heavier fluid (water) in a two-fluid reser-

* For clarity we shall take the lighter fluid to be oil and the heavier to be water. However, this discussion is general for two fluids of different densities.

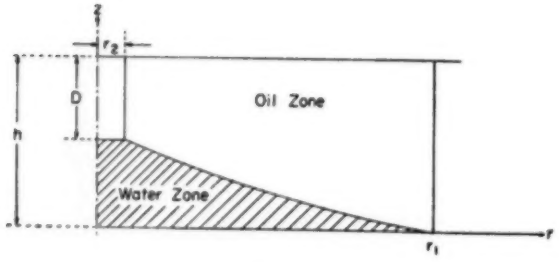

FIG. 2.

voir under a producing well due to the movement of the lighter overlying fluid (oil) toward the well. This phenomenon is usually termed water coning (see Muskat[3]).

If we restrict our consideration to the limiting case of determining the maximum (oil) flow into a well which partially penetrates a formation without producing water, a very simple solution is available.

We define the water and oil potentials as above:

$$\phi_w(r,z)=gz+\frac{p-p'}{\rho_w},$$
$$\phi_0(r,z)=gz+\frac{p-p'}{\rho_0}, \tag{6}$$

where ρ_w and ρ_0 are the densities of water and oil, respectively.

Since the water is at rest, it has a constant potential ϕ_w so that we have from (6)

$$p_w=\phi_w\rho_w-gz\rho_w+p',$$

and in the water zone on the interface

$$\phi_0=gz+\frac{p_w-p'}{\rho_0}$$
$$=\phi_w\frac{\rho_w}{\rho_0}+gz\left[\frac{\rho_0-\rho_w}{\rho_0}\right], \quad 0\leq z\leq h-D.$$

If we choose coordinates so that $z=0$ at the intersection of the oil-water interface and the drainage radius (Fig. 2), then

$$\phi_1=\phi_0(r_1,z)=\phi_w\frac{\rho_w}{\rho_0},$$

so that

$$\phi_0(r_2,z)=\phi_w\frac{\rho_w}{\rho_0}-g(h-D)\left[\frac{\rho_w}{\rho_0}-1\right]$$
$$=\phi_1-g(h-D)\left[\frac{\rho_w}{\rho_0}-1\right], \quad h\geq z\geq h-D, \tag{7}$$

where D is the depth of penetration of the well and h is the depth of the oil layer at the drainage radius.

The relations (7) follow from the continuity of the potential function and from our assumption that the water cone has reached the position shown in Fig. 2.

From (5) and (7) we then obtain

$$\int_0^h \phi_0(r_2,z)dz=\int_0^{h-D}\phi_0(r_2,z)dz+\int_{h-D}^h\phi_0(r_2,z)dz$$
$$=\phi_1 h+\frac{\alpha}{2}[h^2-D^2].$$

If we then take $r=r_2$ in (4), we obtain

$$Q=\frac{\pi\sigma\alpha}{\ln(r_2/r_1)}[h^2-D^2]$$
$$=\frac{\pi k_0 g(\rho_w-\rho_0)(h^2-D^2)}{\mu_0\ln(r_1/r_2)}. \tag{8}$$

This simple formula gives the maximum theoretical flow into a well of outside radius r_2 in a reservoir of radius r_1 which penetrates a depth D into a reservoir of oil saturated thickness h, under the condition that no water shall be produced.

WATER CONING IN A GAS WELL

The analysis of the preceding sections will have to be modified somewhat if the flowing fluid is a gas. Equation (1) is replaced by the equation

$$2\pi\int_0^h \rho_G v_r(r,z)r\,dz=-J, \quad r_2\leq r\leq r_1$$

which is a statement of the conservation of mass. J is the mass flux across any $r=$constant surface in the reservoir; it must also be equal to the mass rate of production from the well. We assume an isothermal system obeying the perfect gas law, i.e.,

$$\rho_G=p\times\text{constant}=\kappa p.$$

Using the coordinate system of Fig. 2, let p be the pressure at $z=0$. Then in the water zone, the hydrostatic law requires

$$p=p_0-\rho_w gz.$$

Proceeding as in the preceding section we obtain the following expression for J, the maximum gas flow

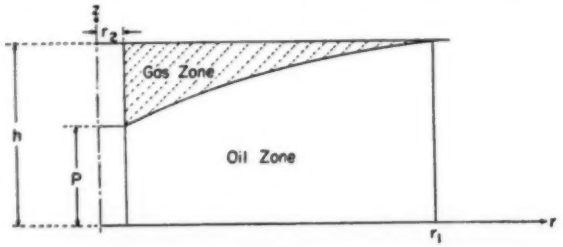

FIG. 3.

rate without water coning,

$$J=\frac{\pi\kappa k}{\mu\ln(r_1/r_2)g}\times\left\{\frac{p_0^2(1-e^{-2\kappa gh})}{2\kappa}+\frac{[p_0-\rho_w g(h-D)]^3-p_0^3}{3\rho_w}-\frac{[p_0-\rho_w g(h-D)]^2(1-e^{-2\kappa gD})}{2\kappa}\right\}. \quad (8')$$

GAS CONING (GAS ZONE OVER OIL)

The gas coning problem is completely analogous.

If, as in Fig. 3, we let P be the height of the producing section in a well of thickness h, then the oil potential at $r=r_2$ will be

$$\phi_0(r_2,z)=\begin{cases}\dfrac{\rho_G}{\rho_0}\phi_G+gP\left(1-\dfrac{\rho_G}{\rho_0}\right), & z\leq P,\\[2ex] \dfrac{\rho_G}{\rho_0}\phi_G+gz\left(1-\dfrac{\rho_G}{\rho_0}\right), & P<z<h_1.\end{cases}$$

Using this expression to evaluate the integral in (4) we obtain

$$Q=\pi\frac{k_0 g(\rho_0-\rho_G)(h^2-P^2)}{\mu_0\ln(r_1/r_2)}. \quad (9)$$

Equation (9) gives the maximum rate of flow into a well of outside radius r_2 in a reservoir with an oil saturation thickness h, which produces through an open area of height P measured from the base of the oil zone, under the condition that no gas shall be produced.

THREE-PHASE RESERVOIR (OIL FLOWING)

Now we consider a reservoir which initially has three parallel zones of water, oil, and gas saturation. The problem is to locate the perforations in the casing so that the oil flow into the well will be a maximum subject to the condition that the gas and water flow into the well will be a minimum.

If the producing section (perforated region) of the well is of height P, we may solve for the depth D to the bottom of this section subject to the condition that the water cone and the gas cone intersect the well at the bottom and top of this producing section, respectively (Fig. 4).

The oil potential in the gas zone will be

$$\phi_0=\frac{\rho_G}{\rho_0}\phi_G-gz\left(\frac{\rho_G}{\rho_0}-1\right),$$

so that we have

$$\phi_0(r_2,z)=\frac{\rho_G}{\rho_0}\phi_G+g(h-D+P)\left(1-\frac{\rho_G}{\rho_0}\right), \quad h-D\leq z\leq h-D+P. \quad (10)$$

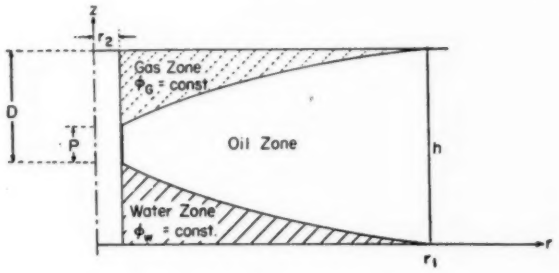

FIG. 4.

Considering the oil potential in the water zone, we obtain

$$\phi_0(r_2,z)=\frac{\rho_w}{\rho_0}\phi_w-g(h-D)\left(\frac{\rho_w}{\rho_0}-1\right), \quad h-D\leq z\leq h-D+P. \quad (11)$$

Equating (10) and (11), and using the continuity of the oil potential at the drainage radius, we obtain

$$D=h-(h-P)\frac{\rho_0-\rho_G}{\rho_w-\rho_G}. \quad (12)$$

As in the previous cases, we may express the oil potential at the well radius as

$$\phi_0(r_2,z)=\begin{cases}\dfrac{\rho_w}{\rho_0}\phi_w-g(h-z)\left(1-\dfrac{\rho_G}{\rho_0}\right), & h\geq z\geq h-D+P,\\[2ex] \dfrac{\rho_w}{\rho_0}\phi_w-g(h-D)\left(\dfrac{\rho_w}{\rho_0}-1\right), & h-D+P\geq z\geq h-D,\\[2ex] \dfrac{\rho_w}{\rho_0}\phi_w-gz\left(\dfrac{\rho_w}{\rho_0}-1\right), & h-D\geq z\geq 0.\end{cases}$$

If we use this expression to evaluate the integral in (4) and if we then use (12) to eliminate D from the equation, we obtain

$$Q=\frac{\pi k_0\rho_0}{\mu_0\ln(r_1/r_2)}\left\{\left(1-\frac{\rho_G}{\rho_0}\right)g\left[(h-P)\left(1-\frac{\rho_0-\rho_G}{\rho_w-\rho_G}\right)\right]^2+\left(\frac{\rho_w}{\rho_0}-1\right)g\left[(h-P)\frac{\rho_0-\rho_G}{\rho_w-\rho_0}\right]\times\left[P+(h-P)\frac{\rho_0-\rho_G}{\rho_w-\rho_G}\right]\right\}. \quad (13)$$

Evidently maximum flow will occur as the height P tends to zero. This gives

$$Q=gh^2\frac{(\rho_0-\rho_G)(\rho_w-\rho_0)}{(\rho_w-\rho_G)}\cdot\frac{\pi k_0}{\mu_0\ln(r_1/r_2)}. \quad (13')$$

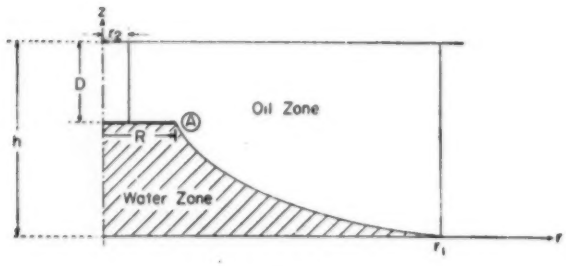

FIG. 5.

For maximum oil production from a three-phase reservoir, with minimum gas and water production, the well should be completed over a narrow interval at a depth

$$D=h\frac{(\rho_w-\rho_0)}{(\rho_w-\rho_G)} \tag{14}$$

from the oil-gas interface, where h is the thickness of the oil-saturated zone. (Both D and h are determined at the drainage radius.) This result follows if we let P tend to zero in (12).

EFFECT OF AN IMPERMEABLE BARRIER BELOW WELL

We return now to the water coning problem, modified by the introduction of an impermeable barrier or "break" extending radially a distance R from the well at its base (Fig. 5). We will derive a theoretical expression which demonstrates how this barrier will increase the maximum flow rate into the well without producing water. In this case, the well potential will have a discontinuity at r_2. Denoting the constant well potential by ϕ_2, we have that

$$\phi_0(r_2,z)=\begin{cases}\phi_2 & h\geq z\geq h-D\\ \phi_1-gz\left(\dfrac{\rho_w}{\rho_0}-1\right) & h-D\geq z\geq 0.\end{cases} \tag{15}$$

We then reduce Eq. (4) to

$$Q=\frac{2\pi k_0\rho_0}{\mu_0\ln(r_1/r_2)}\left\{D(\phi_1-\phi_2)+g\left(\frac{\rho_w}{\rho_0}-1\right)\frac{(h-D)^2}{2}\right\}. \tag{16}$$

We do not know ϕ_2 as a function of the reservoir geometry. If, however, we make the conservative assumption that the flow into the well is radial in the region $r<R$, $z<h-D$, we can deduce a relation which indicates the effect of the impermeable barrier.

At the point $(R, h-D)$, labeled A in Fig. 5, the potential will be

$$\phi_0(R,h-D)=\phi_1-g(h-D)\left(\frac{\rho_w}{\rho_0}-1\right).$$

From the radial flow formula [see Eq. (152)[1]], the potential drop from $r=R$ to $r=r_2$ will be

$$Q\frac{\mu_0\ln(R/r_2)}{k_0\rho_0\cdot 2\pi D}.$$

Hence, we have

$$\phi_2=\left\{\phi_1-g(h-D)\left(\frac{\rho_w}{\rho_0}-1\right)\right\}-Q\frac{\mu_0\ln(R/r_2)}{k_0\rho_0\cdot 2\pi D}.$$

Substituting this into (16), we have

$$Q=\left\{\frac{\pi k_0(\rho_w-\rho_0)g(h^2-D^2)}{\mu_0\ln(r_1/r_2)}\right\}\Big/\left\{1-\frac{\ln(R/r_2)}{\ln(r_1/r_2)}\right\}.$$

If we compare this result with (8), we see that this result reduces to (8) if $R=r_2$. The effect of the barrier is to multiply the allowable flow by the factor

$$1/\left\{1-\frac{\ln(R/r_2)}{\ln(r_1/r_2)}\right\}.$$

That this difference is *not* negligible will be seen from the following table, in which the drainage radius r_1 has been taken to be 660 feet and the well radius r_2 to be 3 inches:

R/r_2	$1/\left\{1-\dfrac{\ln(R/r_2)}{\ln(r_1/r_2)}\right\}$
2	1.10
3	1.16
4	1.21
5	1.26
10	1.41
100	2.40

In this example an R of only 6 inches (3-inch penetration into the producing formation) yields a 10 percent increase in permissible flow rate, while an R of 25 feet more than doubles the allowable production.

COMPARISON OF MAXIMAL FLOW RATES IN GAS AND OIL WELLS

To obtain some notion of the actual magnitudes of the maximal flow rates without production of water as predicted by the equations presented here, we rewrite Eqs. (8) and (8′) in engineering units. From (8) we obtain

$$Q=\frac{1.5351(\rho_w-\rho_0)(h^2-D^2)k}{\mu\ln(r_1/r_2)} \tag{17}$$

in which the units are as follows:

ρ	grams/cc
h,D	feet
μ	centipoises
k	darcies
Q	bbls/day.

If we take $Q^* = Q\mu \ln(r_1/r_2)/k(\rho_w - \rho_0)$, Eq. (17) becomes

$$Q^* = 1.5351(h^2 - D^2). \tag{18}$$

In Fig. 6, Q^* has been plotted as a function of the formation thickness h for six different values of the depth of penetration D.

In Eq. (8′) we write $\kappa = \rho_a/P_a$ in which ρ_a is the density of the gas at atmospheric pressure P_a (= 14.7 lb/sq in.). We take $\rho_a = 0.0450$ lb/cu ft (which is the density of methane at atmospheric pressure and 32°F). We then obtain $\kappa = 7.106(10)^{-10}$ sec²/cm². Using this value of κ and taking $D = 0$, Eq. (8′) becomes

$$J^* = 38.65\left\{-\frac{P_0^2}{2}(4.248)^2(10)^{-10}h^2 + 1.841(10)^{-5}P_0h^2 - 0.2658(10)^{-5}h^3\right\} \tag{19}$$

if we approximate e^{-x} by the first three terms of its power series, where we have written

$$J^* = \frac{\mu \ln(r_1/r_2)}{k} J. \tag{20}$$

The units in this equation are as follows:

J	MCF/day
k	darcies
μ	centipoises
P_0	lb/sq in.
h	feet.

In Fig. 7, J^* has been plotted as a function of the formation thickness h, for five different values of the bottom hole pressure P_0.

Since we have assumed that the depth of penetration is 0, the curves of Fig. 7 should be compared to the curve $D = 0$ of Fig. 6.

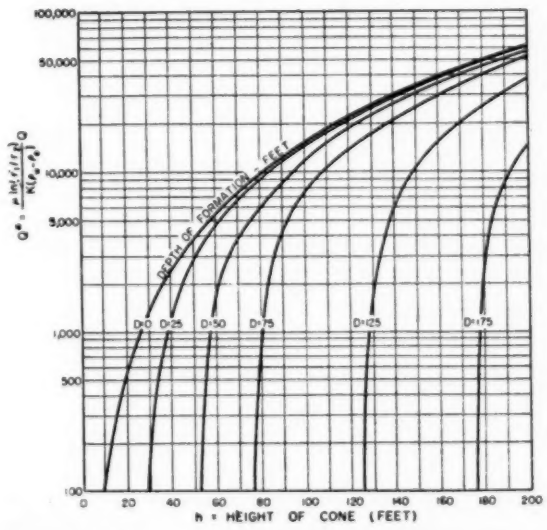

FIG. 6. Maximum oil production from an oil-water system without water production.

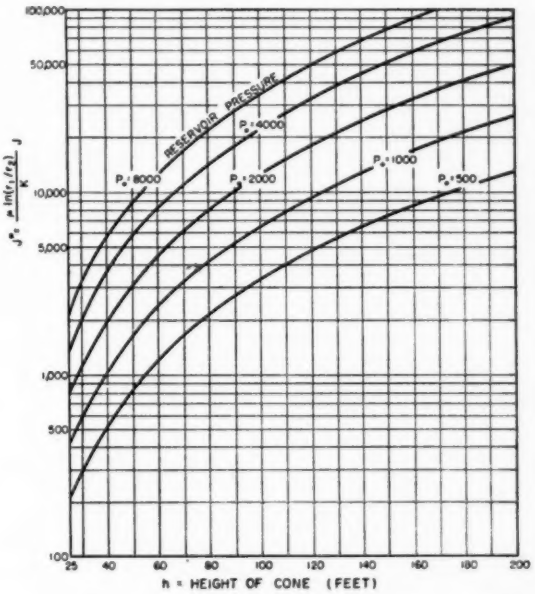

FIG 7. Maximum gas production from a gas-water system without water production.

DISCUSSION

It should be pointed out that this analysis has dealt with highly idealized reservoirs. Also we have assumed the validity of the linear Darcy equation. Inasmuch as these idealizations will not be exactly realized in a naturally occurring producing formation, our results should be used only to give an approximate, rather than an exact picture of the mechanics of a producing reservoir. With this qualification, we draw the following conclusions.

In an oil-bearing sand, which lies above a water-saturated zone, maximum production will be obtained without water entering the well by producing from the top of the oil-saturated zone. In this case the flow rate will be given by Eq. (8).

In an oil-bearing zone, which lies below a gas-saturated zone, and where water coning is not anticipated, it is best to produce from the bottom of the oil zone. The maximum oil flow will be given by Eq. (9). In an actual reservoir, gas will be produced due to its coming out of solution and to the expansion of the gas cap. Therefore, producing from the bottom of the oil zone cannot be expected to eliminate gas production, but only to keep it at a minimum with ordinary completion methods.

In a three-phase reservoir, the well should be completed at a depth D, given by Eqs. (12) or (14) below the top of the initial oil zone. The rate of oil production is then given by Eq. (13) or (13′).

A method of controlling water coning is suggested, *viz.*, the introduction into the formation of an imperme-

able barrier, extending radially from the bottom of the well. Such a barrier might be made by squeeze cementing techniques in reservoirs where the radial permeability is high compared to the vertical; also, it may be possible to locate the completion of the well above a naturally occurring shale break; or, conceivably, the development of new tools to place an artificial barrier might well be justified.

The relatively low production rates (computed in the preceding section) at which water can be expected to enter either a gas or an oil well indicated that the water can be expected to cone into the well in all cases under normal production rates in which the geology of the formation approximates the mathematical models used here. This raises the question: Will enough water enter the well to present a practical problem? We have studied this question by the use of models and also the problem: "How long does it take for the cone for form?" We intend to present the results of this investigation in a second paper.

JOURNAL OF APPLIED PHYSICS VOLUME 25, NUMBER 11 NOVEMBER, 1954

Forming Point-Contact Silicon Transistors

HAROLD JACOBS, FRANK A. BRAND, WESLEY MATTHEI, AND ALEXANDER P. RAMSA
Signal Corps Engineering Laboratories, Fort Monmouth, New Jersey

(Received January 4, 1954)

A new technique is reported in which silicon can be formed to provide transistor action. A suitable impurity is arced at the surface of the silicon causing the impurity to be diffused into a small region. Tests have been carried out using *n*-type and *p*-type silicon with various impurities. Initial results indicated voltage gains as high as 75 and power gains between 15 and 60. Other characteristics, such as variations in current multiplication with emitter current, were examined and the mechanism of alpha was compared with the theories developed by Sittner.

I. INTRODUCTION

DURING the past few years there has been an increasing interest in silicon transistors. This new interest has been due to the fact that the more standard germanium transistors fail to operate at slightly elevated temperatures (about 80°C), while theoretically, silicon should perform usefully at these same temperatures.

It was the purpose of this investigation to study the mechanism of "forming" point-contact silicon transistors. Generally speaking, forming may be thought of as the treatment given to a contact which enables one to obtain a significant transistor action. This treatment may be electrical, chemical, thermal or mechanical in nature.

For the case of *n*-type germanium, it has been found that surging current through the collector of the point-contact transistor in the difficult direction of flow enhanced the performance of the crystal.[1] (This was thought to be due to diffusion or electrolysis of impurities from the collector metal into the germanium crystal.) Initially these techniques were tried with low-resistivity *p*-type silicon, and no enhancement of transistor action was noticed. The techniques finally developed for forming silicon were found to be relatively high energy methods compared with those for forming germanium. Best results were actually obtained using an arc to drive the impurities into the silicon. In the course of these experiments different resistivities of *p*- and *n*-type silicon were used. Some of these silicon samples were furnished by Dr. Paul Keck, who utilized his new floating zone process of purification.[2]

In addition, the mechanism of the enhancement of the silicon transistor performance was examined and it was found that by doping the sample with suitable impurities, carrier injection could be increased at the emitter and current multiplication could be readily obtained in the collector region. The density and types of traps in both emitter and collector regions were estimated as well as the heights of energy barriers. With the interpretation gained by means of these experiments it would appear that silicon will become an increasingly important material for transistor action.

II. ELECTRICAL TESTING

All of the testing in the following experiments was carried out with the grounded base connections. The general test circuit and equivalent circuit are indicated in Figs. 1 and 2.

In the experiments to be described the voltage gains were determined by two methods, the first being a calculated value determined by static characteristics, and the second being a direct dynamic measurement to check the static methods.

The voltage gain can be determined from the static

[1] J. Bardeen and W. G. Pfann, Phys. Rev. **77**, 401–402 (1950).

[2] P. Keck, presented at the Rochester, New York, meeting of the American Physical Soc. (June 1953).

characteristic as follows:

$$\text{Voltage gain} = \alpha \frac{r_{22}}{r_{11}}, \tag{1}$$

$$\alpha = -\left(\frac{I_c}{I_e}\right)_{V_c} \tag{2}$$

and

$$r_{22} = \left(\frac{dV_c}{\partial I_c}\right)_{I_e}, \quad r_{11} = \left(\frac{\partial V_e}{\partial I_e}\right)_{I_c}. \tag{3}$$

The maximum power gain can be calculated by

$$\text{Power gain} = \frac{\alpha^2 r_{22}}{4 r_{11}}. \tag{4}$$

From these equations, we can see that the more important parameters are r_{11}, r_{22}, and α. The parameter α has physical significance and was studied in detail throughout the course of these experiments.

III. FORMING *P*-TYPE SILICON

In the first tests with *p*-type silicon, the samples studied were polycrystalline pieces with resistivities

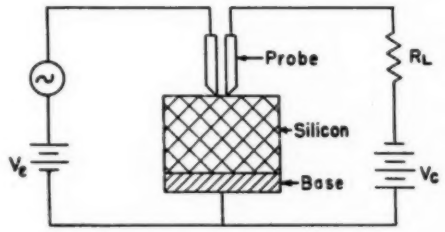

FIG. 1. Test circuit.

ranging from 0.1 to 1.0 ohm-cm. The crystals were large enough, however, to form and test by applying moveable, point-contact emitter and collector electrodes. The silicon was sliced to disks of 0.040 in. in thickness and one side was polished with 600-mesh carborundum. The unpolished side was plated to nickel and lead soldered to the base, which consisted of a large brass block. The exposed surface was then etched in successive rinses of hot sodium hydroxide, distilled water, hydrofluoric acid, and distilled water.

When this sample was tested initially, the results were very poor, and as shown in Table I, the surging of current in the forward direction of the emitter brought no enhancement as it has been reported to do for the case of *p*-type germanium.

After considerable testing with different probe materials and electrical surging of both the emitter currents and collector currents it was concluded that this material would not provide much transistor action with these processes.

Another approach to forming seemed more reasonable after the poor results with electrical surging. This consisted of doping the *p*-type silicon with small quantities of pentavalent impurities. The pentavalent impurities should form an *n*-type region in *p*-type material and might enhance the injection of electrons into the material in the emitter region. In order to test this hypothesis, the following technique was used for chemical forming.

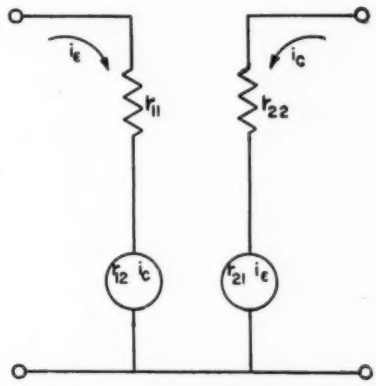

FIG. 2. Equivalent circuit.

A small piece of impurity (such as antimony) was placed on the freshly etched silicon surface. A pointed, 0.080-in. diameter tungsten probe was then placed in such a manner that the point of the tungsten pressed the antimony against the silicon. A sixty cycle current was then passed through the probe, the antimony, and the silicon; while at the same time, all parts were protected by a nitrogen atmosphere. The antimony could be diffused into the silicon by local heating (the silicon sometimes heating to as high as 800°C in the area of the contact).

The diffusion of antimony into the silicon could be further enhanced by arcing between the antimony and silicon. The arcing was induced by lifting the antimony from the silicon and making and breaking the contact. After this treatment, the sample was allowed to cool in nitrogen, etched, and later tested by means of a micromanipulator with two pointed 0.004-in. diameter tungsten wires. Best results were usually obtained with the emitter inside the contaminated region and the collector farther out in a less contaminated region. In addition to the treatment of antimony in this manner, other trivalent, quadrivalent and pentavalent impurities were tested. The results of the initial tests are given in Table II. It should be noted that these results were obtained from 0.1 to 1.0-ohm-cm resistivity silicon. Furthermore, the data in Table II are static

TABLE I. Electroforming.

	r_{22} ohms	r_{11} ohms	α	Voltage gain	V_e volts	V_c volts	I_e ma	I_c ma
Control	15 000	2300	0.04	0.3	2.5	13.5	1.15	0.95
After electroforming	9650	2300	0.02	0.1	2.5	13.5	1.2	1.42

TABLE II. Chemical forming.

Forming element	r_{11} ohms	r_{22} ohms	α	Voltage gain	V_e (dc)	V_c (dc)	I_e (dc)	I_c (dc)
Control (none)	380	2400	0.3	1.9	1.00	17.1	6.0	7.5
Bismuth	500	9120	0.5	9.1	1.35	35.5	3.0	4.5
Antimony	160	1370	1.2	10.0	0.66	15.1	6.0	15.0
Tin	140	2920	0.1	2.1	0.50	29.6	12.0	15.0
Indium	670	750	0.2	0.2	1.80	8.0	9.0	9.0
Aluminum	850	3800	0.1	0.5	1.06	12.7	1.5	3.0
Copper probes electroformed	80	1150	0.3	4.2	0.62	16.7	15.0	15.0
Phosphor bronze probes electroformed	110	1550	0.2	2.0	0.38	11.5	6.0	7.5

test results and hence are not accurate, but only indicative of trends.

Table II illustrates in a relative manner the role of impurity in the injection of electrons into the emitter region of a n-p-n point contact transistor. Referring to this table and Fig. 3, we see that for the control, the value of α was 0.3 After antimony forming, α rose to a value of 1.2. The rise in α indicates that a higher percentage of the emitter current consists of electrons entering the silicon and reaching the collector. In Fig. 3, part b, we see the type of change at the contact of the emitter which would account for an increase in α. In the case of trivalent impurities such as aluminum and indium, α decreased after forming. A condition, such as shown in Fig. 3, part c, where the potential barrier at the surface is raised because of the impurities, could account for the decrease in α from 0.3 to values such as 0.1 and 0.2. In the case of tin (quadravalent), α decreased but the contact was found to be ohmic. This might indicate that the emitter current consisted mainly of holes (since few electrons were injected) and this type of contact resulted from the tin wiping out the effects of surface traps. Because of the ease of using antimony and early favorable results, further tests were continued with antimony-formed silicon. Some of the typical results obtained here are listed in Table III.

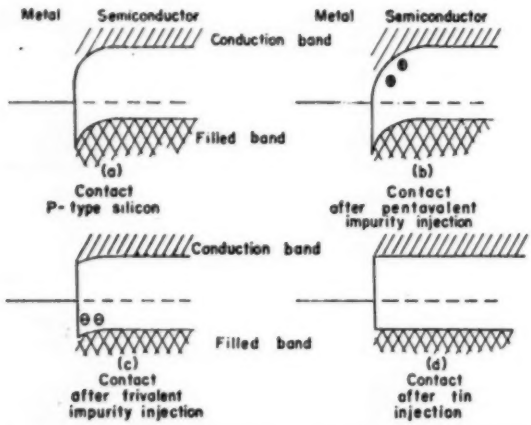

FIG. 3. Energy band distortions resulting from impurities.

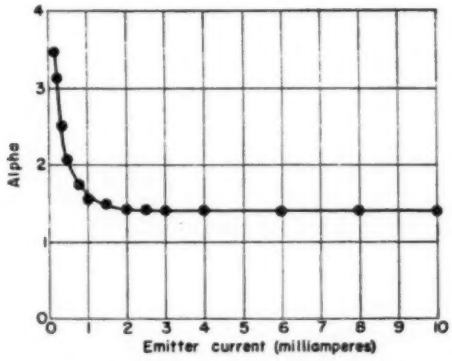

FIG. 4. Alpha *vs* emitter current for 0.1–1.0-ohm-cm silicon (antimony formed).

Here, we are still dealing with low resistivity silicon (0.1 to 1.0 ohm-cm).

In measuring the static characteristics it has been found that the curves for r_{11}, r_{22}, r_{12}, r_{21}, and α *vs* I_e, resemble very much the curves obtained for germanium. Several of these are illustrated in Figs. 4 and 5.

Up until this point we have only discussed p-type silicon with resistivities of from 0.1 to 1.0 ohm-cm. Additional work was carried out using p-type silicon of resistivities ranging from 5 to 10 ohm-cm. In addition to using higher purity silicon, together with the arcing technique of impurity injection, it was found that surging large currents in the reverse direction of the emitter sometimes enhanced the transistor action of the unit.

With these innovations in technique, a fundamental property of the silicon specimens became more apparent. The maximum alphas of the silicon treated in this way, appeared to be much greater than the maximum alphas in average germanium transistors. For instance, while the maximum alpha for typical germanium units range from 4.0 to 5.0, we have consistently observed in the silicon units maximum alphas of about 10. In addition, many silicon units have had alphas greater than this value and in Fig. 6 the data illustrates an alpha of 25. In Fig. 7 another α *vs* I_e curve is given for another area of the same crystal.

Primarily as a result of the increased resistivity, not only were the alphas increased but the voltage gains were greatly enhanced. The operating characteristics of some of the units are shown in Table IV. The improved performance was also noted in unformed samples as well as the formed silicon. In Fig. 8 we see

TABLE III. Operating characteristics for point contact (p-type) silicon transistors.

Sample no.	I_b	I_e	V_e	V_c	R_L	α	Dynamic voltage gain
1	3.0	10.3	0.20	40.5	10K	1.07	23:1
2	4.5	9.0	0.49	25.2	10K	1.00	15:1
3	0.5	7.2	0.74	25.0	20K	0.76	15:1
4	0.6	3.0	0.49	18.5	···	1.60	33:1

TABLE IV. Operating characteristics of silicon transistors.

Description	r_{11} ohms	r_{12} ohms	r_{21} ohms	r_{22} ohms	Calculated voltage gain	Measured voltage gain	α_{max}	$\alpha_{operating}$	Power gain
Control test, 5 ohm-cm, p-type silicon, unformed	1222	165	12 800	8000	10	5	···	1.5	1.8
Sb formed, 5 ohm-cm, p-type silicon	1000	333	32 900	9120	33	44	10.0	3.6	39.6
Sb formed, 5 ohm-cm, p-type silicon (probes in different area)	510	···	46 000	20 000	92	60	···	2.3	34.5
Sb formed p-type silicon, (different specimen)	···	···	···	···	···	75	7.0	1.5	28.3

the α *vs* I_e curve for unformed 5–10 ohm-cm silicon is markedly better than the performance of the unformed lower resistivity material (compared with Table I and Table II control samples). After the antimony forming, the maximum α improved from 4.5 to 7.0 as shown in Fig. 9. This particular sample concurrently showed an increase in dynamic voltage gain from an initial value of 3 to a value of 20 after forming.

IV. BARRIER POTENTIAL AT THE EMITTER CONTACT

It is possible to estimate the potential barrier at the surface of the antimony doped silicon sample when dealing with the n-p-n point contact transistor. Let us assume that since in many cases the asymptotic value of α at higher emitter currents was nearly equal to one, all current flow was due to electrons. In almost all cases, when I_e was one milliampere, α was very near one. In addition, losses due to recombination and diffusion are considered negligibly small.

The equation for current in a semiconductor is

$$j=N_0 evV/L, \tag{5}$$

where j=current density, e=electric charge, v=electron mobility, and V/L=field. In the actual case, we can estimate j, e, v, and V/L and thus compute N_0.

The factor N_0 will in turn determine the height of the barrier by means of the relation

$$N_0=2\left(\frac{2\pi mkT}{h^2}\right)^{\frac{3}{2}} e^{-(\phi-\chi)/kT}. \tag{6}$$

Let us take the current I_e to be 0.001 amp as was found in several typical experiments. The radius near the contact was estimated as 2×10^{-3} cm, a radius sufficiently large to be able to neglect fields just at the point of contact due to surface states. Then, since $A=\pi r^2$, $A=12.56\times10^{-6}$. The factor j is then determined by $I_e=jA$, and $j=78$ amp/cm^2.

Other components of Eq. (5) are $e=1.6\times10^{-19}$ coulomb and $v=3\times10^2$ cm/sec (volt/cm). To compute the field in the vicinity of the emitter V/L we use the following relation:

$$\frac{V}{L}=F=\rho\frac{I_e}{2\pi r^2}, \tag{7}$$

where ρ is the resistivity and is approximately 1.0, I_e is the emitter current (approximately 0.001 amp) and $r=2\times10^{-3}$ cm. With these values, F is 40 volts/cm and substituting into Eq. (5), the value for N_0 is 4×10^{16}.

To obtain the energy term $(\phi-\chi)$, we can refer to Eq. (6), and solving, we find $(\phi-\chi)$ is approximately 0.14 ev.

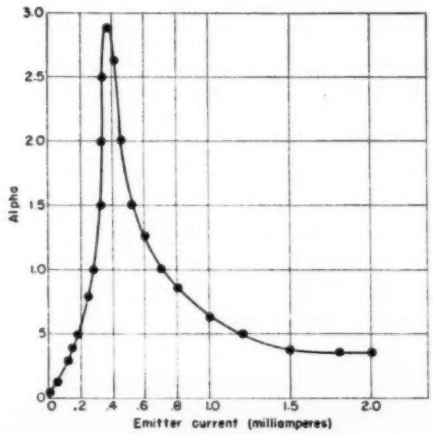

FIG. 5. Alpha *vs* emitter current for 0.1–1.0 ohm-cm silicon (antimony formed).

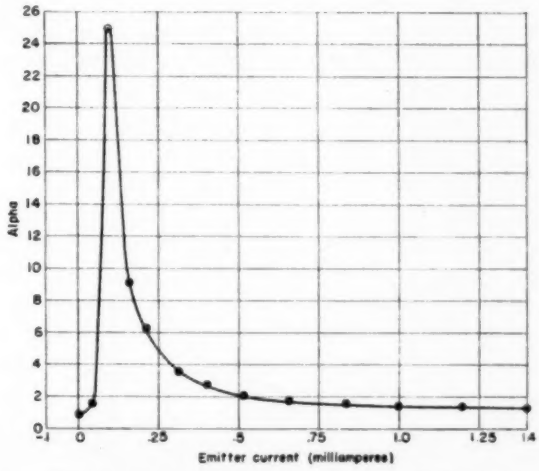

FIG. 6. Alpha *vs* emitter current for 5–10 ohm-cm silicon (antimony formed).

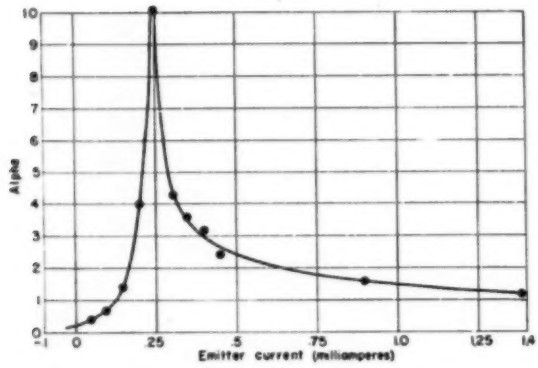

FIG. 7. Alpha *vs* emitter current for 5–10 ohm-cm silicon (antimony formed).

To summarize, using Eq. (5) we have estimated N_0, then using Eq. (6) we have found the value of $(\phi-\chi)$. The energy barrier of 0.14 ev may not necessarily be simple in shape, but does in fact represent a potential barrier limiting the injection of electrons into the emitter region (Fig. 10).

V. FORMING *N*-TYPE SILICON

In working with *n*-type silicon, there is one theoretical advantage. The *n*-type silicon semiconductors should have a maximum α near 4, whereas the *p*-type should only have an α near 1.3 in the higher emitter current range. This is due to the manner in which the dependence of α on mobility differs with *n*-type and *p*-type silicon.

As compared with the *p*-type silicon which relies on electron injection for transistor action, *n*-type crystals depend upon hole injection. In view of this difference, doping agents of the trivalent type were studied intensively. In particular, aluminum and indium were tried using the same forming techniques as described previously.

The results of forming with aluminum are indicated in Table V. It can be seen here, that forming raised the α under typical operating conditions, lowered r_{11}, and raised r_{22}. In Table V, crystal No. 2 was a sample furnished by Dr. P. Keck in which he utilized his new process of purification and crystallization.[2] Sample No. 1 was furnished by a commercial company. The two specimens were formed in a similar manner and the resistivities were in the same range (~5 ohm-cm). The reproducibility in these tests and others appeared good.

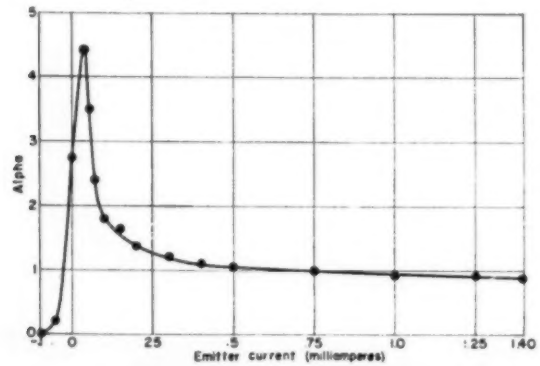

FIG. 8. Alpha *vs* emitter current for unformed high resistivity silicon.

In Fig. 11 the I_c *vs* I_e curves are shown for both samples after forming. It is to be noted that the resistivities of both samples are nearly the same and the slopes of the curves in Fig. 11 are not too different, except in the lower region of emitter current. Although the data described refer to aluminum as an impurity,

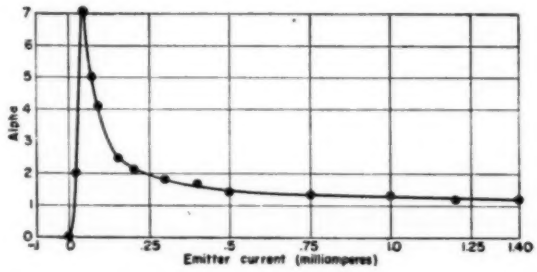

FIG. 9. Alpha *vs* emitter current for antimony formed high resistivity silicon.

similar data were obtained with indium as an impurity. However, due to the difference in physical properties such as melting points, and possible diffusion rates, the aluminum was found to give more reliable and reproducible results.

According to the theory, antimony, which is an *n*-type impurity, should not give hole injection with *n*-type silicon. This was tried, and it was noted that the presence of antimony decreased the interaction between

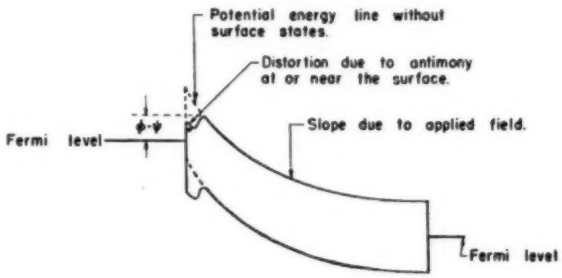
Potential energy line without surface states.
Distortion due to antimony at or near the surface.
Slope due to applied field.
Fermi level
ϕ-ψ
Fermi level

FIG. 10 Energy band distortion due to antimony impurity near the surface.

the emitter and collector, α decreasing and the voltage gain diminishing to much less than one. These results lend support to the ideas previously mentioned concerning the formation of a localized impurity region of the proper sign. That is, for *p*-type silicon we needed an impurity region which formed an *n*-type region and *vice-versa*.

In Fig. 11, α is plotted as a function of I_e, the emitter current. Here we see that α rises to a value of 5.2 for the case of sample No. 2. This peak occurred at small emitter currents (50 μa). It was found that the sample

TABLE V. Aluminum forming.

	Crystal No. 1		Crystal No. 2	
	Control	Al formed	Control	Al formed
α	0.34	1.10	0.067	1.95
r_{11}	5600	1300	1320	800
r_{22}	8700	29 000	8210	13 100
Voltage gain	0.8	34	0.417	36
Power gain	0.068	9.4	0.007	17.5

Typical operating conditions

Crystal No. 1 (After forming)				Crystal No. 2 (After forming)			
Emitter bias (volts)	Collector bias (volts)	Emitter current (ma)	Collector current (ma)	Emitter bias (volts)	Collector bias (volts)	Emitter current (ma)	Collector current (ma)
0.65	28.5	0.5	1.0	0.5	30.0	1.0	4.5

could be dynamically operated at very low emitter currents, with stability at emitter currents as low as 50 μa. Thus due to the enhanced α, a high voltage gain could be achieved.

In the course of these experiments we have also observed a definite photoelectric response for the various crystals although no quantitative data has been obtained as yet. When irradiated with light (and particularly infrared), both the alphas and the voltage gains were observed to decrease. The effect was slightly more pronounced for the n-type crystals than for the p-type samples tested.

VI. INTERPRETATION OF ALPHA

In the previous data, one can see that α rises to a value much greater than one, and then falls rapidly with increasing emitter currents. This effect has been accounted for quantitatively in the work of Sittner[3] and Shockley.

The equation for α as a function of temperature and current is given by Sittner as

$$\alpha=\gamma\left[1+b+\frac{ab}{(1+G'I_e)^2}\right], \tag{8}$$

where

$$\alpha=-\left(\frac{\partial I_c}{\partial I_e}\right)_{V_c},$$

$$\gamma=\frac{\text{hole current}}{\text{emitter current (total)}},$$

b = electron mobility/hole mobility,

I_e = emitter current,

$$G'=\frac{\gamma}{A\left(q\mu_p\frac{N_t}{a}\right)\frac{V_c}{L}},$$

A = area of collector contact,

q = electron charge,

μ_p = mobility of holes,

N_t = number of acceptors in region of collector,

V_c/L = field of vicinity of collector,

$$a=\frac{p_t}{p}=\frac{N_t}{N_v}e^{E_b/kT},$$

$$\frac{p_t}{p}=\frac{\text{number of trapped holes in region of collector}}{\text{number of free holes in region of collector}},$$

N_t = number of traps in region C,

N_v = number of states in filled band,

and

E_b = energy of traps.

In this theory, α is made up of three components. The first is γ. This component represents the number of holes that reach the collector as a result of having been injected in the emitter region. With perfect injection ($\gamma=1$) and no other terms, α would theoretically be 1. In the second term, b (or the ratio of electron mobility to hole mobility) comes as a result of the principle that all free charges must be neutralized. That is, for every free positive charge in the collector region, an electron is drawn from the collector electrode for neutralization. This process occurs in less than 10^{-11} second. The third term $\gamma ab/(1+G'I_e)^2$ represents a still further enhancement of by the ratio of mobility mechanism. If there are acceptor traps in the collector region, the holes in going through this region will be slowed down. The holes will have a certain amount of recombination with the acceptors and then be released, the process con-

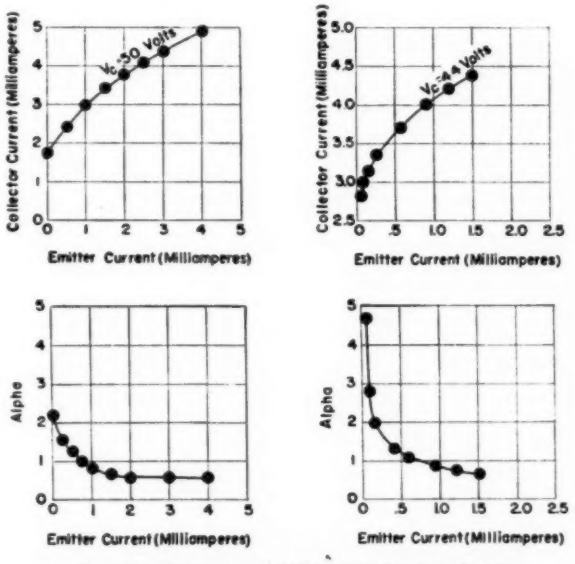

FIG. 11. Current multiplication characteristics for aluminum formed silicon.

[3] W. R. Sittner, Proc. Inst. Radio Engrs. 448–454 (1952).

TABLE VI. Physical constants for silicon and germanium transistors.

Sample	Description	α_{max}	α_{min}	γ	α'	I_e'(ma)	a	N_t	E_b(ev)
Silicon	p type, 5 ohm-cm resistivity, antimony formed	25.0	1.22	0.92	13.1	0.135	78.0	1.94×10^{16}	0.27
Silicon	p type, 5 ohm-cm resistivity, antimony formed, probes in different location	10.0	1.20	0.90	5.6	0.290	29.7	1.58×10^{16}	0.26
Silicon	p type, 0.1 to 1.0 ohm-cm resistivity antimony formed	2.9	0.35	0.26	1.6	0.500	29.4	0.77×10^{16}	0.27
Silicon	n type, crystal No. 1 5 ohm-cm, Al doped	2.2	0.60	0.15	1.4	0.375	3.55	1.21×10^{15}	0.26
Silicon	n type, crystal No. 2 5 ohm-cm, Al doped	5.2	0.60	0.15	2.9	0.100	9.8	9.0×10^{14}	0.31
Germanium	CB 92 (from Sittner) n type	4.4	2.00	0.64	3.2	0.017	2.0	7.2×10^{12}	0.31
Germanium	CB 84 (from Sittner) n type	3.2	...	...	...	...	1.0	6.70×10^{12}	0.31

suming a finite interval of time. This reduction of the hole mobility increases the ratio of electron mobility to hole mobility and is shown as the third component in Eq.(8).

By a graphical analysis of the α *vs* I_e curves determined for the formed silicon, one can find some of the physical constants of the material and compare them with those of germanium samples tested by Sittner. If the theory developed by Sittner is correct, the data shown in Table VI provide a comparison of the physical constants of the silicon point-contact transistors with the constants for germanium.

From the data in Table VI, it would appear that the arc-type forming technique greatly enhances the injection of carriers at the emitter. In the collector region, the enhanced α mechanism is not clear. For instance, we do not know exactly what was done during the experimental procedures to cause the "hook" region at the collector. If we accept the "hook" theory as the explanation of enhanced alphas at low emitter currents, then there are two possible factors which account for the high alphas observed. First, we might assume the high N_t and "hook" are already in the silicon specimens at the start. By increasing γ at the emitter we increase the effects of N_t proportionately. In some cases we have seen evidence to support this theory. The second possibility is that during the chemical forming in the emitter region, some of the impurities do diffuse to the collector region, increasing N_t and setting up a "hook" region. To what extent each of these factors comes into play is still a matter of further research and can be decided only by further experiments.

Acknowledgment should be made to Mr. John B. Freely who has recently experimentally verified that these units can be operated stably at elevated temperatures (150°C), to Dr. D. Dobischek for many consultations, and to the late Dr. J. E. Gorham who suggested this program.

JOURNAL OF APPLIED PHYSICS VOLUME 25, NUMBER 11 NOVEMBER, 1954

Ferrite Phase Shifters in Rectangular Wave Guide*

BENJAMIN LAX,† KENNETH J. BUTTON,† AND LAURA M. ROTH‡
Lincoln Laboratory, Massachusetts Institute of Technology, Cambridge, Massachusetts

(Received January 14, 1954)

The problem of the propagation of electromagnetic energy down an infinitely long rectangular wave guide partially filled by a ferrite slab is solved. The solution is expressed in the form of a transcendental equation involving the propagation constant. Calculations are carried out for a lossless ferrite, and the phase constant is evaluated as a function of the appropriate parameters, namely, the ferrite slab thickness, the lateral position of the slab in the guide, and the applied transverse static magnetic field intensity. The results are plotted in graphic form for values of the static magnetic field in the region of ferrite saturation both above and below ferromagnetic resonance. The electromagnetic field configurations within the wave guide are plotted in detail for values of the parameters of practical interest. Two versions of the nonreciprocal phase shifter are discussed. The first consists of a single slab placed asymmetrically in the wave guide, while the second consists of two symmetrically placed slabs with antiparallel static magnetic fields imposed. The nonreciprocal nature is summarized in terms of the differential phase shift $\beta_+ - \beta_-$ which is pertinent in applications of this phase shifter.

I. INTRODUCTION

PROPAGATION of high-frequency electromagnetic waves in media possessing tensor properties has been treated quite thoroughly by ionospheric physicists. Polder developed a similar treatment[1] for the class of ferromagnetic media which have a tensor permeability much like the dielectric tensor of magneto-ionic media.[2] In recent years, investigators have conducted experiments with magneto-ionic gases[3] and ferromagnetic materials[4,5] in circular wave guides, and have demonstrated a large Faraday effect in such systems. Exact treatment of the electromagnetic problem associated with a ferrite-filled circular wave guide has been presented by a number of workers.[6–8] However, the evaluation of the eigenvalue, namely, the propagation constant, has proved to be very difficult. The circular wave guide partially filled with ferrite has been even more difficult to analyze, and the evaluation of the propagation constant is extremely involved.

Components containing ferrites are being used as elements for microwave gyrators and circulators. Nonreciprocal transmission systems utilize these devices. Very recently, a rectangular wave guide version of a nonreciprocal microwave component has been suggested by Kales *et al.*[9] It employs a ferrite slab placed asymmetrically in the guide, as shown in Fig. 1. When a static magnetic field is imposed transversely, the propagation constants of the *TE* modes prove to be dependent on the direction of propagation.

The independent evaluation of the variables affecting the propagation constants is required in order to develop devices based on this nonreciprocal rectangular wave guide phase shifter. In particular, the ferrite slab thickness, the position of the slab in the guide, and the value of static magnetic field intensity critically affect the propagation in each direction. However, the complicated transcendental equations that have been obtained in this type of problem do not result thus far in explicit expressions for the propagation constant. Furthermore, the usual approximations are not valid over a practical range. Nevertheless, we have formulated a procedure for solving these equations exactly in a relatively simple manner when the losses in the ferrite can be neglected. We present our results in graphic form. An analysis of both the electric and magnetic field configurations has been performed, and illustrations are presented for several practical cases.

II. THEORY

This theoretical analysis is based upon the condition that the phase shifter is operated in the region reasonably below ferromagnetic resonance, hence, the magnetic losses are generally very small. The dielectric loss is known to be negligible. Therefore, Γ, the characteristic

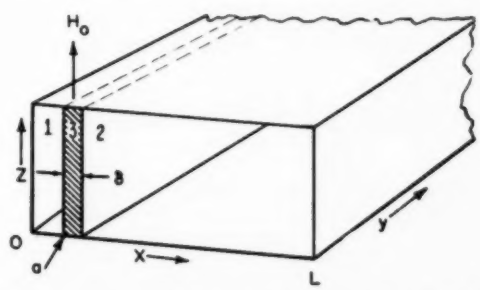

FIG. 1. A single ferrite slab in a rectangular wave guide of internal width *L*.

* The research in this document was supported jointly by the Army, Navy, and Air Force under contract with the Massachusetts Institute of Technology, Cambridge, Massachusetts.

† Staff Members, Lincoln Laboratory, Massachusetts Institute of Technology, Cambridge, Massachusetts.

‡ Now at Harvard University, Cambridge, Massachusetts.

[1] D. Polder, Phil. Mag. **40**, 99 (1949).

[2] B. Lax and A. D. Berk, Convention Record of Institute of Radio Engineers National Convention (1953).

[3] Goldstein, Lampert, and Heney, Phys. Rev. **82**, 956 (1951).

[4] F. F. Roberts, J. phys. radium **12**, 305 (1951).

[5] C. L. Hogan, Bell System Tech. J. **31**, 1 (1952).

[6] H. Suhl and L. R. Walker, Phys. Rev. **86**, 122 (1952).

[7] M. L. Kales, Naval Research Laboratory Report No. 4027 (August 8, 1952).

[8] H. Gamo, J. Phys. Soc. Japan **8**, 176 (1953).

[9] Kales, Chait, and Sakiotis, J. Appl. Phys. **24**, 816 (1953).

propagation constant, has only an imaginary part β when the system is lossless. This condition holds for an infinite line above the cut-off frequency. The cut-off limit is not approached in this treatment.

The boundary value problem is solved exactly. Therefore, the demagnetizing factors associated with the microwave component of magnetic field are automatically taken into account by the boundary conditions imposed at the surface of the ferrite. The demagnetizing factors associated with the static magnetic field are assumed to be those of a sample whose cross section is an elongated ellipse§; the saturation magnetization is in the direction of the major axis.

In each of the cases presented, we assume that the ferrite material is magnetically saturated at the values of static magnetic field intensity used. Experimental observations of some common ferrites indicate that this condition is readily realizable.

If a static magnetic field H_0 is applied in the z direction, Maxwell's equations pertaining to the region occupied by the ferromagnetic medium are

$$\nabla\times\mathbf{E}=-j\omega\mu_0(1+\chi)\cdot\mathbf{h}, \qquad (1)$$
$$\nabla\times\mathbf{h}=j\omega\epsilon\mathbf{E},$$

where the time dependence $\exp[j\omega t]$ is to be assumed throughout. $\mathbf{E}$ and $\mathbf{h}$ are the alternating electric and magnetic fields, respectively. The constants μ_0, ϵ, and ω represent the magnetic permeability of free space, the scalar permittivity of the ferrite, and the angular frequency of the electromagnetic field, respectively. χ denotes the magnetic susceptibility tensor:

$$\begin{pmatrix} \chi_{xx} & \chi_{xy} & 0 \\ -\chi_{xy} & \chi_{xx} & 0 \\ 0 & 0 & 0 \end{pmatrix}. \qquad (2)$$

The expressions for the tensor components in terms of the appropriate parameters may be found in Appendix A.

The wave equation expressed in terms of the *rf* magnetic field is

$$\nabla\times\nabla\times\mathbf{h}=\omega^2\epsilon\mu_0(1+\chi)\cdot\mathbf{h}. \qquad (3)$$

For the transverse electric modes, h_x and h_y have the functional form $\exp[jk_mx]\exp[-j\beta y]$ in the ferrite. Substituting such expressions in the above equation leads to a set of homogeneous linear equations in the components of $\mathbf{h}$ for which the determinant must vanish. The result of the determinantal equation is

$$k_m^2=\omega^2\epsilon\mu_0\left[\frac{(1+\chi_{xx})^2+\chi_{xy}^2}{1+\chi_{xx}}\right]-\beta^2. \qquad (4)$$

§ *Note added in proof.*—The original assumption was that the internal static magnetic field intensity was equal to the applied field. Actually, this is not the case. A correction has to be made for any demagnetizing effects according to the relation $H_0=H_{\text{applied}}-NM$. N is the usual demagnetization factor which depends only upon the geometry of the sample. Then if H_0 is taken to be the internal field the results given in this report are still consistent.

In the portion of the wave guide not occupied by the ferrite material, the appropriate form of Maxwell's equations can be obtained from Eq. (1) by setting $\chi=0$ and $\epsilon=\epsilon_0$. The above procedure, through the use of expressions of the form $\exp[jk_ax]\exp[-j\beta y]$ for the variation of h_x and h_y in this empty region, yields the familiar relation:

$$k_a^2=\omega^2\epsilon_0\mu_0-\beta^2. \qquad (5)$$

III. ASYMMETRICAL PHASE SHIFTER

A. The Boundary Value Problem

We shall consider the "fundamental" transverse electric mode of the asymmetrical system (Fig. 1). A third relation between k_a, k_m and β is obtained from matching boundary conditions which must be imposed upon the components of the electromagnetic field. The electric field intensity $\mathbf{E}=kE_z$ must vanish at the walls of the wave guide so that, omitting the time dependence,

$$\begin{aligned} E_z&=(A\sin k_ax)\exp[-j\beta y], && \text{Region 1}\\ E_z&=[B\sin k_a(L-x)]\exp[-j\beta y], && \text{Region 2} \qquad (6)\\ E_z&=(C\exp[jk_mx]\\ &\quad +D\exp[-jk_mx])\exp[-j\beta y], && \text{Region 3}\end{aligned}$$

where L is the width of the wave guide.

The boundary conditions at the two faces of the ferrites require the continuity of E_z and h_y. [The expressions for h_y may be obtained from Eq. (1); they are given in Appendix B.] These four boundary conditions result in a set of homogeneous linear equations in the coefficients A, B, C, and D, whose determinant must vanish, yielding the following transcendental equation involving the phase constant β:

$$\begin{aligned}&\frac{1}{2}\left(\frac{k_a^2}{\rho^2}+\frac{\beta^2}{\theta^2}-k_m^2\right)\cos k_a(L-\delta-2a)\\ &\quad+\frac{j\beta k_a}{\rho\theta}\sin k_a(L-\delta-2a)\\ &\quad+\frac{1}{2}\left(\frac{k_a^2}{\rho^2}-\frac{\beta^2}{\theta^2}+k_m^2\right)\cos k_a(L-\delta)\\ &\quad+\frac{k_ak_m}{\rho}\cot(k_m\delta)\sin k_a(L-\delta)=0, \qquad (7)\end{aligned}$$

where

$$\rho=\frac{1+\chi_{xx}}{(1+\chi_{xx})^2+\chi_{xy}^2},$$

$$\theta=\frac{1+\chi_{xx}}{\chi_{xy}}.$$

As indicated in Fig. 1, δ is the thickness of the ferrite slab, and a is the distance from the slab to the nearer wall of the wave guide.

This expression is equivalent to that already reported,[9] where it was pointed out that the term that is linear in β indicates that the phase constant is dependent upon the direction of propagation.

B. The Thin-Slab Approximation

An approximate explicit expression for the phase constant for the case of the thin slab may be obtained by expanding β in a Taylor series in powers of δ about the point $\delta=0$. This is accomplished by implicit differentiation of Eq. (7), making use of the relations involving β given by Eqs. (4) and (5). The expansions of the phase constants for the positive and negative y directions are

$$\beta_{\pm}=\beta_0\pm\left(\frac{d\beta}{d\delta}\right)_{\substack{\delta=0\\ \beta=\pm\beta_0}}\delta+\cdots, \tag{8}$$

where β_0 is the phase constant for the completely empty wave guide.

The quantity that is of particular importance in the application of the nonreciprocal phase shifter under discussion is the difference in the phase shift for the two directions of propagation, namely, $\beta_+-\beta_-$, which we shall call the differential phase shift. From Eq. (8)

$$\beta_+-\beta_-=\left[\left(\frac{d\beta}{d\delta}\right)_{\substack{\delta=0\\ \beta=\beta_0}}+\left(\frac{d\beta}{d\delta}\right)_{\substack{\delta=0\\ \beta=-\beta_0}}\right]\delta+\cdots. \tag{9}$$

Expressed in terms of the position of the ferrite, the differential phase shift in the first-order thin-slab approximation is

$$\beta_+-\beta_-=\left(-\frac{2k_0}{L}\frac{j\chi_{xy}}{1+\chi_{xx}}\sin 2k_0a\right)\delta, \tag{10}$$

where $k_0=\pi/L$ (the value of k for the completely empty wave guide).

The range of validity of Eq. (10) is restricted by the condition that the empty wave guide field configurations are not distorted. The magnitude of the perturbation of the electric and magnetic fields is dependent on both the thickness δ and the position a of the ferrite. An estimate based upon perturbation considerations indicates that this approximation is not valid for values of δ greater than $L/100$. Furthermore, higher order terms are required to predict the proper location of the maximum differential phase shift.

The second-order term of the thin-slab approximation has been calculated and evaluated. This term is quite complicated. It does predict the location of the maximum differential phase shift more accurately, but for X-band wave guide used at about 9000 Mcps, it is adequate only for ferrite thicknesses less than $\frac{1}{2}$ millimeter. In this frequency range, thin slab approximations fail to provide an accurate and convenient solution of Eq. (7) for practical values of ferrite thickness and position. We have, therefore, turned to numerical methods for an exact solution.

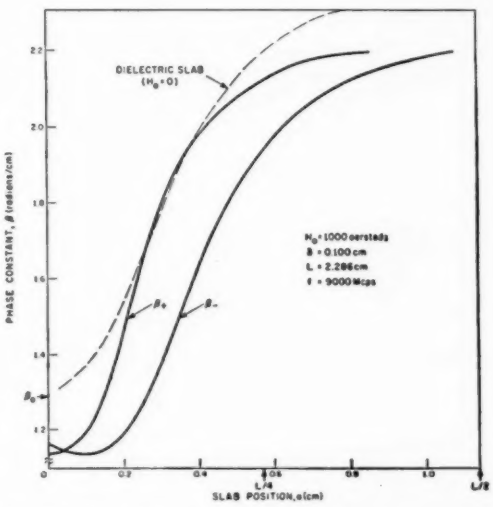

FIG. 2. Phase constant *vs* position of slab. The curves labeled β_+ and β_- refer to the positive and negative directions of propagation, respectively, in a wave guide containing a ferrite slab. The dotted line shows the variation of β for a nonmagnetic dielectric slab having the same dimensions and dielectric constant as the ferrite slab.

C. Numerical Solution of the Transcendental Equation

For the purpose of these computations, we have chosen the following parameters:

Landé g factor for the electron,	$g=2$
Permittivity of ferrite,	$\epsilon=10\epsilon_0$
Saturation magnetization of the ferrite,	$4\pi M_s=3000$ gauss
Microwave frequency,	$f=9000$ Mcps
Internal width of the wave guide,	$L=2.286$ cm.

We have obtained β_+ and β_- as a function of slab position for a series of values of ferrite thickness and static magnetic field intensity. In order to accomplish this, we have expressed Eq. (7) in the form

$$p\cos k_a(L-2a-\delta)+q\sin k_a(L-2a-\delta)+r=0, \tag{11}$$

where

$$p=-\frac{1}{2}\left(\frac{k_a^2}{\rho^2}+\frac{\beta^2}{\theta^2}-k_m^2\right),\quad q=j\frac{\beta k_a}{\theta\rho},$$

$$r=-\frac{1}{2}\left(\frac{k_a^2}{\rho^2}-\frac{\beta^2}{\theta^2}+k_m^2\right)\cos k_a(L-\delta)+k_m\cot(k_m\delta)\frac{k_a}{\rho}\sin k_a(L-\delta).$$

This may be transformed simply into a quadratic equation in $\cos(L-2a-\delta)$ which yields the solution for the unknown position of the slab,

$$a=\frac{L-\delta}{2}-\frac{1}{2k_a}\cos^{-1}\left[-\frac{pr\pm q(p^2+q^2-r^2)^{\frac{1}{2}}}{p^2+q^2}\right]. \tag{12}$$

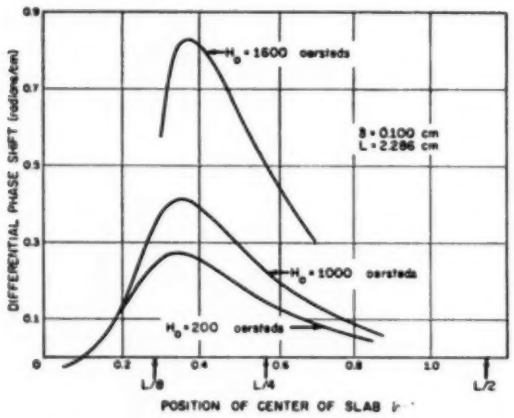

FIG. 3. Differential phase shift vs ferrite position for several values of applied static magnetic field.

The choice of a suitable trial value of β permits the evaluation of k_a and k_m. The subsequent substitution of these into Eq. (12) yields two values of the ferrite position a. One solution represents the required position of the ferrite corresponding to the chosen phase constant for propagation in the positive y direction; the other for propagation in the negative y direction. Figure 2 shows the curves that are traced for a typical case when this procedure is repeated for many choices of β.

D. Discussion of Asymmetrical Phase Shifter

1. Differential Phase Shift

The large deviation of the phase constant from β_0, the empty guide value, suggests that a relatively thin slab is capable of measurably perturbing the empty guide fields and wavelength. This is principally brought about by the dielectric properties of the ferrite, while the differences in the curves of β_+ and β_- are a consequence of the magnetic properties. To illustrate this, a curve showing the β variation for a nonmagnetic dielectric slab having the same dimensions and dielectric constant as the ferrite slab has been superimposed upon the ferrite curves of Fig. 2.

By graphic subtraction of the curves of Fig. 2, the differential phase shift $\beta_+-\beta_-$ has been plotted as a function of slab position. Curves for several values of H_0 are shown in Fig. 3. Near the maximum of a given curve, the differential phase shift is sensitive to the positioning of the ferrite within a few mils. It should also be noted that the maxima of these curves do not occur near the point $a=L/4$, as one might expect if only the empty wave guide magnetic field patterns were considered. These two general characteristics of the asymmetrical phase shifter have been observed experimentally.[10]

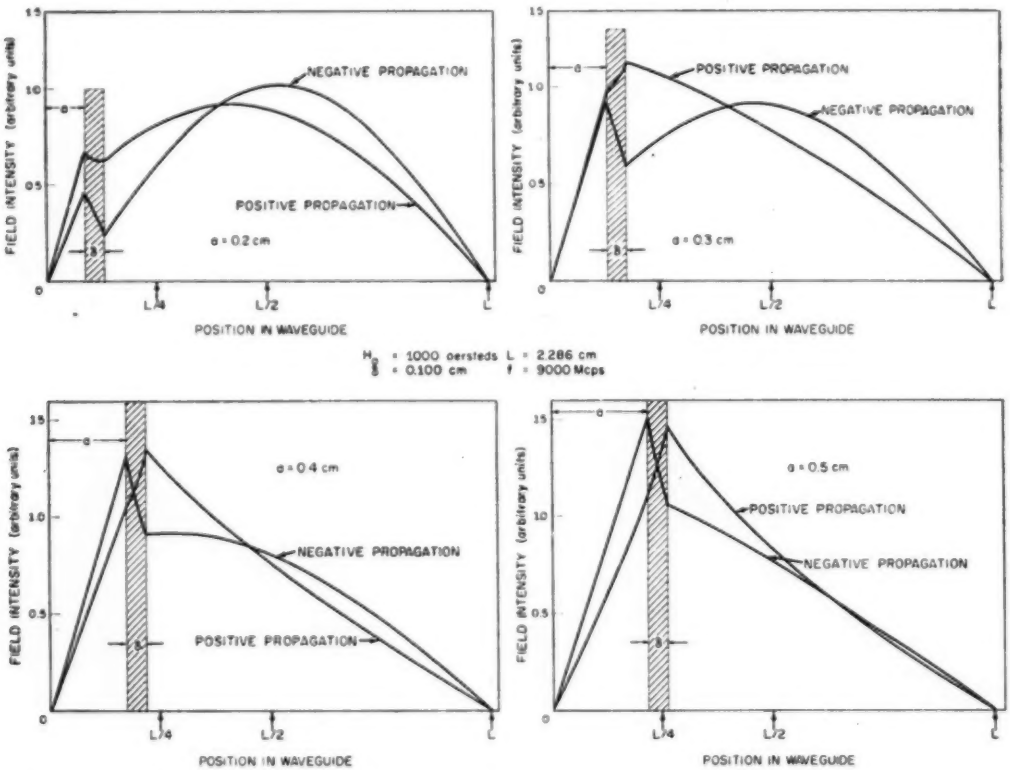

FIG. 4. Electric field intensity in a wave guide containing a ferrite slab. All curves have been normalized to enclose equal area. L is the internal width of the wave guide.

[10] R. H. Fox, Lincoln Laboratory, Massachusetts Institute of Technology, Cambridge, Massachusetts (private communication).

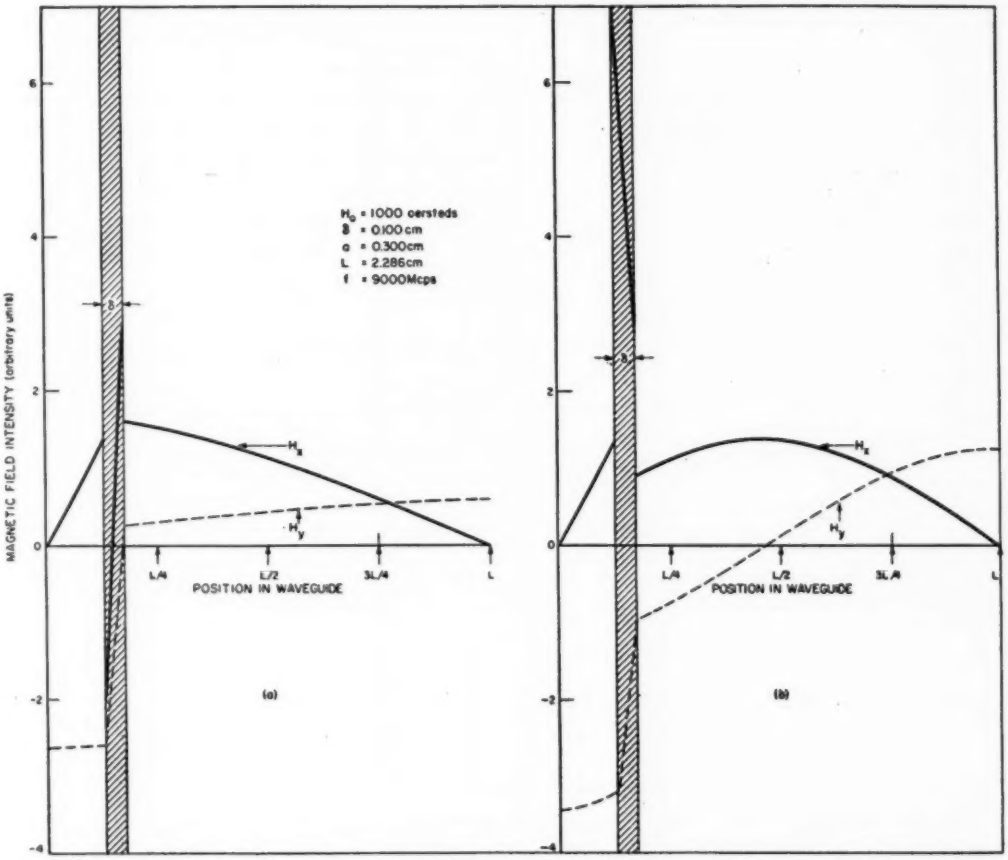

FIG. 5. Magnetic field intensity for the "fundamental" *TE* mode in a wave guide containing a ferrite slab: (a) for propagation in the positive y direction; (b) for propagation in the negative y direction.

2. *Field Configurations*

For the purpose of illustrating the severe distortion of the microwave fields in the presence of ferrite material, we have reproduced in Fig. 4 a detailed plot of the electric field intensity for several positions of the slab. The method of construction of these fields is outlined in Appendix B. The distortion increases sharply with increasing a to the point where the argument of the sine function turns imaginary, and the field intensity decays rapidly outside the ferrite. In the more extreme cases shown, about half of the microwave energy is concentrated within the ferrite. Changes in the applied static magnetic field intensity have little effect on the shape of these electric fields.

The perturbation of the magnetic components of the microwave fields is even more serious. Figure 5 shows the shape of these components when the slab is positioned for maximum differential phase shift. The fields vary over a wide range within the ferrite. The assumption that a circularly rotating magnetic field exists near the point of maximum differential phase shift is no longer appropriate for this ferrite slab thickness. Figure 6 presents a measure of the ellipticity by showing the ratio of the magnetic field components. For positive propagation, the ellipticity assumes nearly all values between positive and negative infinity within the ferrite. For negative propagation, the sign of the ellipticity of the magnetic field within the ferrite is everywhere positive. This corresponds to the case where the microwave field rotates in the same sense as the precession of the spin system.

3. *Properties of the Phase Shifter*

The dependence of the differential phase shift on slab thickness is illustrated in Fig. 7. $\beta_+ - \beta_-$ has been plotted as a function of ferrite location for an applied field of 200 oersteds. The maximum becomes sharper for the thicker slabs and moves closer to the wave guide wall. The actual relation of slab thickness to the position of the maximum is shown in Fig. 8.

The effect of changes in applied magnetic field on the maximum differential phase shift is shown in Fig. 9. Portions of the curve below ferromagnetic resonance show characteristics suitable for a variable phase shifter that can be controlled by the applied magnetic field. The location of the maximum differential phase shift is relatively insensitive to changes in magnetic field over a wide range.

The dependence of the magnitude of maximum differential phase shift on ferrite thickness is shown in

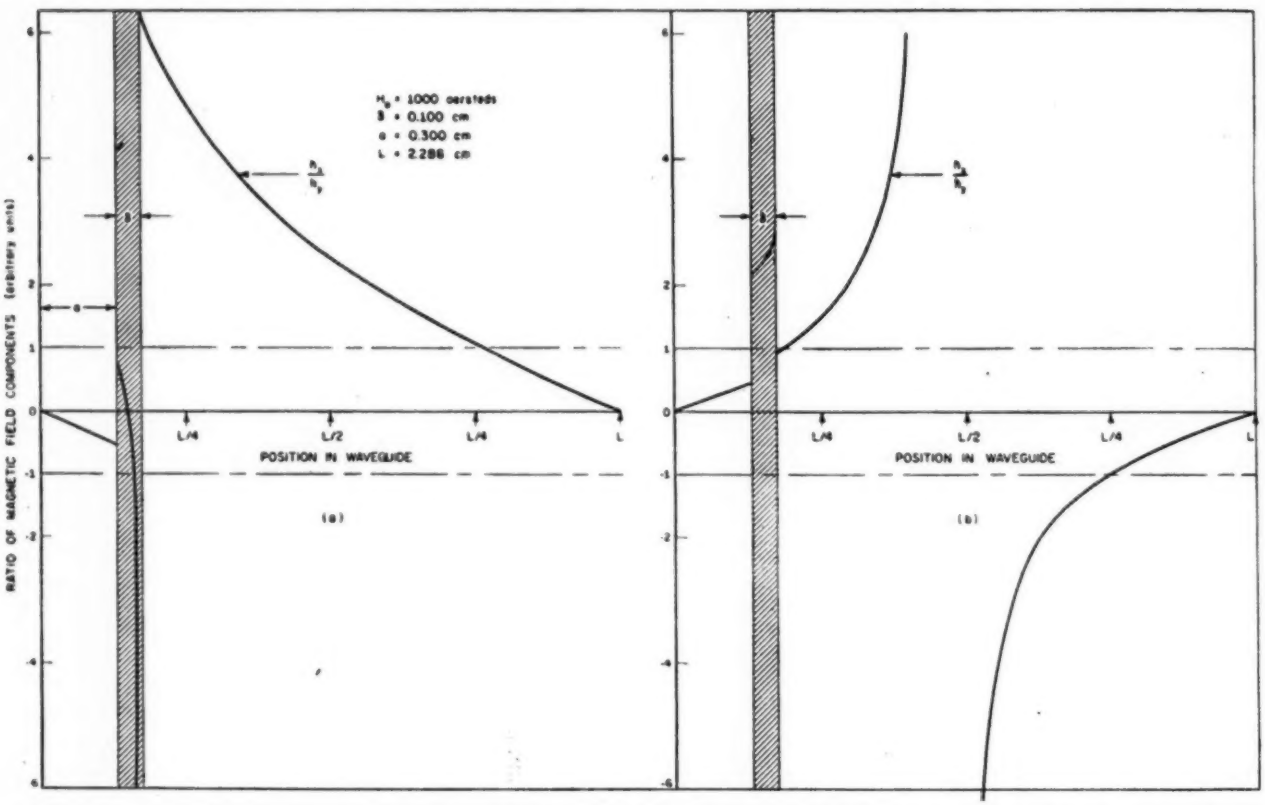

FIG. 6. The ratio of the components of magnetic field intensity for the "fundamental" *TE* mode in a wave guide containing a ferrite slab: (a) for propagation in the positive *y* direction; (b) for propagation in the negative *y* direction. The slab is shown in the position for maximum differential phase shift.

Fig. 10. The first-order thin-slab approximation was used to construct the portion of the curve near $\delta=0$.

IV. SYMMETRICAL NONRECIPROCAL PHASE SHIFTER

Another version of the nonreciprocal phase shifter is shown in Fig. 11. The analytical expressions for this case appear in Appendix C. Such an arrangement preserves the symmetry of the electromagnetic fields with respect to the vertical center plane of the wave guide. This feature may prove useful in attempting to effect a matched transition to an empty wave guide section. Several examples of the electric field configurations are shown in Fig. 12. For some locations, an ideal plane wave exists between the slabs within the wave guide.

For all practical slab positions near the walls, the

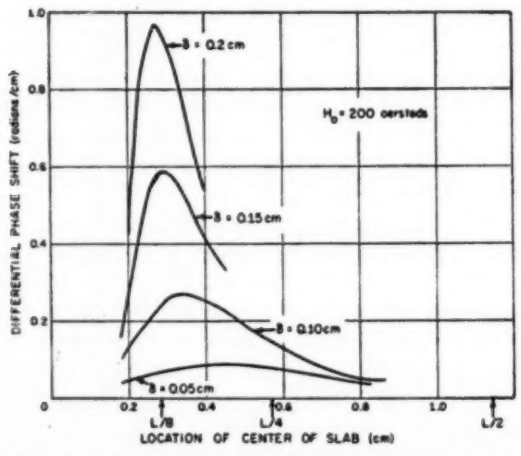

FIG. 7. Differential phase shift *vs* ferrite slab location for several values of ferrite slab thickness.

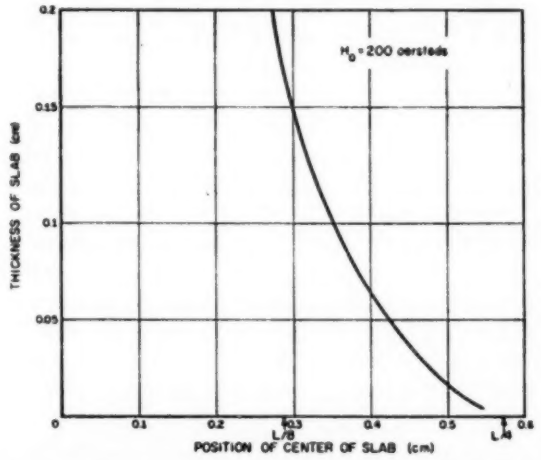

FIG. 8. Dependence of location of maximum differential phase shift on slab thickness. For a given thickness of ferrite, the curve indicates where the slab should be placed in the wave guide to obtain maximum differential phase shift.

phase shift characteristics for this device are similar to the asymmetrical case, as indicated in Fig. 13. If the slabs are placed near the center of the wave guide, the differential phase shift increases sharply. Figure 14 shows a plot of the differential phase shift for all positions up to the point where the slabs are in contact at the center. The problem of actually obtaining the appropriate configuration of the dc magnetic field near the center would prevent the realization of these large phase shifts.

V. REMARKS

The parameters chosen for the purposes of the computations correspond most closely to a nickel zinc ferrite, but they were not taken from an actual sample. The development carried out in this memorandum demonstrates the method of solution. The computations can be repeated for a particular ferrite using parameters easily and accurately measured by cavity techniques.[11]

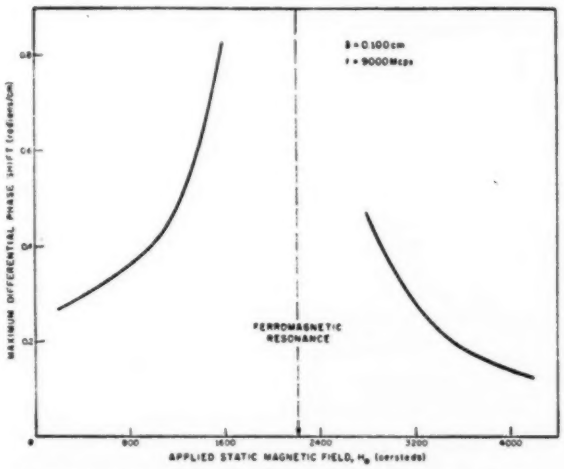

FIG. 9. Maximum differential phase shift *vs* applied static magnetic field intensity. The region below magnetic saturation was not investigated.

Although the region near ferromagnetic resonance is avoided, since it is not practical for applications of the phase shifters discussed here, it would be of interest for nonreciprocal attenuators. The analysis carried out above can, in principle, be extended to include the resonance region by expressing the parameters as complex quantities. The resultant propagation constant would involve an attenuation constant. The field configurations near resonance would be expected to have the same general character as illustrated above. However, for quantitative analysis, it would be worth while to plot them in detail.

VI. APPENDIX

A. The Magnetic Susceptibility Tensor Components

The evaluation of the magnetic susceptibility tensor is accomplished by substitution in the following ex-

[11] J. O. Artman and P. E. Tannenwald, Phys. Rev. **91**, 1014 (1953).

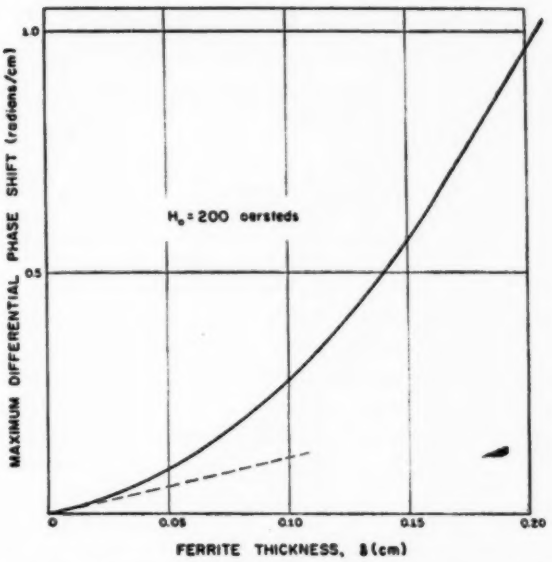

FIG. 10. Maximum differential phase shift *vs* ferrite slab thickness. The solid line is the solution obtained from the transcendental equation. The dotted line is the curve obtained from the first-order thin-slab approximation.

pressions which, essentially, have been derived by Polder:[1]

$$\chi_{xx}=\frac{4\pi M_s\gamma\omega_0}{\omega_0^2-\omega^2},$$
$$\chi_{xy}=-\frac{j\omega\gamma 4\pi M_s}{\omega_0^2-\omega^2}, \tag{13}$$

where $\gamma=ge/2mc$ is the gyromagnetic ratio for the electron, g is the Landé g factor for the electron, H_0 is the applied static magnetic field intensity (oersteds), $4\pi M_s$ is the saturation magnetization of the ferrite (gauss), $\omega_0=\gamma H_0$ is the ferromagnetic resonance frequency for this geometry, and ω is the applied rf angular frequency. The cgs system of units is used in these expressions.

B. The Microwave Electric Field Configurations

The x dependence of the electric field intensity for the asymmetrical phase shifter is given by Eq. (6). To evaluate the coefficients A, B, C, and D, it is only

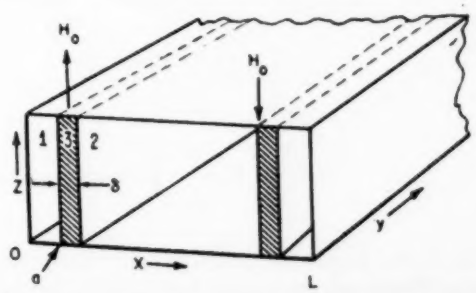

FIG. 11. Symmetrical nonreciprocal phase shifter.

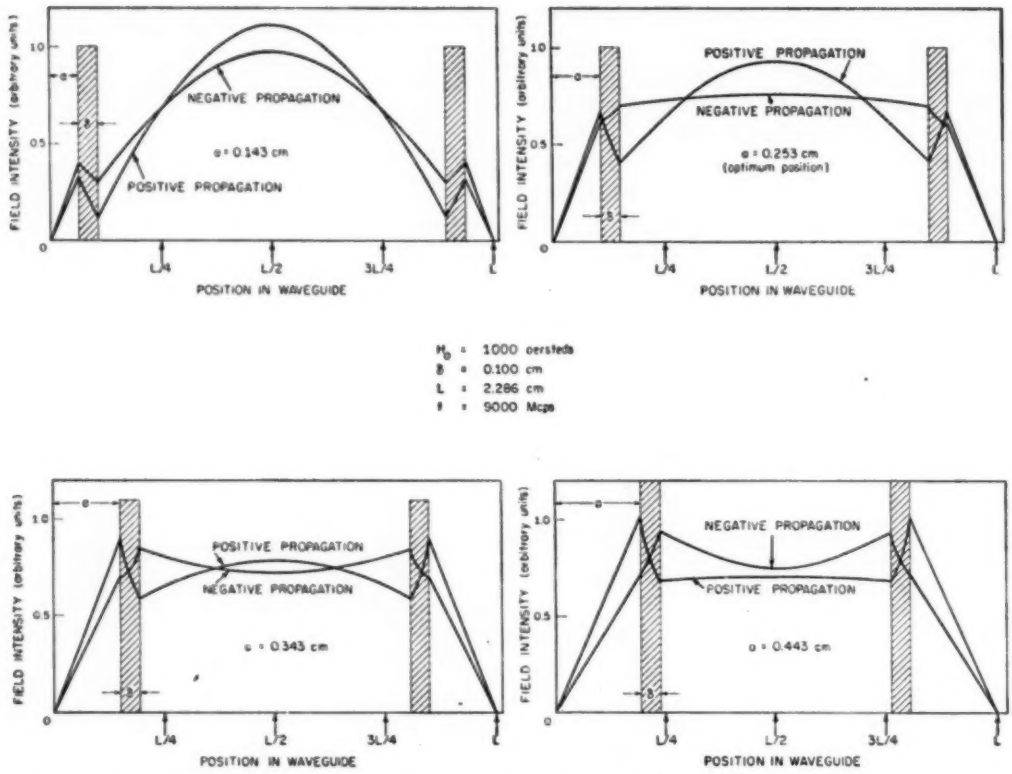

FIG. 12. Electric field intensity for the "fundamental" TE mode in the symmetrical nonreciprocal phase shifter. All curves have been normalized to enclose equal area. L is the internal width of the wave guide.

necessary to impose the boundary conditions at the two faces of the ferrite slab. These conditions require the continuity of E_z and h_y. The expressions for h_y in the three regions specified in Fig. 1 are obtained by substituting from Eq. (6) into Maxwell's equation, $(1+\chi)\cdot\mathbf{h} = -(1/j\omega\mu_0)\nabla\times\mathbf{E}$, where $\chi=0$ in Regions 1 and 2. Retaining only the x dependence, the resulting expressions for h_y are

$$h_y=(1/j\omega\mu_0)Ak_a\cos k_a x,$$

$$h_y=-(1/j\omega\mu_0)Bk_a\cos k_a(L-x),$$

$$h_y=\frac{k_m\rho}{\omega\mu_0}[C\exp(jk_m x)-D\exp(-jk_m x)] \qquad (14)$$
$$+\frac{\beta\rho}{\omega\mu_0\theta}[C\exp(jk_m x)+D\exp(-jk_m x)].$$

After imposing boundary conditions, explicit expressions for the coefficients are obtained:

$$A=\frac{\left[\left(1-\frac{\beta}{k_m\theta}\right)\sin k_a(L-a-\delta)+j\frac{k_a}{k_m\rho}\cos k_a(L-a-\delta)\right]\exp(-jk_m\delta)}{\left(1-\frac{\beta}{k_m\theta}\right)\sin k_a a-j\frac{k_a}{k_m\rho}\cos k_a a},$$

$$B=1, \qquad (15)$$

$$C=\frac{1}{2}\left[\left(1-\frac{\beta}{k_m\theta}\right)\sin k_a(L-a-\delta)+j\frac{k_a}{k_m\rho}\cos k_a(L-a-\delta)\right]\exp[-jk_m(a+\delta)],$$

$$D=\frac{1}{2}\left[\left(1+\frac{\beta}{k_m\theta}\right)\sin k_a(L-a-\delta)-j\frac{k_a}{k_m\rho}\cos k_a(L-a-\delta)\right]\exp[+jk_m(a+\delta)],$$

where B is set equal to unity for mathematical convenience. These are evaluated by choosing the proper values of a and β for a given thickness and static magnetic field intensity. The evaluated coefficients are used in Eq. (6), and the curves are normalized to enclose equal area for convenient comparison.

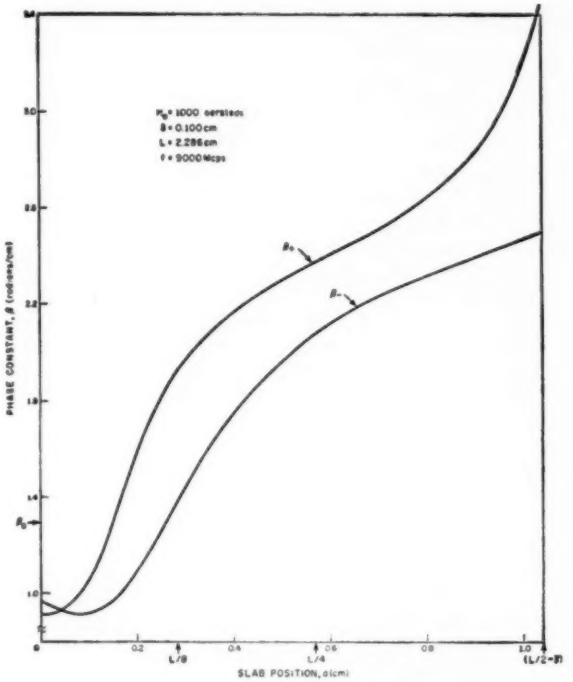

FIG. 13. Phase constant *vs* position of ferrite slabs for the symmetrical nonreciprocal phase shifter. β_+ and β_- refer to propagation in the positive and negative y directions, respectively.

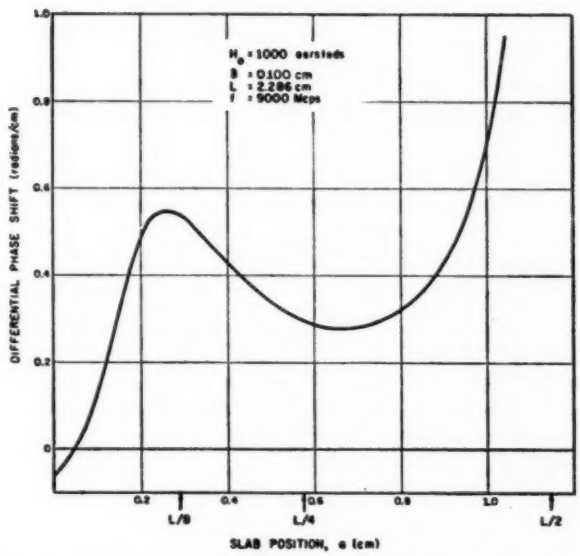

FIG. 14. Differential phase shift *vs* location of ferrite slabs for the symmetrical nonreciprocal phase shifter.

C. The Transcendental Equation for the Symmetrical Nonreciprocal Phase Shifter

The electric field intensity E_z for the symmetrical nonreciprocal phase shifter shown in Fig. 11 is given by

$$E_z = A_z(\sin k_a x)\exp[-j\beta y], \qquad \text{Region 1}$$

$$E_z = B_z[\cos k_a(L/2-x)]\exp[-j\beta y], \qquad \text{Region 2}$$

$$E_z = (C_z\exp[jk_m x] + D_z\exp[-jk_m x])\exp[-j\beta y], \qquad \text{Region 3}$$

where the symmetry with respect to the vertical longitudinal center plane of the guide is preserved. When, as in the asymmetrical case, boundary conditions are imposed at the surfaces of the ferrites, the following transcendental equation is obtained involving the phase constant β:

$$\frac{1}{2}\left(\frac{k_a^2}{\rho^2}+\frac{\beta^2}{\theta^2}-k_m^2\right)\sin k_a\left(\frac{L}{2}-\delta-2a\right) - \frac{j\beta k_a}{\theta\rho}\cos k_a\left(\frac{L}{2}-\delta-2a\right) - \frac{1}{2}\left(\frac{k_a^2}{\rho^2}-\frac{\beta^2}{\theta^2}+k_m^2\right)\sin k_a\left(\frac{L}{2}-\delta\right) + k_m\cot(k_m\delta)\frac{k_a}{\rho}\cos k_a\left(\frac{L}{2}-\delta\right)=0. \quad (16)$$

This has the form of Eq. (7), and the explicit expression for a is obtained by the method already described.‖

ACKNOWLEDGMENTS

We wish to thank Dr. R. H. Fox of Lincoln Laboratory for his helpful suggestions in this problem. We also wish to express our thanks to Dr. B. S. Gourary of the Applied Physics Laboratory of Johns Hopkins University for his criticism of some of our theoretical work. We are pleased to acknowledge the assistance of Miss M. C. Glennon, as well as other members of Group 77 of Lincoln Laboratory, in computing and plotting much of the data presented in this article.

‖ *Note added in proof.*—The parameter a used in Appendix C represents the distance from the center of the wave guide. This reference point was chosen for mathematical simplicity. In order to be consistent, however, the graphs for the symmetrical phase shifter have been plotted in terms of a as measured from the side of the wave guide.

JOURNAL OF APPLIED PHYSICS VOLUME 25, NUMBER 11 NOVEMBER, 1954

Radioactive and Photoelectric *p-n* Junction Power Sources

W. G. PFANN AND W. VAN ROOSBROECK
Bell Telephone Laboratories, Murray Hill, New Jersey
(Received June 3, 1954)

An electrical power source can be made by exposing a *p-n* junction to radioactivity or light, so that the junction field separates electron-hole pairs produced by the radiation. Expressions for maximum power, optimum load resistance, and efficiency are derived from an equivalent circuit and rectification theory. Power and efficiency increase with source current I_g of separated charges and zero-bias junction resistance. I_g increases with energy and intensity of radiation, but is limited by self-absorption in the radioactive isotopes. Estimates of attainable power and efficiency for silicon cells are $3\cdot10^{-3}$ watt cm^{-2} and 15 percent for solar radiation, averaged, allowing for night, weather, and varying angle of incidence; and $3\cdot10^{-4}$ watt cm^{-2} and 8 percent, for beta radiation from $Sr^{90}-Y^{90}$ of activity 32 Curie/g. However, lattice defects produced by $Sr^{90}-Y^{90}$ beta radiation impair cell performance by increasing electron-hole recombination. A theoretical estimate of threshold energy for radiation damage in silicon is about 0.3 Mev, about half the experimental value reported for germanium. Avoiding radiation damage by annealing, by absorbers, and by use of less energetic isotopes is discussed. The Y^{90} beta spectrum is given; it is used in estimating damage rates in germanium, which are high, and efficiencies obtainable with absorbers, which are low. Theory and experiment are compared for $Sr^{90}-Y^{90}$ cells of silicon and of germanium.

1. INTRODUCTION

RADIOACTIVITY can be converted to useful electrical power by means of a *p-n* junction. Electron-hole pairs produced in the semiconductor by beta radiation, for example, are separated by the junction field; the separated pairs bias the junction in the forward direction and deliver power to a load. Since each beta produces many pairs, junction cells convert a small current of high-energy betas to a much larger current of low-voltage electrons. Optical radiation —sunlight, for example—may similarly be employed; each absorbed photon in a characteristic absorption band of germanium or silicon produces one electron-hole pair.

Other methods for obtaining electrical power from radioactivity have been described. Mosely[1] suspended a sphere containing radon in vacuum and determined that a potential difference of 150 000 volts could be developed by the emission of charged particles. Linder and Christian[2] obtained 365 000 volts from 250 millicuries of $Sr^{90}-Y^{90}$, using an improved form of this device. Rappaport and Linder[3] recently described a charging device in which the vacuum is replaced by a thin sheet of insulating medium. Kramer[4] in 1924 and, more recently, Ohmart[5] described devices in which a gas is ionized by radiation and the ions are separated by the electrical field arising from the difference in contact potential between two dissimilar metallic electrodes. Open-circuit voltages of the order of a volt were reported.

That electrical power can be obtained by directing light at a rectifying junction is well known; comparatively high efficiencies for such devices have recently been obtained by Chapin, Fuller, and Pearson.[6] Attention has been called also to the current multiplication observed when an electron beam is directed at a selenium or copper oxide cell.[7] Independent work on the use of a radioactive beta emitter with a *p-n* junction to produce power was reported recently by Rappaport.[8]

Two applications of radiactive junction cells are of particular interest. The first consists of a small, durable source of bias voltage for devices such as the junction transistor.[9] Construction of cells to meet such needs appears feasible. Output powers of the order of microwatts, at voltages of a few tenths of a volt, are attainable with single *p-n* junctions and moderate amounts of radioactive material. While such material is expensive at present, it has been estimated that $Sr^{90}-Y^{90}$, a pure beta emitter of 20-year half-life, could be made available at reasonably low cost.[10] A second application is the large-scale conversion of the radioactivity of unrefined or partly refined fission products into electrical power. Use would be made of both gamma and beta radiation; heavy external shielding and large volumes of semiconductor would be required.

Results of a detailed theoretical and experimental investigation of *p-n* junction power sources are given in this paper, principal emphasis being placed on the radioactive case. In Section 2, design criteria for radioactive cells are considered briefly. In Section 3, from the equivalent circuit and rectification theory, expressions are derived for maximum available power, the corresponding load resistance, and ideal efficiency.

[1] H. G. J. Mosely, Proc. Roy. Soc. (London) **A88**, 471 (1913).
[2] E. G. Linder and S. M. Christian, J. Appl. Phys. **23**, 1213 (1952).
[3] P. Rappaport and E. G. Linder, J. Appl. Phys. **24**, 1110 (1953).
[4] J. B. Kramer, The Electrician **93**, 497 (1924).
[5] P. E. Ohmart, J. Appl. Phys. **22**, 1504 (1951).
[6] Chapin, Fuller, and Pearson, J. Appl. Phys. **25**, 676 (1954).
[7] Ehrenberg, Lang, and West, Proc. Phys. Soc. (London) **A64**, 424 (1951).
[8] P. Rappaport, Phys. Rev. **93**, 246 (1954).
[9] Shockley, Sparks, and Teal, Phys. Rev. **83**, 151 (1951); R. L. Wallace, Jr., and W. J. Pietenpol, Bell System Tech. J. **30**, 530 (1951).
[10] A preliminary estimate of $2.00 per Curie for Sr^{90}—Y^{90} at a specific activity of 33 Curies per gram appears in "Industrial Uses of Radioactive Fission Products," SRI Project 361, Stanford Research Institute, Stanford, California (1951).

These are based on a given source current I_g and apply to any p-n junction cell, being independent of the manner of production of electron-hole pairs. It is shown that output power and efficiency increase with I_g and with zero-voltage junction resistance, R_0. Specific examples are given for a representative case and for the case of solar radiation. In Section 4 available source currents for layers of $Sr^{90}-Y^{90}$ are estimated, and properties of other isotopes of interest are discussed. Available I_g increases with energy and activity of the radioactive isotope but is limited by self-absorption. If the energy of the beta radiation exceeds a certain minimum, cell life will be shortened by the production of lattice defects in the semiconductor. Such radiation damage can be prevented or reduced in rate by a layer of energy-absorbing material between source and junction, or by annealing. In Section 5, the rate of lattice defect formation for an unshielded $Sr^{90}-Y^{90}$ source on germanium is calculated from the beta spectrum and found to be high. It is shown that an absorber thick enough to prevent such damage materially reduces efficiency and power. In Section 6, experimental results for silicon and germanium cells powered by $Sr^{90}-Y^{90}$ are discussed. In Section 7 are considered the potentialities of p-n junction power sources, on the basis of results given in this paper.

2. RADIOACTIVE CELL DESIGN

A principal objective in cell design is to absorb as much radiation as possible as close to a suitable junction as possible. The problem may be resolved into three parts: (1) the radioactive source; (2) its disposition with respect to the p-n junction; and (3) the rectifying junction and the semiconductor.

(1) The Radioactive Source

Type of radiation, energy, half-life, activity, and range are of concern. Pure beta emitters appear well suited as to range and energy, and heavy external shielding is unnecessary. The radiation is strongly absorbed, the range for 0.5-Mev betas in germanium being 0.03 cm, and a few emitters have reasonably high energy, activity, and half-life. Gamma rays, by various processes, give rise to betas which in turn produce electron-hole pairs. Although gammas are not strongly absorbed, their use in combination with other beta and gamma emitters appears feasible for larger scale applications. Alpha particles can produce electron-hole pairs, but their use may be less desirable because they severely damage the lattice.

While beta radiation of high energy is desirable from the viewpoints of power and efficiency, a limit is imposed by the threshold energy E_t for radiation damage. One way out of this difficulty is to use only beta emitters which have maximum energy less than E_t. This procedure can in principle provide better efficiencies than are obtainable with a higher energy source whose maximum energy is reduced to E_t by an absorber. The use of absorbers as well as the removal of defects by annealing will also be discussed later in context.

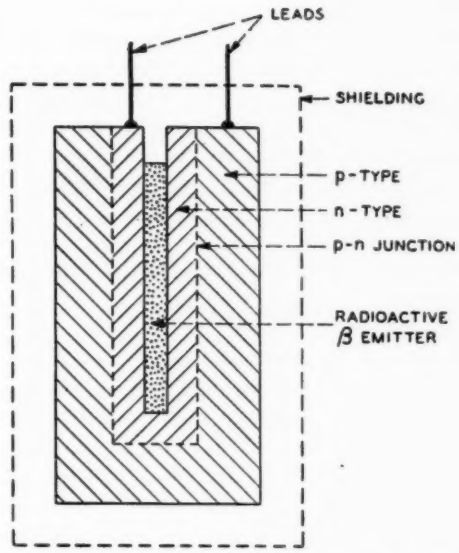

FIG. 1. Schematic representation of a radioactive p-n junction cell.

(2) Disposition with Respect to the p-n Junction

The cell design which will be used for analysis is a planar layer of radioactive material on a slab of semiconductor having a p-n junction parallel to the layer and less than a diffusion length from it. The layer may be very thin, or of appreciable thickness, though little will be gained by having it thicker than a beta range in the isotope. A more efficient design comprises two slabs of semiconductor, one on each side of the layer, as suggested in Fig. 1. Still more efficient is an array of alternate parallel layers and slabs, in which essentially all betas are utilized and each junction is bombarded from both sides. Note that the rectifying junction may be a junction of the semiconductor with a metallic radiation source or metallic absorber.

(3) The Junction and the Semiconductor

Desiderata for both must be considered. For the junction these are: large zero-voltage resistance R_0 and large diffusion lengths for electrons and holes in the p-type and n-type regions, respectively. For the semiconductor these are: small beta range, large energy gap, large threshold energy E_t for formation of lattice defects by betas, and small energy ϵ for formation of of an electron-hole pair by betas. Certain of these properties are interrelated. In general, one diffusion length, or the sum of both, should be large compared to the range over which betas of less than threshold energy are absorbed. For one diffusion length small, the junction should be located away from the center of the beta range so as to allow the other diffusion length to encompass the beta range. Large energy gap E_g is desirable because E_g is an upper limit for attainable

cell voltage and because large E_g makes for large R_0. A qualitative comparison of germanium and silicon shows silicon to be superior in R_0 and germanium to be superior in beta range, E_t, ϵ, and in the diffusion lengths presently obtainable. Of junction cells which have been made, those from silicon have had output power and voltage greater by at least an order of magnitude because of the controlling influence of larger R_0.

3. AVAILABLE POWER AND CIRCUIT EFFICIENCY

3.1. General Theory

On the basis of an equivalent circuit and the current-voltage characteristic of the junction, cell voltage and external current and power may be determined. In particular, the maximum power in a matched load and an ideal efficiency may be specified in terms of given I_g and R_0.

Electron-hole pairs produced within a distance from a p-n junction which is small compared with a diffusion length will substantially all flow across the junction, holes flowing into the p-type side and electrons into the n-type side. Denote by I_g the current which corresponds to this flow. Since the p-type and n-type sides become charged, respectively, positively and negatively,[11] a forward bias across the junction results, which causes a current I_f to flow in the semiconductor opposite to I_g. The current $I=I_g-I_f$ flows in an external circuit. A simple equivalent circuit is accordingly that of Fig. 2, which consists of a current generator I_g in parallel with the rectifying junction and the load resistance R. This resistance is the only linear resistance in this somewhat idealized equivalent circuit, for which the short-circuit current is equal to the source current, I_g. This circuit is frequently an adequate approximation, and it exhibits the principal qualitative features of interest; generalizations that may be necessary in some cases to account for cell behavior can be introduced without difficulty.

Equations for this equivalent circuit are:

$$I_g=I_f+I, \tag{1}$$

$$I_f=(kT/eR_0)[\exp(eV/kT)-1], \tag{2}$$

$$IR=V, \tag{3}$$

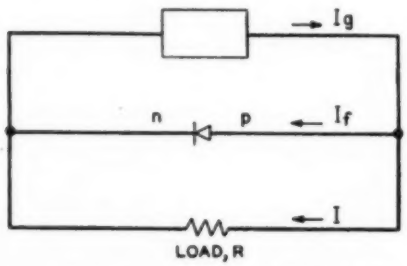

FIG. 2. Equivalent circuit for a p-n junction power source.

[11] It is a convenient mnemonic to recall that this charging effect is the origin of the terms "p-type" and "n-type": E. F. Kingsbury and R. S. Ohl, Bell System Tech. J. 31 (4), 802 (1952).

in which e denotes the electronic charge, k is Boltzmann's constant, T is absolute temperature, and V is cell voltage. Equation (2) is a simple current-voltage characteristic[12] applicable to p-n junctions (such as certain germanium junctions) that exhibit comparatively rapid voltage saturation in the forward direction (positive I and V), with negligible ohmic resistance of the semiconductor. For many silicon junctions, currents under appreciable forward bias are proportional to $\exp(eV/AkT)$, with $A>1$, rather than to $\exp(eV/kT)$; the requisite generalization is easily made. Such behavior may be associated with comparatively gradual transition from n- to p-type, with appreciable increases in local conductivity by carrier injection, with junction non-uniformity, and with non-uniform junction bias.

It follows from the circuit equations that cell voltage V is related to source current I_g as follows:

$$(kT/e)(R/R_0)(\exp(eV/kT)-1)+V=I_gR. \tag{4}$$

Determination of the available power involves finding the load resistance R such that the power,

$$W=I^2R=IV, \tag{5}$$

is maximum. The condition $dW/dR=0$ for a maximum gives

$$\exp(eV/kT)=R_0/R \tag{6}$$

and, hence,

$$I_g=(kT/eR)\ln(R_0/R)+(kT/e)(1/R-1/R_0). \tag{7}$$

This equation permits determination of R for maximum W in terms of R_0 and I_g.

It is convenient to write (7) in dimensionless form by introducing the reduced source current,

$$G\equiv eI_gR_0/kT, \tag{8}$$

which is the ratio of I_g to reverse saturation current, and writing

$$z\equiv R_0/R. \tag{9}$$

Then the equation becomes

$$G=z\ln z+z-1. \tag{10}$$

The quantity z, which will be called the load conductance factor, is plotted against reduced source current, G, in Fig. 3. Given R_0, I_g, and T, the optimum load resistance $R=R_0/z$ may be found from this curve.

The load resistance R which provides maximum power W_m is (independently of the form of the characteristic) equal to the differential resistance of the junction under the operating conditions. In the present case, the nonlinearity is such that it is even smaller than the corresponding actual resistance $R_j\equiv V/I_f$ of the junction, since

$$R/R_j=(z-1)/z\ln z\leq 1. \tag{11}$$

While R approaches R_0 in the limit of zero I_g, it is, for example, $0.5R_j$ (and $0.2R_0$) for $G=12$.

[12] W. Shockley, Bell System Tech. J. 28, 435 (1949); C. Wagner, Physik. Z. 32, 641 (1931).

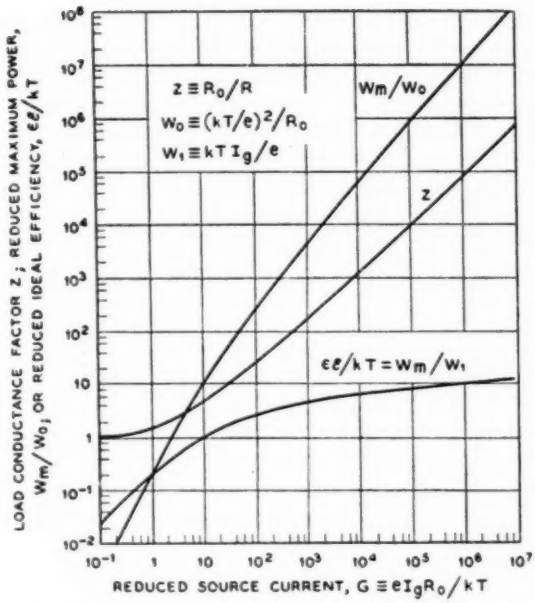
LOAD CONDUCTANCE FACTOR z; REDUCED MAXIMUM POWER, Wm/Wo; OR REDUCED IDEAL EFFICIENCY, εℰ/kT
z ≡ Ro/R
Wo ≡ (kT/e)²/Ro
W1 ≡ kT Ig/e
Wm/Wo
z
εℰ/kT = Wm/W1
REDUCED SOURCE CURRENT, G ≡ eIgRo/kT

FIG. 3. The dependence on reduced source current G of load conductance factor z, reduced maximum power W_m/W_0, and reduced ideal efficiency, $\epsilon\mathcal{E}/kT$.

Since current and voltage for maximum power are, from (3), (6), and (9),

$$I=(kT/eR_0)z\ln z \tag{12}$$

$$V=(kT/e)\ln z, \tag{13}$$

the maximum power W_m is given by

$$W_m=W_0z(\ln z)^2, \quad W_0\equiv(kT/e)^2/R_0. \tag{14}$$

The reduced maximum power W_m/W_0 is plotted against G in Fig. 3.

The open-circuit voltage V_0 of the cell is given by

$$V_0=(kT/e)\ln(1+eI_gR_0/kT), \tag{15}$$

from (4). This equation relates short-circuit current I_0, which equals I_g for the circuit under consideration, to open-circuit voltage V_0. From a more general viewpoint, the dependence of V_0 on I_g should, aside from ohmic drop in the semiconductor, be the same as the dependence of V on I_f without generated carriers, which is the forward characteristic of the rectifier.

An ideal efficiency $\mathcal{E}$ may be derived on the assumption that there is no recombination in the semiconductor, so that all the added current carriers produced by the radiation are collected by the junction. If energy ϵ of the radiation is required to produce one electron-hole pair, then since each pair results in a carrier of charge e which is subject to potential drop V, and since a fraction I/I_g of carriers flows in the load, the efficiency is

$$\mathcal{E}=(eV/\epsilon)(I/I_g)=eV^2/R\epsilon I_g=(kT/\epsilon)z(\ln z)^2/G. \tag{16}$$

The first two expressions for $\mathcal{E}$ are completely general, while the third, which follows from (8) and (12), applies only if R has the value for maximum power. The reduced ideal efficiency at maximum power,

$$\epsilon\mathcal{E}/kT=z(\ln z)^2/G=W_m/W_1,$$

$$W_1\equiv kTI_g/e=GW_0, \tag{17}$$

is plotted against G in Fig. 3. Use of W_1 as power unit is convenient because it is proportional to I_g and because it permits the determination of maximum power W_m as well from the efficiency curve. It will be observed that $\mathcal{E}$ is small for G small and increases with G, and is approximately $(kT/\epsilon)\ln z=(kT/\epsilon)(eV/kT)$ if the second factor is large compared with unity. It may be shown from an appropriate generalization that if, for G large, $A>1$ applies, then V_0, W_m, and $\mathcal{E}$ are multiplied by A, while I remains unchanged, provided the mechanism that gives $A>1$ is associated with that of charge separation.[13]

For high-energy electrons, estimates of ϵ are: 3.0 ev for germanium, and 3.6 ev for silicon.[14] With the use of these constant energies in calculations of G resulting from beta radiation, rates of electron-hole pair production are simply proportional to absorbed power, and ideal efficiencies at 300°K in percent are 0.86 and 0.72 times the reduced efficiency, respectively.

In the optical case, ϵ is equal to the photon energy $h\nu=hc/\lambda$, in a familiar notation. For any specified spectral distribution, an average energy ϵ_{av} applies, to which corresponds an average wavelength λ_{av}. This average energy is equal to the integral, over the entire spectrum, of the monochromatic incident power distribution divided by an integral of the distribution of monochromatic photon incidence rate. The latter integral extends over the spectrum from short wavelengths to the long-wavelength limit λ_m of the characteristic absorption band for electron-hole pair production, which is about 2.2 microns for germanium and about 1.2 microns for silicon.[15] Another property of the semiconductor is involved in that correction should be made for the loss by reflection. For the semi-infinite semiconductor, to which sharp cutoff at λ_m applies, it suffices for this correction to multiply the photon distribution by $(1-r)$, where r is the reflection coefficient. By simultaneously taking into account reflection loss and the cutoff near λ_m in their dependence on semiconductor thickness x, a less idealized ϵ_{av} may be determined. For this purpose, the photon distribution is multiplied by the fraction

$$\Phi\equiv[1-r][1-(1-r)e^{-\alpha x}-re^{-2\alpha x}]/[1-r^2e^{-2\alpha x}] \tag{18}$$

of photons absorbed. Here α is the absorption coefficient, which, with r, depends on λ. This readily-derived expression takes account of multiple internal reflections and applies if x is large compared with λ_m, so that

[13] Detailed consideration of these matters is beyond the intended scope of the present discussion.

[14] K. G. McKay (private communication).

[15] H. B. Briggs, Phys. Rev. 77, 287 (1950); Phys. Rev. 77, 727 (1950); J. Opt. Soc. Am. 42, 686 (1952).

interference may be neglected. It is evident that Φ becomes small, with α, near λ_m.

These considerations apply directly only if there is negligible recombination of added carriers on the surface of the semiconductor or in its volume. Theoretical correction for recombination seems impractical for beta radiation because, with scattering, the distribution of volume rate of carrier production is not easily specified. For optical radiation, however, such correction is easily made. The relevant theory is given in Section 8.1 of the Appendix.

3.2. Illustrative Applications

Radioactive Source

For an illustrative numerical estimate that applies, for example, to an unshielded layer of $Sr^{90}-Y^{90}$ of about 0.2 Curie on silicon, let $I_g=10^{-4}$ amp and (for an area of about 1 cm²) $R_0=10^6$ ohm. Then, at room temperature, $G=3870$, $s=500$, $R=2000$ ohm, $I=81$ μamp, $V=0.16$ volt, $W_m=13$ microwatt, and $\mathcal{E}=3.8$ percent is the ideal efficiency.

Solar Radiation

A numerical estimate of some interest is one for solar radiation. By suitably modifying the distribution in wavelength of solar energy outside the atmosphere[16] for (wavelength-dependent) atmospheric absorption with the sun 60° from the zenith for average cloudless weather at sea level,[17] total incident power, aside from a minor contribution of diffuse sky radiation, is found to be 0.089 watt cm^{-2} at normal incidence (which is 15 percent less than the value for the sun at the zenith). From the corresponding distribution of photon incidence rate multiplied by 0.68 to allow for a reflection coefficient of 0.32 for silicon,[18] it is found that $2.47\cdot10^{17}$ cm^{-2} sec^{-1} is the photon incidence rate up to 1.2 microns, which corresponds to an ideal source current I_g of 0.027 amp cm^{-2}. Thus, for a thick silicon cell under these conditions, $\epsilon_{av}=3.3$ ev, $\lambda_{av}=0.37$ micron, and if $R_0=10^6$ ohm cm², then $G=1.04\cdot10^6$ at 300°K, $s=8.4\cdot10^4$, $R=11.9$ ohm cm², $I=0.024$ amp cm^{-2}, $V=0.29$ volt, $W_m=7.0\cdot10^{-3}$ watt cm^{-2}, and $\mathcal{E}=7.8$ percent is the ideal efficiency.

The circumstance that photocurrents not much less than this value of I (which is nearly I_g) have been observed indicates that recombination did not cause a major reduction of output in the thin-surface layer, boron-diffused silicon cells tested.[19] For these cells, A is about 2 or 3, one interpretation for which is that an R_0 of the order of 10^8 ohm cm² properly applies, measured values being of the order of 10^4 ohm cm² perhaps as a result of junction nonuniformity or edge leakage. With no reflection loss, $I_g=0.040$ amp cm^{-2}, $\epsilon_{av}=2.25$ ev, and $\lambda_{av}=0.55$ micron for the conditions specified; and if $R_0=10^8$ ohm cm², then, at 300°K, $R=10.5$ ohm cm², $W_m=16.3\cdot10^{-3}$ watt cm^{-2}, and $\mathcal{E}=18$ percent is the ideal efficiency. Note that R is approximately independent of R_0 in the nonlinear range in which z is approximately proportional to G.

4. AVAILABLE RADIOACTIVE SOURCE POWERS

Available source power may be defined for the radioactive case as the rate at which beta energy is absorbed in the semiconductor. Dividing it by the energy ϵ required to produce an electron-hole pair gives the flux of current carriers across the junction, assuming that all are collected. It is determined by the activity of the isotope and by the fraction of the energy of the isotope layer which is transferred to the semiconductor. These quantities will be considered separately. The latter applies particularly to thick layers.

Properties[20] of a number of pure beta emitters of interest are listed in Table I. Included also are Co^{60} and $Cs^{137}-Ba^{137}$ which emit both betas and gammas. Ideal activities have been computed as follows: If all the atoms were radioactive, the mass per Curie would be $CM\tau/A$ g/Curie, where M is molecular weight; $C=3.7\cdot10^{10}$, the number of disintegrations per Curie per sec; and $A=6.03\cdot10^{23}$, Avogadro's number. Since $\tau=\tau_{\frac{1}{2}}/\ln 2=1.44\tau_{\frac{1}{2}}$, the corresponding number of Curies per unit mass, or the ideal activity, is $1.13\cdot10^{13}/M\tau_{\frac{1}{2}}$ Curie g^{-1}. For the fission products, the specific activity is taken as roughly 0.1 of the ideal activity, unless otherwise known from published data.

TABLE I. Properties of radioactive elements.

Element	Half-life $\tau_{\frac{1}{2}}$	Maximum energy Mev	Density g/cm³	Range of betas in Al in g/cm²	Ideal activity Curie/g	Specific activity Curie/g (estimated)
Cobalt 60	5.2*y*	0.31β 1.17,1.33γ	8.9	0.083	1.15×10^3	1.10
Strontium 89	53*d*	1.5β	2.55	0.68	2.8×10^4	3000
Strontium 90	20*y*	0.54β	2.55	0.22	200	16
Yttrium 90 daughter	62*h*	2.2β	5.5	1.06	200	16
Promethium 147	4.4*y*	0.22β		0.049	500	50
Thallium 204	2.7*y*	0.78β	11.9	0.30	650	65
Calcium 45	180*d*	0.25β	1.54	0.06	1.6×10^4	1600
Cesium 137	33*y*	0.5β 95% 1.2β 5%	1.9	0.16 0.51	79	11
Barium 137 daughter	2.6*m*	0.66γ	3.5		79	11

[16] *Smithsonian Meteorological Tables* (The Smithsonian Institution, Washington, 1951) Sixth revised edition, Table 131.

[17] As observed at Washington: W. E. Forsyth (Editor), *Measurement of Radiant Energy* (McGraw-Hill Book Co., Inc. New York and London, 1937), p. 77.

[18] M. Becker, "The Infra-Red Optical Properties of Silicon and Germanium," thesis, Purdue University, June, 1951. A selenium film over germanium or silicon surfaces has been found to reduce reflection loss: H. B. Briggs, Phys. Rev. 77, 287 (1950).

[19] See reference 6, also G. L. Pearson and C. S. Fuller, Proc. Inst. Radio Engrs. 42, 760 (1954). Measured values of I and W_m are 0.018 amp cm^{-2} and $6\cdot10^{-3}$ watt cm^{-2} (D. M. Chapin, unpublished).

[20] See reference 10, also R. I. Powers and A. F. Voight, AECU-840, May 1, 1950.

For a thin layer of isotope, self-absorption is negligible, and substantially one-half of the radiated beta energy is absorbed in a semiconductor to one side of the layer. As previously indicated, the layer can be confined between two slabs; but illustrative analyses are based on the simpler arrangement utilizing radiation from one side only. While backscattering may cause some 40 percent of incident betas to leave the semiconductor,[21] this effect can be nullified (and, in fact, overcompensated for) by placing a thickness of backscattering material behind the isotope layer. Hence, backscattering will be neglected.

Self-absorption sharply reduces the fraction of beta energy which emerges from a thick isotope layer. The energy spectrum of emergent electrons for a thick layer of $Sr^{90}-Y^{90}$ may be calculated from the theory of Weymouth[22] for a semi-infinite beta-emitting solid. While the exact beta spectrum could be taken into account, it will be an adequate approximation to assume source electrons of the average energy for Y^{90}, 0.89 Mev. Weymouth's distribution of emergent flux in path length can be transformed into a distribution in energy,[23] and for an assumed density of metallic strontium, the spectrum so obtained gives $2.9\cdot10^{-2}$ $\mathfrak{N}$ per cm³ electrons emergent, for $\mathfrak{N}$ electrons per cm³ in the source, with an average emergent energy of 0.57 Mev. The $\mathfrak{N}$ per sec for 41 Curie cm^{-3} (or 16 Curie g^{-1}) then gives $4.3\cdot10^{10}$ cm^{-2} sec^{-1} for the flux of emergent electrons and an energy flux of $2.5\cdot10^{10}$ Mev cm^{-2} sec^{-1}. This energy flux corresponds to a "thin" layer, or layer without self-absorption, of 1.49 Curie cm^{-2}.

It appears, therefore, that 1 Curie cm^{-2} (assumed in the illustrative numerical examples of the following section) is approximately representative of the largest available source powers for planar sources of Y^{90} of a specific activity of 16 Curie g^{-1}. The assumption that such a source is "thin," namely that its spectrum is the beta spectrum of Y^{90}, is not strictly correct, but provides a reasonable approximation.

Note that if scattering is neglected (as discussed in Section 8.4 of the Appendix) and also if proportionality of range and energy is assumed, then the emergent electron flux is $5.4\cdot10^{10}$ cm^{-2} sec^{-1} and the energy flux is $2.4\cdot10^{10}$ Mev cm^{-2} sec^{-1}, which do not differ much from the more accurate values.[24]

5. RADIATION DAMAGE

5.1. Introduction

As determined from studies of the effect on conductivity, high-speed electrons introduce acceptor centers,

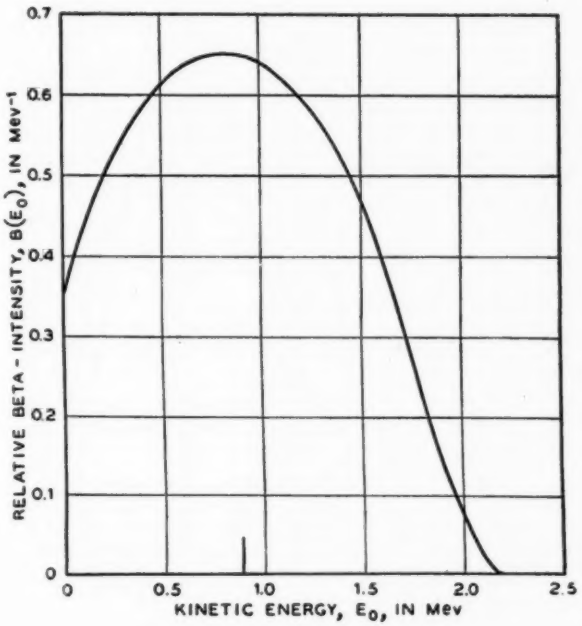

FIG. 4. The Y^{90} beta spectrum.

and these are presumed to be associated with vacancy-interstitial pairs in the lattice.[25] Lifetime is materially reduced by radiation which produces any appreciable conductivity change. Radiation damage reduces cell efficiency primarily by bringing about recombination of the added current carriers before they can diffuse to the collector junction. It may also lower R_0, and, if n-type semiconductor faces the radiation source, an opposing junction may be introduced by the conversion the n-type material in part to p-type. Radiation damage does not occur below a threshhold energy E_t which is about 0.63 Mev for germanium[26] and probably, as will be estimated theoretically, about 0.3 Mev for silicon.

In the following, the total rate of lattice defect formation for an unshielded source of $Sr^{90}-Y^{90}$ on germanium is estimated. It is shown to be comparatively large. With an absorber thick enough to obviate all radiation damage, ideal over-all efficiency, estimated for 1 Curie per cm² of the isotope, is found to be very small for germanium: less than 10^{-6} percent. For a thinner absorber that permits damage at a rate roughly commensurate with the half-life of the isotope, the corresponding efficiency is found to be appreciably larger, but still small: less than 10^{-4} percent. No allowance is made for "self-annealing" of lattice defects which, taking place at ordinary temperatures, may presumably result at least in part from local heating by betas. At the steady state of defect concentration, lifetime would in general be much reduced below its initial value.

[21] H. H. Seliger, Phys. Rev. **88**, 408 (1952).
[22] J. W. Weymouth, Phys. Rev. **84**, 766 (1951).
[23] The transport mean free path κ^{-1} employed as length unit is evaluated as $4.8\cdot10^{-2}$ cm, and use is made of the dependence of energy E and dE/ds on range s. See Sections 8.3, 8.4, and 8.6 of the Appendix.
[24] The empirical treatment of beta intensity in terms of an absorption coefficient also gives essentially the same electron flux. If energy is not too small, electrons emerge equal in number to those in about 0.2 of a beta range: R. G. Baker and L. Katz, Nucleonics **11** (2), 14 (1953).
[25] Brown, Fletcher, and Wright, Phys. Rev. **92**, 591 (1953).
[26] E. Klontz and K. Lark-Horovitz, Phys. Rev. **82**, 763 (1951); **86**, 643 (1952).

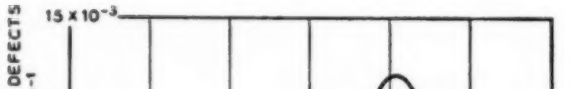

FIG. 5. The distribution in initial kinetic energy E_0 of total number of lattice defects produced in germanium by an unshielded $Sr^{90}-Y^{90}$ source.

5.2. The Y^{90} Beta Spectrum

For estimating rates of lattice-defect formation by $Sr^{90}-Y^{90}$ in germanium, it will suffice to consider the Y^{90} beta spectrum only, since the maximum energy for Sr^{90} is less than E_t for germanium. The Y^{90} beta spectrum is calculated in Section 8.2 of the Appendix[27] and is shown in Fig. 4, normalized to give one electron over the entire range. It is found from the figure that electrons from Y^{90} have a mean kinetic energy of 0.89 Mev.

5.3. The Unshielded $Sr^{90}-Y^{90}$ Source on Germanium

From appropriate theory and the Y^{90} beta spectrum, it is shown in Section 8.3 of the Appendix that the number of lattice defects produced in germanium by a thin layer of $Sr^{90}-Y^{90}$ is 0.010 per source electron. This number is the integral over the distribution of relative number in initial energy shown in Fig. 5. In particular, 1 Curie of Y^{90} per cm^2 will produce defects at the rate $3.6\cdot10^5$ cm^{-2} sec^{-1}. Since they are produced to a depth of 0.156 cm, the space-average rate of increase of defect concentration is $2.3\cdot10^9$ cm^{-3} sec^{-1}, provided all defects that are produced remain. By taking the electron-hole recombination cross section[28] as 10^{-16} cm^2, and thermal velocity as 10^7 cm sec^{-1}, the average lifetime τ after t seconds resulting from the defects alone is $[(2.3\cdot10^9 t)(10^7)(10^{-16})]^{-1}$ sec. For $t=8.64\ 10^4$ sec or 1 day, it is found that $\tau=5$ μsec for the particular surface concentration of the isotope, if no self-annealing occurs.

[27] If needed, the Sr^{90} spectrum may be obtained by a procedure similar to that given.

[28] W. T. Read (private communication). There is evidence that this cross section may be even larger: P. Rappaport, Phys. Rev. 94, 1409 (1954).

5.4. Absorber for Complete Protection

To prevent formation of lattice defects an absorber of thickness $x=s_m-s_t$ may be placed between the layer of isotope and the semiconductor, where s_m and s_t are, respectively, the ranges for electrons of maximum energy, E_m, and of threshold energy, E_t. For Y^{90} and germanium, $E_m=2.20$ Mev and $E_t=0.63$ Mev. In Section 8.4 of the Appendix, the emergent energy spectrum and also the distribution of total emergent energy in initial energy are calculated for this absorber (of thickness 829 mg cm^{-2}, or 0.307 cm of aluminum), using the simplifying assumption that there is no scattering. These spectra are shown in Fig. 6. From them, an upper limit of $2.8\cdot10^{-4}$ is obtained for the fraction F of total energy which penetrates the absorber. For a layer of 1 Curie per cm^2, this corresponds to $I_g=2.5\cdot10^{-7}$ amp, assuming collection to one side of the layer only. Taking R_0 as 10^3 ohm cm^2, a representative value for germanium, the ideal efficiency for the electrons that penetrate is $2.1\cdot10^{-3}$ percent, and the ideal overall efficiency (ignoring the Sr^{90} electrons) is $5.8\cdot10^{-7}$ percent.

A rather small fraction of the energy penetrates this absorber. As Fig. 6 shows, all electrons from the Y^{90} spectrum whose initial energies are less than 1.78 Mev are completely stopped. Since maximum initial energy is only 0.42 Mev larger, electrons that penetrate the absorber from a point in the source have paths that lie within a comparatively narrow cone. In addition, multiple scattering, which ultimately makes the path of an electron more or less statistically random in direction, makes F a good deal smaller than the calculated upper limit.

5.5. An Absorber for Partial Protection

Considerably higher efficiency is obtainable with a somewhat thinner absorber, since F depends rather critically on thickness. Because of multiple scattering, a fairly rigorous calculation of rates of energy transmission and lattice defect formation for such an

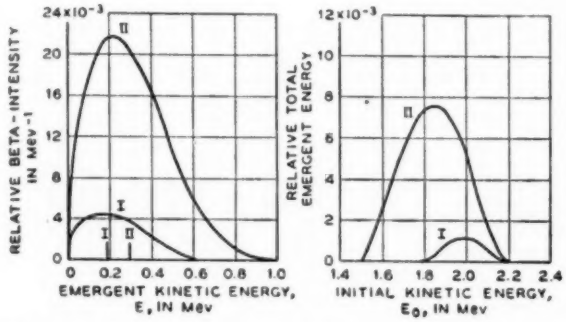

FIG. 6. Emergent energy spectra from $Sr^{90}-Y^{90}$ for each of two absorbers, and the corresponding distributions in initial energy of total emergent energy. (I) Absorber of thickness 829 mg cm^{-2} (or 0.307 cm of aluminum) for complete protection of germanium. (II) Absorber of thickness 669 mg cm^{-2} (or 0.248 cm of aluminum).

absorber would be rather involved.[29] The neglect of scattering appears, however, to be quite adequate in that it provides comparative estimates of the rates of energy transmission and defect production, the calculated rates themselves actually applying approximately to a thickness smaller than that assumed. These points are discussed in Section 8.6 of the Appendix, and in Section 8.5 is given the theory employed for the volume rate of defect production.

For a hypothetical nonscattering absorber of thickness 669 mg cm^{-2}, or 0.248 cm of aluminum, about 20 percent thinner than the one for complete protection, the maximum energy of emergent electrons is 0.94 Mev. The volume rate of defect production in the semiconductor just beyond this absorber is found to equal $4.8\cdot10^{-5}$ $\mathfrak{R}$ cm^{-3} sec^{-1}, where $\mathfrak{R}$ is the number of source electrons per cm^2 per sec. Thus, for $\mathfrak{R}=3.7\cdot10^{10}$ cm^{-2} sec^{-1}, or 1 Curie per cm^2, the defect concentration would increase at the rate $1.78\cdot10^{6}$ cm^{-3} sec^{-1} to a concentration of about 10^{15} cm^{-3} in the 20-year half-life of the isotope, provided all defects that are produced remain. The corresponding lifetime would be of the order of 1 μsec. Curves II of Fig. 6 give the emergent energy spectrum and the distribution of total emergent energy in initial energy; a fraction $9.9\cdot10^{-3}$ of electrons emerge with an average energy of 0.29 Mev, and the fraction F of total energy which penetrates the absorber is $3.3\cdot10^{-3}$. For 1 Curie per cm^2, the over-all ideal efficiency (ignoring the Sr^{90} electrons), taking R_0 as 10^3 ohm cm^2, is $7.8\cdot10^{-5}$ percent.

5.6. Threshold for Radiation Damage in Silicon

Silicon seems more promising than germanium for p-n junction power sources, principally because the larger junction resistance R_0 obtainable with silicon makes for higher efficiencies; the estimates of radiation damage have been given for germanium because the relevant physical magnitudes are known with adequate accuracy for this material. A theoretical estimate of the radiation damage threshold for silicon[30] is about 0.3 Mev. This estimate is obtained by assuming that a minimum energy E_L of 30 ev must be imparted to the atom to displace it to an interstitial site, the same as that calculated[31] for germanium from the experimental threshold electron energy, E_t, in accordance with

$$E_L/mc^2=2(m/M)[(E_t/mc^2)^2+2(E_t/mc^2)], \quad (19)$$

in which m and M are the electronic and atomic masses, respectively. The assumption is plausible, since the lattice constants differ but slightly, and the molar cohesive energies are considered to be equal.[32] A somewhat qualitative refinement of the estimate involves assuming that[33] E_L is inversely proportional to volume compressibility divided by atomic volume, whence[34] E_L for silicon is 17 percent larger than for germanium, and the estimate of E_t is increased by 15 percent. It seems likely that the estimated threshold for radiation damage in silicon of 0.3 Mev is good to within 20 percent. Thus, for silicon the advantage of larger R_0 is probably offset by lower E_t.

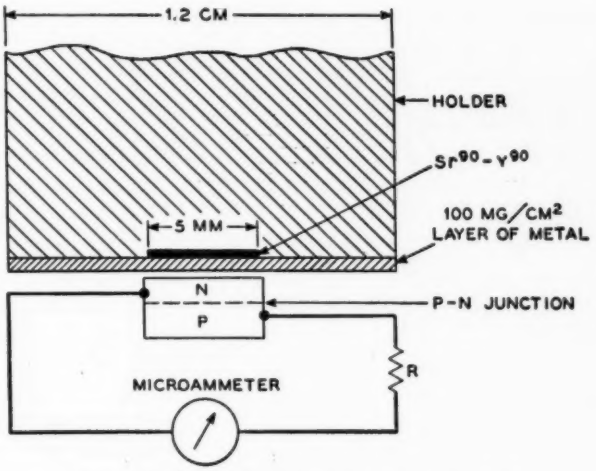

FIG. 7. Experimental Sr^{90}—Y^{90} p-n junction cell.

6. EXPERIMENTAL RESULTS

A variety of silicon and germanium junctions were exposed to beta radiation from Sr^{90}—Y^{90}, as shown in Fig. 7. The source was an RA2 medical applicator (of Tracerlab, Inc., Boston) in which the isotope was a thin layer, about 0.5 cm in diameter, containing 0.05 Curie each of Sr^{90} and Y^{90} as carbonate. The weight of isotope was about 0.025 g, giving a specific activity of 4 Curie g^{-1}.

The layer of isotope was covered by 100 mg cm^{-2} of metallic shielding, which stopped most of the Sr^{90} betas and materially lowered the energy of emergent Y^{90} betas. An approximate calculation, based on the Y^{90} beta spectrum of Fig. 4, shows that only about 16 percent of the Y^{90} beta energy in the layer penetrated the shield.

Silicon Cell

A junction prepared by diffusion of lithium, a donor, into p-type silicon by a method attributed to Fuller[35] was tested as a power source. Its area was 0.15 cm^2 and it lay about 0.002 cm below the upper face of the silicon slab, 0.05 cm thick. The diffusion length in the p-type silicon, measured before the junction was prepared, was about 0.02 cm. It is estimated that about 60 percent of the emergent betas were intercepted by the junction and that about 25 percent of the energy of those

[29] Theory similar to that of Weymouth (reference 22) can furnish reasonably accurate estimates.
[30] W. Kohn (private communication).
[31] W. Kohn (unpublished). For copper, E_L is about 25 ev, and there is evidence that there is not much variation of E_L with different materials.
[32] L. Pauling, *The Nature of the Chemical Bond* (Cornell University Press, Ithaca, New York, 1940), p. 53.
[33] Conyers Herring (private communication).
[34] E. M. Conwell, Proc. Inst. Radio Engrs. **40**, 1327 (1952).
[35] C. S. Fuller and J. A. Ditzenberger, Phys. Rev. **91**, 193 (1953).

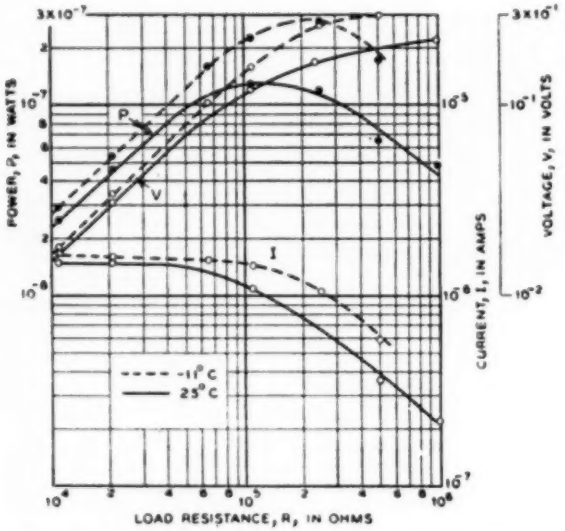

FIG. 8. Electrical characteristics of a $Sr^{90}-Y^{90}$ silicon p-n junction cell.

intercepted, neglecting backscattering, was absorbed within a diffusion length of the junction.

Electrical characteristics of this cell are shown in Fig. 8. The apparent maximum power W_m was $0.13\cdot10^{-6}$ watt at 25°C, for a load resistance R of about $1.2\cdot10^{5}$ ohm. At −11°C the apparent W_m was $0.3\cdot10^{-6}$ watt for R of about $2\cdot10^{5}$ ohm. This junction had an unusually high series ohmic resistance, R_s, the value being about $8\cdot10^{4}$ ohm. Considering R_s as part of the load, it is found that W_m is $0.23\cdot10^{-6}$ watt and R is about $1.5\cdot10^{5}$ ohm, at 25°C.

The following efficiencies will be computed: $\mathcal{E}_1$, that based on total source power; $\mathcal{E}_2$, that based on power incident on the semiconductor; $\mathcal{E}_3$, that based on power absorbed within a diffusion length of the junction. From data given, these are estimated to be:

$$\mathcal{E}_1=\frac{(0.13\cdot10^{-6})(100)}{(0.1)(3.7\cdot10^{10})(1.6\cdot10^{-19})(0.55\cdot10^{6})}$$

$$=\frac{1.3\cdot10^{-5}}{3.3\cdot10^{-4}}=0.040\%, \quad (20)$$

where 0.55 Mev is the mean energy of $Sr^{90}-Y^{90}$ betas computed from the beta spectra;

$$\mathcal{E}_2=\mathcal{E}_1/(0.16)(0.60)(0.80)=0.5\%, \quad (21)$$

where 0.80 is the fraction of the energy of the mixture which arises from Y^{90} betas, the energy of Sr^{90} betas being assumed lost; and

$$\mathcal{E}_3=\mathcal{E}_2/(0.25)=2.0\%. \quad (22)$$

If R_s is included as part of the load, then $\mathcal{E}_3\sim3.5$ percent.

Of these, $\mathcal{E}_1$ and $\mathcal{E}_2$ are of incidental interest only, because they depend largely on experimental geometry, which was not too favorable. They indicate the expected order of magnitude for a planar silicon junction. They are high in that the shielding has been insufficient to lower the beta energy below E_t; but they are low in that larger R_0 and diffusion length can be expected.

For comparison of these efficiencies with the ideal efficiency $\mathcal{E}$ the quantities G, z, and ϵ are required. Taking the short-circuit current, $1.5\cdot10^{-6}$ amp, as I_0, and taking the value $5\cdot10^{6}$, obtained from the current-voltage characteristic of the junction (in the absence of radioactivity) as R_0, we obtain 290 for G, which corresponds, from Fig. 3, to $z=58$. Using the value $\epsilon=3.6$ ev for silicon, we obtain $\mathcal{E}=2.4$ percent from Eq. (16), which is of the order of $\mathcal{E}_3$ above. Accuracy of the various estimates involved is insufficient for more detailed comparison.

Lowering the temperature can be expected to increase the output power of a radioactive junction cell in two ways: by increasing R_0, thereby increasing the cell voltage, and by increasing the diffusion length, thereby increasing the cell current by increasing the fraction of carriers collected. Both of these effects can be observed in the curves of Fig. 8.

Germanium Cell

A germanium junction prepared by crystal pulling[36] was tested. Its area was 0.4 cm²; it lay, n side uppermost, 0.1 cm below the upper face of the block. Diffusion lengths were about 0.06 cm and about 0.03 cm in the n-type and p-type regions, respectively. It is estimated that 90 percent of the emergent betas were intercepted by the semiconductor and that about 40 percent of the energy of intercepted betas was absorbed within a diffusion length of the junction.

Cell characteristics at room temperature appear in Fig. 9. While the short-circuit current, about $4\cdot10^{-6}$ amp, was greater than for the silicon cell, the W_m of $3.3\cdot10^{-9}$ watt was far less because of lower junction resistance. Measured R_0 was about 1000 ohms; R from the cell data was about 800 ohms. For the observed low output voltage, one would expect $z=R_0/R$ to be close to unity.

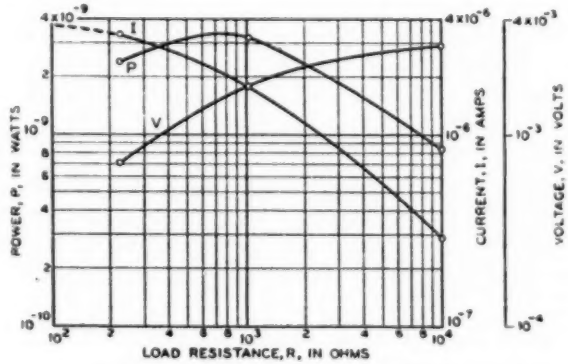

FIG. 9. Electrical characteristics of a $Sr^{90}-Y^{90}$ germanium p-n junction cell.

[36] Teal, Sparks, and Buehler, Proc. Inst. Radio Engrs. **40**, 906 (1952).

Efficiencies are: 0.001 percent for $\mathcal{E}_1$; 0.009 percent for $\mathcal{E}_2$; and about 0.021 percent for $\mathcal{E}_3$. These may be compared with an ideal efficiency of 0.034 percent, computed from R_0 and the short-circuit current.

The influence of diffusion length and geometry for junctions such as these is illustrated by the following: A junction identical to the above, except that the n-type layer was 0.2 cm thick, instead of 0.1 cm, had a maximum power of $2.2 \cdot 10^{-10}$ watt, lower by a factor of 15. Testing with the p-type side uppermost lowered W_m by a further factor of 10, because of lower diffusion length on this side.

Lowering the ambient temperature of the cell of Fig. 9 from 25°C to −10°C increased W_m to 0.8×10^{-7} watt, a factor of 24, and increased R by a factor of about 10.

Radiation Damage

While the average energy of incident betas was less than E_t, for germanium at least, betas of energy greater than E_t were present for both silicon and germanium and formation of lattice defects was to be expected. The short-circuit current I_0 of the silicon cell did, indeed, decrease by about 45 percent in two days. However, after 5 weeks at room temperature, in the absence of radiation, I_0 rose to 62 percent of its original value, and after an additional 24-hour anneal at 110°C, I_0 returned to its original value. While further experimentation is indicated, these preliminary results suggest that it may be possible to prevent cumulative radiation damage at this level of irradiation by periodic anneals at 110°C or by operation at an elevated temperature.

7. DISCUSSION

The structures and materials which have here been considered for radioactive junction cells by no means exhaust the design possibilities. They do provide a basis, however, for a preliminary evaluation of the potentialities of such devices, and such evaluation will be made in this section.

It has been shown that the maximum source power available to one side of a thick layer of isotope is roughly one-eighth of that generated in a mean beta range, and this was verified by a more exact calculation for Y^{90}. For an activity of 16 Curie g^{-1}, this maximum power is $2.5 \cdot 10^{10}$ Mev cm^{-2} sec^{-1}. If all electron-hole pairs are utilized, this source power corresponds in germanium (for $R_0 = 10^3$ ohm cm^2) to: $I_g = 0.0013$ amp cm^{-2}, $W_m = 65$ microwatt cm^{-2}, and ideal efficiency, $\mathcal{E} = 1.7$ percent; and in silicon (for $R_0 = 10^8$ ohm cm^2) to: $I_g = 0.0011$ amp cm^{-2}, $W_m = 340$ microwatt cm^{-2}, and ideal efficiency, $\mathcal{E} = 8.6$ percent.

These ideal efficiencies do not take into account the fact that all of the beta energy is not used. For a layer thickness equal to a beta range, these efficiencies should be divided by 8. However, by using a thinner layer of the order of one-eighth beta range in thickness, and by using an array of alternate layers and junctions, efficiencies not much less than the values given above can in principle be obtained.

However, for these cases, the energy and intensity of the radiation are such that radiation damage occurs at an excessive rate. It may be circumvented by using a less energetic isotope, by an absorber, or by annealing. The first means is preferable to the second: It has been shown that considerably less than 0.03 percent of the energy from a thin Y^{90} layer would penetrate an absorber for complete protection of germanium. On the other hand, from a layer of a hypothetical beta emitter of maximum energy equal to the threshold energy for lattice defect formation, energy equal to about 5 percent of that in the Y^{90} layer would emerge, assuming equal activities.

For silicon cells and solar radiation, the ideal efficiency of 18 percent given in Section 3 applies, for the conditions specified, while the sun is shining. The value given for incident power is larger by a factor of 5 than the corresponding average over the entire year which takes night, weather, and varying angle of incidence into account. It follows that for the conversion of solar energy an average W_m of about $3 \cdot 10^{-3}$ watt cm^{-2} may be obtainable, with an $\mathcal{E}$ (equal to the ratio of this power to the average solar input power) of about 15 percent.[37]

Increased efficiency may be realized by increasing $G \equiv eI_gR_0/kT$, hence by increasing I_g or R_0; and, principally through the effect on R_0, by decreasing the temperature T. It is obtainable also by use of junctions for which voltage increases comparatively rapidly with forward current. A necessary condition for this behavior is $A > 1$, as discussed in Section 3; values of A of about 3 have been observed. For given R_0 and I_g, in junctions of suitable types, cell voltage V, power W_m, and ideal efficiency $\mathcal{E}$ are proportional to A. It is readily shown for the optical case that $\mathcal{E}$ can attain values not much less than λ_{av}/λ_G, where λ_G is the long-wavelength limit, if V is less than the energy-gap voltage only by the amount required for charge separation. For solar radiation* with no reflection loss, a theoretical upper limit for $\mathcal{E}$ is accordingly 46 percent.† For essentially monochromatic radiation of wavelength near λ_G, and A of suitable magnitude, $\mathcal{E}$ could in principle be a major fraction of 100 percent.

ACKNOWLEDGMENT

Throughout this study we have had the benefit of help from many of our associates at Bell Telephone

[37] See: reference 16; *Smithsonian Physical Tables* (The Smithsonian Institution, Washington, 1933), eighth revised edition, pp. 610*ff*; and The President's Materials Policy Commission, *Resources for Freedom*, A Report to the President, June 1952, Vol. IV, Chap. 15, "The Possibilities of Solar Energy." Note that a minor effect of load mismatch has been neglected, and that there are no readily available data from which the error that may be involved in the assumption of no change in energy spectrum can be estimated.

* See Section 3.2.

† An estimate of about 23 percent is based on an assumed cell voltage of 0.5 for silicon.

Laboratories. In particular, we are indebted to J. D. Struthers for assistance with radioactive isotopes, to A. J. Goss and D. Dorsi for experimental assistance with radioactive cells, to H. Christensen, C. S. Fuller, and D. M. Chapin for *p-n* junctions; to J. H. Bollman for dc measurements; to C. Herring, W. Kohn, H. W. Lewis, D. A. Kleinman, W. L. Brown, R. C. Fletcher, J. A. Burton, A. Uhlir, J. L. Moll, M. B. Prince, T. S. Benedict, and P. A. Wolff for helpful information and advice; and to K. G. McKay for valued discussions, as well as suggestions concerning the manuscript.

APPENDIX

8.1. The Effect of Recombination in the Photoelectric Case

A quantum efficiency Q may be defined as the ratio of the number of current carriers, or electron-hole pairs separated by the junction, to the number of absorbed photons, each of which produces one electron-hole pair in germanium and silicon. Consider a semi-infinite semiconductor with a plane junction (at which added carrier concentration is zero) at depth $x=x_s$; recombination on the surface with velocity s; diffusion lengths L_s and L, respectively, for recombination in surface layer and in the bulk of the semiconductor; and added carrier generation rate proportional to exp $(-\alpha x)$, as given by Lambert's law of photon absorption, where α is the absorption coefficient at a given wavelength.

The small-signal differential equation[38] for added carrier concentration written for zero total current density[39] provides solutions from which carrier flow into the junction may be evaluated. Contributions from both sides are added, and Q is found to be given by

$$Q=\frac{[1-\exp(L_s^{-1}-\alpha)x_s]/[1-(\alpha L_s)^{-1}]-[(S-1)/(S+1)][1-\exp(-L_s^{-1}-\alpha)x_s]/[1+(\alpha L_s)^{-1}]}{\exp(x_s/L_s)-[(S-1)/(S+1)]\exp(-x_s/L_s)}$$
$$+[\exp(-\alpha x_s)]/[1+(\alpha L)^{-1}], \quad (23)$$

in which

$$S\equiv sL_s/D_0, \quad (24)$$

with

$$D_0\equiv kT\mu_n\mu_p(n_0+p_0)/\sigma_0 = (n_0+p_0)/(n_0/D_p+p_0/D_n) \quad (25)$$

the small-signal ambipolar diffusivity, in a familiar notation.[38]

Various special cases of (23) may be of interest, such as those for s zero or infinite. If the wavelength is short so that $(\alpha L_s)^{-1}$ is small, then, to the first order in this quantity,

$$Q\sim\frac{2(1+S/\alpha L_s)}{(S+1)\exp(x_s/L_s)-(S-1)\exp(-x_s/L_s)}. \quad (26)$$

8.2. The Y^{90} Beta Spectrum

The spectrum may be obtained from the same approximation[40] of Bethe that was employed to represent spectral data in the modified Kurie plot which gives a straight line.[41] The distribution of relative beta intensity $B(E_0)$ in kinetic energy E_0 is accordingly given by

$$B(E_0)\propto\gamma^2(\gamma_m-\gamma)^2[(1+4\alpha^2)\gamma^2-1]^{\sigma-1} \times[1-\exp(-2\pi\alpha\gamma/(\gamma^2-1)^{\frac{1}{2}}]^{-1} \cdot[(\gamma^2-1)+(\gamma_m-\gamma)^2], \quad (27)$$

where

$$\gamma\equiv 1+E_0/m_0c^2 \quad (28)$$

is the total energy of the electron in units of its rest energy, $m_0c^2=0.511$ Mev; $\gamma_m=5.31$ (or $E_0=2.20$ Mev), determined from the Kurie plots, is the upper limit of the spectrum; and the other constants are

$$\alpha\equiv Z/137, \quad Z=40; \quad \sigma\equiv(1-\alpha^2)^{\frac{1}{2}}. \quad (28a)$$

The expression for $B(E_0)$ is the approximation rewritten in accordance with Fermi theory and modified by introduction of the last factor on the right.

8.3. Total Lattice Defect Production Rate: Unshielded Y^{90} and Germanium

It will suffice to assume linear variation with path length of the cross section Σ for lattice defect production. (From theory for Σ in germanium, a linear increase with electron energy from the threshold value, 0.63 Mev, to 2.20 Mev underestimates it near the center of this range by no more than 20 percent.[42] The range-energy relationship is such that the error is somewhat less with the assumption of linear variation with path length.) Thus, if Σ equals[25] $50\cdot10^{-24}$ cm^2 at 2.20 Mev, then

$$\Sigma=3.2\cdot10^{-22}\Delta s \text{ cm}^2, \quad \Delta s\equiv s-s_t, \quad (29)$$

where s_t is the range s in cm that corresponds to the threshold energy. For a rate of generation $\mathfrak{R}$ of electrons of given initial energy E_0 and range s_0 by the isotope layer per unit area, $\frac{1}{2}\mathfrak{R}N\Sigma d(s_0-s)$ defects are produced in path length $d(s_0-s)$, where $N=4.42\cdot10^{22}$ cm^{-3} is the concentration of germanium atoms. The defect

[38] W. van Roosbroeck, Phys. Rev. **91**, 282 (1953).
[39] W. van Roosbroeck, J. Appl. Phys. (to be published).
[40] H. A. Bethe and R. F. Bacher, Revs. Modern Phys. **8**, 82 (1936), Eq. (215b).
[41] E. N. Jensen and L. J. Laslett, Phys. Rev. **75**, 1949 (1949); Braden, Slack, and Shull, Phys. Rev. **75**, 1964 (1949); H. C. Price, Jr., and L. M. Langer, Phys. Rev. **76**, 454 (1949); and L. M. Langer and H. C. Price, Jr., Phys. Rev. **76**, 641 (1949).
[42] W. Kohn (unpublished).

production rate for E_0, neglecting backscattering, obtained by integrating from 0 to $\Delta s_0 \equiv (s_0 - s_t)$, is thus $\frac{1}{4}\mathfrak{R}NA\Delta s_0^2$, in which $A = 3.2 \cdot 10^{-22}$ cm for germanium. This expression is $D(O)$, a special case of a function calculated in Section 8.5.

Multiplication by $B(E_0)$ gives the distribution in E_0 of defect production rate for the unshielded isotope, provided Δs_0 is expressed in terms of E_0. This is accomplished by means of the empirical range-energy relationship,[43]

$$s = 0.412\rho^{-1}E_0^{1.265-0.0954\ \ln E_0}\ \text{cm}, \tag{30}$$

where ρ is the density[34] of the semiconductor in g cm^{-3}, and E_0 is in Mev. The relative distribution (for $\mathfrak{R}=1$) so obtained for Y^{90} is shown in Fig. 5. Its integral over E_0 equals $9.6 \cdot 10^{-3}$, in accordance with which, for $\mathfrak{R} = 3.7 \cdot 10^{10}$ cm^{-2} sec^{-1}, or a Curie per cm^2, defects are produced at the rate $3.6 \cdot 10^8$ cm^{-2} sec^{-1} or 0.010 defect per source electron.

Note that $\frac{1}{4}\mathfrak{R}NA\Delta s_0^2/(10^6 E_0/\epsilon)$ is the ratio of total electron-hole pair production rate for initial energy E_0 (with E_0 in Mev, ϵ in ev). For germanium, this ratio increases from zero at the damage threshold to about $2 \cdot 10^{-7}$ at 2.20 Mev. For any specified distribution of electrons in initial energy, the number of lattice defects per carrier pair is the ratio of the integral for total defect formation to the corresponding integral of $10^6 E_0/\epsilon$.

8.4. Electron Transport through an Absorber with Negligible Scattering

With no scattering, the emergent energy E of electrons which leave a thin-layer source on an absorber of thickness x at angle θ to the perpendicular, for initial energy E_0, is that which corresponds to s in

$$s = s_0 - x\ \sec\theta. \tag{31}$$

The relative number of electrons in the element of angle $d\theta$ is

$$n(\theta)d\theta = \tfrac{1}{2}\ \sin\theta d\theta, \tag{32}$$

the expression on the right being the solid angle. The distribution in E, obtained by eliminating θ from (32) in favor of E by means of (31), is

$$n(E)dE = \begin{cases} \dfrac{x\,dE}{2(s_0-s)^2(dE/ds)}, & 0 \le E \le E(s_0-x) \\ 0 \cdot dE, & E > E(s_0-x). \end{cases} \tag{33}$$

The energy spectrum of emergent electrons is

$$\int_{E_0(s+x)}^{E_m} n(E)B(E_0)dE_0 = \frac{x}{2(dE/ds)} \int_{E_0(s+x)}^{E_m} \frac{B(E_0)dE_0}{(s_0-s)^2}, \tag{34}$$

in which $E_0(s+x)$ is the E_0 that corresponds to s_0 in

$$s_0 = s + x. \tag{35}$$

The derivative in (34) may be evaluated from

$$\frac{dE}{ds} = \frac{1.919\rho E^{-0.265+0.0954\ln E}}{1 - 0.151\ \ln E}\ \text{Mev cm}^{-1} \tag{36}$$

with ρ as in (30). It is instructive to consider also the distribution of total emergent energy in incident energy E_0, which is given by

$$B(E_0)dE_0 \cdot \int_0^{s=s_0-x} En(E)dE = \tfrac{1}{2}xB(E_0)dE_0 \cdot \int_x^{s_0} \frac{Ed(s_0-s)}{(s_0-s)^2} \tag{37}$$

per source electron.[44]

Curves I of Fig. 6 are these distributions, for the 829 mg cm^{-2} absorber, computed from (34) and (27). From the energy spectrum shown at the left, it is found that the fraction of emergent Y^{90} electrons is $1.38 \cdot 10^{-3}$, with average energy 0.185 Mev. The total energy per source electron is thus $2.5 \cdot 10^{-4}$ Mev, or 250 volts, which may also be obtained by integrating the distribution of total emergent energy in E_0 shown at the right in the figure.

The number and energy of electrons that would emerge from a thick isotope layer if there were no scattering is given by the spectrum,

$$\mathfrak{N}\int_0^{s_0-s} n(E)dx \cdot dE = \begin{cases} \dfrac{\mathfrak{N}dE}{4dE/ds}, & 0 \le E \le E_0 \\ 0 \cdot dE, & E > E_0, \end{cases} \tag{38}$$

for $\mathfrak{N}$ source electrons, each of energy E_0, per unit volume. Since dE/ds is roughly constant over most of the range, this result shows that the total number of emergent electrons is approximately $\frac{1}{4}s_0\mathfrak{N}$ per unit area, with average energy $\frac{1}{2}E_0$, so that the average emergent energy $\bar{E}$ is about one-eighth of the energy of electrons within a beta range. For $E_0 = 0.89$ Mev, $\bar{E} = 0.111 s_0\mathfrak{N}$ Mev cm^{-2}, while Weymouth's theory[22] gives $\bar{E} = 0.116\ s_0\mathfrak{N}$ Mev cm^{-2} for this E_0 and metallic strontium.

8.5. Volume Rate of Lattice Defect Formation for Negligible Scattering

The number of defects per source electron of initial energy E_0 produced in the element of angle $d\theta$ and in path length $d(s_0-s)$ or in dx is

$$\tfrac{1}{2}N\Sigma\ \sin\theta d\theta d(s_0-s) = \tfrac{1}{2}N\Sigma\ \tan\theta d\theta dx, \tag{39}$$

[43] L. Katz and A. S. Penfold, Revs. Modern Phys. 24, 28 (1952).

[44] Note that the distribution in E_0 of total emergent number is given by $\frac{1}{2}(1-x/s_0)B(E_0)dE_0$ per source electron.

introducing dx by means of (31). Since, from (29) and (31),

$$\Sigma = A(\Delta s_0 - x\sec\theta)\ \text{cm}^2, \quad A = 3.2\cdot 10^{-22}\ \text{cm}, \quad (40)$$

the relative number of defects per cm² in dx is

$$\tfrac{1}{2}N dx \cdot \int_0^{\cos^{-1}x/\Delta s_0} \Sigma \tan\theta d\theta = \tfrac{1}{2}NAx \times [(\Delta s_0/x)\ln(\Delta s_0/x) - ((\Delta s_0/x)-1)]dx, \quad (41)$$

with $0 \leq x \leq \Delta s_0 \equiv s_0 - s_t$. The coefficient of dx, for given x, multiplied by $\mathfrak{R}B(E_0)$ provides the distribution in E_0 of the rate of formation of defects per unit volume.

The total rate of defect formation $D(x)$ beyond depth x is $\mathfrak{R}$ times the integral of (41) from x to Δs_0, or

$$D(x) = \tfrac{1}{2}\mathfrak{R}NAx^2[\tfrac{1}{2}((\Delta s_0/x)^2 - 1) - (\Delta s_0/x)\ln(\Delta s_0/x)]. \quad (42)$$

Note that $D(O)$, which is derived directly in Section 8.3, is not subject to error from the neglect of scattering.

It is consistent with the assumption of no scattering that the volume rate of defect formation beyond an external absorber at the semiconductor surface is that which would obtain without the absorber at the corresponding depth in the semiconductor. Thus, the rate in germanium at a depth of 0.126 cm is the rate at the surface for an absorber of thickness 669 mg cm^{-2}. This rate for Y^{90}, calculated from (41) and the beta spectrum, is found to equal $4.8\cdot 10^{-5}\ \mathfrak{R}$ cm^{-3} sec^{-1}.

8.6. The Effect of Multiple Scattering

As a result of multiple scattering, beta electrons travel in paths that are substantially straight only for an initial fraction of total range. This fraction (about 0.3 in aluminum[45] for $E_0 = 0.89$ Mev) changes comparatively slowly with E_0. Beyond the corresponding path length, or diffusion limit, the transport is largely random in direction and diffusive in nature. Approximate corrections to the dependence on perpendicular distances calculated according to the theory that neglects scattering may be obtained from the diffusion theory.[46] The "detour factor" (*Umwegfaktor*) is the ratio of actual path length to average perpendicular transport distance for electrons at the end of their range. The rate of radiation damage and average emergent energy calculated for a nonscattering absorber do not apply to the thickness assumed, but approximately to a smaller thickness equal to the diffusion limit plus the remaining thickness divided by the detour factor $\mathfrak{U}$.

The average initial energy of emergent electrons for the thinner absorber is 1.85 Mev, from Fig. 6. The corresponding diffusion limit in aluminum is 0.145 cm, at which the energy, E_d, is to be taken as[45] 1.0 Mev. If s_d is the range for energy E_d, the detour factor is[46]

$$\mathfrak{U} = s_d/\mathfrak{p}, \quad \mathfrak{p}^2 = \int_0^{E_d} \frac{dE}{\kappa_1 dE/ds}, \quad (43)$$

where κ_1 is the reciprocal of the transport mean free path. By employing Eq. (36) and an approximation of Lewis[47] for κ_1, evaluating the integral, and noting that s_d is 0.155 cm, it is found that $\mathfrak{U}$ equals 1.6. Hence the estimates of defect production and energy transmission obtained by neglecting scattering apply actually to an aluminum absorber of approximately 0.21 cm rather than to the 0.248 cm assumed.

Tacit in these considerations is the assumption that multiple scattering does not appreciably affect the shape of the emergent energy spectrum, namely that the spectrum computed for 0.248 cm and straight-path transport is substantially that which obtains for an aluminum absorber 0.21 cm thick. Since the diffusion limit occurs at a roughly constant fraction of total range, multiple scattering will result in a somewhat greater relative number of emergent electrons of the higher energies, compared to the spectrum for the straight-path case. Thus, since there is a threshold for radiation damage, the damage rate is probably slightly larger for the given rate of pair production than the straight-path estimates have indicated.

[45] F. Rohrlich and B. C. Carlson, Phys. Rev. **93**, 38 (1954).

[46] Bethe, Rose, and Smith, Proc. Am. Phil. Soc. **78**, 573 (1938). Direct application of diffusion theory is unsatisfactory because it assumes small energy loss in a transport mean free path, which in aluminum is of the order of the residual range after straight-path transport.

[47] H. W. Lewis, Phys. Rev. **78**, 526 (1950).

Letters to the Editor

Failure and Survival in Fatigue*

A. M. FREUDENTHAL AND E. J. GUMBEL
Columbia University, New York, New York
(Received April 16, 1954)

BECAUSE of the considerable scatter of fatigue life at constant stress amplitude, a reasonable assumption concerning the statistical distribution-function of the fatigue life is a prerequisite for the rational interpretation of fatigue tests. It has recently been shown[1,2] that the cumulative distribution function of extreme (smallest) values

$$l(N)_S=\exp[-(N-N_{0,S})/(V_S-N_{0,S})]^{\alpha_S}, \quad (1)$$

where N denotes the number of cycles to failure, and $N_{0,S}$, the "minimum life" (which may or may not be zero), V_S and α_S are three parameters, represents a physically justified survivorship function of fatigue specimens tested at constant stress amplitude S.

Obviously, the form of this function implies that at any stress amplitude all specimens will fail after a finite number of stress applications $N>N_{0,S}$. However, it is generally observed in fatigue tests as well as in other types of life tests that a certain percentage of specimens will survive a number of stress applications so large that it can practically be considered as $N\to\infty$, provided the applied stress amplitude is sufficiently low; the percentage of specimens surviving on "infinite" number of stress applications increases with decreasing stress amplitude.

It appears, therefore, that, within this range of stress amplitudes, a finite probability $0<l(S)_\infty\leq 1$ must be introduced. With increasing S this probability decreases towards zero; at a certain stress amplitude it will be either zero or differ from zero by so little that, for all practical purposes, the variation of life is governed by Eq. (1). The stress amplitude S_0 for which $l(S_0)_\infty\to 1$ is known as the "endurance limit"; the difficulty of its actual determination by experiment is implied by this definition.

The range $0<l(S)_\infty<1$ within which a number n' out of the total number n of specimens tested survive, while the remaining specimens break after various numbers N of stress applications, has, so far, presented a major difficulty in the rational interpretation of fatigue tests. The purpose of the present note is to show that this difficulty can be easily overcome by introducing an auxiliary survivorship function

$$L(N)_S=[l'(N)_S-l(S)_\infty]/[1-l(S)_\infty], \quad (2)$$

which is itself an extreme value distribution of a form identical with Eq. (1), but with different parameters V_S' and α_S', while $l'(N)_S$ is the true distribution of the test results. Hence, all procedures for the estimation of parameters derived for $l(N)_S$ remain valid for $L(N)_S$; only the plotting position of the n test results, arranged in ascending order from $m=1$ to $m=n-n'$, is now $[1-m/(n+1)(1-l(S)_\infty]$ instead of $[1-m/(n+1)]$, where $n'/(n+1)$ represents a first estimate of $l(S)_\infty$. Thus, $L(N)_S$ is the survivorship function based on the results of only those $(n-n')$ tests that were terminated by failure.

After this function has been determined by the standard procedure, the true distribution of N is easily obtained from Eq. (2):

$$l'(N)_S=L(N)_S+l(S)_\infty[1-L(N)_S]>L(N)_S. \quad (2a)$$

This function fulfills the boundary conditions $l'(N)_S=l(S)_\infty$ for $N\to\infty$ and $l'(N)_S=l(N)_S$ for $l(S)_\infty\to 0$. Hence, the skewness of the distribution $l'(N)_S$ within the range $0<l(S)_\infty<1$ exceeds that of the distribution associated with Eq. (1) and increases with increasing $l(S)_\infty$, a conclusion that is born out by recent tests[3]. On extreme value probability paper on which, for $N_{0,S}=0$, the functions $l(N)_S$ and $L(N_S)$ plot as straight lines, $l'(N)_S$ is a curve with an asymptote at $l(S)_\infty$.

* This work is supported in part by the Office of Ordnance Research under Contract No. DA-30-069-ORD-1061.
[1] A. M. Freudenthal and E. J. Gumbel, Proc. Roy. Soc. (London) **A216**, 309 (1953).
[2] A. M. Freudenthal and E. J. Gumbel, J. Am. Statistical Assoc. **49** (September, 1954).
[3] A. Bender and E. Hamm, unpublished report, Delco Remy Division of General Motors Corporation, Anderson, Indiana (1954).

Effect of Moving Striations on Microwave Conductivity of a Coaxial Discharge

HOWARD L. STEELE, JR., AND PETER J. WALSH
Research Department, Westinghouse Electric Corporation, Bloomfield, New Jersey
(Received June 25, 1954)

IN connection with a means of switching microwave power, the conductivity of 10-cm microwave energy along a dc gas discharge has been studied. A discharge tube is placed within the hollow center conductor of a coaxial transmission line with a short section of its plasma filling a gap in that conductor. The fraction of microwave energy transmitted across this gap has been measured as a function of dc discharge current. The microwave power must be low enough so that it will not disturb the discharge. As the tube current is varied in the range from one milliampere to one ampere, the fraction of energy transmitted first drops and then rises to a value close to one. This is in agreement with what has been found by others.[1] Theories[1-3] have been presented to explain this behavior. If experiments are carried out in rare gases[4] or rare gas mixtures (including mixtures with mercury[5]), moving striations will occur at these low currents.

A discharge which appears perfectly homogeneous to the eye may be composed of bright and dark regions located periodically with distance along the tube axis and travelling thousands of centimeters per second from the anode toward the cathode. These are the moving striations[5,6] and may be detected with a photocell or in a mirror rotating on an axis parallel to that of the discharge. Pupp[7] has investigated the variation of electron density in the light and dark regions of travelling striations and found that the density was highest in the bright region and fell to ½ this value in the dark region. The microwave conductivity would thus be expected to oscillate considerably when moving striations were present.

The microwave signal that has passed a gap, such as previously described, can be displayed on an oscilloscope. If the tube in the gap is operated at a low current in a rare gas, an amplitude jitter

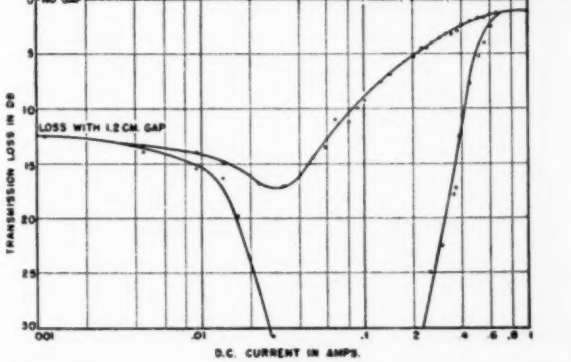

FIG. 1. Maximum and minimum attenuation for 10-cm waves in coaxial transmission line containing a 1.2-cm length of gas discharge exposed in the center conductor. Current external to discharge shows very little fluctuation although discharge contains moving striations.

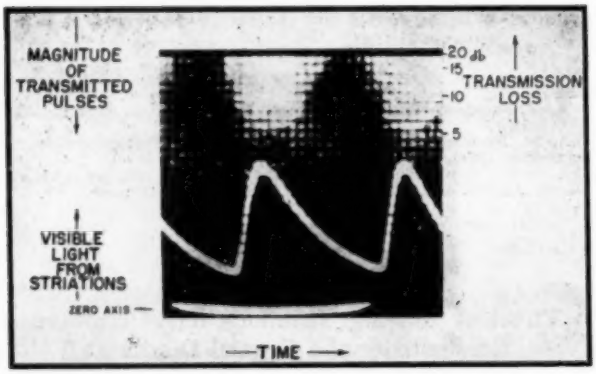

FIG. 2. Magnitude of microwave pulse transmitted past striating gap and light intensity from gap as a function of time. Upper trace is envelope created by shifting phase of arrival of rf at gap with respect to arrival of bright region. Time scales of two traces are the same. Discharge current is 0.175 amperes through 2-mm krypton with 1.2-cm gap exposed.

of considerable magnitude may be noted in the microwave signal trace. Striations are passing through the gap and the jitter is due to the varying phase of the rf signal with repect to striations. The jitter amplitude is a measure of the change in transmission associated with different parts of the striation cycle. Figure 1 shows the maximum and minimum of the jitter amplitude. The fraction of microwave energy transmitted is given as a function of discharge current in krypton at a pressure of 2 millimeters. The gap was short compared to the distance between bright regions. The striations, of course, can be considered stationary compared to the time of travel of microwave energy across the gap. The upper curve gives the transmission when the electron cloud attending the bright region is in the most favorable position. The lower curve gives the minimum transmission obtainable in the striation cycle at various discharge currents.

In order to prove conclusively that striations cause the jitter mentioned, the oscilloscope was synchronized to the frequency of the striations. The envelope in the upper part of Fig. 2 is that obtained as the microwave energy pulse crosses the gap of different times in the striation cycle. The lower trace is that obtained with a highly directive photomultiplier responding to the light from the striations as they pass the generator edge of the gap. The time scales of the two parameters are thus the same in magnitude and phase.

The results presented demonstrate a pronounced change in the microwave conductivity as striations move past a gap. The effect is strong enough to suggest[8] the use of moving striations to block and pass periodically (switch) microwave energy from a pulsed source.

[1] L. Goldstein and N. L. Cohen, Phys. Rev. **73**, 83 (1948).
[2] Kerr, Brown, and Kern, Phys. Rev. **71**, 480 (1947).
[3] P. Rosen, J. Appl. Phys. **20**, 868 (1949).
[4] M. J. Druyvesteyn, Revs. Modern Phys. **12**, 87 (1940), Fig. 80.
[5] H. L. Steele, Jr., Phys. Rev. **82**, 571 (1951).
[6] T. Donahue and G. H. Dieke, Phys. Rev. **81**, 248 (1951).
[7] W. Pupp, Physik. Z. **36**, 61 (1935), Fig. 3.
[8] Patent Pending, U. S. Patent Office.

Germanium-Stabilized Gray Tin

A. W. EWALD
Department of Physics, Northwestern University, Evanston, Illinois
(Received June 30, 1954)

IT is well known that the transformation of white tin to the gray modification is strongly influenced by impurities. A concentration of 0.001 percent bismuth for example, inhibits the transformation, whereas aluminum and zinc have an accelerating effect when present in concentrations of the order of 0.1 percent.[1] To the author's knowledge no mention is made in the literature of corresponding effects of impurities on the reverse transformation (i.e., from gray to white). The purpose of this note is to report an observed high degree of stability at elevated temperatures of germanium-doped gray tin.

In the course of an investigation of the semiconducting properties of gray tin it was noted that samples containing 0.75 weight percent germanium did not reconvert to the metallic (white) phase when exposed to room temperature for many months, whereas pure gray tin transforms within a few hours under the same conditions. To investigate this stabilization a quantity of the germanium-doped gray tin powder was divided into two samples. One, the test sample, was heated in an oven to successively higher temperatures while the other was kept at room temperature. The oven was maintained at fixed temperatures, starting with 30°C, for 24 hour periods. At the end of each period the two samples were compared for any color difference, and when none was observed the test sample was replaced in the oven at a temperature 10 degrees higher for the next 24 hours. This procedure

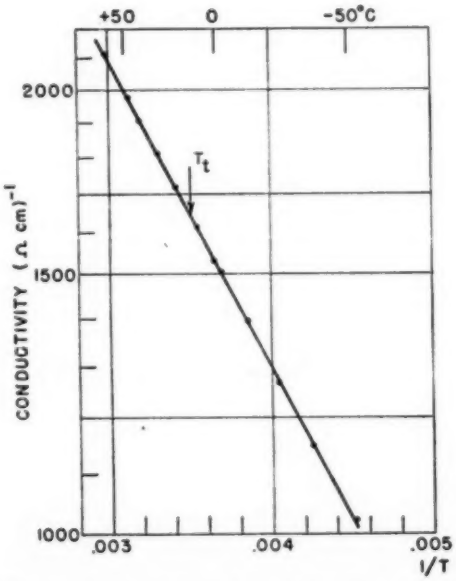

FIG. 1. Extension of the intrinsic conductivity line 50°C above the normal transition temperature T_t.

was continued for four consecutive days with no apparent change in color of the test sample. Before the end of the next period, during which the oven temperature was 70°C, the test sample showed the expected color change. The results of this test indicate that gray tin containing 0.75 percent germanium reconverts to the metal at an appreciable rate only at temperatures above 60°C.

To make certain that there was not a partial reconversion at lower temperatures before the color change was apparent the temperature dependence of the conductivity was investigated at these higher temperatures. Since the conductivity of the metal (at room temperature) is approximately 30 times that of the semiconducting phase, the presence of a small percentage of the former would result in a discontinuity in the intrinsic line of the conductivity plot. The sample was in the form of a filament[2] which had been completely transformed to gray tin. It was found possible to solder electrical leads to it with Wood's metal (melting point 72°C) without reconverting it to the metal. The results of the measurements up to 60°C are shown in Fig. 1. There is no indication of a phase change. When the sample was maintained at 63°C for an hour the conductivity increased by 20 percent. This, however, was an irreversible change due not to the phase transition

but to diffusion of the solder (near its melting point) into the sample. The added conductivity could not be removed by prolonged refrigeration at the optimum temperature for the white-to-gray transition.

The possibility of gaining increased stability at still higher temperatures by increasing the concentration of germanium is limited by the solubility of germanium in metallic tin.[3] Also, attempts to produce comparable stabilization of the gray phase by doping with silicon have not been successful, probably because of the very small solubility of silicon in the metal.

[1] E. Cohen and A. K. W. A. van Lieshout, Z. physik. Chem. **117A**, 331 (1936).
[2] A. W. Ewald, Phys. Rev. **91**, 244 (1953).
[3] H. Stöhr and W. Klemm, Z. anorg. Chem. **241**, 305 (1939).

Protective Films on Magnesium Observed by Electron Diffraction and Microscopy

SHIGETO YAMAGUCHI
Scientific Research Institute, Ltd., Hongo, Toyko, Japan
(Received June 30, 1954)

THE protective films of hydroxide and fluoride formed on magnesium[1] were freed from the substrata by using the Grignard reagent. The isolated films were examined by means of electron diffraction and microscopy.

A magnesium ingot with a lustrous surface, prepared by etching with a hydrochloric acid solution (35 percent), was immersed in boiling water for about 10 minutes. The surface of the magnesium was rendered mat by this treatment. The mat surface of the ingot was sliced with a knife edge in order to prepare shavings. The shavings obtained were immersed in a Grignard reagent. The reagent here employed was a solution consisting of methyl iodide and ethyl ether (1:10 by volume).[2] In this solution the metallic component of the shavings was dissolved away at room temperature. The nonmetallic surface films thus freed remained suspended in the solution. The films were collected and washed with ethyl ether and with absolute alcohol.

The thin films thus prepared and obtained gave a diffraction pattern and a micrograph shown in Figs. 1 and 2. Figure 1 verifies the existence of oriented crystallites of magnesium hydroxide (hexagonal, $Cd(OH)_2$ type). The c axes of the crystallites in Fig. 1 lie almost parallel to the incident beam. Table I is a comparison of the interplanar spacings measured in Fig. 1 with those of magnesium hydroxide crystal determined by x-ray diffraction.

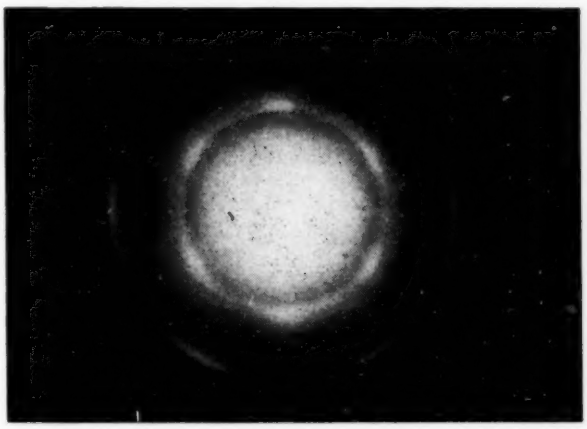

FIG. 1. Diffraction pattern obtained from the protective film formed on magnesium in boiling water. The pattern verifies the existence of magnesium hydroxide [$Mg(OH)_2$]. Here the hydroxide crystallites of $Cd(OH)_2$ type are regularly oriented. The c axes of the crystallites lie almost parallel to the incident beam. Wavelength: 0.0306 A. Specimen-plate distance: 495 mm. Positive enlarged 2.33 times.

FIG. 2. Micrograph of the protective film of magnesium formed in boiling water. The film gave the diffraction pattern (Fig. 1) characteristic of magnesium hydroxide.

An etched surface of magnesium was immersed in a sodium fluoride solution (10 percent) for about 5 minutes at room temperature. Thin films were freed from the mat surface of magnesium by the same process as for the specimen treated with boiling water. The films obtained gave Figs. 3 and 4. The diffraction pattern

TABLE I. A comparison of the interplanar spacings (d) measured in Fig. 1 with those (d^*) of magnesium hydroxide crystal calculated using x-ray data.[a]

d	d^*	hkl
2.69 A	2.69	100
1.55	1.555	110
1.02	1.02	210
0.898	0.898	300

[a] R. W. G. Wyckoff, *Crystal Structure* (Interscience Publishers, Inc., New York, 1948).

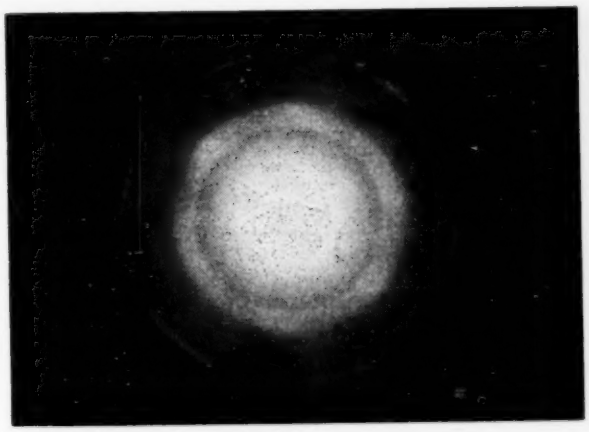

FIG. 3. Diffraction pattern obtained from the protective film formed on magnesium in a fluoride solution. The pattern verifies the coexistence of magnesium fluoride and hydroxide. Wavelength: 0.0296 A. Specimen-plate distance: 495 mm. Positive enlarged 2.33 times.

TABLE II. A comparison of the interplanar spacings (d) measured in Fig. 3 with those of magnesium fluoride crystal (d^*) determined by x-ray diffraction.* d^{**}: interplanar spacings of magnesium hydroxide given in Table I. ( ): diffraction intensity approximated on an arbitrary scale of 10.

d	d^*	d^{**}
3.29 A (0.5)	3.29 (8)	...
...	3.14 (0.5)	...
2.69 (4)	...	2.69
2.56 (1)	2.56 (2)	...
2.24 (6)	2.24 (10)	...
...	2.07 (3)	...
1.93 (3)	1.93 (1)	...
1.72 (3)	1.72 (10)	...
...	1.64 (3)	...
1.55 (10)	...	1.55
1.53 (1)	1.53 (2)	...

* Hanawalt, Rinn, and Frevel, Ind. Eng. Chem., Anal. Ed. 10, 457 (1938).

of Fig. 3 verifies the coexistence of magnesium fluoride and hydroxide. Table II is a comparison of the interplanar spacings measured in Fig. 3 with those of magnesium fluoride and hydroxide determined by x-ray diffraction. It is noticed that the fluoride-

FIG. 4. Micrograph of the protective film of magnesium formed in a fluoride solution. The film is composed of magnesium fluoride and hydroxide. This film is coarser than that of Fig. 2.

hydroxide composite film of Fig. 4 is coarser than the hydroxide film of Fig. 2. The rather fine film of Fig. 2 may be used as a replica of the substrate.

The experimental procedures here described are useful for the detection of protective films formed on magnesium.

[1] U. R. Evans, *Metallic Corrosion, Passivity and Protection* (Edward Arnold and Company, London, 1948), p. 608.
[2] O. Diels, *Einführung in die organische Chemie* (Verlag Chemie GmbH, Weinheim, 1953), p. 78.

Entropy of Information and the Odd Ball Problem*

PAUL J. KELLOGG AND DOROTHY J. KELLOGG
Laboratory of Nuclear Studies, Cornell University, Ithaca, New York
(Received July 8, 1954)

THERE is a well-known puzzle in which one is asked to sort out from twelve balls, one of which has a different weight from the rest, and determine whether it is heavier or lighter, in three weighings. This problem and many generalizations of it can readily be solved by considering the entropy of information.

Suppose, for example, that one wishes to find the odd ball out of N balls. Then there are $2N$ possibilities; first ball is heavier, first ball is lighter, etc. They are equally probable by assumption, so the entropy of the system is:

$$S=-k\Sigma\rho\ln\rho=k\ln 2N.$$

Each weighing can have three results: left pan heavier, right pan heavier, or both pans same weight. If initially all three results are equally probable, then before weighing there will be entropy $S=k\ln 3$, and after the weighing the entropy will be zero. If the three results are not equally probable, then the change in entropy will be smaller, a well-known property of the entropy function.

When we have found which ball is odd, and found its weight, the entropy of information will be zero, and this much change in entropy will require at least

$$\frac{\Delta S\ (\text{total})}{\Delta S\ (\text{per weighing})}=\frac{\ln 2N}{\ln 3}$$

weighings, which gives a lower limit on the number of weighings required for a systematic solution.

Weighing involves the conversion of energy into entropy of information in a transparent way, thus providing a demonstration of the equivalence of informational entropy to negative thermodynamic entropy. When the balls are put into the pans of the balance, the heavier pan must be allowed to sink until the deflection of the balance is greater than the random thermal deflections, so that approximately kT of energy is used up. If the outcome of a particular weighing is that the contents of the pans have the same weight, then there is no loss of energy to this source. However, there are other sources of energy loss, because one must use up energy in order to observe the pointer position, say with a light beam, as discussed by Brillouin,[1] and these also give energy losses of the order of kT.

In the usual ball problem, there are twelve balls, and one is supposed to find the odd ball in three weighings. Initially (dropping the unit k from now on) $S=\ln 24$, and since for three weighings $\Delta S=-3\ln 3=-\ln 27$, it appears that there is just a little more than enough negative entropy to do the job. In fact, it would appear that one could get enough information from three weighings to separate thirteen balls, but actually one cannot get enough information from the first weighing. For suppose that one begins by balancing two piles of four balls each. If they balance, the odd ball is in the remaining pile of five balls, and one requires $\Delta S=-\ln 10$ to sort it out, which is more than one can get from the two remaining weighings. On the other hand, if initially one weighs two piles of five balls each, and the odd ball belongs to one of these piles, one again requires $\Delta S=-\ln 10$ to sort it out. Clearly any other choice for the initial weighing gives even more unequal probabilities, and less entropy of information.

The twelve ball problem can be solved in an almost straightforward fashion. It is clear that the maximum gain of information is obtained if the first move is to divide the balls into three equal piles, A, B, and C, and to weigh two of them, say A and B. Then the probability of balance is the probability that the odd ball is in C, $\frac{1}{3}$, and is equal to the probability that either side is

TABLE I.

n_1	n_2	Left pan heavy	Right pan heavy	Balance	ΔS
1	1	$\frac{1}{4}$	$\frac{1}{4}$	$\frac{1}{2}$	1.040
1	0	$\frac{1}{3}$	$\frac{1}{3}$	$\frac{1}{3}$	0.736
2	2	$\frac{1}{4}$	$\frac{1}{4}$	0	0.693
2	1	$\frac{1}{5}$	$\frac{1}{5}$	$\frac{1}{5}$	1.082
2	0	$\frac{1}{4}$	$\frac{1}{4}$	$\frac{1}{2}$	1.040
3	1	$\frac{1}{4}$	$\frac{1}{4}$	0	0.693
3	0	$\frac{1}{3}$	$\frac{1}{3}$	$\frac{1}{3}$	1.082
4	0	$\frac{1}{2}$	$\frac{1}{2}$	0	0.693

TABLE II.

Contents of left pan A	B	Contents of right pan A	B	C	Balance	Right pan heavy	Left pan heavy	ΔS
1	2	1	2	0	‡	‡	‡	1.082
1	2	1	1	1	‡	‡	‡	1.082
1	2	0	2	1	‡	‡	‡	1.082
1	3	0	1	3	Same as one of above.			
2	1	2	1	0				
2	1	2	0	1				
2	2	1	1	2				
2	2	0	1	3				
2	3	0	1	4				
2	2	1	0	3				
2	1	1	1	1				
3	1	1	0	3				
3	2	1	0	4				

heavier. So one gets the maximum possible gain in entropy $\Delta S = -\ln 3$.

Suppose that A and B balance, so that the odd ball is in pile C. It can easily be shown that the odd ball of four cannot be separated in two weighings, by reasoning similar to that used above for thirteen balls. Hence one must use the knowledge that the other eight balls have normal weight. Suppose one puts n_1 balls of pile C into the left pan of the balance, and n_2 balls of pile C together with $n_1 - n_2$ balls of normal weight into the right pan. Table I gives the various possibilities, together with the probability of balance, left pan heavier and right pan heavier, and decrease of entropy. Either of the two choices which give the largest entropy change can easily be shown to lead to a solution.

Now suppose that piles A and B do not balance, so that (say) either one of the balls in A is heavy, or one of those in B is light. In this case, the list of all possible combinations becomes rather long. The following considerations serve to eliminate all but a few of the possibilities. The third balancing can contribute at most ln3 to the negentropy. Hence after the second weighing, the odd ball must have been determined to be one of three at most, and for each of the three it must be known whether it would be heavy or light, should it prove to be the odd one. The only combinations for the second weighing which fulfill these conditions are given in Table II, together with the probabilities. All of these combinations lead to the same entropy change, and all lead to a solution. For example, in the first case listed, if the pans balance, then one of the two A balls is heavy, and weighing them against each other shows which; if the left pan is heavy, then either the A ball is heavy or one of the B balls in the right pan is light, and weighing these two B balls against each other determines the odd one; the same procedure works if the right pan is heavy.

Clearly these principles will also apply to more complicated problems, such as when more than one odd ball, or an unknown number of odd balls are present.

The authors are grateful to Professor Philip Morrison for discussion of this matter.

* Supported by the joint program of the Office of Naval Research and the U. S. Atomic Energy Commission.

[1] L. Brillouin, J. Appl. Phys. 22, 334 (1951).

Diffusion of Boron and Phosphorus into Silicon*

C. S. FULLER AND J. A. DITZENBERGER
Bell Telephone Laboratories, Murray Hill, New Jersey
(Received July 20, 1954)

LARGE area p-n junctions adjacent to the surface of silicon wafers or slabs are useful in the construction of many electronic devices, including power rectifiers[1] and photocells.[2] It is the purpose of this letter to present some preliminary results on the diffusions of boron and phosphorus into silicon which provide convenient methods of obtaining these junctions.

Specimens of single crystal silicon,[3] ranging in resistivities between 1 and 10 ohm cm, of both n and p types were heated in the presence of boron trichloride and phosphorus vapor,[4] respectively. Temperatures from 1050 to 1250°C and times ranging from 16 to 112 hours were employed. Diffusion constants were calculated from measurements of the p-n junction depths and values of the surface concentrations of the elements. The latter were estimated from surface resistance measurements[5] and values of electron and hole mobilities as determined from Hall measurements on highly doped crystals.[6] Solid solubilities between 3 to 6×10^{20} cm^{-3} at 1250°C were calculated for boron and phosphorus. The latter solubility appears to decrease more rapidly with temperature.

Fick's law was assumed valid and junction depths, normalized to 16 hours diffusion time, were plotted against temperature. Within the rather large error of the experiments the values for both phosphorus and boron fall on one curve. Values for penetration depths were interpolated from the aforementioned penetration-temperature curve at 1000, 1100, 1200, and 1300°C and diffusion constants calculated in the usual manner for a semi-infinite slab. The results are given approximately (Fig. 1) by the equation

$$D = 0.001 \exp(-58000/RT) \qquad (1)$$

for both elements, where D is the diffusion constant in cm^2 per sec. The probable error in D is estimated as ± 50 percent and in the activation energy as ± 15 percent.

Preliminary work by J. D. Struthers using radioactive phosphorus at 970°C is in approximate agreement with the results of Fig. 1. The close similarity between the diffusion characteristics for phosphorus and boron in silicon suggests a mechanism based

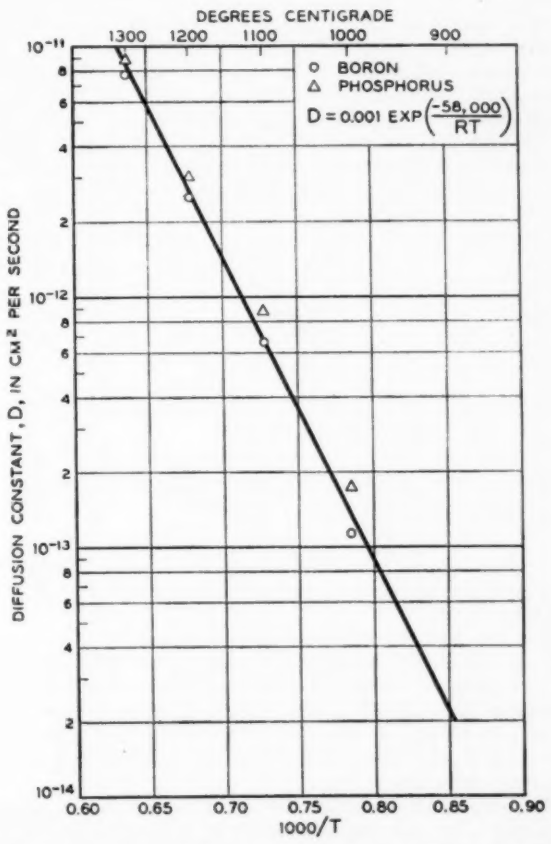

FIG. 1. Diffusion constants of boron and phosphorus in silicon as a function of reciprocal of absolute temperature.

on the self-diffusion of silicon, although there is some indication that the activation energy for diffusion may be somewhat higher for phosphorus.

Although the carrier lifetimes in junctions produced by the above method are in general low, reverse current densities of 10^{-6} amperes per cm² at 1–10 volts are obtainable. Abrupt voltage saturation behavior in the range 90 to 200 volts (rms) has also been observed. Average surface resistivities for boron and phosphorus diffused at 1260°C are approximately 0.001 ohm cm, a fact which enables low resistance contacts to be made to the diffusion layers.

* Presented before I.R.E. Semiconductor Devices Conference, Minneapolis, Minnesota, June 28, 1954. Work along similar lines was reported to Am. Phys. Soc. meeting, Minneapolis, Minnesota, June 28, 1954. See Dunlap, Bohm, and Mahon, Bull. Am. Phys. Soc. 29, 11 (1954).
[1] G. L. Pearson and C. S. Fuller, Proc. Inst. Radio Engrs. 42, 760 (1954).
[2] Chapin, Fuller, and Pearson, J. Appl. Phys. 25, 676 (1954).
[3] The authors are indebted to E. Buehler, E. D. Kolb, and N. B. Hannay for silicon crystals.
[4] J. H. Scaff and H. C. Theuerer, U. S. Patent 2 567 970, September 18, 1951.
[5] A. Uhlir (private communication).
[6] Measurements of F. J. Morin and J. P. Maita.

Stress Measurement by X-Ray Diffraction

H. R. LETNER, *Mellon Institute of Industrial Research, Pittsburgh, Pennsylvania*
AND
S. R. MALOOF, *Raytheon Manufacturing Company, Waltham, Massachusetts*
(Received July 26, 1954)

A LIMITATION of the x-ray method in measuring surface stresses having steep gradients normal to the surface is revealed by an experiment in which the principal stresses in a biaxial system were measured by two independent methods. The stresses, induced by surface grinding annealed tool steel, were first measured by the two-exposure method, using unfiltered CrKα radiation reflected from the (211) planes of α iron. Line positions and intensities were measured with a Geiger-counter diffractometer.[1] Later the surface was sectioned and the stresses were determined by the deflection technique.[2]

The complete distributions for the principal stresses σ_1 and σ_2, obtained by the latter method, are shown in Fig. 1 in which positive values represent tension and negative values compression. The steep gradients close to the surface are an important feature of these curves.

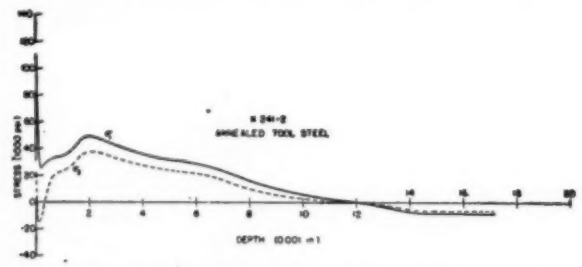

FIG. 1. Residual grinding stresses in annealed tool steel specimen K241–2; σ_1 and σ_2 are parallel and perpendicular, respectively, to the direction of abrasive (see reference 2) travel.

The first 0.001 in. below the surface is plotted on an enlarged scale in Fig. 2. The cross-hatched areas within 0.0001 in. of the surface represent ranges of values which uncertainties in the deflection data would permit. The x-ray values, indicated by circles, lie well below these ranges at the surface. This in not surprising in view of the contribution of the subsurface metal to the x-ray diffraction pattern.

The ratio of the intensity diffracted from a surface layer of thickness z to that diffracted from an infinitely thick layer is $I_z/I_\infty = 1-e^{-\mu l}$, in which μ is the linear absorption coefficient and l is the path length of the radiation in the surface.[3] Application of this equation to the diffraction of CrKα radiation from the (211) planes making an angle of 45° with the plane of the surface discloses that 50.2 percent of the total line intensity comes from the first 0.0001 in., 25.0 percent from the second, 12.6 percent from the third, 6.3 percent from the fourth, and so on. The first 0.001 in. contributes 99.9 percent of the total line intensity. The position of the diffraction peak is a weighted average of the peak positions which each incremental layer, acting alone, would define; consequently, the x-ray stress value corresponding to the peak position is likewise a weighted average of the stresses throughout the volume irradiated. If the values of σ_1 and σ_2, indicated in Fig. 2 for each incremental layer, are multiplied by the fractional contribution of that layer to the total line intensity, the products added together, and the sum divided by 0.999, weighted averages for σ_1 and σ_2 are obtained which are also shown in Fig. 2. The ranges of uncertainty in the averages are the result of the uncertainties in σ_1 and σ_2 close to the surface.

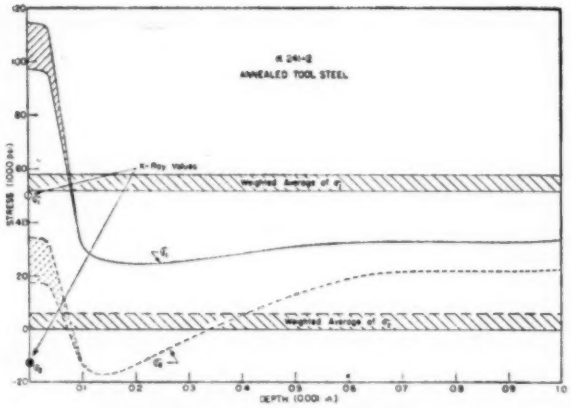

FIG. 2. Stresses in the first 0.001 in. below the surface of specimen K241–2.

Although x-ray diffraction does not give the true surface stress when the gradient is steep, it gives a value nearly equal to the weighted average of the stresses in the volume diffracting. If the gradient is not steep, the difference between the stress at the surface and the weighted average is small, and the x-ray method should closely approximate the actual surface stress.

The experimentally determined constant of proportionality between stress and lattice strain used in obtaining the x-ray values is about 30 percent higher than that calculated from engineering values of Young's modulus and Poisson's ratio.[1] The agreement between the x-ray values and the weighted averages supports previous evidence that mechanical values of the elastic constants (particularly Young's modulus) cannot be used in the x-ray stress equation.

[1] S. R. Maloof, Norelco Reporter 1, No. 3, 35–39 (1954).
[2] H. R. Letner, Proc. Soc. Exp. Stress Anal. 10, 23–36 (1953).
[3] A. Taylor, Phil. Mag. 35, 632–638 (1944).

Surface Leakage Current in Rectifiers

MELVIN CUTLER AND HUBERT M. BATH
Hughes Aircraft Company, Research and Development Department, Semiconductor Division, Culver City, California
(Received July 31, 1954)

A THEORY has been developed for surface leakage which is based on a relatively simple model, and which shows agreement with the experimental behavior of several types of rectifiers. The leakage current I_2 is added to the rectifier current I_1; the latter obeys the classical diode equation.

The behavior of I_2 is derived from the following model, illustrated in Fig. 1: The semiconductor on one side of the rectifier

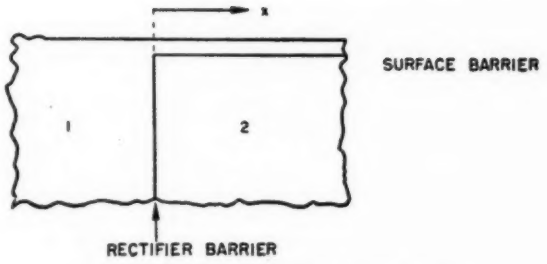

FIG. 1. Diagram of the surface leakage model.

barrier (region 2) is assumed to be separated from a thin conducting surface film by a surface barrier; the film connects with region 1. I_2 flows from region 1 through the surface film, with an ohmic voltage drop, and across the surface barrier to region 2.

The equations of the system depend on the geometry of the rectifier. For a filament with a p-n junction across it, whose perimeter has a length L, the equations are

$$dV/dx = -\rho I_2/tL, \tag{1}$$

$$dI_2/dx = -I_s L[\exp(qV/kT)-1], \tag{2}$$

where x is the distance from the rectifier junction, t is the film thickness, ρ is the film resistivity, and I_s is the saturation current per unit area for the surface barrier. The solution is

$$I^2 = (2tL^2 I_s kT/\rho q)(e^v - v - 1), \tag{3}$$

where $v = qV/kT$. (V and I_2 are functions of x in equations (1) and (2); elsewhere, the symbols refer to the values at $x=0$.)

For a junction with circular geometry, such as a fused junction, Eq. (3) is an approximation to the solution, which is accurate when $v \gg 1$. In the reverse direction, theory indicates that I_2 may be nearly proportional to V rather than $V^{\frac{1}{2}}$.

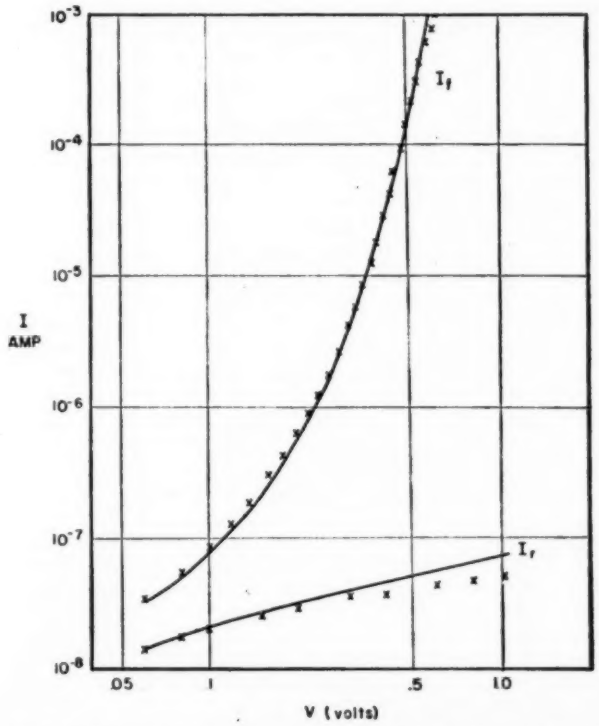

FIG. 2. Comparison of experimental points with the theoretical curve for the leakage current in a drawn p-n junction; $I_h = 1.2\times10^{-4}$ amp, $I_s = 2\times10^{-12}$ amp.

The current-voltage characteristics of different types of rectifiers have been examined, and agreement with equations above over a considerable range has been found in a number of cases. These include evaporated contacts on n-type germanium, fused junctions on p-type silicon, and drawn silicon p-n junctions (see Fig. 2). The rectifiers obey the equation

$$I = I_c(e^v - 1) + I_h(e^v - v - 1)^{\frac{1}{2}} \tag{4}$$

in the forward direction up to the range where the voltage drop in the base becomes appreciable. Typical values for the constants for silicon fusion diodes at room temperature are $I_c = 3\times10^{-15}$ amp, $I_h = 2\times10^{-10}$ amp. According to Eq. (4), the value of $d(\ln I)/dV$ in the forward direction should vary with bias between q/kT and $q/2kT$. This is in general agreement with reported properties of silicon fusion diodes.

There is little doubt that the leakage current is closely related to other surface phenomena reported recently.[1,2] It is of interest that the simple model used here is adequate for many rectifier systems, although it seems likely that a more involved model would be necessary for a general treatment of the problem.

[1] S. R. Morrison, J. Phys. Chem. 57, 860 (1953).
[2] W. L. Brown, Phys. Rev. 91, 518 (1953).

All-Glass Valves for Use in Obtaining Ultra High Vacua

RICHARD W. DECKER
Westinghouse Research Laboratories, East Pittsburgh, Pennsylvania
(Received July 31, 1954)

THE production of ultra high vacua is necessary to a large number of experiments. D. Alpert[1] has described a system employing a metal valve and an ion gauge that would produce ultra high vacua. The procedure described was to place the valve in the vacuum system between the manifold and the vacuum pumps. An ion gauge was attached to the manifold, and the manifold, ion gauge, and the valve were evacuated and thoroughly baked to degas. The valve was closed and the pumping action of the ion gauge evacuated the manifold to an extremely low pressure. A discussion of ion gauge pumping is also included in Alpert's paper.

In experiments that demand ultra high vacuum it is imperative that the vapor pressures of all the constituents be considered.

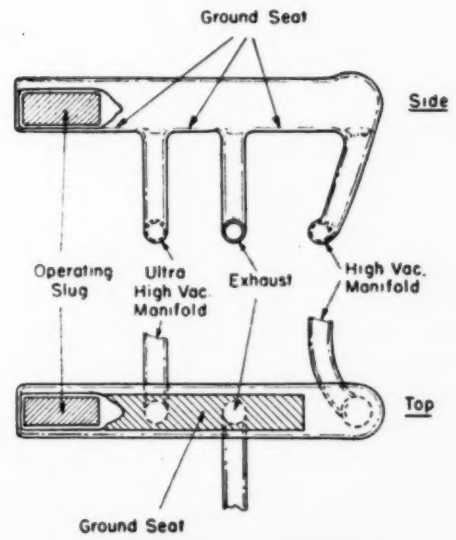

FIG. 1. Sliding ground glass valve.

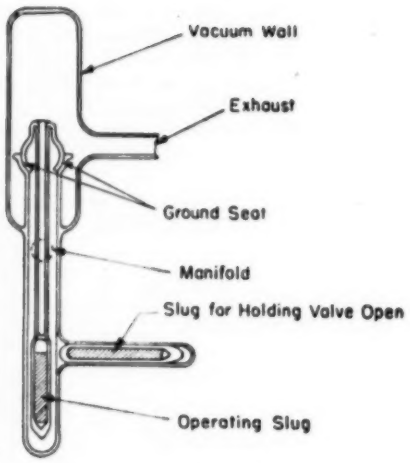

FIG. 2. Ball joint ground glass valve.

In this aspect glass is a valuable material. Glass has the desirable properties of being easily cleaned, chemically inert, and physically stable. It has been found that in some experiments, performed in ultra high vacua, the presence of a metal would cause an unwanted reaction.

An all-glass valve may be constructed as shown in Fig. 1. The valve consists of a ground seat, sealed in glass tubing with a glass-enclosed iron slug ground to fit the seat. Pyrex glass is used to allow high temperature bakeouts. The valve is opened and closed by moving the ground slug in and out of the seat by an external magnet. In Figs. 2 and 3 alternative constructions are shown in which the valve joint is constructed of a standard ground glass ball joint. The use of standard ball joints reduces the cost and in general provides a better seat.

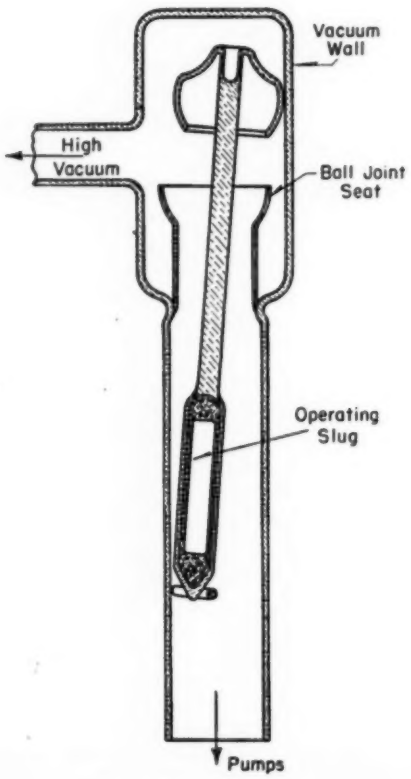

FIG. 3. Single slug glass valve.

The gas passage through the closed valve is extremely small when the pressures on both sides of the valve are in the molecular flow region. Tolerances of $\pm 10^{-4}$ inches are readily available in standard ball joints and 10^{-5} inches is obtained with slight lapping of the seats. The conductance of a 1 cm i.d. valve when closed has been determined to be approximately 0.4 cm³/sec. The pumping speed of an ion gauge is approximately 100 cm³/sec for a representative system. It is possible with the use of a molecular pump, such as an ion gauge, to reduce the pressure of the manifold side of the valve to 10^{-9} mm Hg if the other side of the valve is at a pressure in the molecular flow region.

In a vacuum system with a manifold volume of 1 liter, a pressure of less than 1×10^{-9} mm Hg was obtained and maintained for one week, with the valve shown in Fig. 1. In the processing of demountable experimental tubes of several liters in volume, it has been possible to obtain some of the advantages of sealed-off tubes. The experimental tube is isolated from the vacuum pump by the all-glass valve and an ion gauge is used to pump the tube.

In summarizing, the advantage of the use of this valve for obtaining ultra high vacua is that the vacuum is contained entirely in glass, which reduces the probability of undesirable reaction.

The author is indebted to R. O. McIntosh and Charles J. Cassidy for their original suggestions on the glass valve.

[1] D. Alpert, J. Appl. Phys. **24**, 860 (1953).

Method for Elimination of Thermal Convection*

ALEXANDER KOLIN
University of Chicago, Chicago, Illinois
(Received August 2, 1954)

IN our work on electromagnetophoresis, thermal convection engendered by the current traversing the cell is one of the main disturbing factors. The same problem is also encountered in electrophoresis. In the latter case thermal convection is minimized by using a small current, and by operating at a temperature near the density maximum of the aqueous solution. A method suppressing thermal convection in the presence of steep temperature gradients would be very useful, since it would permit the use of intense currents in conjunction with a cooling system.

It has proved possible to establish and maintain extremely steep temperature gradients in a liquid without engendering large scale thermal convection by a very simple device. Thermal convection is essentially a gravitational phenomenon caused by the density differences between cool and warm liquid masses. It can be effectively eliminated if we expose our fluid to an alternating gravitational field instead of the usual exposure to the unidirectional field of gravity. This is simply accomplished by rotating the cell containing the liquid at a rate at which the centripetal acceleration is small as compared to the acceleration due to gravity. In this case, suspended particles (which include heated fluid elements of differing density) describe circles of small radii about stationary centers, and, thus, nearly stand still relative to the cell.

The effectiveness of this method can be demonstrated by means of a closed cell containing a heating spiral or two adjacent electrodes between which a current passes, heating the liquid between them. When the cell is at rest, the convection can be seen by suspending small polystyrene spheres in the liquid. To demonstrate the suppression of thermal convection in the rotating cell a rotoscope[1] can be used which consists of a Dove prism rotating with half the angular speed of the thermal convection cell. When viewed through the rotoscope the cell appears stationary and the absence of convection is clearly established by inspection. In our experiments a cell of 16×18×41 mm has been used, rotating at

a frequency of 1.3 rps. The heating was accomplished by passing an ac of 3 amperes at 4 volts between 2.5×35 mm silver electrodes 4 mm apart, immersed in a NaCl solution.

The same principle can also be used to suppress convection caused by concentration gradients of a solute.

The author wishes to thank the Research Corporation for a grant supporting his work.

* This work has been supported by the Office of Naval Research.
[1] K. Fischer, Mitt. Hydr. Inst. Tech. Hochsch. (Munchen) **4**, 7–27 (1931).

Reproducibility of Diffusion Measurements: Time of Anneal and Method of Counting Radiation*

C. T. Tomizuka and D. Lazarus
Department of Physics, University of Illinois, Urbana, Illinois
(Received August 2, 1954)

In recent measurements of the diffusion of gold in copper, Martin, Johnson, and Asaro[1] noted a dependence of the measured diffusion coefficient on diffusing time at high temperatures. Similar effects had previously been observed by Johnson[2] in measurements of self-diffusion in silver. The method employed in both instances involved the use of radioactive tracers and sectioning techniques. Since the reproducibility of diffusion data is a matter of serious concern to workers in the field, it was decided to reinvestigate this effect. For convenience, the measurements have been confined to a re-examination of self-diffusion in silver near the melting point, using techniques described elsewhere.[3]

Single and coarse-grained crystal specimens were prepared from Handy and Harmon silver of 99.99 percent purity. Both ends of the cylindrical specimens of 2 cm diameter were plated with high specific activity Ag^{110}. Three specimens were then annealed in vacuum at 903.5°C for periods of 5, 24, and 110 hours, respectively. This range of annealing time is larger than the one covered by Martin, Johnson, and Asaro. It should be noted that the range of annealing time covered in this investigation represents a practical limit beyond which experimental accuracy has to be sacrificed. For a period shorter than 5 hours, the transient time for the specimen to reach an equilibrium temperature becomes too large relative to the actual time of anneal, and for an annealing time longer than our limit, the amount of material left becomes too little after a sufficient amount is taken off from the side of a specimen prior to sectioning, to eliminate effects of surface diffusion. Independent measurements of the diffusion coefficient were made using material removed from each end of the specimen, employing beta counting technique with an immersion counter for one end, and gamma counting for the other. Least-squares calculations were made from these analyses to obtain diffusion coefficients.

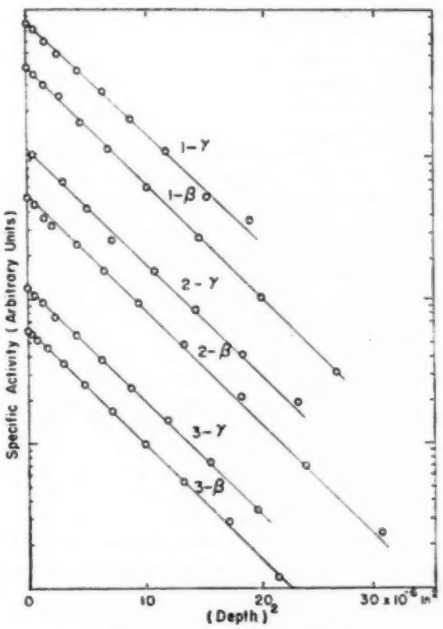

FIG. 1. Penetration curves for self-diffusion in Ag at 903.5°C

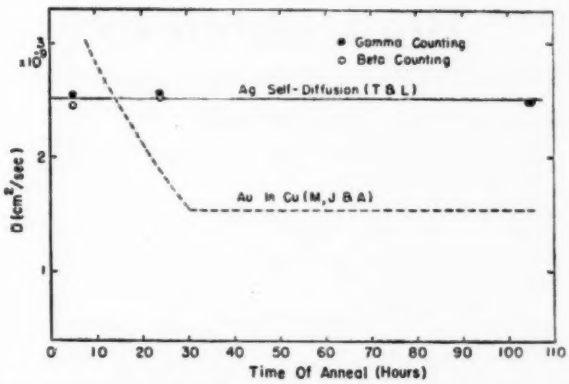

FIG. 2. Diffusion coefficient *versus* annealing time. The solid line represents the results of the present work. The broken line represents the results of the diffusion of Au in Cu by Martin, Johnson, and Asaro in reference 1.

TABLE I. Self-diffusion in silver at 903.5°C.

Specimen No.		Annealing time (hours)	Counting method	Diffusion coefficient (cm^2/sec)	Curve in Fig. 2
1	coarse-grained crystal	5	Gamma	2.55×10^{-9}	$1-\gamma$
			Beta	2.45×10^{-9}	$1-\beta$
2	single crystal	24	Gamma	2.57×10^{-9}	$2-\gamma$
			Beta	2.55×10^{-9}	$2-\beta$
3	single crystal	110	Gamma	2.51×10^{-9}	$3-\gamma$
			Beta	2.50×10^{-9}	$3-\beta$

The plots of the activity against the square of penetration are represented in Fig. 1, where the distance is normalized by a factor $1/t^{\frac{1}{2}}$. Diffusion coefficients are plotted as a function of t in Fig. 2. Pertinent numerical results are listed in Table I.[4] It is apparent that, within the precision of this experiment, *the measured diffusion coefficient is independent of the time of anneal and method of counting radiations.*

The authors wish to thank Dr. L. Slifkin for enlightening discussions.

* Supported in part by the U. S. Atomic Energy Commission and Office of Naval Research.
[1] Martin, Johnson, and Asaro, J. Appl. Phys. **25**, 364 (1954).
[2] R. D. Johnson (private communication).
[3] Slifkin, Lazarus, and Tomizuka, J. Appl. Phys. **23**, 1032 (1952); C. T. Tomizuka and L. Slifkin (to be published).
[4] Previous results (see reference 3) on self-diffusion in silver give a value of 2.4×10^{-9} cm^2/sec at 903.5°C. The activation energy for this process will have to be raised slightly in the light of the present data.

Book Reviews

Diffusion in Solids, Liquids, and Gases

By W. Jost, Academic Press, Inc., New York, 1952. Price $10.96.

Diffusion in Solids, Liquids, and Gases is not just a revision of the author's well-known earlier book *Diffusion und Chemische Reaktion in festen Stoffen*, but a new and more complete treatment of diffusion. The scope and viewpoint of the book are fairly well indicated by the following quotation from the preface: "Although the present monograph contains several theoretical chapters, it is the work of a physical chemist who time and again encountered diffusion problems. Its chief aim is to assist in planning, evaluating, and understanding diffusion experiments, at the same time giving a survey of the results obtained to date."

The main emphasis is placed on diffusion in solids. Diffusion in gases and liquids is discussed much less completely in the last quarter of the book. The first part of the book treats Fick's laws and their solutions, imperfections in crystals, and the theory of diffusion in solids. Following this treatment there is an extensive discussion of the important experimental results on diffusion in solids and their interpretation. Subjects included in this discussion are electrolytic conduction and diffusion in ionic crystals, kinetics of oxidation, diffusion in metals and molecular crystals, diffusion of gases in metals, and others. Diffusion in gases and liquids is then taken up and there is a final chapter on thermal diffusion.

The book should be valuable as a handbook on diffusion since it contains probably the most complete and up to date bibliography and tabulations of data on diffusion in existence.

In my opinion the subject of diffusion along free and internal boundaries of solids deserves a more complete and unified treatment than Jost gives.

I found one important error. It is reported (pp. 225) that Radavich and Smoluchowski [Phys. Rev. 65, 62 (1944)] found a marked effect of pressure on the rate of diffusion in a Cu-Al alloy. Actually these authors state in a subsequent erratum [Phys. Rev. 65, 248 (1944)] that the effect of pressure was nil, within experimental error.

Much of the book is devoted to the description of experiments and discussion of their significance. Usually the author selects the most pertinent experiments and describes accurately and concisely their content and importance. However, the organization of the book is rather loose and there is a tendency to take up particulars before the broad background of a subject has been developed.

The book should prove very valuable to readers who desire information on the content and significance of the most important diffusion experiments, but it will probably disappoint those expecting a broad and critical evaluation of the state of knowledge on diffusion.

D. Turnbull
G-E Knolls Research Laboratory

Cloud Chamber Photographs of the Cosmic Radiation

By G. D. Rochester and J. G. Wilson. Foreword by P. M. S. Blackett. Pp. 128+viii. 123 plates. Academic Press, Inc., New York, 1952. Price $9.88.

Recently, plans were being made for the revision of the twelve-year-old *Atlas typischer Nebelkammerbilder* of Genter, Maier-Leibnitz, and Bothe. However, it appeared that the cloud chamber field has grown sufficiently to justify a separate volume dealing principally with cosmic ray work. Professors Rochester and Wilson therefore collected a fascinating set of 123 photographs, which includes many fine examples of cascade showers, meson decays, nuclear disintegrations, and V-particle events.

The first section of *Cloud Chamber Photographs of the Cosmic Radiation* deals with techniques. It contains photographs illustrating various types of distortion and contamination which are often troublesome, as well as examples of various internal counter arrangements and methods of estimating ionization densities and ages of tracks. This section could have been improved by the addition of a brief description of the principles of the cloud chamber and a few sketches of expansion mechanisms, for the book will prove interesting for the uninitiated as well as for the practicing physicist.

The selection of the cosmic ray photographs is slanted toward recent work—that is, high-energy nuclear disintegrations and V-particle events are represented better than mu mesons and electron cascades. The value of the plates is enchanced by rather complete descriptive legends which give details of the experimental conditions, and which discuss carefully the analyses leading to the interpretations of the pictures. The section dealing with V particles will be received with particular interest; each photograph is accompanied by a lucid discussion which rules out explanations in terms of previously known particles.

The technical qualities of both the original pictures selected and of the reproductions in this volume are, in general, good. There are, of course, some cases for which few examples are available and poorer samples had to be used; it is comforting to note that occasionally even the greatest cloud-chamber practitioners are troubled with poor tracks and excessive background fog.

Cloud Chamber Photographs of the Cosmic Radiation is certain to be received well, both by the specialist who wants information and by the layman who enjoys looking at beautiful pictures.

Rolf G. Winter
Western Reserve University

Lectures on Theoretical Physics. Vol. I. Mechanics; Vol. III. Electrodynamics

By Arnold Sommerfield, Academic Press, Inc., New York, 1952. Price $5.97.

Volume I is paced to the abilities of a first or second year graduate student who has mastered a course in intermediate mechanics. This book will also be welcomed by the serious student of mechanics. It is, for example, one of the few texts which contain a correct treatment of problems involving variable masses, i.e., rocket problems. One of the most unique features of the book is the choice of examples. Two samples are "The Mechanics of Billiards" and "Mass Balancing of Marine Engines."

The level of Vol. III is about the same as that of Vol. I, but a solid preparation is essential. The first part of the book is concerned with the definition of electromagnetic quantities and the deduction of Maxwell's equations. The second part is devoted to solving the equations in special cases. The third and fourth parts of the book are concerned with electron theory, relativity, and the electrodynamics of moving bodies.

The Physics of the Stratosphere

By R. M. Goody. Pp. 187+x, Figs. 61. Cambridge University Press, New York, 1954. Price $5.00.

This book is one of the latest additions to the Cambridge Monograph series which has been extended in the last few years to report on recent advances in pure physics. This book treats the investigations concerning the main physical properties of the stratosphere. It is directed toward physicists who are interested in the advances made in a field which is not necessarily connected with their own work. The theoretical developments are therefore not stressed, and the main discussions are more concerned with the stating of recent findings in this field. In introducing the subject, information on the discovery of the stratosphere and the various methods of obtaining data have been included. Then the book describes the various observed characteristics of temperature, composition, winds, and radiation-absorbing effects of

the stratosphere. A separate chapter is included to cover the complexities involved in the measurement of the properties of the ozone constituent.

Thermal Diffusion in Gases

By K. E. Grew and T. L. Ibbs. Pp. 143+xii, Figs. 40. Cambridge University Press, New York, 1952. Price $4.50.

This work is one of the interesting series of Cambridge Monographs on Physics. The book begins with a brief history of research on thermal diffusion and a survey of the phenomena involved. The assumptions and results of the theory are quoted, but the reader is referred to the treatise by Chapman and Cowling for all details. The emphasis in the first half of the book is on the dependence of the thermal diffusion ratio (the ratio of thermal to concentration diffusion coefficients) upon the intermolecular force law. Experimental methods for determining the small changes of composition are described, and the experimental results are quoted with emphasis on mixtures of different inert gases and mixtures of isotopes of inert gases. A chapter is devoted to comparison of theory and experiment and to the knowledge of intermolecular force laws derived from the experiments. The last three chapters discuss the Clausius-Dickel separation column, the inverse effect to thermal diffusion (temperature difference caused by diffusion) and thermal diffusion in liquids (Soret effect).

An Introduction to the Theory of Control in Mechanical Engineering

By R. H. Macmillan. Pp. 195+xiii. Cambridge University Press, New York, 1951. Price $6.00.

This text is intended for use in an introductory course in the analytical theory of servomechanisms for engineers and physicists. Starting with the principles of control, the author proceeds to a discussion of control system elements and system operation. A treatment of criteria of performance, stability, and the system transfer function is followed by a chapter on Laplace transforms and a chapter on graphical methods, including the application of attenuation and phase diagrams. The book departs from the usual American practice in postponing the use of the Laplace transform and frequency response functions until the last half, the early discussion being based on the use of ordinary differential equations. Another unusual feature is the analysis of a large number of mechanical and hydraulic components which are not usually treated so thoroughly in American books. An interesting historical summary and bibliography is given.

Dictionary of Conformal Representation

By H. Kober. Pp. 208+xvi with 447 diagrams. Dover Publications, New York, 1952. Price $3.95.

This book assembles under one cover a large collection of formulas effecting conformal representations, classified according to the analytic functions describing the transformations. Most transformations are accompanied by pairs of illustrative diagrams which show corresponding curves and regions. While the author disclaims any pretensions toward completeness of the collection, the number of mappings and their possible combinations is so large that practically any explicit mapping problem will be related to some part of the text. Part One treats mappings by linear and bilinear transformations and their construction. Part Two deals with algebraic functions, mappings of region bounded by the familiar algebraic plane curves, Joukowski's aerofoil, and concludes with a bibliography of original papers on aerofoil theory. Part Three discusses mapping by the exponential and logarithmic functions and their combinations. In Part Four the theory of the general Schwartz-Christoffel transformation is reviewed together with a discussion of the mappings effected by this transformation. The last part catalogs mappings resulting from the elliptic functions and the elliptic modular functions. The book should be especially helpful to anyone interested in fluid and gas dynamics, heat flow, magnetic field theory, map projections, and other fields in which the conformal mapping technique is used.

Tables for Predicting the Performance of Fixed Bed Ion Exchange and Similar Mass Transfer Processes

By Ascher Opler and Nevin K. Hiester. Pp. 111, Figs. 4. Stanford Research Institute and Dow Chemical Company, 1954.

These tables represent the first complete numerical evaluation of the concentration history equation of Professor Henry C. Thomas of Yale University. They should prove valuable in problems in which the performance of fixed-bed ion exchange or adsorption columns is to be studied. They have further application in heat-transfer calculations. The paper bound book includes the discussion of the basic equations, their derivation and use. The mathematical methods used in computation are also described. A limited number of complimentary copies may be obtained on request from either the Public Relations Office, Stanford Research Institute, Stanford, California, or the Research Department, The Dow Chemical Company, Pittsburgh, California.

An Introduction to Mathematical Physics

By R. A. Houstoun. Blackie and Son Ltd., London, 1952.

For many years the earlier versions of this work have been a source of knowledge, inspiration, and delight to many readers wishing to appreciate better the many interrelations between mathematics and physics. This new volume is substantially a moderate revision of the earlier edition with the addition of chapters on quantum mechanics and relativity theory. Even with the added chapters, the subject matter of this book is most appropriately designated as classical mathematical physics. But those for whom the book is primarily intended, the graduate student and advanced undergraduate in physics, will find it a compact and substantial source for extending and strengthening their knowledge of the mathematical substructure of their field. The volume is equally well recommended to students of mathematics who wish to extend their physical knowledge in terms of a language they already understand, and to all others, in classroom or out, who wish to enlarge their knowledge of both mathematics and physics.

Since many an academic generation has passed since the appearance of the first version of this book, a brief summary of subject matter may be in order. Chapter I begins with Newton's law of gravitation, its application to attractions of rods, disks, shells, follows with more general discussion of potential, force fields, Gauss' theorem, Laplace's and Poisson's equation. Chapter II discusses the basic notions of hydrodynamics, equations of continuity, motion, and energy, and their integration, with numerous applications to flows in two and three dimensions. Chapter III presents a discussion of Fourier series, derives the heat conduction equation, and solves heat conduction problems in a variety of coordinate systems and dimensions. Chapter IV deals with wave motion, the derivation of the fundamental equations, and their solutions for vibrating strings, torsional vibrations, sound waves, waves in elastic solids, tidal waves, etc. Chapter V presents electromagnetic theory beginning with the method of images followed by such topics as the electrostatic field, magnetic induction, electromagnetic field, and Hertzian oscillator. Chapter VI discusses the principles of thermodynamics, properties of a perfect gas, the Stefan-Boltzmann law, entropy, and the kinetic theory of gases.

Chapter VII, the first of the new chapters, follows the foregoing chapter with a study of energy distribution and radiative equilibrium. This is followed by the Bohr theory of the hydrogen atom and discussion of electron spin, the Zeeman effect, electron diffraction, and wave mechanics. The final Chapter VIII is devoted to the minimal principles and relativity. The exposition of the principles of Fermat, Maupertius, D'Alembert, and Hamilton leads to a discussion of Lagrange's equations, relativity effects, the Lorentz transformation, the principle of relativity,

and the application of minimal principles to the prediction of relativity effects. The plan of exposition in this last chapter exhibits the material at hand in a most interesting arrangement and brings the book to a close with great periodic effect.

Each chapter is augmented by a set of exercises with which the reader may test his own strength. While at times one regrets that some topics can be discussed only briefly, one is more often surprised that so great an amount of interesting material is contained in a volume having such modest length. It is altogether good to have this book again available.

PAUL E. GUENTHER
Case Institute of Technology

Physics in Chemical Industry

BY R. C. L. BOSWORTH. Pp. 928+xix, Figs. 327. MacMillan and Company, Ltd., London, 1950. Price $12.75.

Dr. Bosworth has done a remarkably good job of covering the major physical principles encountered by industrial chemists and chemical engineers in problems of research, development, and plant practice. The arrangement of the subjects is logical and convenient. The test is divided into four parts with a total of 36 chapters. The first part is entitled Mathematical Introduction and treats vector and tensor quantities, mechanical mathematics, dimensional analysis, and statistical methods.

The second part deals with the properties of matter. All three forms of matter are discussed with approximately equal attention given to gases, liquids, and solids. Both surface and internal phenomena are separately discussed for solids and liquids. In addition, chapters are devoted to atomic theory and the thermodynamics of equilibrium.

The third part treats the movement of matter and energy. This section consisting of 10 chapters is perhaps the best in the book. Types of motion are discussed in a general manner and the phenomenon of diffusion treated specifically. Diffusion is applied to the movement of mass, momentum, energy, and electric charge in separate chapters. Additional chapters are devoted to thermal radiation, transflux phenomena, and combinations of the diffusion of matter and energy.

The final part discusses scientific instruments. The author has presented an excellent treatment of the fundamentals and theoretical considerations pertaining to the extremely broad field of scientific and industrial instrumentation. The chapters are divided according to quantity to be measured such as mass, pressure, viscosity, elasticity, flow, temperature, electrical quantities, light, etc. This arrangement is particularly convenient when the book is used for reference.

The book is very readable, and the subject matter is clearly presented. It appears to be well edited and remarkably free of errors. Perhaps its best application will be its use as a reference. Because of its wide scope, it has not been possible for the author to treat individual subjects in complete detail. Industrial chemists and chemical engineers in the United States may be somewhat handicapped by the fact that a majority of the literature references are from European publications which are frequently not available in many industrial laboratories in this country.

A. L. JONES and WARREN JACKSON, JR.
The Standard Oil Company (Ohio)

Coloured Glasses

BY WOLDEMAR A. WEYL. Pp. 541+xvi, Figs. 116. The Society of Glass Technology, Sheffield, 1951.

This monograph is concerned with a critical survey of the information available in the field of colored glasses. The approach of the book is from the viewpoint of the physical chemist. The analysis is not one of batch formulas, but rather an explanation as to the "why" of different colors. The introduction is concerned with an extended survey of the constitution of the glasses themselves, with a particular reference to the structure of glass. In the second section of the book, different ionic colors are discussed in detail. This section contains the necessary chemical information about compounds and the state of oxidation of coloring elements. The resemblance between solutions and glasses is emphasized throughout this work. The third section is concerned with the fluorescence, thermoluminescence, and solarization of glass. Numerous references as well as a detailed cross index of subjects and authors add to the usefulness of the book.

Reihenentwicklungen in der mathematischen Physik

BY J. LENSE. Pp. 216. Walter deGruyter & Company Berlin, 1953, Third Edition. Price DM 26.

Except for elimination of typographical errors and certain simplifications in proofs the present edition is substantially the same as earlier editions. For those not acquainted with earlier editions it may be remarked that the subject matter includes very thorough yet compact discussions of asymptotic representations, Euler's summation formula, the gamma function and its various representations, the general theory of orthogonal functions with special details for the functions of Laguerre, Hermite, and Tschebyscheff. Later chapters are devoted to Bessel's functions, spherical harmonics, and Lame's functions. The book will be of value as a reference work for students and research workers in science and technology to whom these special functions are of interest.

Gmelin's Handbuch der Anorganischen Chemie. 8th Edition. Verlag Chemie. G.m.b.h. Weinheim/Bergstr. Germany

System No. 3. Sauerstoff (Oxygen)
Part 2. 1952, 218 pages. Price $15.48.

System No. 27. Magnesium
Part A4, 1952, 336 pages. Price $23.81.

System No. 41. Titanium
1951, 481 pages. Price $27.20.

These three volumes are a welcome addition to the encyclopedic and authoritative series of Gmelin reference books. The first volume, dealing with oxygen, covers its distribution, physical, and chemical properties. Oxygen isotopes are treated in a special section. The occurrence, chemistry, and technology of ozone are discussed in detail. A special section of the book is devoted to the distribution of water, the geochemistry of the hydrosphere, and the treatment, distribution, and purification of water.

The second volume, dealing with magnesium, will be of equal importance to scientists and engineers. It covers a wide range of binary and ternary alloys giving extensive data on intermetallic compounds, production processes, casting methods, hardening characteristics, as well as thermic, optical, electric, magnetic, electrochemical, and crystal-structure data. Chemical behavior, corrosion resistance, and surface treatments are described in great detail. The alloy equilibrium diagrams represent the very latest information and are well drawn. The only exception is that of the very important Mg-Zr system, unless the slope of the peritectoid line, which should be horizontal, is an indication that either equilibrium conditions were not reached or that impurities were present in solid solution.

The third volume, on titanium, maintains the exceedingly high standard of the series. Its compass ranges from the occurrence of titanium, through the extraction of the metal to the physical and chemical properties of the element, its alloys, and its compounds. Among the many excellent sections is a comprehensive discussion of the TiC, TiO, TiN phase structures and a detailed account of the properties and crystallographic transformations of $BaTiO_3$. The reader must be wary of lattice parameter data presented in these volumes, since much of it is stated to be in absolute angstroms, while actually the data are in unconverted kX units.

A. TAYLOR
Horizons, Inc.

Elementary Introduction to Molecular Spectra

By Børge Bak. Pp. 125+x, Figs. 35. Interscience Publishers, Inc., New York, 1954. Price $2.90.

The author presents in this book the basic features and experimental possibilities of molecular spectra studies. This book is especially valuable for those people who wish to gain a broad knowledge of this field without recourse to the specialized literature on the subject. The opening chapter concerns itself with the characteristics of spectra in the microwave, the infrared, and the visible and ultraviolet regions and a description of the experimental equipment used in the three regions. Derivations of equations used in spectroscopy are made in the second chapter. This chapter is complete in itself and is included so that the reader who is not acquainted with quantum mechanics will be able to understand the concepts encountered later in the book. The remainder of the book is divided into three chapters, devoted to the three spectral regions mentioned above. Each chapter indicates possibilities for further research and includes a quantitative discussion of the origin of each spectral group in terms of transitions between energy levels and the selection rules. Also included are discussions of such important features as the Stark effect in the microwave region, Raman spectra, qualitative aspects of molecular constitution, and thermodynamic properties. The book contains 17 tables and is rich in footnote references.

Transactions of the Symposium on Fluid Mechanics and Computing

By the American Mathematical Society and the Office of Ordnance Research, U. S. Army. (Editorial Committee: G. Birkhoff, K. O. Friedrichs, T. E. Sterne) Interscience Publishers, Inc., New York, 1954. Price $5.00.

This book contains the contributions of fourteen authorities in the mathematical analysis of the problems of fluid mechanics and in the adaptation of large scale computing machines to the solutions of such problems. One paper presented at the symposium, that of von Neumann, is not included.

Perhaps the clearest picture of the contents of the volume may be given by listing the titles of the papers. They are: (1) Mathematical methods in compressible flow theory, (2) Boundary layer problems in applied mathematics, (3) Fourier synthesis of homogeneous turbulence, (4) One-dimensional anisotropic flows, (5) Approximate methods for computing flow fields, (6) Results and conjectures in the mathematical theory of subsonic and transonic gas flow, (7) The singular solutions and the Cauchy problem for generalized Tricomi equations, (8) Remarks on the theory of partial differential equations of mixed type and applications to the study of transonic flow, (9) Discussion on transonic flow, (10) Some problems solvable on computing machines, (11) Weak solutions of nonlinear hyperbolic equations and their numerical computation, (12) Computation of one-dimensional compressible flows including shocks, (13) The deformation of a thin material shell of nonuniform thickness by a detonation wave, (14) Measurement of spherical shock waves.

The papers cover broad analyses of the mathematical attack on problems of an applied nature as well as detailed and penetrating studies of certain aspects. Critical problems facing the investigator in these fields are kept in the forefront of the discussion.

Physical Similarity and Dimensional Analysis

By W. J. Duncan. Pp. 156+vii. Longmans Green and Company, New York. Price $5.75.

Physical Similarity and Dimensional Analysis is a slender volume which presents clearly and concisely the principles and interrelationships of dimensional analysis and physical similarity. This material is presented in the first sixty pages with simple examples which clarify any vestige of obscurity which may remain after the abstract explanation. The remainder of the book is devoted to the application of dimensional analysis to diverse topics. These applications include: fluid dynamics, heat transfer, electromagnetism, and the use of dimensional analysis in design. The book is well worth a careful reading by any physicist or research engineer whose work involves the analysis of complex engineering problems.

Thermodynamics and Statistical Mechanics

By W. P. Allis and M. A. Herlin, Pp. 239+iii. McGraw-Hill Book Company, Inc., New York, 1952. Price $4.92.

This book is intended as a text for college seniors in physics. The authors assume that the physicist is less interested in chemical equilibrium and the efficiency of heat engines and more interested in understanding the basic principles of thermodynamics and their relation to the properties of matter. To this end some topics usually covered in a course in thermodynamics are omitted in order to provide time in the course for a treatment of statistical mechanics from the viewpoint of Boltzmann and Planck. This combination of thermodynamics with statistical mechanics emphasizes the similarities of the two subjects. After a brief review of related mathematics, chapters discuss the equation of state, the gas laws, the laws of thermodynamics and their immediate consequences, entropy and probability, Maxwell-Boltzmann statistics, equipartition of energy, quantum statistics, and degenerate gases.

Harmonics, Sidebands, and Transients in Communication Engineering

By C. Louis Cuccia. Pp. 465+ix, Figs. 253, McGraw-Hill Book Company, Inc., New York, 1952. Price $9.00.

The aim of this book is to acquaint the student or engineer with the application of the Fourier and Laplace transform methods to network analysis and to problems often encountered in communication engineering. The first few chapters are devoted to a brief treatment of the requisite mathematical tools, the theory of the complex variable, Fourier series and the Fourier integral, and the Laplace transformation. Having developed this mathematical foundation, the author proceeds to apply this approach to linear networks and subsequently to filters, amplifiers, and integrating and differentiating circuits. The latter half of the book is devoted to modulation systems: amplitude modulation, single-tone frequency and phase modulation, and multitone FM and pulse-width modulation. Finite wave trains, wave transmission through linear networks, and traveling waves are also treated. The book closes with a brief discussion of reception in electrical communications which includes the television receiver. The point of view maintained throughout is that of the communications engineer. Many problems and review exercises accompany each chapter.

Signal, Noise and Resolution in Nuclear Counter Amplifiers

By A. B. Gillespie. Pp. 155+xii, Figs. 58. McGraw-Hill Book Company, Inc., New York, 1953. Price $4.50.

This book, by a member of the British Atomic Energy Establishment at Harwell, is the first of a series of monographs on electronics and waves which is being produced under the general editorship of D. W. Fry, also of Harwell.

Mr. Gillespie has produced a very readable discussion of the noise and resolution problems which face those who use particle counters. The approach is essentially theoretical, with no detailed accounts of specific pieces of completed apparatus. A short chapter on the nature of signals from ionization chambers precedes a detailed discussion of the origin and nature of the various sorts of "valve noise," together with means for reducing its effects. The next major section of the book is devoted to signal-to-noise ratio and its relation to circuit parameters. Amplifier sensitivity is discussed in connection with energy measurements, and the book ends with a chapter on proportional and scintillation counters.

The style is informal, with much physical reasoning; the major mathematical steps being outlined in sufficient detail that the nature and limitations of the calculation can be clearly understood. More difficult or tedious matters are removed to one of the numerous appendices at the back of the book. Considerable care went into the preparation of this book, as shown by the frequent cross referencing and the display equations, diagrams, and curves, all of which are designed for easy use by the man who wants to look up some particular point, but does not want to reread the whole chapter. At the front of the book is a table of symbols listed in the order in which they appear, and at the back is a rather interesting list of references for further reading.

The author has succeeded very well in his effort to give a "comprehensive, yet essentially simple treatment of a far from simple subject." The book is a convenient reference source for anyone interested in the design of experiments and equipment for particle counting, and at the same time provides newcomers with an excellent introduction to the field.

A. H. Benade
Case Institute of Technology

Fundamentals of Electronic Motion

By Willis W. Harman. Pp. 319+x, Figs. 257. McGraw-Hill Book Company, Inc., New York, 1953. Price $6.50.

Basically this is an engineering text concerning itself with the analysis of electronic motion under the influence of electric and magnetic fields. In approaching this subject much emphasis is placed upon specific problems related to electron tube operation. The book commences with the study of motion in a static electric field, developing the necessary differential equations of motion and then extending this to the magnetic field case, and finally to combinations of both fields. The problem of negative and positive space charges as encountered in the parallel-plane and cylindrical diode as well as other type tubes is then approached. This is followed by a study of motion in time varying fields. The theory of space charge waves is taken up in reference to the klystron tube, covering the aspects of amplification and oscillation. This topic is continued with a study of the cascade klystron amplifier introducing the analysis of traveling-wave amplification. The linear electron accelerator, which in many ways is similar to the traveling-wave tube, is treated by analogy. The closing two chapters of the book are devoted to magnetrons and relativistic electrodynamics. This book is primarily intended to stimulate an understanding of the mechanisms concerned with electron tube operation. The techniques involved can easily be extended to cope with new problems. The author assumes no previous background in electromagnetic theory or mathematics beyond the calculus.

Short-Wave Radiation Phenomena

By August Hund. Pp. 1382+xiv (in two volumes), Figs. 394. McGraw-Hill Book Company, Inc., New York, 1952. Price $20 for two volumes, not sold separately.

The purpose of this text is to present radiation phenomena with their many applications to radio communication and to guidance and detection. *Short-Wave Radiation Phenomena* is divided into nine large sections and an appendix. The book begins with a numerical, practical discussion of electromagnetic properties and their applications. The fundamentals of electromagnetic theory are introduced later, where the author feels they may be better appreciated. The MKS system of units is used throughout. The first three chapters cover relations of currents and electromagnetic fields, elementary electric and magnetic dipole space fields, and fundamentals of electromagnetic theory. The book proceeds with a treatment of wave propagation characteristics, transmission lines, unobstructed space radiation, radiation in the presence of obstructions, diffraction, and, finally, wave guides and cavities. A comprehensive list of references closes the book. A subject and name index is included at the end of the second volume. The body of the text is quite detailed in its presentation, little information being left to the footnotes and the appendix. The emphasis is kept on the practical and experimental side, and the author strives continually to present his ideas in concrete, physical form.

Electromagnetics

By John D. Kraus. Pp. 604+xiii, Figs. 663. McGraw-Hill Book Company, Inc., New York, 1953. Price $9.00.

This volume presents a comprehensive treatment of the electromagnetic field both in theory and application. Recently developed topics such as transmission lines and wave guides are also treated. It is valuable as a textbook or as a reference for electrical and electronic engineers.

The first part of the book is devoted to a study of the static, electric, and magnetic fields, time changing fields, and Maxwell's equations. All concepts are clearly expanded and explained through the use of diagrams and charts. The units used are the rationalized MKS system. Vector notation is developed where needed throughout the text. The second half of the book is an intermediate study of plane waves in dielectric and conducting media, boundary value problems, transmission lines, wave guides, and antennas. Many practical methods for calculations are included such as the rectangular impedance chart, the Smith impedance chart, conformal transformations, and the field mapping technique developed by A. D. Moore. This book has a bibliography, many illustrations, and problem sets at the end of each topic.

Analysis of Alternating-Current Circuits

By W. A. LePage. Pp. 444+xiii. McGraw-Hill Book Company, Inc., New York, 1952. Price $6.50.

The analytical trend in the training of engineers is reflected in this book. Although most of the content is the classical material for a first course, the precise development of the concepts of circuit theory and the careful use of mathematics are noteworthy. Nodal analysis is given adequate space and a good treatment of Fourier series is given. An appendix on dc network analysis is included.

Musical Engineering

By Harry F. Olson. Pp. 369+vii, Figs. 303, Tables 28. McGraw-Hill Book Company, Inc., New York, 1952. Price $6.50.

This prolifically illustrated book is intended "as a textbook, as a handbook, or as an instruction book for students, teachers, musicians, engineers, laymen and enthusiasts interested in the subjects of speech, music, musical instruments, acoustics, sound reproducers and hearing." An opening chapter introduces semi-quantitatively the elements of acoustics. The concepts of sound velocity, wavelength, frequency, intensity, and impedance are discussed, and the relevant formulas are given brief physical justification. The "physical optics" of sound waves is considered. Chapters follow on musical terminology, scales, and resonators and radiators. A long chapter on the various musical instruments describes their mechanical construction and gives elaborate electrical analogs for many of them. The sound of each instrument is then discussed in the language of Fourier analysis, this being described well enough for the semiqualitative use to which it is put. There are considerable tabular and graphical data presented on such topics as the transient behavior, spectra, power output, and angular distribution of sound from different orchestral instruments. The book closes with chapters on the psychological and physiological properties of music, room acoustics, and on sound reproducing instruments.

Dislocations in Crystals

By W. T. Read, Jr. Pp. 228+xvii. McGraw-Hill Book Company, Inc., New York, 1953. Price $5.00.

The field to which this book is devoted is a very new one which was first conceived only some twenty years ago and has developed most rapidly over the past five or so years. In his presentation Dr. Read has succeeded in conveying a sense of an expanding subject, in which many of the ideas are necessarily tentative, without neglecting the established achievements. At the same time he has provided an excellent introduction to the basic notions of dislocation theory suited to a reader with only a fairly elementary background in mathematics, elasticity, and crystallography. In achieving these somewhat disparate objectives he has been greatly assisted by a style which combines the virtues of lucidity and informality. The treatment of forces on dislocations—which includes an introduction to the notion of generalized forces—is unfortunately not done with the same clarity that characterizes the remainder of the work.

The book is divided into two parts. In the first, the nature of a dislocation is explained in some detail and the mechanical properties of dislocations are discussed. In this development the ideas of edge and screw dislocations are first introduced on essentially a pictorial basis via the notion of slip; and the concepts thus developed serve as a starting point for the introduction of the notion of the Burgers vector, of the more general dislocation lines, and of partial dislocations in noncubic crystals. The statics of dislocations are discussed and expressions are derived for the force exerted on a dislocation by external stress fields and by the interaction with another dislocation, the latter in terms of the stress distribution produced by a dislocation as calculated according to elasticity theory. The expression for the stress field is also employed to estimate the stored energy associated with a dislocation. The author deliberately avoids any discussion of details of the slip process in actual crystals because he considers this as not yet established, but he does present the newer concepts of the mechanism of the production of dislocations in the course of the deformation.

The second part of the book is devoted to a presentation of the two applications of dislocation theory which Dr. Read considers best established, namely, the explanation of the mechanism of crystal growth and the calculation of the dependence of grain boundary energy on the angle between grains. In each case he develops the underlying theory and shows how its consequences are in striking agreement with experimental results. The two topics are nicely complementary in that the discussion of crystal growth can be given in a rather qualitative fashion and leads to something very close to pictorial proof of the existence of dislocations while the grain boundary calculations are quite quantitative and have been verified experimentally in a satisfactory numerical fashion.

In conclusion, this book can be highly recommended as an introduction to dislocation theory for physicists or engineers unfamiliar with the field and as a fairly complete summary for those already acquainted with the basic notions. It might have been helpful, in view of the sparsity of quantitative experimental data available, if mention had been made of the results of stored energy and resistivity change measurements made on cold-worked metals.

Gerhart Groetzinger
NACA Lewis Flight Propulsion Laboratory

Principles of Mathematical Analysis

By Walter Rudin. Pp. 227+ix. McGraw-Hill Book Company, Inc., New York, 1953. Price $5.00.

The author first considers the real number system, the algebra of sets, and elements of topology. Continuity and differentiability of real functions both of a single and of several real variables are discussed. Numerical sequences and series, followed by uniform convergence, integrability, and differentiability of sequences and series of functions, are treated in detail with applications related to the elementary functions and function representation by series. The integrals of Riemann, Stieltjes, and Lebesgue are developed in adequate detail for a first encounter. The book serves very well as a text for a year course offered to junior and senior level students, and should also be excellent for individual study.

Water

By Sir Cyril S. Fox. Pp. 148+xxvii, Figs. 4, Plates 25. Philosophical Library, New York, 1952. Price $8.75.

This is the first of a series of books in preparation by the Technical Press, Ltd., on the various aspects of water supply. It is a nontechnical account written in three parts: the natural history of water, the work done by water, and the utilization of water. Part I describes the constitution, distribution, and circulation of water. A comparison is made of sea water, the fresh waters of lakes and rivers, ice caps, and ground water. Discussion of the hydrologic cycle includes energy requirements, evaporation, precipitation, runoff, percolation weathering, and virginal water from volcanic sources. Part II is a brief resumé of the erosional activity of water and ice on the land surface, of the geological activity of ground water, and of the deposition of sediments. Part III deals with the engineering aspects of water supply, storage, contamination, and power. Much statistical information is incorporated in this small book. The pictorial examples are largely English and American.

Radioisotopes, Industrial Applications

By G. H. Guest. Pp. 185, Figs. 65. Pitman Publishing Corporation, New York, 1951. Price $4.50.

Radioisotopes, Industrial Applications, presents a cross section of industrial uses of radioisotopes for the layman, technician, and industrial scientist. Sufficient basic atomic and nuclear background is presented in the first three chapters to acquaint the reader with the language and theory employed in the use of isotopes. The use of radioactive tracers in several industries is then developed, as is the use of isotopes for radiographic work. Important to those interested in using radioisotopes are discussions of laboratory facilities needed and precautions necessary for safe handling of isotopes. Lists of available isotopes and their emanations are included in the appendix. Generous use of illustrations adds to the inherent clarity of the text, while a good list of references at the end of each chapter enables the reader to find more specific information in his particular field of interest.

Radio and Radar Technique

By A. T. Starr. Pp. 812+xviii, Figs. 926. Pitman Publishing Corporation, New York, 1953. Price $15.00.

The author, Dr. Starr, has attempted in this new volume to compile all the essential elements of the rapidly expanding field of radio and radar. Although the book is comprehensive in all subjects related to radio and radar, Dr. Starr has placed emphasis on the time dependence of system properties, microwave technique, noise phenomena such as shot and thermal noise, and the fundamental behavior of electronic tubes. In order that the main body of the text be clear and more readable, Dr. Starr has placed the more involved theoretical verifications in an extensive appendix. In addition a large set of useful references is included at the end of each chapter.

This book should be an exceedingly useful reference for designers, electrical engineers, and physicists of the graduate and post-graduate level. The main emphasis of the book is on physical interpetation, analysis, and techniques, and not on specific application. It is for this reason the book supplies a wealth of material for all types of electronic application. This book is not designed for the beginner in the field of electronics but for the experienced worker in need of a complete and useful reference.

Electronics—Principles and Applications

By Ralph R. Wright. Pp. 388+x, Figs. 314. Ronald Press Company, New York, 1950. Price $5.50.

This book has been designed to serve as a textbook for an introductory course in electronics primarily for the nonelectrical engineering student. Only basic mathematical equations have been included in the text and most of them have not been derived. In a few places simple calculus has been used to analyze certain phenomena that could not have been treated by any other means. Starting with the basic electronic principles of electrons and their behavior in vacuum and gases this book discusses different types of electron emission, the different types of high-vacuum and gas-filled tubes that conduct the emission currents, and the functions and applications of these tubes. A review chapter of basic dc and ac circuits is included. The largest portion of the book is devoted to a detailed discussion of the five basic functions of the vacuum tube: amplification, oscillation, modulation, detection, and rectification. In connection with these functions the characteristic circuits for each of the functions are discussed.

Some special electronic devices and circuits are discussed in the last part of the book. These include the cathode-ray tube, various light-sensitive tubes, the production and utilization of x-rays, high-frequency heating, and basic control circuits.

The Design of Switching Circuits

By W. Keister, A. E. Ritchie and S. H. Washburn. Pp. 556+xviii. D. Van Nostrand Company, Inc., New York, 1951. Price $8.00.

This text book is a result of the growing interest and importance in the designing of machines which automatically carry out complex sequences of instructions and logical operations. The magnitude and difficulty of the problems which arise are beyond the cut-and-try stage. They require specialized techniques, not only of electrical engineering but also of symbolic logic. The text was used in a one-semester graduate course for electrical engineers, and has for prerequisites, in the words of the authors, "a logical mind and a knowledge of elementary circuit theory." The first three chapters are of an introductory nature, dealing with the fundamental concepts of control and the structure of relays, switches, and circuits. The next five chapters contain an exposition based on Shannon's work of parts of Boolean Algebra and the Calculus of Propositions applied to relay and switching circuits. The ninth chapter concerns switch control circuits and the tenth chapter discusses the characteristics of electron tubes and semiconductors as switching elements. The next eleven chapters treat basic "unifunctional" circuits such as circuits for counting, translating, selecting, connecting, lockout, hunting and finding, timing, pulse generation, checking, registration, and calculating. The remaining three chapters are concerned with multifunctional circuit design.

The emphasis is on design principles. Useful diagrams and many problems are included. The text can well form a foundation for a one- or two-semester course in relay and switching circuits.

Circuit Theory of Electron Devices

By E. Milton Boone. Pp. 483+vii, Figs. 333, Tables 17. John Wiley and Sons, Inc., New York, 1953. Price $8.50.

In this book the author has emphasized circuit theory involved with the use of such devices rather than the physical analysis of the internal complexities of individual components. With some exceptions the primary theoretical emphasis is on the properties of electronic devices that can be measured at the available terminals of such devices. Alternating equivalent circuits are introduced early in the book and are used very effectively throughout. The author generally uses the four-terminal networks representation of circuit elements. This is also true in the last chapter, which is concerned with the transistor theory.

The book has been constructed from notes compiled by Mr. Boone while teaching electronic courses at The Ohio State University. The text is designed for the student who has had approximately two years of college physics (including circuit theory) and mathematics through differential and integral calculus. It is not intended as a beginning course in circuit theory. There is material in the text for a two-semester course. Each chapter contains a large number of representative problems at the end and well explained examples throughout.

The Thermodynamics of the Steady State

By K. G. Denbigh. John Wiley and Sons, Inc., New York, 1951. Price $1.75.

This is a clearly written survey of the thermodynamics of irreversible processes. After a historical introduction, the thermo-pressure effect is treated in the pre-Onsager way and the different implications are discussed. Chapter III is a condensed treatment of Onsager's theory. The exclusion of the "triangle reaction" is shown and the assumption about the regression of fluctuations is mentioned.

Chapter IV discusses whether the entropy can be defined in a nonequilibrium system. The entropy production is calculated in several one-component models, the "continuity equation" of entropy is demonstrated in the case of simultaneous heat flow and diffusion, and finally the results are gathered together in general expressions. In the last section of the chapter a rather formal argument is given why the quantity $T(\partial S/\partial T)$ acts as a potential. In the "applications of the theory," Chapter V, the thermo-pressure effect is considered again, now on the basis of Onsager's theory, together with a treatment of the thermal diffusion. At the end some remarks are made about the difficult field of the application to biology. The concluding chapter is a valuable discussion about the relation of Thomson's hypothesis to the theory of Onsager.

This little book serves its goal very well. There are abundant references to the literature and the reader does not lose his way in unnecessarily complicated notation.

Mechanics of Vibrations

By H. M. Hansen and P. F. Chenea. Pp. 417+xiii. John Wiley and Sons, Inc., New York, 1952. Price $8.00.

The emphasis in this textbook for advanced undergraduate or beginning graduate engineering students is on underlying principles rather then specific applications. The prerequisites are elementary dynamics and the usual undergraduate engineering mathematics. The book is divided into three parts. The first part concerns systems with one degree of freedom, and energy methods are utilized. The second part treats systems with several degrees of freedom and includes Lagrange's equations. A chapter on the mobility methods and the use of the complex impedance or frequency response is given. In addition the solution of the frequency equation, by the methods of Holzer and Graeffe, is discussed. In the third part, distributed-parameter systems are treated by separation of variables. Transient vibrations in lumped-constant systems are introduced and a superposition integral formula is established without the use of the Laplace transform. Nonlinear vibrations are also discussed. A large number of problems is included.

Designing by Photoelasticity

By R. B. Heywood. Pp. 414+xvi, Figs. 178. Chapman and Hall, Ltd., London, 1952. Price 65s.

The modern designer of industrial parts will find this book on photoelastic techniques valuable. It is known that local "stress concentrations" have a large effect on fatigue or failure of mechanical parts. The purpose of this book is, then, to present a practical method of stress analysis based upon elastic material models. The method used is that of photoelasticity and depends on the effect of stressed transparent materials under polarized light. A variation in the magnitude of the principal stresses at points in a model will cause varying degrees of interference,

causing "fringe" effects, from which the magnitude of the stresses can be obtained by applying suitable equations.

Heywood discusses in part I the principles involved in photoelastic interpretation, as well as the construction and materials used in the models under examination. Three-dimensional analysis of stresses in a complicated part is treated by the remarkable "freezing" method of stress analysis in which the fringes are locked or frozen into the model as a result of heat treatment. Part II concerns itself with stress concentration in notches, screw threads, bolts, nuts, and holes. Much of the data relevant to these design problems have been correlated and presented in graphical form for ease of reference. The final chapters discuss improvement of designs and establishment of criteria for failure. An extensive, well classified list of references is given so that one may easily find additional information on any subject matter in the text.

Electric Control Systems

By R. W. Jones. Pp. 511+xiv. John Wiley and Sons. Inc., New York, 1953, 3rd edition. Price $7.75.

This text is intended for advanced undergraduate electrical engineering students. It begins with a discussion of ac and dc motor characteristics. This is followed by a considerable amount of material on relay and switching circuits covering both electromagnetic and electronic relays and switches as well as Boolean Algebra and its application to switching circuit analysis and synthesis. Motor acceleration, speed control, braking, and protection are treated, and a chapter is included on feedback control systems. Power amplifiers, including the magnetic amplifier, are also considered. The author has emphasized the integration of the subjects of circuits, electrical machines, and electronics. There are many problems and a good bibliography is given at the end of each chapter.

Principles of Geochemistry

By Brian Mason. Pp. 276+vii, Figs. 42, Tables 39. John Wiley and Sons, Inc., New York, 1952. Price $5.00.

This volume is a well organized presentation of the geochemical principles underlying the evolution of the earth, supported by pertinent experimental and geological data. Emphasis is "on interpretation rather than description and on what is yet to be learned as well as what is already known." The author assumes that the reader has a basic knowledge of geology, chemistry, and physics, and, although the book is designed for geology students, it should also be a valuable reference for physicists and chemists. The first part of the book deals with the earth as a planet, its relationship to the solar system and universe, and also its internal structure and composition. A study of the relative abundance of the elements and isotopes in the earth and in the universe is the basis for a reconstruction of the earth's pre-geologic history. Chapter 4, the background for the remainder of the book, introduces some principles of thermodynamics and crystal chemistry, especially the chemistry of the solid state. The remaining portion of the book discusses magnetism and igneous rocks, sedimentation and sedimentary rocks, the hydrosphere, the atmosphere, the biosphere, and metamorphism and metamorphic rocks. Other questions discussed in this part of the book are the origin and evolution of the ocean and atmosphere and the role of organisms in the concentration and deposition of individual elements. A final chapter is devoted to a brief summary and synthesis in terms of the geochemical cycle. Excellent selected bibliographies appear at the end of each chapter.

Essentials of Microwaves

By Robert B. Muchmore. Pp. 236+vii, Figs. 202. John Wiley and Sons, Inc., New York, and Chapman and Hall, Ltd., London, 1952. Price $4.50.

This book is a survey of the field of microwaves. Starting with the fundamental laws and principles of electricity and magnetism this book shows how by combining them and extending them they explain all microwave phenomena. Various types of wave guides, cavity resonators, filters, and microwave antennas are explained. The rest of the book deals with electronic devices that use the principles of microwaves in their operation. These include grid control tubes, klystrons, magnetrons, microwave radio systems and relays, and radar.

The final chapters discuss microwave measurements and their application in physical research. This includes the application of microwave principles to the linear accelerator, microwave spectroscopy, and the "atomic clock."

In order to simplify the book very little mathematics is used in explaining microwave phenomena and no attempt has been made to develop any of the formulas. However, in order to give the mathematical expression some physical meaning, detailed explanation in words is given for each one of the mathematical equations.

Measurement Techniques in Mechanical Engineering

By R. J. Sweeney. Pp. 309+x, Figs. 132. John Wiley and Sons, Inc., New York, and Chapman and Hall, Ltd., London, 1953. Price $5.50.

This book is a collection of information about modern measurement techniques used in mechanical engineering. It discusses thoroughly the methods of testing power equipment. Among these methods are electrical and mechanical measurements, chemical analysis, and automatic controls. The author stresses the principles upon which the instruments have been designed. The many difficulties encountered in obtaining correct measurements of physical quantities with the instruments available are discussed at considerable length. Discussion of methods of calibration have been included as well as many of the standard points that are necessary for such calibration. In discussing automatic control devices, the author deals with measuring instruments as signaling devices to the automatic controllers. This book has been designed to serve either as a laboratory textbook for the mechanical engineering student or as a reference book for the practicing mechanical engineer. In either case some knowledge of physics, calculus, and thermodynamics is necessary in order to have a complete understanding of the text.

The Foundations of Mathematics

By Raymond L. Wilder. Pp. 305+xiv. John Wiley and Sons, Inc., New York, 1952. Price $5.75.

To the nonmathematician it may come as a surprise that mathematics, reputedly the most exact of sciences, should undergo questioning and examining at the hands of its own practitioners as to what ultimately it is all about and what is its precise nature. For example, is it a study of actual and intrinsic properties—say, of space, in the case of geometry—or is it a body of doctrine developed deductively from a number of assumed (unproved) propositions relating to a number of undefined terms? The non-Euclidean geometries of Bolyai, Gauss, and Riemann in some ways contradict each other and contradict the traditional geometry of Euclid, and yet are all logically consistent in themselves. This would give pause to one who might be inclined to view the mathematician as the scientist who aims to penetrate ever deeper into certain immutable laws, laws expressed in terms of numbers, figures, or other mathematical entities. Another example is the study of infinite sets by nineteenth century analysts which revealed the need for clarifying such apparently unambiguous ideas as to what is meant by "equal to" or "greater than." In short, the richer the accumulation of mathematical knowledge becomes, the greater the urge to examine the nature of that knowledge, its validity, and its basic concepts. The book under review provides an orderly study of the problems involved in the logic of mathematics and the way these problems have been treated, from their first inception down to our own day.

Other Books Received

The Physics of Viruses. ERNEST C. POLLARD. Pp. 230+xi. Academic Press, Inc., New York, 1953. Price $5.50.

Sir James Jeans. E. A. MILNE. Pp. 176+xvi. Cambridge University Press, New York, 1953. Price $4.00.

Lectures on Cauchy's Problem. JACQUES HADAMARD. Pp. 316+v, Dover Publications, New York, 1952. Price $1.70 paperbound, $3.50 clothbound.

On the Sensations of Tone. HERMANN L. F. HELMHOLTZ. Pp. 576+xix. Dover Publications, New York, 1954. Price $4.95.

Elements of the Theory of Functions. KONRAD KNOPP, translated by FREDERICK BAGEMIHL. Pp. 140, Figs. 23. Dover Publications, New York, 1952. Price $2.25 clothbound, $1.25 paperbound.

Selected Papers on Noise and Stochastic Processes. NELSON WAX, Editor. Pp. 337. Dover Publications, New York. Price $2.00.

The Design and Use of Instruments and Accurate Mechanism Underlying Principles. T. N. WHITEHEAD. Pp. 283+xiv. Dover Publications, New York, 1954. Price $1.95.

A History of Mechanical Inventions. ABBOTT PAYSON USHER. Pp. 450+xi, Illustrations 159. Harvard University Press, Cambridge, 1954. Price $9.00.

Gas Dynamics of Thin Bodies. F. I. FRANKL AND E. A. KARPOVICH. Pp. 175+viii, Illustrations 33. Interscience Publishers, Inc., New York, 1953. Price $5.75.

Analytical Geometry of Three Dimensions. WILLIAM H. MCREA. Pp. 144+vii, Figs. 12. Interscience Publishers, Inc., New York, 1953. Price $1.25.

Linear Equations in Applied Mechanics. H. F. P. PURDY. Pp. 240+xiv. Interscience Publishers, Inc., New York, 1953. Price $3.50.

Flames, Their Structure, Radiation and Temperature. A. G. GAYDON AND H. G. WOLFHARD. Pp. 340+xi. Macmillan Company, New York, 1954. Price $11.00.

Analysis of Deformation. Volume I. KEITH SWAINGER. Pp. 285+xix. Chapman and Hall, Ltd., London, 1954. Price $12.75.

Millimicrosecond Pulse Techniques. I. A. D. LEWIS AND F. H. WELLS. Pp. 310+xiv. McGraw-Hill Book Company, Inc., New York, 1954. Price $7.50

Analog Methods in Computation and Simulation. WALTER W. SOROKA. Pp. 390+xii. McGraw-Hill Book Company, Inc., New York, 1954. Price $7.50.

Calculus. C. R. WYLIE, JR. Pp. 565+v. McGraw-Hill Book Company, Inc., New York, 1953. Price $6.00.

Essays in Science. ALBERT EINSTEIN. Pp. 114+xi. Philosophical Library, Inc., New York. Price $2.75.

The Composition and Assaying of Minerals. J. S. REMINGTON AND W. FRANCIS. Pp. 128+viii. Philosophical Library, Inc., New York, 1953. Price $5.50.

Elements of Statistical Mechanics. D. TER HAAR. Pp. 468 +xix. Rinehart and Company, Inc., New York, 1954. Price $8.50.

The Science Book of Space Travel. HAROLD LELAND GOODWIN. Pp. 213+vii. Franklin Watts, Inc., New York, 1954. Price $2.95.

Theoretical Petrology. A textbook on the origin and the evolution of rocks. TOM F. W. BARTH. Pp. 387+vii. Figs. 146. John Wiley and Sons, Inc., New York, 1952. Price $6.50.

Alternating Current Machines. Third Edition. PUCHSTEIN, LLOYD, AND CONRAD. Pp. 721+xii, Illustrations 422. John Wiley and Sons, Inc., New York, 1954. Price $8.50.

Introduction to the Theory of Functions of a Complex Variable. W. J. THRON. Pp. 230+x. John Wiley and Sons, Inc., New York, 1953. Price $6.50.

Gmelin's Handbook of Inorganic Chemistry, Boron. System No. 13, Supplement Volume. Edited by the Gmelin Institute under the direction of E. H. E PIETSCH, VII. Pp. 253, graphs 28. D. R. Stein, New York, 1954. Price $34.80.

Gmelin's Handbook of Inorganic Chemistry. Gold. System No. 62, Part 2. Edited by the Gmelin Institute under the direction of E. H. E. PIETSCH. V, Pp. 306, Graphs 20. D. R. Stein, New York, 1954. Price $40.32.

Gmelin's Handbook of Inorganic Chemistry. Gold. System No. 62, Part 3. Edited by the Gmelin Institute under the direction of E. H. E. PIETSCH. XXI, Pp. 558, Graphs 201. D. R. Stein, New York, 1954. Price $74.88.

Gmelin's Handbook of Inorganic Chemistry. Selenium. System No. 10, Part A, Section 3. Edited by the Gmelin Institute under the direction of E. H. E. PIETSCH. XVII, Pp. 184, Graphs 158. D. R. Stein, New York, 1953. Price $26.64.

Scientific and Technical Papers. SEINEN YOKOTA. Pp. 206 +xx. Yokota Memorial Committee, University of Tokyo, Tokyo, 1954.

Bibliography of the Submarine, 1557 to 1953. Pp. 261+xiii. National Research Council, Washington, D. C., 1954.

Rotating Electrical Machinery. Pp. 256, illustrated. Crow Electri-Craft Corporation, division of Universal Scientific Company, Vincennes, Indiana, 1954. Price $3.50.

Advanced Calculus. C. A. STEWART. Pp. 523+xviii, Figs. 166. British Book Centre, Inc., New York, 1951. Price $5.50.

Cover Photograph

A millimeter wave backward-wave oscillator, built at Stanford University. The tube, which is shown together with a crystal detector to measure its output, covers the wavelength range, 4.5 to 6 mm. The internal structure of the tube consists of a 0.025 in. diameter tungsten helix wound with 0.002 in. by 0.005 in. tape. The helix is supported by quartz knife edges and is flooded internally with an electron beam of 4.0 ma. The frequency of oscillation is determined entirely by the accelerating voltage which is tuned from 2400 to 850 volts to cover the range. The output of the device is taken from the helix by means of a transition from helix to waveguide inside the glass envelope. This waveguide then meets the inside of the glass at an angle. A second piece of waveguide is placed outside the vacuum envelope at the same angle to continue the transition. Coupling loss is about 50 percent. The device requires an axial magnetic field of 2000 gauss for beam focusing and is believed to deliver more than one milliwatt over the entire range.

This photograph and explanation were supplied by Professor D. A. Watkins of Stanford University.

PROGRAM

Proceedings of the Electron Microscope Society of America

The annual meeting of the Electron Microscope Society of America was held at Moraine-on-the-Lake Hotel, Highland Park, Illinois, on October 14, 15, and 16, 1954. Titles and abstracts of the papers are presented below.

Preface. R. G. PICARD

Session A

Contributed Papers on General Subjects, Instrumentation, and Techniques

CO-CHAIRMEN: THOMAS F. ANDERSON, *The Johnson Foundation, University of Pennsylvania Hospital, Philadelphia 4, Pennsylvania.*

S. G. ELLIS, *Radio Corporation of America, RCA Laboratories Division, Princeton, New Jersey.*

General

A1. Report on the *International Conference on Electron Microscopy*. THOMAS F. ANDERSON, *an Official Representative of the EMSA* (address above).—This "International Conference on Electron Microscopy" was held in London, England, from July 15 to 21, 1954.

Instrumentation and Techniques

A2. The Optical System of the RCA EMU-3A Electron Microscope. J. H. REISNER, *Scientific Instruments Engineering, Electronic Products, Radio Corporation of America, Camden, New Jersey.*—Without fundamentally changing the optical system of the EMU-2 Electron Microscope, modifications have been incorporated in it to provide a new optical system with better aperturing, less distortion, and simplified adjustment. The illuminating system provides complete adjustment through one mechanical gun transverse motion and two magnetic deflection (tilt) systems. The deflection magnets precede and follow the condenser lens and are fixed with the condenser in a single rigid assembly. Electrostatic compensation means are provided in the objective lens gap, while the objective contrast aperture has been placed at the rear focal plane of the objective. This aperture is retractable and centerable from controls outside the vacuum enclosure and may be manipulated while the instrument is in operation. A single intermediate lens is used to cover the whole range of magnification, acting as a reducing lens below 8000 times and as a magnifying lens at higher magnifications. Lens distortions at low magnification have been minimized by balancing the barrel distortion of the intermediate lens against the pincushion distortion from the projector lens.

A3. A Medium Power 75-kv Electron Microscope of Simplified Construction. A. C. VAN DORSTEN, *Philips Research Laboratories, Eindhoven, Holland.*—The EM 75 is a medium power electron microscope capable of resolving 100 angstrom units or better with a useful photographic enlargement of up to 50 000×. The unit employs a fully adjustable lens system with its main characteristics being a very short focal objective lens, a magnetic shunt type projector lens, and a variable accelerating potential of 20 to 75 kv.

A4. A Film Camera for the RCA Type EMU Electron Microscope. H. HALMA, *RCA Laboratories Division, Princeton, New Jersey.*—This film camera is substituted in place of the left-hand viewing chamber window. No instrument modifications are required. Thirty-five-millimeter unperforated film is used in a standard Leica type cassette. Thirty-five 32-×42-mm exposures can be taken per loading. The unit has a separate fluorescent screen and is thus completely independent of the standard EMU plate camera and viewing screen. Provision is made to prevent double exposures.

A5. A Strong-Focusing Electron Lens. BENJAMIN M. SIEGEL,* *Department of Engineering Physics,* AND ELIAS REISMAN, *Department of Physics, Cornell University, Ithaca, New York.*—The field of a quadrupole magnet with hyperbolic pole faces will cause an electron beam to converge in one dimension and diverge in the other.[1] By using two section, rotated 90° to one another and with appropriate parameters, the cardinal points can be made independent of angle. A convergent lens giving a true Gaussian image is obtained. The spherical aberration coefficient depending on third-order terms can be adjusted by introducing a third-order correction in the magnetic field to give positive, negative, or vanishingly small values. Such a lens is being constructed in these laboratories to be used in combination with an axially symmetric lens. This should give an objective lens for the electron microscope with corrected third-order spherical aberration.

* Probable speaker.

[1] Courrant, Livingston, and Snyder, Phys. Rev. **88**, 1190 (1952).

A6. Operating Considerations in the Design of the Electron Microscope. S. M. ZOLLERS AND A. A. LITWAK, *Scientific Instruments Engineering, Electronic Products, Radio Corporation of America, Camden, New Jersey.*—In the light of many man years of electron microscope operation and extensive findings in the field of "Human Engineering," arbitrary choice is being replaced by a studied determination of such engineer-

ing particulars as position of controls, viewing angles, dimensions, illumination, and automation of functions. Less arbitrary, but still controversial, is the choice of magnification range and the use of the "step" system or the "continuous" range of magnifications. A discussion of factors influencing such engineering choices will be given. Examples of automation in photographic systems and valving systems will be described. Advantages of the step system of magnification selection will be considered.

A7. Recent Advances in Instrumentation for the Philips EM 100 Electron Microscope. T. P. TURNBULL, *North American Philips Company, Inc., Mt. Vernon, New York.*—Presentation of a new high resolution objective lens for the Philips EM 100 Electron Microscope and other accessories of recent development.

A8. A Model Field for Electrostatic Electron Lenses. W. GLASER, *Farrand Optical Company, Inc., New York, New York.*—To know the general relations between the optical properties of electrostatic electron lenses, there is need to have an image forming field typical for electrostatic lenses of the electron microscope and suitable for rigorous calculation of its optical properties. The axial potential distribution

$$\Phi(z) = U + \frac{U_L}{[1+(z/a)^2]}$$

is a model field which has the required typical bell-shape of electrostatic lens fields. Fortunately, the general equations of electron motion in this field can be integrated in a rigorous way. Together with P. Schiske, we have explicitly carried out these calculations. The Gaussian electron trajectories and the optical constants, the chromatic and spherical aberration, and the other image aberrations of the third order have been determined. Further, the general electron trajectories of any axial distance could be calculated, and an application was given to the dispersion of the velocity analyzer. Fitting the foregoing bell-shaped field to empirical lens fields, we can use the developed formulas for investigation of electrostatic electron lenses.

A9. Extensible Area Specimen Holder for RCA-EMU Models Electron Microscope.[1] RUBIN BORASKY, *Biology Section, Radiological Sciences Department, General Electric Company, Richland, Washington.*—The area of an electron microscope specimen grid that can be surveyed in an RCA-EMU electron microscope with the conventional stage is limited to about 0.35 square millimeters. This limitation has been overcome by designing and fabricating a specimen holder with a movable specimen holding component controlled by a mechanical stage. With the extensible area specimen holder it is possible to survey the entire area of the specimen grid. The application and advantages of the extensible area specimen holder will be discussed.

[1] This paper is based on work performed under Contract No. W-31-109-Eng-52 for the U. S. Atomic Energy Commission.

A10. On the Effects of Hysteresis on Magnification. H. FROULA* AND E. S. C. BOWLER, *Department of Engineering, University of California, Los Angeles 24, California.*—For each of several magnification settings, different hysteretic conditions were established in the projector lens of an RCA-EMU electron microscope. From micrographs prepared under these various conditions, a study was made of effects of hysteresis on magnification.

A11. Some New Applications of the Magnetic Lens X-Ray Microscope. W. C. NIXON, *Cavendish Laboratory, Cambridge, England.*—The x-ray shadow microscope with magnetic lenses has been used at low magnification to obtain stereographs of a relatively thick insect specimen without dissection and possible damage of the interesting region. Metallurgical results have shown improved resolution using a good contrast specimen such as aluminum–5 percent tin where the two constituents have widely different atomic numbers. Brass and bronze with much poorer inherent contrast have also shown structure at 1000× magnification. A comparison of resolution is made with the ultraviolet microscope, and the magnetic lens x-ray microscope approaches this resolution. This high-intensity x-ray source has been used to obtain x-ray diffraction patterns in one-tenth the time when using a normal x-ray tube of much lower specific loading.

Session A (*continued*)

Contributed Papers on General Subjects, Instrumentation, and Techniques

CO-CHAIRMEN: R. G. PICARD, *Radio Corporation of America, RCA Victor Division, Camden, New Jersey.*
ROBLEY C. WILLIAMS, *Virus Laboratory, University of California, Berkeley, California.*

Instrumentation and Techniques (continued)

A12. X-Ray Microscope Operation and Inherent Properties. STERLING P. NEWBERRY, *General Engineering Laboratory, General Electric Company, Schenectady, New York.*—A critical review is given of the operation and properties of the x-ray microscope, pointing out what specimens may be photographed and what structures one may hope to reveal. The interdependence of wavelength, contrast, resolution, and specimen thickness will be discussed.

A13. A New Shadow X-Ray Microscope. SELBY E. SUMMERS, *General Engineering Laboratory, General Electric Company, Schenectady, New York.*—The development progress on the shadow x-ray microscope will be discussed. The instrument employs electrostatic optics with a biased electron gun. Resolution is better than one micron and stability sufficient for one-hour exposures.

A14. Specimen Techniques for Use with the X-Ray Shadow Microscope. JAMES F. NORTON AND STERLING P. NEWBERRY, *General Engineering Laboratory, General Electric Company, Schenectady, New York.*—Development has continued in the use of the x-ray microscope for biological sections. By using lower energy x-rays, contrast is increased in certain specimens. Latest results will be shown. The conditions for optimum thickness of specimens to yield greatest amount of information will be described. Stereo techniques give additional information and will be described.

A15. The Practical Attainment of High Resolving Power. M. E. HAINE AND T. MULVEY, *Research Laboratory, Associated Electrical Industries, Limited, Aldermaston Court, Aldermaston, Berkshire, England.*—The use of the Fresnel edge diffraction fringe for measuring astigmatism and other instrumental defects has been analyzed, and its use in assisting the attainment of resolving powers in the region 3–8 A.U. investigated. These methods allow a regular attainment of resolving powers between 5–10 A.U. A definition for instrumental resolving power, based on the edge fringe, is proposed.

A16. A Survey of X-Radiation Dosage from the EMU with Special Ionization Chambers. L. E. PREUSS* AND JOHN H. L. WATSON, *Edsel B. Ford Institute for Medical Research, Detroit 2, Michigan.*—Earlier reports[1] of the x-ray dosage from the electron microscope have largely ignored the errors which may be interjected by detector energy response and geometry conditions. In light of recent work by Cogan, Rugh,[2] and others on the eye's radiation sensitivity, special, small ionization chambers were designed for an accurate assay of the radiation flux by obviating the two errors mentioned. The chambers were read with an altered quartz string electrometer using null method calibration. Dosages were first determined for a nonroutine operation and these data correlated with dosage change found for other operation modes. Roentgen values in excess of maximum tolerable *total body radiation* were found, being of the order of 2×10^2 mr/hr for special operating conditions. Although safe for most normal operation, the instrument has potential for increase to high dosage levels. Values from these chambers are in significant difference to earlier data. (15 min.)

[1] L. B. Silvermann *et al.*, Science **110**, 376 (1949); M. L. Watson, Biochim et Biophys. Acta **10**, 349 (1953); and J. H. L. Watson and L. E. Preuss, Science **112**, 407 (1950).
[2] R. Rugh, University of Michigan Biological Symposium (July, 1953); D. G. Cogan *et al.*, Arch. Ophthalmol. (Chicago) **50**, 597 (1953).

A17. An Electron Microscope Study of Sodium Chloride Particles as Used in Aerosol Generation. JAMES P. LODGE AND BARBARA J. TUFTS,* *Department of Meteorology, University of Chicago, Chicago, Illinois.*—The effects of temperature, moisture, and filament age on sodium chloride particles evaporated from the hot-wire source used in the LaMer generator were studied with the RCA EMU-2E electron microscope. The size appears to vary with temperature and filament age, while concentration seems to be a function of temperature. The shape of the sodium chloride crystals is related to the amount of moisture present. Model equations are given which show the trend of events in any apparatus similar to the one described.

A18. Electron Microscopy of Monodisperse Latexes. E. B. BRADFORD AND J. W. VANDERHOFF, *Physical Research Laboratory, The Dow Chemical Company, Midland, Michigan.*—Monodisperse polystyrene and polyvinyltoluene latexes with particle-diameters ranging from 0.1 to 1.2 microns have been prepared. The particle diameters of these latexes have been determined by electron microscopy using two techniques: 1. Measurement of the individual particles dispersed on a collodion membrane. 2. Measurement of the individual particles dispersed on replicas of a 30 000-line/inch diffraction grating. The average particle diameter has been expressed by a calculated arithmetic mean. The uniformity of the particles and the reproducibility of the measurements have been expressed by the standard deviation. Possible sources of error in latex particle-diameter measurements are discussed.

A19. A Simple Ultramicrotome. H. HALMA AND G. B. CHAPMAN, *RCA Laboratories Division, Princeton, New Jersey.*—The microtome described previously[1] was improved by employing "vee" block bearings to provide more precise rotor alignment and by using a stiffer thermal advance rod to overcome frictional effects. The microtome is motor driven. Some slides of typical sections are shown.

[1] J. Hillier and G. B. Chapman, J. Appl. Phys. **24**, 1415 (1953).

A20. Serial Sections for Electron Microscopy. HELEN GAY, *Department of Zoology, University of Pennsylvania, Philadelphia, Pennsylvania.*[1]—A method has been developed for obtaining ultrathin serial sections for electron microscopy in any quantity desired. The method eliminates the difficulties inherent in earlier techniques of aligning the material to be studied over the openings in the grid. The ribbon, which is produced by sectioning onto the surface of a liquid in a collecting trough, is detached from the knife edge and picked up in the center of a Formvar-coated wire loop. When dry, the straight ribbon of sections is optically aligned over a slit in the grid by using a microscope, and the grid is then brought into contact with the film. These grids are then ready for examination in the microscope. A series of 18 consecutive sections will be shown of a salivary-gland cell fixed in buffered osmium tetroxide, imbedded in methacrylate, sectioned with a glass knife, and mounted on a Sjöstrand-type grid.

[1] Present address: Department of Genetics, Carnegie Institution, Cold Spring Harbor, Long Island, New York.

A21. Examination of Tissue-Cultured Hela Cells by Electron Microscopy of Serial Sections. ROBLEY C. WILLIAMS AND FRANCES KALLMAN, *Virus Laboratory, University of California, Berkeley, California.*—A technique is described for conveniently mounting serial sections for microscopy. As many as eight sections are picked up upon a collodion-filmed ring and are then mounted in precise position over one opening of an unfilmed microscope grid with the aid of a dissecting microscope. Hela cells, grown on the lower surfaces of stationary test tubes oriented horizontally, are fixed *in situ* with buffered osmic acid and subsequently scraped from the tubes. They are then washed, dehydrated, and embedded in methacrylate with centrifugation preceding each change of fluid. Cells at the advancing margin of culture growth show a dense cortical area and pseudopial extensions containing finely structured cytoplasm. In the tightly packed center of the culture area the cells in juxtaposition often form a syncitium. Various cytoplasmic inclusions can be reconstructed in three-dimensional representation from serial sections. The structures evidently differ in form with differing physiological state.

A22. Void Formation During Drying of Plastic Films. C. J. CALBICK AND MISS S. E. KOONCE, *Bell Telephone Laboratories, Murray Hill, New Jersey.*—Examination of many surfaces by shadowed plastic replicas or by intermediate pressure-temperature or polymerized plastic molds is not practicable. Many ceramic materials are somewhat porous, rendering impossible the removal of very thin plastic films. They are also brittle, often fracturing during separation of the specimen from its P-T mold. Cast films 20–100 μ thick may be stripped from porous surfaces. Their flexibility eliminates fracturing, caused by the large instantaneous forces necessary to separate the rigid P-T mold from the specimen. Films prepared by drying from solution in the usual solvents show certain surface features not found on P-T mold surfaces or on similar films for which the solvent was the monomer. These features are believed to show the presence of voids about 500 A.U. in size within the plastic, formed during the last stages of drying by diffusion of the solvent away from the interface. Polymerization of the monomer eliminates void formation.

A23. Electron and Light Microscopy of Film Surfaces. JOHN J. KELSCH, *Research Laboratories, Interchemical Corporation, 432 West 45th Street, New York, New York.*—This will be a

description of methods and instrumentation used in a study of the surfaces of films used in can linings. Silicon monoxide and pva replicas for electron microscopy are compared with the film surface itself as studied with a Leitz Ultrapak vertical darkfield objective.

A24. The Carbon Replica Method. D. E. BRADLEY, *Research Laboratory, Associated Electrical Industries, Limited, Aldermaston Court, Aldermaston, Berkshire, England.*—The main features of the evaporation of carbon and associated replica methods are described. Micrographs of some recent applications are discussed, and an assessment is made of the resolution and capabilities of the technique.

A25. Silicon Monoxide and Its Use in Electron Microscopy. GEORG HASS, *Engineer Research and Development Laboratory, Fort Belvoir, Virginia,* AND H. T. MERYMAN,[1] *Naval Medical Research Institute, Bethesda, Maryland.*—The composition and physical characteristics of silicon monoxide are described including discussion of its optical properties and some of its applications in this field. Its uses in electron microscopy are enumerated with emphasis on the practical technical aspects. Detailed consideration is given to the problems and technique of vacuum evaporation, the production of support films and one- and two-step replicas. (15 min.)

[1] Present address: Department of Biophysics, Yale University, New Haven, Connecticut.

A26. An Investigation on the Shape and Resolution of Formvar Replica Films. A. W. AGAR AND R. S. M. REVELL, *Research Laboratory, Associated Electrical Industries, Limited, Aldermaston Court, Aldermaston, Berkshire, England.*—True sections of Formvar replicas of typical surface structure have been deduced from measurements on the replicas and interferometric measurement of height. It is shown that true negative replicas of structure can be obtained when the replica film thickness is about twice the structure height. The replica films used had a resolution of better than 100 A.U. when shadowed. The factors limiting improved resolution or increased replica thickness are discussed.

A27. Replication of Crystals Sensitive to the Atmosphere: A Study of Dispersions of Colloidal Potassium in Potassium Chloride. BENJAMIN M. SIEGEL, *Department of Engineering Physics,* RALPH E. SIMON, AND ROBERT L. SPROULL, *Department of Physics, Cornell University, Ithaca, New York.*—An apparatus has been constructed for the study of cleavage surfaces of crystals which are sensitive to attack by components of the atmosphere. A mercury diffusion pump and liquid nitrogen trap are used to remove the water vapor and evacuate the chamber in which the crystal is mounted. A fresh surface is obtained on the crystal by cleaving with external controls. This surface is shadowed immediately, and a substrate is evaporated onto it without exposure to air. If cleavage at a reduced temperature is necessary, the crystal can be cooled by thermal contact to a liquid nitrogen reservoir. This apparatus has been used to study colloid dispersions of potassium in potassium chloride. A range of particle sizes has been observed which depends on the heat treatment of the crystal. Spectral transmission measurements have been made on each of the crystals replicated to determine the correlation between particle size and wavelength of the extinction maximum.

Session B

Symposium on Electron Diffraction

CHAIRMAN: L. O. BROCKWAY, *Department of Chemistry, University of Michigan, Ann Arbor, Michigan.*

This Symposium will be directed by the Chairman assisted by the Discussion Moderators. The types of prepared presentation are Contributed Papers and Invited Discussions. An informal, five-minute discussion period will follow each prepared presentation and will include spontaneous audience participation where slides may be used when relevant. The presentation time for a Contributed Paper or an Invited Discussion will be ten minutes. **The Chairman will announce the program order for the presentations.**

Discussion Moderators

L. S. BIRKS, *Naval Research Laboratory, Anacostia Station, Washington 25, D. C.*
C. J. CALBICK, *Bell Telephone Laboratories, Murray Hill, New Jersey.*
S. G. ELLIS, *Radio Corporation of America, RCA Laboratories Division, Princeton, New Jersey.*
W. L. GRUBE, *Research Laboratories Division, General Motors Corporation, Detroit 2, Michigan.*
N. A. NIELSEN, *Experimental Station, E. I. du Pont de Nemours and Company, Wilmington, Delaware.*
R. G. PICARD, *Radio Corporation of America, RCA Victor Division, Camden, New Jersey.*
LEROY G. SCHULZ, *Institute for the Study of Metals, University of Chicago, Chicago, Illinois.*
C. M. SCHWARTZ, *Battelle Memorial Institute, Columbus, Ohio.*
BENJAMIN M. SIEGEL, *Department of Engineering Physics, Cornell University, Ithaca, New York.*
C. F. TUFTS, *Sylvania Electric Products, Inc., Atomic Energy Division, Bayside, New York.*

Contributed Papers

B1. A Low-Temperature Chamber for Electron Diffraction Studies. MAYNARD J. COLUMBE, *General Engineering Laboratory, General Electric Company, Schenectady, New York.*—Description of a recently designed attachment for the electron diffraction instrument will be given. A thermocouple is provided for indicating the temperature which is adjustable from +100 degrees to −170 degrees centigrade. Both transmission and reflection samples are accommodated. The chamber is connected to the regular manipulator of the instrument imparting to the sample all necessary motions.

B2. Growth of Oxide Layers on Nickel Single Crystals. W. W. HARRIS AND FRANCES L. BALL, *Carbide and Carbon Chemicals Company, Oak Ridge, Tennessee.*—Oxide films formed at intermediate temperatures on three faces of copper single crystals have been described previously to differ in structure relative to the three faces corresponding to maximum, intermediate, and low rates of oxidation at atmospheric pressure.[1] Electron optical evidence of nucleation of the initial oxide film was presented. Bardolle and Benard[2] and Gulbransen and McMillan[3] have shown that nucleation of an initial oxide layer is a part of the growth process occurring on iron crystals at high temperatures. The present work extends these observations of nucleation to the oxide formed on the 100, 111, and 311 faces of electropolished and annealed nickel single crystals. Examination of several degrees of oxidation in the region of 450°C for varying times has shown a systematic development of nucleated oxide layers characteristic of each of the three faces studied. Electron diffraction patterns of these films show, as for copper, a progression from an oriented powder pattern for the initial oxide through mixed powder and fiber patterns to intricate single crystal patterns for films several hundred angstrom units thick. The thick film diffraction patterns show doubling of diffraction spots, tailed arcs, and rotational displacement of spots, and for the oxide formed on the 100 face at 500°C and 30 minutes exposure to oxygen the diffraction pattern indicates at least seven diffraction phenomena.

[1] W. W. Harris and Frances L. Ball, J. Appl. Phys. **24**, 1416(A) (1953).
[2] J. Bardolle and J. Benard, Rev. Met. 613–622 (1952).
[3] E. A. Gulbransen and W. R. McMillan, J. Appl. Phys. **24**, 1416(A) (1953).

B3. Epitaxies Studied by Electron Microscopy and Electron Diffraction.[1] A. OBERLIN-MATHIEU-SICAUD AND R. HOCART, *Laboratoire de Mineralogie, Faculte des Sciences, Paris, France.*—Gold particles prepared by the reduction of solutions of $AuCl_3$, HCl, and particles of MoO_3 obtained by sublimation orient themselves on graphite. The latter is cleaved in platelets thin enough to serve as specimen supports for electron microscopy. Electron diffraction limited to micro-monocrystals demonstrates the correlation of lattices. Gold orients its [110] row parallel to the [100] row of the graphite. The experiments show that the epitaxy favors crystallization, suppresses the curvature normally observed on these particles, and constrains the parameters of the gold. MoO_3 leads to two orientations: (1) the [001] MoO_3 row parallel to the graphite [100] row. (2) The MoO_3 [001] row parallel to the graphite [310] row. The classical law of the correlation of lattices (Friedel-Royer) allows for a third orientation with the [001] row of the MoO_3 parallel to the [210] row of the graphite. This epitaxy was not observed. A new hypothesis considering short atomic bonds accounts for these anomalies.

[1] To be read by H. Halma.

B4. Nucleation in the Hydration of Tricalcium Silicate. MAX SWERDLOW* AND F. A. HECKMAN, *National Bureau of Standards, Washington 25, D. C.*—A cooperative program with the Portland Cement Association has been directed toward new studies of products formed by the action of water on portland cement and its pure clinker phases by means of electron microscopy and electron diffraction. Tricalcium silicate, hydrated in the form of a neat paste, in a ball mill or in an ultrasonorator, was examined. A fine-grained particulate structure of about 150A was observed in many of the solid phases developed during various stages of hydration. In the fully hydrated, ball-milled material, particles ranging from about 50 to 200A in diameter occurred. These findings constitute a visual experimental confirmation of the theoretical deductions of others regarding the size of the ultimate gel particles and provide additional information about the crystalline state of these colloidal systems, the mechanism of the hydration process of portland cement, and the nature of the cementing action.

B5. Motion Picture Studies of Electron Bombardment of Evaporated Bismuth Films.[1] LORN L. HOWARD, *Conducting Thin Films Laboratory, Department of Electrical Engineering, University of Illinois, Urbana, Illinois.*—The orientation of crystallites in evaporated bismuth films under study in the electron microscope often undergoes changes which have been reported previously.[2] It is possible to record this activity on motion pictures without modification of the RCA model EMU electron microscope and with film recently made commercially available, Eastman Tri-X Negative Panchromatic. Motion pictures were made of these changes in a bismuth film approximately 1000 A thick and having an initial resistance per square of 100 ohms.

[1] Abstract received too late to be placed in normal program order.
[2] Lorn L. Howard, J. Appl. Phys. **25**, 125 (1954).

Invited Discussions

Developments in Gas Diffraction. L. O. BROCKWAY (address above)

Identification of Patterns for Micro Single Crystals. R. M. FISHER, *Fundamental Research Laboratory, United States Steel Corporation, Kearney, New Jersey.*

Problems in Reflection Electron Diffraction. R. D. HEIDENREICH, *Bell Telephone Laboratories, Murray Hill, New Jersey.*

Stripping Techniques Useful with Selected Area Diffraction. WILLIAM R. MCMILLAN, *Research Laboratories, Westinghouse Electric Corporation, East Pittsburgh, Pennsylvania.*

Microdiffraction, Its Theory and Application. NORMAN M. WALTER, *Metallurgy Research Department, General Electric Company, Schenectady, New York.*

Session C

Symposium on Problems Involved in the Electron Microscopy of Viruses

CHAIRMAN: C. E. HALL, *Department of Biology, Massachusetts Institute of Technology, Cambridge, Massachusetts.*

This Symposium will present three Invited Discussions. Each of these will be a thirty-minute presentation. One-half of the Symposium program is allotted to informal discussion periods during which spontaneous audience participation will be encouraged. **The Chairman will announce the program order for the Invited Discussions and for the informal discussion periods.**

Invited Discussions

THOMAS F. ANDERSON, *The Johnson Foundation, University of Pennsylvania Hospital, Philadelphia 4, Pennsylvania.*
D. GORDON SHARP, *Duke University, Durham, North Carolina.*
ROBLEY C. WILLIAMS, *Virus Laboratory, University of California, Berkeley, California.*

Session D

Symposium on Electron Metallography

HONORARY CHAIRMAN: CYRIL S. SMITH, *Director, Institute for the Study of Metals, University of Chicago, Chicago, Illinois.*

CHAIRMAN: GEORGE E. PELLISSIER, *United States Steel Corporation, Pittsburgh, Pennsylvania.*

This Symposium will be directed by the Chairman assisted by the Honorary Chairman and the Discussion Moderators. The types of prepared presentation are Contributed Papers and Invited Discussions. An informal five-minute discussion period will follow each prepared presentation and will include spontaneous audience participation where slides may be used when relevant. The presentation time for a Contributed Paper or an Invited Discussion will be ten minutes. **The Chairman will announce the program order for the presentations.**

Discussion Moderators

L. S. BIRKS, *Naval Research Laboratory, Anacostia Station, Washington 25, D. C.*
L. O. BROCKWAY, *Department of Chemistry, University of Michigan, Ann Arbor, Michigan.*
ALFRED L. ELLIS, *International Harvester Company, Chicago, Illinois.*
ERNEST F. FULLAM, *Ernest F. Fullam, Inc., Schenectady, New York.*
W. L. GRUBE, *Research Laboratories Division, General Motors Corporation, Detroit 2, Michigan.*
R. D. HEIDENREICH, *Bell Telephone Laboratories, Murray Hill, New Jersey.*
WILLIAM R. MCMILLAN, *Research Laboratories, Westinghouse Electric Corporation, East Pittsburgh, Pennsylvania.*
LEROY G. SCHULZ, *Institute for the Study of Metals, University of Chicago, Chicago, Illinois.*
C. M. SCHWARTZ, *Battelle Memorial Institute, Columbus, Ohio.*
C. F. TUFTS, *Sylvania Electric Products, Inc., Atomic Energy Division, Bayside, New York.*

Contributed Papers

D1. Cathodic Vacuum Etching of Uranium. T. K. BIERLEIN, *Hanford Atomic Products Operation, General Electric Company, Richland, Washington.*—Uranium of various histories has been etched by krypton ions. The etching chamber which utilizes a water-cooled zirconium sample mount sealed directly to glass, as well as the etching procedure used, is described. Optical and electron micrographs of specimens representing three different fabrication and heat treatment histories illustrate the range of utility of cathodic vacuum etching for macro and micro examination of uranium. Shadowed silicon monoxide films from primary Faxfilm replicas show: (1) inclusions etch preferentially and at a rate slower than that for the matrix uranium; (2) one specimen is characterized by pyramidal type mounds, presumably twins; (3) the configuration of the second specimen consists of a marked subdomain structure with an associated width of about 0.5 micron; (4) the third specimen is characterized by impurities at prior grain boundaries, and by a coarse, fibrous structure.

D2. Some Studies in Nickel Plating. ROBERT B. FISCHER AND CHARLES E. RING, *Chemistry Department, Indiana University, Bloomington, Indiana.*—Thick (~25μ) and thin (~500A) layers of nickel were plated onto strips of electropolished, electrolytic copper from a low *p*H Watt's bath modified only by known additions of 1,5-naphthalene disulfonic acid as a brightening agent. Deposits were examined by several experimental techniques: surface replication by electron microscopy; surface brightness and/or roughness by two optical methods; x-ray diffraction; electron microscopy; and electron diffraction of deposits after separation from the base metal. The several types of experimental data are correlated with each other and with the conditions of preparing the sample. The thin deposits all exhibit preferred orientation and small, but random variations in brightness. The thick deposits exhibit, as the brightener concentration is increased to an optimum value, decreasing grain size as indicated both microscopically and by diffraction patterns, markedly increasing brightness, and decreasing roughness.

D3. Recent Applications of the "Extraction Replica" Technique. R. M. FISHER, *Fundamental Research Laboratory, United States Steel Corporation, Kearny, New Jersey.*—The combination of electron diffraction and electron microscopy through the "Extraction Replica" technique has proven very useful in investigating fine precipitates in ferrous metals. Recent applications of the method including studies of carbide formation during the first stages of tempering carbon steels and examination of grain boundary carbides influencing intergranular corrosion will be described. Possible artifacts of the method such as stain formation will also be discussed and illustrated.

D4. The Formation and Growth of Cuprous Oxide Nuclei on the 311 Face of Copper Single Crystals. W. W. HARRIS AND FRANCES L. BALL, *Carbide and Carbon Chemicals Company, Oak Ridge, Tennessee.*—Electron optical evidence for nucleation of initial oxide layers formed on copper single crystals has been presented previously.[1] This work extends the investigation relative to detailing the development of oxide nuclei on the 311 faces of copper single crystals. For 150°C oxidations, oxide layers too thin to show visible color have been examined electron optically, and data have been obtained for the number per square centimeter and size of nuclei for oxygen exposures as short as 20 seconds and as long as 5000 seconds. The number of nuclei per square centimeter rises from 4×10^{11} at 20 seconds to 12×10^{11} at 910 seconds and then falls to a limiting value around 4×10^{11} at 5000 seconds. The nucleus diameter increases from about 15A at 20 seconds to 30A at 900 seconds then rises rapidly to a limiting value of about 80A at 5000 seconds.

[1] See abstract B2, this program.

D5. The Application of Cathodic Vacuum Etching to Electron Metallography. THOMAS R. PADDEN, *Atomic Power Division, Westinghouse Electric Corporation, Pittsburgh, Pennsylvania.*—A cathodic vacuum etching procedure was developed in which one set of electrical, geometric, and vacuum conditions can be used to develop the microstructures of a wide variety of metals and alloys cut in various cross-sectional sizes and shapes. The controlling variable is the etching time which is of the order 1–3 minutes for light microscopy and about twice as long for electron microscopy. Most of the advantages of the procedure are derived from a cooled cathode design which facilitates the use of high ion current densities while the sample is held below 232°C. A description of the equipment design along with recent improvements will be included, but the main topic will be the application of the technique to electron metallography. (The basic equipment design and procedure as well as applications in light microscopy have been published elsewhere.) The characteristic of developing unstained microstructures requiring no washing or rinsing subsequent to etching make this technique particularly useful in electron metallography. A number of micrographs will be presented to demonstrate this and other characteristics of the technique as well as to indicate its wide range of applicability.

D6. Recent Advances in Emission Electron Microscopy. A. C. VANDORSTEN, *Philips Research Laboratories, Eindhoven, Holland.*—An instrument will be described which has a resolution of the order of 1000 angstrom units. The image of the emitting surface is formed by means of an immersion type lens and further enlarged with two magnetic type lenses. Provision is made to evaporate an activating medium, such as Cs, Ba, or Sr, while the specimen is in position for examination. Four such evaporation filaments are incorporated. Temperatures up to 1250°C are used.

Invited Discussions

Studies of Minor Phases in Heat Resistant Alloys. W. C. BIGELOW, *Engineering Research Institute, University of Michigan, Ann Arbor, Michigan.*

Field Emission Microscopy. ROBERT GOMER, *Institute for the Study of Metals, University of Chicago, Chicago, Illinois.*

Sub-Grain Structure of Aluminum and Commercial Aluminum Alloys. M. S. HUNTER, *Research Laboratory, Aluminum Company of America, New Kensington, Pennsylvania.*

Preparation of Surfaces for Electron Metallography. FRED KELLER, SR., *Research Laboratory, Aluminum Company of America, New Kensington, Pennsylvania.*

The X-Ray Microscopy of Metals. STERLING P. NEWBERRY, *General Engineering Laboratory, General Electric Company, Schenectady, New York.*

Studies of Oxide Films from Stainless Steels. N. A. NIELSEN, *Experimental Station, E. I. du Pont de Nemours and Company, Wilmington, Delaware.*

Etch Figures as Seen with the Electron Microscope in Tungsten and Copper. L. DELISLE PELLIER, *Research Division, American Cyanamid Company, Stamford, Connecticut.*

Electropolishing and Electroetching for Electron Metallography. D. M. TEAGUE, *Chrysler Corporation, Engineering Division, Detroit, Michigan.*

Sample Preparation for Light and Electron Metallography. J. R. VILELLA, *Fundamental Research Laboratory, United States Steel Corporation, Kearny, New Jersey.*

Activities of the A.S.T.M. Subcommittee XI on Electron Microstructure of Metals. R. M. FISHER, present chairman of Subcommittee XI (address above). (5 min.)

Session D (*continued*)

1:30 P.M.–2:45 P.M.

Symposium on Electron Metallography (*continued*)

See the Friday morning program of Session D for names of the contributors.

Session E

Symposium on Electron Microscopy in Petroleum Technology

CHAIRMAN: HARRY M. ALLRED, *Beacon Laboratories, The Texas Company, Beacon, New York.*

This Symposium will be directed by the Chairman, assisted by the Discussion Moderators. The types of prepared presentation are Contributed Papers and Invited Discussions. Since some of the data to be presented are of an argumentative nature, one-half of the Symposium program will be allotted to informal discussion periods during which spontaneous audience participation will be encouraged. During these informal discussion periods, slides may be used when relevant. The presentation time for a Contributed Paper or an Invited Discussion will be ten minutes. **The Chairman will announce program order for the prepared presentations and for the informal discussion periods.**

Discussion Moderators

L. O. BROCKWAY, *Department of Chemistry, University of Michigan, Ann Arbor, Michigan.*
ERNEST F. FULLAM, *Ernest F. Fullam, Inc., Schenectady, New York.*
C. M. SCHWARTZ, *Battelle Memorial Institute, Columbus, Ohio.*
JOHN H. L. WATSON, *Edsel B. Ford Institute for Medical Research, Detroit 2, Michigan.*

Contributed Papers

E1. Applications of Electron Microscopy to Studies of Metallic Wear. D. M. TEAGUE, C. R. LEWIS, AND S. B. TWISS, *Chrysler Corporation, Engineering Division, Detroit, Michigan.*—Some aspects of wear and lubrication have been studied by observation of wear specimens with the electron microscope. The specimens used were crossed steel cylinders, one cylinder rotating, the other being stationary. It has been shown that under these conditions of high unit loading, wear particle size, damage of the metal contact surface, and wear rate increase with increasing original surface roughness of the moving metal part. The smoothness of the wear area in the stationary member is most closely related to the finish of the rotor and tends to be smoother than the original surfaces, except in the case of rough rotor finish. This characteristic is undoubtedly important in the mating or breaking-in of moving parts since, during this process, wear is known to decrease progressively. The type of lubricant strongly affects the wear process. Wear with purified mineral oil produces extremely minute particles, possibly by extensive and continuous microscopic welding of the sliding surfaces, due to rupture of the simple hydrocarbon film under the high unit loads. In contrast, ethyl palmitate or a 5 percent addition of sperm oil to mineral oil provides improved boundary lubrication, larger and fewer wear particles, little welding, and an extremely smooth surface except for occasional deep scratches.

E2. Shadowcasting Lubricating Greases for Electron Microscope Examination. JOHN W. WILSON, JR., AND GERARD S. MAPES, *Socony-Vacuum Laboratories, 412 Greenpoint Avenue, Brooklyn, New York.*—In the examination of lubricating greases with the electron microscope, shadowing with metals gives an improved image. Three metals—gold, chromium, and uranium—were used in shadowing four types of lubricating greases. Best results were obtained on all four greases with uranium. Modifications of the RCA Model EMV-6 Vacuum Shadowing Unit are described which allow the use of a 50-ampere filament current. This gives a relatively inexpensive instrument for shadowing with uranium.

Invited Discussions

Preparation of Lubricating Grease Specimens. JOHN A. BROWN, *Sinclair Research Laboratories, Inc., Harvey, Illinois.*

Preparation of Lubricating Oils and Liquid Fuels for Electron Microscopy. W. L. GRUBE, *Research Laboratories Division, General Motors Corporation, Detroit 2, Michigan.*

Informal Discussions

Additional contributions will be made during the informal discussion periods by PAUL SKIBA, *Research Division, Esso Laboratories, Linden, New Jersey.*

Session F

Contributed Papers on Viruses

CHAIRMAN: F. B. BANG, *Departments of Parasitology and Medicine, The Johns Hopkins University, Baltimore, Maryland.*

F1. The Morphological Structure of Anopheles A Virus. MARLENE FRIEDLAENDER, *Columbia University, College of Physicians and Surgeons, New York.*—The action of an oncolytic virus, Anopheles A, on cells of Ehrlich ascites tumor was studied in ultrathin sections, and the virus identified both in the tumor cells and in chorioallantoic membranes used as independent controls. The virus showed characteristic internal structure, and various stages and sites of development were observed. The mature spheroid virus appeared to consist of a core of low electron density, about 35 mμ in diameter, surrounded by a complex dense shell, up to 15 mμ thick which gave an over-all diameter of about 65–70 mμ. At a different, possibly earlier, stage, a surrounding, apparently structureless, zone of medium to low electron density could be identified. Its thickness of about 30 mμ varied from 20 to 40 mμ, and its boundary consisted of a thin additional shell structure. Accompanying changes in the cytoplasm from early infection to final breakdown of the cell were compared with the action of another oncolytic virus, Bunyamwera, under similar conditions.

F2. Virus-Like Particles as Seen in Sections of Rous Sarcoma Tumors. WILLIAM H. GAYLORD, JR., *Department of Microbiology and Department of Pathology, Yale University School of Medicine, New Haven, Connecticut.*—Round, dense, particles about 500A in diameter have been observed in sections of two Rous sarcoma tumors but not in a third. They correspond in appearance to the particles seen in cells cultured from Rous tumors as reported previously by others[1,2] and they were not seen in tissues studied for comparison. The particles consist of thin limiting membranes and dense, round, or stellate central masses. They occur singly, in pairs, or in small clusters on the outer surface of cell membranes. Intracellular particles were rarely seen, and no other structure presumed to be related to the particles has been identified. If the virus-like particles have an intracellular phase, it is either of a low order of incidence or it is in a form not yet recognized.

[1] Claude, Porter, and Pickels, Cancer Research **7**, 421 (1947).
[2] Bernhard, Dontcheff, Oberling, and Vigier, Bull. du Cancer **40**, 311 (1953).

F3. A Comparison of Normal and Infected Mouse Lung by Means of the Electron Microscope. H. KARRER, *Departments of Parasitology and Medicine, The Johns Hopkins University, Baltimore, Maryland.*—Adult mice were infected intranasally with different agents, notably influenza virus and feline pneumonitis virus, and osmium-fixed lung tissue was studied in thin sections and compared with normal lung tissue. Infected lungs showed an increased number of free cells in air spaces and other signs of pneumonia. Influenza virus could be seen in bronchioles, and feline pneumonitis virus seemed to be located primarily in the alveolar epithelium. In normal lung, certain alveolar cells were seen, the mitochondria of which were undergoing a cystic change. The capillary and alveolar endothelial lining of normal lung was studied in serial sections. Small vacuole-like structures in a capillary endothelial cell are interpreted as products either of pinocytosis or of gas transfer from the blood stream to the air space or *vice versa*.

F4. Measurements of Electron Stains Absorbed by Virus. C. E. HALL, *Department of Biology, Massachusetts Institute of Technology, Cambridge, Massachusetts.*—Densitometric methods will be described with which the mass thickness through the center of stained virus particles was measured. Such measurements were made on tomato bushy stunt virus (BSV) and tobacco mosaic virus (TMV) after they had been treated with a variety of electron stains. Very little stain is taken up in the *p*H range where the viruses are stable, but, as the *p*H is decreased to about 1.5 and below, the amount of stain absorbed rises rapidly. Under these drastic conditions stains, such as phosphotungstic acid and heavy metal ions such as platinum and thorium, when present in sufficient concentration, preserve the morphology of the virus particles. With phosphotungstic acid alone or in combination with other heavy reagents, the estimated mass of BSV particles can be increased by a factor of three to four times without noticeable increase in diameter. Maximum masses of TMV were about 2.5 times that of the unstained particles. Some artifacts associated with the use of electron stains will be shown.

F5. Further Data on the Nature of Avian Erythromyeloblastic Leukosis Virus. D. GORDON SHARP, *Duke University, Durham, North Carolina.*—The size and shape of these virus particles as they appear on electron micrographs prepared for counting (agar sedimentation method) is dependent on extent of osmic acid fixation. Without treatment the particles are excessively flattened, while 30-minute exposure to the vapor produces almost spherical shape. From sedimentation velocity H_2O saline, D_2O saline, and bovine serum albumin solutions, we calculate virus particle densities of 1.29 and 1.06 for the penetrating and nonpenetrating solutions, respectively. Minimum associated water must be 80 percent or more. Still, titration and particle count show that no destruction results from severe osmotic shock. The virus particle is probably soft, wet, and sponge-like. Larger bodies, presumably mitochondria found in both normal and infected material, can be seen to contain particles which look like virus. Such bodies, when broken, seem to be emitting these particles much as bacteria can be seen emitting phage.

F6. The Effect of Drying on the Structure and Shape of Certain Viruses. COUNCILMAN MORGAN, SOLON A. ELLISON, HARRY M. ROSE, AND DAN H. MOORE, *Departments of Microbiology and of Medicine, College of Physicians and Surgeons, Columbia University, New York.*—Thin sections of methacrylate embedded tissues revealed vaccinia and fowlpox viruses to be spherical within the host cell and to possess a cytoplasm-like component, an eccentric nuclear-like structure, and a single limiting membrane. In the extracellular space they appeared to be oblong and to consist of a central body, possibly disk-shaped, and a double limiting membrane. When thick sections were cut, the methacrylate removed by immersion in amyl acetate, and the preparations dried, brick-shaped particles were produced which resembled forms encountered by other investigators in ultracentrifuged preparations. Drying of ultracentrifuged preparations of influenza virus generally caused flattening of the particles with increase in their apparent diameter. Disruption of viral membranes with loss of inner components produced ring forms or "doughnuts."

F7. Intracellular Development of Herpes-B Virus. MAGDALENA REISSIG AND JOSEPH L. MELNICK, *Section of Preventive Medicine, Yale University School of Medicine, New Haven,*

Connecticut.—Herpes-B virus produces characteristic cytopathogenic changes in cultures of monkey kidney epithelium. Monolayer cultures were inoculated with a large dose of virus to obtain the simultaneous infection of all cells present. The cultures were harvested at different time intervals after inoculation, tested for production of mature infective virus, and examined with the electron microscope. Infected cells become swollen and are too thick for direct observation in the electron microscope. Therefore, a technique was devised by means of which ultrathin sections of the cultures were made. A close relationship was found between the appearance of cytological changes and the presence of virus particles within the infected cells. A few hours after inoculation, virus-like particles characterized by their internal structure began to appear both in the nucleus and in the cytoplasm. These particles, which range in size from 100 to 180 mμ, have a dense center surrounded by either one or two membranes. In some instances they were present between the two layers of the nuclear membrane. They have not been found in normal cells, and appear in infected ones a few hours after inoculation. At about the time when new *infective* virus first becomes detectable in the culture fluid, particles also appear on the external surface of the cells.

F8. "Virus" Particles in "Normal" Chick Embryo Cells and Their Similarity in Appearance to the Rous Tumor Virus Particles. F. B. BANG, *Departments of Parasitology and Medicine, The Johns Hopkins University, Baltimore, Maryland.*—Previous reports by Porter and by Bernhard have indicated that certain 70 mμ particles found in clumps in cells and free in the cytoplasm of chicken tumor cells may be the tumor virus particles. During the last three years about 10 percent of our "normal" tissue cultures from chick embryos have shown similar particles in large numbers. These are seen in primary explants either on coverslips or in roller tubes in 50 percent chicken serum. They are identical in size, shape, appearance, and arrangement with those described as tumor viruses. They do not occur in most cultures, and thus are not "normal" to the cell, but when present are there in large numbers in many fields. The best preparations were obtained from roller tube cultures which had been in heterologous media for two weeks. They have not been seen in cells other than the chick embryo. That they may be virus particles is indicated by their size, shape, arrangement, and internal density. They are found in partially disintegrating cells and are associated with changes in cell morphology. Despite their occurrence in normal chick embryos, their relation to the virus of Rous sarcoma cannot be excluded.

The Round Table

This Session will consist of several informal, spontaneous Round Table Discussions under the direction of Discussion Leaders. This affords a meeting place for discussion groups to consider topics that, because of time limitations, were not included in the regular sessions of the Twelfth Annual Meeting. Specific topics and Discussion Leaders will be announced at the Annual Banquet.

Session H

Contributed Papers on General Biology

CHAIRMAN: JEROME GROSS, *Massachusetts General Hospital, Department of Medicine, Boston, Massachusetts.*

H1. Further Observations on the Submicroscopic Vesicular Component of the Synapse. E. DE ROBERTIS AND C. M. FRANCHI, *Departamento de Ultrastructura Celular, Instituto de Investigacion de Ciencias Biologicas.*—De Robertis and Bennett (1954)[1] recently described a submicroscopic component consisting in dense vesicles of 200–500A in the synapses of the sympathetic ganglia of the frog and in the neuropile of the annelids nerve cord. In the frog material this component was essentially found in presynaptic terminals. Now these observations have been extended, and similar vesicles have been found in the neuropile of nerve ganglia of certain arthropods and in the central nervous system of mammals. This component has been seen in the neuropile and axo-somatic synapses of the ventral acoustic ganglion, in the plexiform layer of the cerebellum, and in the cerebral cortex. Particularly interesting are the synaptic junctions at the level of the glomeruli of the cerebellum in which the vesicles are very abundant in the large endings of the mossy fibers. In view of these observations it is postulated that the simple contact of membranes between nerve endings does not constitute a synapse and that the presence of the submicroscopic vesicular component, in addition to the membrane contact, is the specific character of most synaptic junctions.

[1] De Robertis and Bennett, Fed. Proc. March 13, 1954.

H2. The Ultrastructure of Crayfish Giant Synapses. J. DAVID ROBERTSON, *Department of Pathology and Oncology, University of Kansas Medical School, Kansas City, Kansas.*—Recent work on the crayfish median-to-motor giant synapse will be reviewed. Evidence will be presented for the following conclusions: (1) The median giant and motor giant fiber axon-Schwann membranes appear in sections as dense edged structures of about 200–300A over-all thickness. (2) These two membranes fuse to form a single membrane of apparently identical structure at the synapse. (3) The motor axoplasm of the synaptic processes terminating in median giant Schwann cytoplasm is peculiar for a relatively high concentration of dense concentrically lamellated bodies measuring about 0.1–0.8μ in diameter, a relatively high concentration of axoplasmic filaments and concentrations of vesicular bodies measuring from about 250A to 1000A in diameter. (4) Motor fiber and median giant fiber Schwann cells fuse at the synapse. (5) The motor fibers synapse with one another as they decussate just cranial to the median-to-motor giant synapse.

H3. Width and Length of Collagen Fibrils during the Development of Human Skin, in Granulation Tissue and in the Skin of Adult Animals. WILLIAM G. BANFIELD, *Department of Pathology, Yale University School of Medicine, New Haven, Connecticut.*—Using the electron microscope, a determination was made of the widths and the comparative length of collagen fibrils from the skin of fetal and adult humans, granulation tissue, dense scar tissue, and the skin of adult animals. During fetal development there was an increase in the widths of the collagen fibrils in the human skin, and a corresponding increase in the comparative lengths. Young granulation tissue con-

tained a high proportion of narrow tapered fibrils while the dense scar tissue contained a high proportion of wide fibrils with a low incidence of tapering. There was virtually no difference in widths and percentages of tapered fibrils from the skins of adult humans, rabbits, guinea pigs, rats, hamsters, and mice. The immaturity and not the size of the animal is responsible for a high percentage of narrow tapered fibrils in the skin.

H4. A Technique for Electron Microscopic Observation of Intact Loose Connective Tissue and Ground Substance. GEORGE W. COCHRAN, A. M. ASADI, AND T. F. DOUGHERTY.—*Department of Botany and Plant Pathology, Utah State Agricultural College, Logan, Utah, and Department of Anatomy, College of Medicine, University of Utah, Salt Lake City, Utah.*—A new technique for electron microscopic observation of loose connective tissue elements is described. It utilizes the air-dried tissue spread technique which was originally introduced by Ranvier (1889). Subcutaneous loose connective tissues of mice were dissected by fine ocular surgical instruments so that one-layer cuticles were produced. A trapezoidal electrolytic copper grid was placed adjacent to and in firm contact with the one-layer sheets of connective tissue and immediately air-dried. Several such specimens were prepared from each animal, either shadowed or unshadowed, and observed with an RCA electron microscope (Model EMU). The use of artificial plastic membranes, chemical fixatives, or other treatments, enzymatic or otherwise, was avoided. Marked changes in the morphology of the ground substance resulting from various chemical and physical treatments of the animals were demonstrated.

H5. The Ultrastructure of the Epithelial Cells in the Trachea of the Albino Rat. J. RHODIN* AND T. DALHAMN, *Department of Anatomy, Karolinska Institutet, and The Institute of Public Health, Stockholm, Sweden.*—Studies were made on the ultrastructure of the epithelial cells in the trachea of the albino rat. The tissues were fixed in buffered osmium tetroxide solution, embedded in methacrylate, and sectioned with the ultramicrotome designed by F. Sjöstrand. The sections, approximately 200 A thick, have been studied in an RCA EMU 2 c electron microscope without dissolving or subliming the embedding medium. The tracheal epithelium consists of the nonciliated goblet cells with characteristic cytoplasmic structures and the ciliated cells. The cilia, about 3μ in length and 0.3μ in width, are bordered by a 100 A thick membrane and the internal structure consists of one central and nine peripheral longitudinal filaments. The latter prove to be tubules with a 100 A thick wall, the total thickness being 300 A. The basal corpuscles are formed by junction of the tubules to a solid structure. No ciliary rootlets or any kind of fibrils are observed in connection with the basal corpuscles.

H6. Functional Implications of the Fine Structure of the Renal Glomerulus. JAMES F. RINEHART AND MARILYN GIST FARQUHAR, *Department of Pathology, University of California, School of Medicine, San Francisco, California.*—Electron micrographs of the normal renal glomerular loop reveal three distinct components: (1) a complete inner layer of endothelial cytoplasm of variable thickness, (2) a basement membrane which is a derivative of the endothelium, and (3) an outer layer of epithelium with "innumerable" foot processes anchored on the basement membrane. This elaborate organization practically precludes the commonly held concept of glomerular function as one of simple filtration across a semipermeable membrane. The highly vesicular nature of the endothelial cytoplasm indicates that fluid is transferred across this layer via vesicles as suggested by Palade (1953) for certain other endothelia. The basement membrane proper is probably of the nature of a gel (a modified glycoprotein) and serves as an ultrafilter. This appears finely vesicular under the stress of overloading with water. The possible role of the epithelium in elaboration of the glomerular filtrate will be discussed. It is believed that that the epithelial cell foot processes inserted on the basement membrane may act as hydrophilic "wicks" in drawing fluid across the basement membrane.

H7. Evidence of Nucleocytoplasmic Interchange in Frog Oocytes.[1] A. W. POLLISTER, M. E. GETTNER, AND R. WARD, *Columbia University.*—In early oocytes, before yolk deposition, the nuclear boundary, or membrane, approximately 1000A thick, in vertical section appears as a series of evenly spaced dense areas interspaced in a continuum of much lower density. In tangential section the former dense areas appear circular, 500 to 900A in diameter, with a peripheral ring of very dense bodies, 100 to 200A in diameter. Commonly, there is also a central dense body similar in size to the latter. From the outer surface of each of the large dense areas, in vertical section, there projects into the cytoplasm an unbranched, threadlike body 50 to 150A in diameter, which frequently appears to be nodulated, or to show a suggestion of helical structure 250 to 500A in diameter. From the inner surface of each large dense area a delicate, highly contorted thread extends into the nucleus, sometimes terminating in the nucleolus. Occasionally these also appear nodulated. In sum, these appearances at the nucleocytoplasmic boundary seem consistent with the view that the large dense areas may be regions where a threadlike substance is continuous from nucleus to cytoplasm.

[1] Supported by a grant in aid of research (contract 1776) from The National Cancer Institute, Public Health Service, Department of Health, Education, and Welfare.

H8. Further Studies on the Ultrastructure of the Nucleus and Its Components. G. YASUZUMI, *Electron Microscope Laboratory, Anatomical Department, Nara Medical College, Naraken, Unebicho, Japan.*—The work attempted at the Electron Microscope Laboratory, Anatomical Department, Nara Medical College and Medical School of Osaka University, will be briefly reported. The head of bull spermatozoa treated with 5 percent *Saccharas ferricus medicus* was composed of helical elements which give an appearance of granular structure at low magnifications. The metabolic (interphase) chromosomes isolated from erythrocyte nuclei of various vertebrates was composed of double-coiled and double-stranded helices identical with telophase chromosomes in somatic cells. Thin sections of erythrocyte nuclei of carp confirmed the same structure as obtained by mechanical agitation. The salivary chromosomes of Diptera showed clearly a number of chromofilaments running longitudinally in the specimen treated with ultrasonic vibration, Carnoy's solution, and 45 percent acetic acid. Thin sections of testes of albino rats demonstrated various stages of spermatogenesis in which mitochondria and nuclear membranes play an important role.

H9. Fine Structure of *Nitella* Chloroplasts. A. J. HODGE, *Chemical Physics Section, Division of Industrial Chemistry, Commonwealth Scientific and Industrial Research Organization, Melbourne, Australia,* AND A. B. HOPE, D. J. MCLEAN, AND F. V. MERCER, *Plant Physiology Unit, Botany School, University of Sydney, Sydney, Australia.*—Cells of *Nitella cristata* fixed in buffered osmium tetroxide were examined by ultra-thin sectioning. The disk-shaped chloroplasts contain bands of well-ordered lamellae. The interband regions usually contain starch granules, apparently formed within a thin-walled starch vacuole, and a number of dense spherical bodies. The minimum interlamellar spacing in well-ordered regions is about 70A. A well-defined chloroplast limiting membrane is present. Space not occupied by lamellae or the inclusions mentioned previously is filled with a granular substance which will be termed chloroplasm. The cytoplasm, which is bounded by a thin membrane (the tonoplast), contains, besides chloroplasts, a number of thin-walled vacuoles and bodies resembling mitochondria. The latter possess a thin limiting membrane and contain membrane-like structures. In addition, structures

tentatively identified as elements of the endoplasmic reticulum occur in the cytoplasm. Isolated swollen chloroplasts were examined by both conventional and sectioning techniques. Swelling is accompanied initially by increased interlamellar spacing and some vacuolization, but eventually the entire chloroplast is vacuolated. The lamellae round up to form closed vacuoles containing remnants of chloroplasm. The limiting membrane usually remains intact. The results emphasize the highly pleomorphic character of lipo-protein layer structures and suggest that the chloroplasm may contribute to swelling by virtue of its fixed charges.

H10. Cytochondria and Myofibril Interrelationships in Pigeon Breast Muscle. STANLEY WEINREB* AND JOHN W. HARMAN, *University of Wisconsin, Department of Pathology, Madison 6, Wisconsin.*—Electron microscopic studies of pigeon breast muscle have revealed a symplasmic relationship between mitochondria, sarcosomes, and myofibrils. These structures generally appear to present a weakly defined interface between adjoining components and the surrounding sarcoplasm. Numerous projections and areas were observed which are confluent with those of closely approximated structures. Such connections are especially apparent between mitochondria and the "*Z*" line regions of myofibrils. Mitochondria have been observed in three forms: (1) nonlaminated; (2) coarse, irregular lamination; (3) fine, regular lamination. It is postulated that the finely laminated appearance is the result of the regular folding of an internal "ribbon" structure many times the length of the mitochondrion. Sarcosomes have been regularly observed in positions and numbers which correlate with phase microscope observations. They usually are positioned at the poles of mitochondria or within mitochondrial depressions. They are the most electron-opaque structures in the section and appear partially surrounded by a clear area.

H11. Further Studies in the Electron Microscope of Thin Sections of Normal and Malignant Mammary Tissues of Mice of High- and Low-Breast-Cancer Strains. LEON DMOCHOWSKI,* CUSHMAN D. HAAGENSEN, AND DAN H. MOORE, *Department of Experimental Pathology and Cancer Research, University of Leeds, Leeds, England, and Departments of Microbiology and Surgery, College of Physicians and Surgeons, Columbia University, New York.*—A number of additional spontaneous mammary tumors and lactating mammary glands of mice from strains harboring the mammary-tumor-inducing agent and agent-free strains have been examined in ultrathin sections. Spherical particles varying in diameter from 500 to 1500A have been observed in the cytoplasm, frequently in the intercellular spaces and small ducts, but not in the nucleus of the cells. The particles show an internal dense region, varying in diameter from 180 to 350A, surrounded by an outer pale zone which in turn is surrounded by a well-defined outer boundary. They have been observed in most of the high-cancer-strain tumors, in a number of low-cancer-strain tumors supposedly free of the agent, and in lactating breast tissues of agent-containing mice. These characteristic particles can be differentiated easily, by their internal structure, from similar size casein-calcium-phosphate and lipoprotein particles present in the milk of high- and low-cancer-strain mice. The significance of these observations is discussed.

Session I

Symposium on Industrial and Applied Microscopy

CHAIRMAN: THEODORE G. ROCHOW, *Research Division, American Cyanamid Company, Stamford, Connecticut.*

This Symposium will be directed by the Chairman, assisted by the Discussion Moderators. The program is divided into two parts. The first portion will present Contributed Papers dealing with industrial and applied microscopy. The second portion is an Industrial Clinic where a series of invited discussions, in the form of Progress Reports, will present additional microscopical applications as found in a number of diversified industries. The presentation time for a Contributed Paper or a Progress Report will be ten minutes. An informal discussion period of at least five minutes will follow each presentation and will include spontaneous audience participation where slides may be used when relevant. **The Chairman will announce the program order for the presentations.**

Discussion Moderators

S. G. ELLIS, *Radio Corporation of America, RCA Laboratories Division, Princeton, New Jersey.*
ROBERT B. FISCHER, *Chemistry Department, Indiana University, Bloomington, Indiana.*
R. M. FISHER, *Fundamental Research Laboratory, United States Steel Corporation, Kearny, New Jersey.*
ERNEST F. FULLAM, *Ernest F. Fullam, Inc., Schenectady, New York.*
R. G. PICARD, *Radio Corporation of America, RCA Victor Division, Camden, New Jersey.*
MAX SWERDLOW (address below).
C. F. TUFTS, *Sylvania Electric Products, Inc., Atomic Energy Division, Bayside, New York.*
CARL E. WILLOUGHBY, *Experimental Station, E. I. du Pont de Nemours and Company, Wilmington, Delaware.*

Contributed Papers

I1. The Fine Histology of Wool and Wool Follicles. J. L. FARRANT AND G. E. ROGERS, *Chemical Physics Section, Division of Industrial Chemistry and Biochemistry Unit, Wool Textile Research Laboratories; Commonwealth Scientific and Industrial Research Organization, Melbourne, Australia.*—Although considerable knowledge of the fine structure of wool fibers has been obtained from early electron microscope studies of material fragmented by chemical, enzymic, and mechanical means, little information has hitherto been gained by electron microscopic examination of thin sections. Recent demonstra-

tions that wool cortex has a bilateral structure have made it desirable that electron microscopic studies be made of sections cut by means of the improved techniques now available. In this way it has been possible to investigate the morphology of nonmedullated wool fibers at various levels within the follicle.

I2. Distant Packing of Synthetic Latices. J. F. HAMILTON* AND F. A. HAMM, *Research Laboratories, Eastman Kodak Company, Rochester, New York.*—A hydrosol formed by the graft polymerization of acrylate esters with a succinyl gelatin derivative has been found under certain conditions to dry, leaving a regular two-dimensional network of particles on the substrate. Such a geometrical array appears not to have been described before. It is believed that prior to drying the particles exist in a similar three-dimensional array whose lattice parameter is dependent upon an electrostatic force of repulsion in equilibrium with the surface tension at the liquid-air interface. The magnitude of the electrostatic force determined by a diffuse double layer of ionic charge surrounding the particle is discussed quantitatively. Correlation with published data on proteins gives reasonable values of surface charge and potential.

I3. Behavior of Crystallites in Polyethylene. VIRGIL PECK* AND WILBUR KAYE, *Research Laboratories, Tennessee Eastman Company, Division of Eastman Kodak Company, Kingsport, Tennessee.*—Polyethylene has been studied in an effort to obtain visual confirmation of existing theories concerning the nature of crystalline polymers. This molecule was selected because it is relatively simple and has high crystallinity. Degree of crystallinity and orientation of crystallites can be controlled by regulation of heating and drafting conditions. Generally, the crystalline regions are lamellar. The lamellae orient or slip according to the draft history. The observed behavior of crystallites agrees with known x-ray diffraction data. The optical study of polyethylene provides part of the necessary background for a study of other crystalline polymers.

I4. Pores in Collagen and Leather. MAX SWERDLOW* AND ROBERT R. STROMBERG, *National Bureau of Standards, Washington 25, D. C.*—Theoretical deductions based on pore-size distributions determined by a pressure porosimeter method indicate the existence of a large volume and number of capillary pores of the order of 100A, in radius, within the structure of dried collagenous tissue and leather. Electron microscopy provides visual confirmation about the probable size, shape, and location of such pores within collagen fibrils obtained from kangaroo tail tendon. A helical configuration of subfibrillar elements is suggested by the electron micrographs. The use of mercury under hydrostatic pressure as a technique in staining and preserving the structure of biological materials for electron microscopy is advanced.

I5. Electron Microscopy of Limited Swelling in Cotton. VERNE W. TRIPP* AND RUTH GIUFFRIA, *Southern Regional Research Laboratory, New Orleans 19, Louisiana.*—Swelling of the cell wall is a familiar phenomenon in natural cellulose fibers treated with cuprammonium hydroxide or similar reagents. When water- or glycerol-wet fibers are embedded for sectioning by methacrylate polymerization, a microscopically similar effect is observed. Under these conditions polymethacrylate is deposited within the fiber cell wall. Examination of cross sections of cotton after removal of the polymethacrylate shows separation of the cell wall into unswollen concentric cellulose layers. The layers consist of highly parallelized microfibrils having strong lateral cohesion. Possible applications of the phenomenon to fiber cell wall studies are discussed.

Industrial Clinic

Progress Reports

C. J. CALBICK, *Bell Telephone Laboratories, Murray Hill, New Jersey.*
R. M. FISHER (address above).
J. F. HAMILTON (address above).
RUSSELL B. KELLER, JR., *Columbia-Southern Chemical Corporation, Barberton, Ohio.*
JOHN J. KELSCH, *Research Laboratories, Interchemical Corporation, 432 West 45th Street, New York, New York.*
CHARLES MARESH, *Research Division, American Cyanamid Company, Bound Brook, New Jersey.*
VIRGIL PECK (address above).
FREDERICK ROWE, *Research Division, American Cyanamid Company, Stamford, Connecticut.*
EDGAR L. SAUNDERS, *RCA Service Company, Inc., Camden, New Jersey.*
D. M. TEAGUE, *Chrysler Corporation, Engineering Division, Detroit, Michigan.*
JOHN W. WILSON, JR., *Socony-Vacuum Laboratories, 412 Greenpoint Avenue, Brooklyn, New York.*

Informal Discussions

Additional contributions will be made during the informal discussion periods by:

GEORGE C. CLAVER, *Plastics Division, Monsanto Chemical Company, Springfield, Massachusetts.*
WILLIAM R. MCMILLAN, *Research Laboratories, Westinghouse Electric Corporation, East Pittsburgh, Pennsylvania.*
SELBY E. SUMMERS, *General Engineering Laboratory, General Electric Company, Schenectady, New York.*

Session H (*continued*)

Contributed Papers on General Biology (*continued*)

CHAIRMAN: JEROME GROSS, *Massachusetts General Hospital, Department of Medicine, Boston, Massachusetts.*

H12. The Effects of Solvent Treatment on Biological Thin Sections. L. E. ROTH, *Argonne National Laboratory, Lemont, Illinois.*—The results of studies on the treatment of electron microscope sections with organic solvents after mounting on membrane-covered grids and before observation in the microscope are discussed. Cytological structures including mitochondria from ciliate protozoa are shown; these structures are compared in sections both treated and not treated with solvents to illustrate the advantages and disadvantages of both methods.

H13. The Influence of Stress and Other Factors on the Structure of Urinary Colloids. D. E. BEISCHER, *U. S. Naval School of Aviation Medicine, Pensacola, Florida.*—Sparse information is available about urinary colloids which are excreted by man in a daily amount of 0.25–2.5 grams. The electron microscope offers a valuable method for a study of these dispersions, which range in size from protein molecules to cell debris and fibers visible in the light microscope. Considerable unexpected changes in the structure of urinary colloids were observed in man under the influence of physical and mental stress. In most cases these influences were leading to an aggregation of the colloidal particles. The observations will be discussed in their relationship to kidney function and kidney stone formation.

H14. Effect of Thioacetamide upon Rat Liver Cells. RUTH G. KLEINFELD,[1] MILTON A. LESSLER, MARIE H. GREIDER, AND WALTER J. FRAJOLA, *The Department of Physiology and The Herman A. Hoster Research Laboratory of the Department of Medicine, Ohio State University.*—Upon administration of thioacetamide (CH_3CSNH_2) to the rat, within two days, characteristic morphological changes of a dramatic nature occur in the hepatic cells. The increased nuclear and nucleolar volumes, correlated to the changed cytoplasmic basophilia and increased cell volume were first noted by Rather.[2] Quantitative cytochemical studies of individual Feulgen-stained nuclei have shown that the early increase in nuclear volume was not associated with DNA synthesis. As the nucleoli enlarge they become very dense (increased RNA protein) and appear to migrate to the nuclear membrane. There is a threefold increase in nucleolar RNA and a twofold increase in nucleolar protein, resulting in a nucleolus of a different chemical nature. The cytoplasmic basophilia changes from the typically coarse clumps to become more finely dispersed and homogeneous in character, very much resembling the cytoplasm of a cell during mitosis. Upon continued treatment, i.e., 14 days of subcutaneous injections at a dose of 3 mg per 100 grams by weight, various stages of "degenerating nucleoli" appear. The "degenerating nucleoli" show an apparent leeching out of RNA protein. Rat liver cells were examined in the electron microscope before and after the thioacetamide treatment. Correlation of the results obtained by light microscopy with those obtained by electron microscopy was attempted. Light and electron micrographs demonstrating the above changes will be presented.

[1] P. H. S. Postdoctoral Fellow of the National Cancer Institute aided in part by U. S. P. H. S. grants C-2148 and C-1084(C4).
[2] Bull. Johns Hopkins Hospital **88**, 38 (1951).

H15. The Fine Vascular Organization of the Anterior Pituitary Gland. MARILYN G. FARQUHAR AND JAMES F. RINEHART, *Department of Pathology, University of California School of Medicine, San Francisco, California.*—Current studies of the cytology of the anterior pituitary gland have revealed detail of fine vascular and perivascular structure that would appear to be of significance in relationship to nutrient exchange and hormonal secretion and to have an important bearing on time-honored problems of reticuloendothelium, reticulin, and basement membranes. The sinusoids are found to be lined continuously by endothelial cells possessing very delicate cytoplasm containing mitochondria, minute particles, "endoplasmic reticulum," and numerous small vesicles. Palade (1953) observed these features in other capillary endothelia. Each sinusoid is surrounded by an actual or potential "space" bordered by basement membranes, one applied to the sinusoidal endothelium and the other to the parenchymal cells. The perisinusoidal spaces contain reticulin or collagen fibrils and cells which react as histiocytes to injected trypan blue. Portions of parenchymal cell cytoplasm containing secretory granules are frequently seen within the perisinusoidal spaces. The extrusion of such material into the space would appear to afford a mechanism for solubilization and slow absorption of pituitary hormones. The reticuloendothelial cells in the perisinusoidal spaces probably play an active role in these processes. The fact that the spaces not only surround sinusoids but extend between them affords a mechanism which greatly increases the bed of contact between the parenchymal cells and fluids from the blood stream. The nature of the basement membranes and the extent to which this organization may exist in other tissues will be discussed briefly.

H16. Colloidal Iron Reactions in the Kidney. RICHARD F. BAKER AND OLIVER WARREN, *School of Medicine, University of Southern California, Los Angeles, California.*—Colloidal iron staining of acid mucopolysaccharides as described by Hale[1] and Rinehart and Abul-Haj[2] has been modified to meet the special requirements of thin sectioning and electron microscopy. After formalin fixation, small pieces of tissue are soaked in acetic acid-iron colloid for several hours. Washing, dehydration, and plastic embedding follow. In thin sections of rat kidney, iron is seen deposited on the surfaces of pedicels of the glomerular capillaries and lining the cell walls of epithelial cells, in the form of filaments approximately 60 A.U. in diameter and 1500 A.U. long. The filaments are also observed on the luminal walls of intertubular capillaries. Pretreatment with hyaluronidase (Wyeth) removes the iron-reacting material from these sites.

[1] C. W. Hale, Nature **157**, 802 (1946).
[2] Rinehart and Abul-Haj, AMA Arch. Pathol. **52**, 189 (1951).

H17. The Ultrastructure of a Reptilian Myoneural Junction. J. DAVID ROBERTSON, *Department of Pathology and Oncology, University of Kansas Medical School, Kansas City, Kansas.*—Evidence for the following conclusions concerning the ultrastructure of chameleon skeletal myoneural junctions will be presented. (1) The terminal axon twigs are divested of Schwann cytoplasm and enveloped by a single double-edged membrane. (2) These terminal twigs are embedded in troughs formed by an invagination of the sarcolemma which is thrown into deep folds within the troughs. (3) The sarcolemma consists

of a double-edged membrane in certain ways analogous to the terminal axolemma. (4) The outer dense edge of the axolemma fuses with the outer dense edge of the sarcolemma in the troughs. (5) The sarcolemmal junctional folds compose the "stroma" of Kühne, "perilemma" of Tiegs, or the "subneural apparatus" of Conteaux. (6) Axoplasm does not dip into the folds. (7) Mitochondria are concentrated in both axoplasm and sarcoplasm at the junction. (8) Sarcolemmal nuclei are accumulated in sole sarcoplasm. (9) No evidence for attachment of "*Z*" bands to the junctional folds has been found.

H18. Effects of X-Radiation on the Gland Cell.[1] JAMES F. MARVIN, *Department of Radiology, University of Minnesota Hospitals, Minneapolis, Minnesota.*—Morphology of the exocrine cells of the pancreas and the cells of the glandular stomach of the mouse has been studied following doses of 600 to 4500 roentgens of ionizing radiation. Some evidence has been found of localized areas of damage. Also found is evidence of inhibition of activity of the cell (particularly in the development of the ergastoplasm[2]) following larger doses of radiation.

[1] Abstract received too late to be placed in normal program order.
[2] J. M. Weiss, J. Exptl. Medicine 98, 607 (1953).

H19. Quantitative Assay of the Binding to Proteins by Iodinated Dyes and Phosphotungstic Acid. Application of Data to Cellular Stains.[1] JAMES F. MARVIN, *Department of Radiology, University of Minnesota Hospitals, Minneapolis, Minnesota.*—Quantitative assay was made of the binding of sodium diiodo fluorescein and of phosphotungstic acid to proteins in connection with studies on porosity of collodion membranes. These electron stains were found to bind firmly, mole for mole, to all the available quaternary nitrogen groups of the amino acid; studies utilizing I^{131} and W^{187} indicated that either of these stains would displace the other stain. Techniques were developed to utilize these stains for observation of collodion molecules, membrane porosity, and cellular staining.

[1] Abstract received too late to be placed in normal program order.

H20. Cytochemical Studies of Thrombocytes Utilizing Dark-field, Phase-Contrast, and Electron Optics.[1] GEORGE L. DEAVER AND WALTER J. FRAJOLA, *The Herman A. Hoster Research Laboratory of the Department of Medicine, and the Department of Anatomy, The Ohio State University, Columbus, Ohio.*—Procedures, utilizing the phase contrast hemocytometer, cover slip preparations, a modified Gey culture chamber, and collodion covered grids on small glass slides, have been developed which permit direct correlation of dark-field, phase, and electron microscopy of blood platelets. Phase-contrast photomicrographs comparable in detail to many published electron micrographs have been obtained. The effects of enzymes, isolated coagulation factors, and other reagents upon viable thrombocytes were studied directly for extended periods of time and were photographed by the time-lapse method. This composite approach is indeed more dynamic than electron microscopy *per se*. When osmium tetroxide vapors were used for fixation, very little internal detail was observed in the hyalomere. However, when the thrombocytes were allowed to adhere and spread upon the collodion membrane for several hours, rather than the usual thirty minutes or less, they became very thin. Greater internal architecture was thereby revealed. To facilitate description, spread or extended form platelets have been classified, on the basis of chromomere morphology, as *nucleoid* or *granuloid*. The chromomere of the nucleoid type is an electron opaque mass limited by a membrane which is continuous, through fiber-like extensions, with a limiting membrane at the periphery. Treatment with different reagents indicated that this nucleoid body was a composite of at least two moieties: a dense component and a more hyaline constituent, possibly a ground substance. In the granuloid type the chromomere appears as a zone of dense spherical or ovoid units of varying sizes. Vacuoles may occur in either nucleoid or granuloid types. However, they were observed most frequently in the latter. Studies of the thrombocyte remnant subsequent to the action of ribonuclease revealed three major effects. Many platelets in preparations treated with desoxyribonuclease exhibited no salient differences from the controls. However, some altered forms were observed. One of the earliest effects of thrombin, as revealed by phase microscopy, was a swelling of the chromomere in some nucleoid forms. Digestion of the hyalomere was also observed. In preparations fixed in platinum or gold chloride, at low *p*H, direct continuity of the nucleoid chromomere and the peripheral limiting membrane was demonstrated, and a remarkable three-dimensional reticular architecture was discovered in the hyalomere. Short-range order was demonstrable. The micellar strands appeared as a network of linear aggregates of macromolecules resembling strings of beads. This data is interpreted as evidence for a thesis that the ultrastructural elements of the human thrombocyte are fibrillo-granular and spatially oriented.

[1] Abstract received too late to be placed in normal program order.

Session I (*continued*)

Symposium on Industrial and Applied Microscopy (*continued*)

See the Saturday morning program of Session I for names of the contributors.

Index of Contributors to This Twelfth Annual Meeting

The capital letter following a name indicates the Session where the contribution was made.
The number indicates the program position for a Contributed Paper.
Multiple entries for a single Session indicate more than one contribution to that Session.

Agar, A. W.—A26
Allred, Harry M.—E
Anderson, Thomas F.—A, A1, C
Asadi, A. M.—H4
Baker, Richard F.—H16
Ball, Frances L.—B2, D4
Banfield, William G.—H3
Bang, F. B.—F, F8
Beischer, D. E.—H13
Bierlein, T. K.—D1

Bigelow, W. C.—D
Birks, L. S.—B, D
Borasky, Rubin—A9
Bowler, E. S. C.—A10
Bradford, E. B.—A18
Bradley, D. E.—A24
Brockway, L. O.—B, B, D, E
Brown, John A.—E
Calbick, C. J.—A22, B, I
Chapman, G. B.—A19
Claver, George C.—I
Cochran, George W.—H4
Columbe, Maynard J.—B1
Dalhamn, T.—H5
Deaver, George L.—H20
De Robertis, E.—H1
Dmochowski, Leon—H11
Dougherty, T. F.—H4
Ellis, Alfred L.—D
Ellis, S. G.—A, B, I
Ellison, Solon A.—F6
Farquhar, Marilyn Gist—H6, H15
Farrant, J. L.—I1
Fischer, Robert B.—D2, I
Fisher, R. M.—B, D, D3, I, I
Frajola, Walter J.—H14, H20
Franchi, C. M.—H1
Friedlaender, Marlene—F1
Froula, H.—A10
Fullam, Ernest F.—D, E, I
Gay, Helen—A20
Gaylord, William H., Jr.—F2
Gettner, M. E.—H7
Giuffria, Ruth—I5
Glaser, W.—A8
Gomer, Robert—D
Greider, Marie H.—H14
Gross, Jerome—H
Grube, W. L.—B, D, E
Haagensen, Cushman D.—H11
Haine, M. E.—A15
Hall, C. E.—C, F4
Halma, H.—A4, A19
Hamilton, J. F.—I, I2
Hamm, F. A.—I2
Harman, John W.—H10
Harris, W. W.—B2, D4
Hass, Georg—A25
Heckman, F. A.—B4
Heidenreich, R. D.—B, D
Hocart, R.—B3
Hodge, A. J.—H9
Hope, A. B.—H9
Howard, Lorn L.—B5
Hunter, M. S.—D
Kallman, Frances—A21
Karrer, H.—F3
Kaye, Wilbur—I3
Keller, Fred, Sr.—D
Keller, Russell B., Jr.—I
Kelsch, John J.—A23, I
Kleinfeld, Ruth G.—H14
Koonce, S. E.—A22
Lessler, Milton A.—H14
Litwak, A. A.—A6
Lodge, James P.—A17
Mapes, Gerard S.—E2
Maresh, Charles—I
Marvin, James F.—H18, H19
McLean, D. J.—H9
McMillan, William R.—B, D, I
Melnick, Joseph L.—F7
Mercer, F. V.—H9
Meryman, H. T.—A25
Moore, Dan H.—F6, H11
Morgan, Councilman—F6
Mulvey, T.—A15
Newberry, Sterling P.—A12, A14, D
Nielsen, N. A.—B, D
Nixon, W. C.—A11
Norton, James F.—A14
Oberlin-Mathieu-Sicaud, A.—B3
Padden, Thomas R.—D5
Peck, Virgil—I, I3
Pellier, L. Delisle—D
Pellissier, George E.—D
Picard, R. G.—P,[1] A, B, I
Pollister, A. W.—H7
Preuss, L. E.—A16
Reisman, Elias—A5
Reisner, J. H.—A2
Reissig, Magdalena—F7
Revell, R. S. M.—A26
Rhodin, J.—H5
Rinehart, James F.—H6, H15
Ring, Charles E.—D2
Robertson, J. David—H2, H17
Rochow, Theodore G.—I
Rogers, G. E.—I1
Rose, Harry M.—F6
Roth, L. E.—H12
Rowe, Frederick—I
Saunders, Edgar L.—I
Schulz, LeRoy G.—B, D
Schwartz, C. M.—B, D, E
Sharp, Gordon D.—C, F5
Siegel, Benjamin M.—A5, A27, B
Simon, Ralph E.—A27
Skiba, Paul—E
Smith, Cyril S.—D
Sproull, Robert L.—A27
Stromberg, Robert R.—I4
Summers, Selby E.—A13, I
Swerdlow, Max—B4, I, I4
Teague, D. M.—D, E1, I
Tripp, Verne W.—I5
Tufts, Barbara J.—A17
Tufts, C. F.—B, D, I
Turnbull, T. P.—A7
Twiss, S. B.—E1
Vanderhoff, J. W.—A18
Van Dorsten, A. C.—A3, D6
Vilella, J. R.—D
Walter, Norman M.—B
Ward, R.—H7
Warren, Oliver—H16
Watson, John H. L.—A16, E
Weinreb, Stanley—H10
Williams, Robley C.—A, A21, C
Willoughby, Carl E.—I
Wilson, John W., Jr.—E2, I
Yasuzumi, G.—H8
Zollers, S. M.—A6

[1] "Preface."